

**PHTHALATE ESTERS DEGRADATION
MECHANISMS BY ENZYMES**

**A Thesis Submitted to
the Graduate School of Engineering and Sciences of
İzmir Institute of Technology
In Partial Fulfillment of the Requirements for the Degree of**

DOCTOR OF PHILOSOPHY

in Environmental Engineering

**by
ESİN BALCI**

**December 2023
İZMİR**

We approve the thesis of **Esin BALCI**

Examining Committee Members:

Prof. Dr. Aysun SOFUOĞLU

Department of Chemical Engineering, İzmir Institute of Technology

Prof. Dr. Nurdan BÜYÜKKAMACI

Department of Environmental Engineering, Dokuz Eylül University

Assoc. Prof. Dr. Hatice Eser ÖKTEN

Department of Environmental Engineering, İzmir Institute of Technology

Assoc. Prof. Dr. Nur Başak SÜRMEİ-ERALTUĞ

Department of Bioengineering, İzmir Institute of Technology

Assoc. Prof. Dr. Serpil ÖZMIHÇI

Department of Environmental Engineering, Dokuz Eylül University

7 December 2023

Prof. Dr. Aysun SOFUOĞLU

Supervisor

Department of Chemical Engineering
İzmir Institute of Technology

Prof. Dr. Gülşah ŞANLI-MOHAMED

Co-supervisor

Department of Chemistry
İzmir Institute of Technology

Prof. Dr. Sait Cemil SOFUOĞLU

Head of Department of Environmental
Engineering
İzmir Institute of Technology

Prof. Dr. Mehtap EANES

Dean of the Graduate School of
Engineering and Sciences
İzmir Institute of Technology

ACKNOWLEDGMENT

First of all, I would like to express my deepest and most sincere gratitude to my advisor Prof. Dr. Aysun SOFUOGLU for her supervision, support, continuous feedback, encouragement, guidance, and patience throughout the thesis. I would also like to extend my gratitude to my co-advisor, Prof. Dr. Gülşah ŞANLI-MOHAMED, for her invaluable guidance and support.

I am grateful to Prof. Dr. Maria Angeles SANROMAN BRAGA, Prof. Dr. Marta M. PAZOS CURRAS, and Assoc. Prof. Dr. Emilio ROSALES VILLANUEVA for accepting me to their laboratory as a researcher, providing invaluable support and continuous feedback and offering guidance throughout my studies. Furthermore, I would like to thank each of my colleagues in the Bioengineering & Sustainable Processes Group (BIOSUV) laboratory at the University of Vigo for their hospitality.

I would like to thank my thesis monitoring jury members, Assoc. Prof. Dr. Hatice Eser ÖKTEN and Assoc. Prof. Dr. Nur Başak SÜRMEİ-ERALTUĞ for their help and valuable suggestions throughout the thesis. I want to thank all my jury members for their constructive feedback to improve the overall quality of my thesis.

I warmly express my special thanks to Baki Sonat DEMİRDİREK, Filiz KURUCAOVALI, Dr. Bilal Orkan OLCAY, and my close friends for their help and support. I would like to thank valuable specialists working in the Environmental Development Application and Research Center, Biotechnology and Bioengineering Application and Research Center and the Center for Materials Research at İzmir Institute of Technology for providing technical support.

I would like to thank the Scientific and Technological Research Council of Türkiye (TUBITAK) for financially supporting me with 2214-A Doctoral Research Fellowship Program for my international Ph.D. studies.

Finally, I would like to thank my beloved family; my father Şahin BALCI, my mother Yıldız BALCI, my brother-in-law Murat GELMEZ, and my dear sister Sezin GELMEZ for their never-ending love, support, and encouragement.

ABSTRACT

PHTHALATE ESTERS DEGRADATION MECHANISMS BY ENZYMES

Phthalate esters (PAEs) stand out as the priority toxicants due to their carcinogenic, mutagenic, and teratogenic properties. The enzymatic degradation is hailed for its recognized safe and environmentally friendly properties. This study delved into PAEs' degradation, especially dibutyl phthalate (DBP) and diethylhexyl phthalate (DEHP) by recombinant esterase from *Geobacillus* sp. isolated from Balçova Geothermal region in İzmir. The esterase exhibited efficient degradation of DBP but had limited effectiveness in degrading DEHP. Many experiments were conducted to compare the ability of recombinant esterase to degrade DBP and DEHP with that of commercially available enzymes secreted from various microorganisms. Among these enzymes, *Bacillus subtilis* esterase and *Rhizomucor miehei* lipase had the highest ability. They were immobilized on halloysite nanotubes (HNTs) by adsorption method to enhance their stability and prolong their activity in applications. To investigate the impact of immobilization methods, two bionanocomposites were formed by immobilization of *Bacillus subtilis* esterase to HNTs with chitosan (CTS) and alginate (ALG) by the cross-linking method. Two fixed-bed reactors with CTS-HNT-EST and ALG-HNT-EST were operated in batch and continuous modes for PAEs' degradation. CTS-HNT-EST exhibited superior efficacy and durability in PAEs' removal for both modes. Lastly, bioremediation experiments were conducted in PAEs-contaminated soils using *Bacillus subtilis* esterase and recombinant esterase. Although both esterase had the same active site triad, recombinant esterase had a less significant effect on PAEs' degradation. This fact can be attributed to different substrate specificity and enzyme dynamics. Despite variations in their degradation capabilities, both commercial and newly engineered recombinant enzymes demonstrate considerable potential for breaking down PAEs.

ÖZET

FİTALAT ESTERLERİNİN ENZİMLERLE BOZUNMA MEKANİZMALARI

Fitalat Esterleri (PAE'ler) kanserojen ve teratojenik özellikler gösteren ve endokrin bozulmasıyla ilişkilendirilmiş öncelikli toksik maddeler olarak bilinmektedir. Enzimatik degradasyon güvenli ve çevre dostudur. Bu çalışma İzmir Balçova Jeotermal bölgesinden izole edilen termofilik *Geobacillus* sp.'lerden rekombinant esteraz enzimi elde edilip, kullanılarak DBP ve DEHP'lerin enzimatik degradasyonuna odaklandı. Rekombinant esteraz, DBP'yi etkili bir şekilde degrade etmesine rağmen, DEHP'nin degradasyonunda daha düşük bir performans sergilemiştir. Rekombinant esterazın DBP ve DEHP'yi parçalama yeteneğini, çeşitli mikroorganizmalardan salgılanan ticari enzimlerle karşılaştırmak için pek çok deney gerçekleştirildi. Bu enzimler arasında *Bacillus subtilis* esterazı ve *Rhizomucor miehei* lipazı, dibütil ftalat (DBP) ve dietilhekzil ftalat (DEHP) için kısa sürede yüksek degradasyon performansı sergilemiştir. Enzimler, stabiliteilerini geliştirmek, kullanım sürelerini artırmak ve uygulamalarda aktivitelerini korumak için haloysite nanotüplere (HNT'ler) adsorpsiyon yöntemiyle immobilize edildi. Immobilizasyon metodlarının etkisini araştırmak amacıyla, *Bacillus subtilis* esterazı kitosan (CTS) ve aljinat (ALG) ile modifiye edilmiş HNT'lere çapraz bağlama yöntemiyle immobilize edildi ve iki biyokompozit oluşturuldu. CTS-HNT-EST ve ALG-HNT-EST biyokompozitleriyle doldurulmuş iki sabit yataklı reaktör, PAE'leri degrade etmek için kesikli ve sürekli modlarda çalıştırılmıştır. CTS-HNT-EST iki modta da PAE'lerin degradasyonunda üstün bir performans ve dayanıklılık göstermiştir. Son olarak, PAE'lerce kirlenmiş topraklarda, rekombinant ve *Bacillus subtilis* esterazları varlığında enzimatik biyoremediasyon deneyleri gerçekleştirilmiştir. İki esteraz aynı aktif bölge üçlüsüne sahip olmasına rağmen, rekombinant esterazın DBP ve DEHP degradasyonu üzerinde daha az etkisi olmuştur. Bu durum, farklı substrat spesifisitesine ve enzim dinamiklerine bağlanmaktadır. Bozunma yeteneklerindeki farklılıklara rağmen, hem ticari hem de yeni tasarlanmış rekombinant enzimlerin, PAE'leri parçalamak için önemli bir potansiyel gösterir.

TABLE OF CONTENTS

LIST OF FIGURES	xii
LIST OF TABLES	xiv
CHAPTER 1. INTRODUCTION	1
1.1. Physical and chemical properties of PAEs.....	2
1.2. Main sources of PAEs	3
1.3. PAE toxicity	5
1.3.1. Human toxicity	5
1.3.2. Ecological toxicity	6
1.4. Occurrence of PAEs in the environment.....	8
1.5. Removal of PAEs in the environment.....	8
1.6. Immobilization	13
1.7. Research Objectives	14
1.8. Thesis Overview.....	15
1.9. Significance and Impact	16
CHAPTER 2. IMMOBILIZATION OF ESTERASE FROM BACILLUS SUBTILIS ON HALLOYSITE NANOTUBES AND APPLICATIONS ON DIBUTYL PHTHALATE DEGRADATION.....	17
2.1. Introduction	17
2.2. Material and Method	20
2.2.1. Materials	20
2.2.2. DBP degradation in the presence of free enzymes	20
2.2.3. Enzyme immobilization on HNT and optimization	21
2.2.3.1. HNT-enzyme composite	21
2.2.3.2. Optimization of the parameters for the immobilization procedure.....	21
2.2.4. Characterization analysis	22
2.2.4.1. Structural characterization of the composite	23
2.2.4.2. Nanotextural and chemical characterization of the composite	23
2.2.5. Degradation studies in presence of the HNT-enzyme composite	24

2.2.6. Analytical procedures	24
2.2.6.1. Determination of the enzyme activity and protein concentration	24
2.2.6.2. Enzyme stability and reusability tests	25
2.2.6.3. Determination of kinetic parameters	26
2.2.6.4. Analysis of DBP and its metabolites	26
2.3. Results and Discussion	27
2.3.1. Determination of the most suitable enzyme for DBP degradation	27
2.3.2. Esterase Immobilization	28
2.3.2.1. HNT-enzyme composite adsorption efficiency	29
2.3.2.2. HNT-enzyme composite specific activity	31
2.3.2.3. Optimization of the conditions for the enzyme immobilization	32
2.3.3. Characterization Analysis	35
2.3.3.1. Structural characterization of HNTs and HNT-enzyme composite	35
2.3.3.2. Nanotextural and chemical characterization of HNT-enzyme composite	36
2.3.4. Stability Test	37
2.3.4.1. Thermal stability	37
2.3.4.2. Storage stability	38
2.3.4.3. Reusability of HNT-enzyme composite	40
2.3.5. Determination of kinetic parameters	40
2.3.6. DBP degradation study by HNT-enzyme composite	41
2.3.7. Investigation of DBP metabolites	43
2.4. Conclusion	44

CHAPTER 3. DEGRADATION OF DIBUTYL AND DIETHYLHEXYL

PHTHALATES BY RHIZOMUCOR MIEHEI LIPASE: SUBSTRATE SPECIFICITY, IMMOBILIZATION, CATALYTIC PERFORMANCE

.....	46
3.1. Introduction	46
3.2. Material and Method	48
3.2.1. Materials	48
3.2.2. Enzyme immobilization onto HNTs	49
3.2.3. Enzyme characteristic properties	49
3.2.4. Material characterization	50

3.2.5. Sequence analysis	50
3.2.6. Circular Dichroism (CD) Analysis	51
3.2.7. Stability tests	52
3.2.8. Degradation assays	52
3.2.8.1. Degradation assay by free palatase	52
3.2.8.2. Degradation assay by HNTs-P composite	53
3.2.9. Analysis of PAEs and their metabolites	53
3.3. Results and Discussion.....	54
3.3.1. Enzyme immobilization and characterization	54
3.3.1.1. Morphological properties.....	55
3.3.1.2. Physical and chemical properties.....	55
3.3.2. Sequence analysis	56
3.3.3. Conformational change in the enzyme structure	59
3.3.4. Stability test assays.....	61
3.3.4.1. Temperature stability	61
3.3.4.2. Storage stability test.....	62
3.3.4.3. pH stability test	63
3.3.5. DBP degradation by free palatase and HNTs-P composites	63
3.3.6. Degradation metabolites	65
3.4. Conclusion.....	67

CHAPTER 4. CONTINUOUS TREATMENT OF DIETHYLHEXYL AND DIBUTYL PHTHALATES BY FIXED-BED REACTOR: COMPARISON OF TWO ESTERASE BIONANOCOMPOSITES..... 69

4.1. Introduction	69
4.2. Material and method	71
4.2.1. Materials	71
4.2.2. Immobilization study	72
4.2.2.1. Preparation of chitosan-halloysite beads	72
4.2.2.2. Preparation of alginate-halloysite beads	72
4.2.2.3. Immobilization of esterase on chitosan-halloysite and alginate-halloysite beads.....	73
4.2.3. Protein determination	73
4.2.4. Enzyme activity assay	74

4.2.5. Material Characterization	75
4.2.5.1. Scanning Electron Microscopy analysis	75
4.2.5.2. Transmission Electron Microscopy analysis	75
4.2.5.3. Fourier-Transform Infrared Spectroscopy analysis	76
4.2.5.4. Thermogravimetric analysis	76
4.2.6. Degradation assay	76
4.2.6.1. Assays with free esterase	76
4.2.6.2. Assays with bionanocomposites	77
4.2.6.3. Analysis of PAEs and their metabolites	77
4.3. Results and Discussion.....	78
4.3.1. Assays with free enzymes	78
4.3.1.1. Effect of the operational condition on the esterase activity	78
4.3.1.2. Degradation assays	79
4.3.2. Characterization of bionanocomposites	80
4.3.3. Batch degradation assays with bionanocomposites.....	83
4.3.4. Continuous degradation.....	87
4.3.4.1. Dibutyl phthalate bionanocomposite degradation	88
4.3.4.2. Diethylhexyl phthalate bionanocomposite degradation.....	90
4.4. Conclusion.....	91
CHAPTER 5. CHARACTERIZATION AND EXPRESSION OF RECOMBINANT THERMOALKALOPHILIC ESTERASE FROM GEOBACILLUS SP. AND PAES' DEGRADATION	92
5.1. Introduction	92
5.2. Material and Method	94
5.2.1. Materials	94
5.2.2. Enzyme preparation.....	94
5.2.3. Recombinant esterase' molecular mass	95
5.2.4. Affinity chromatography	96
5.2.5. Protein concentration and enzyme activity.....	96
5.2.6. Kinetic parameters of enzyme	97
5.2.7. Enzymatic degradation experiments.....	98
5.2.8. Chromatographic analysis of PAEs.....	98
5.3. Results and discussion.....	99

5.3.1. Expression and purification of esterase enzyme	99
5.3.2. Enzyme activity assay	100
5.3.3. Enzyme kinetics.....	101
5.3.4. Degradation experiments.....	102
5.3.5. Degradation products of PAEs	104
5.4. Conclusion.....	106
CHAPTER 6. ENZYME-MEDIATED DEGRADATION OF PHTHALATE ESTERS IN SOIL.....	107
6.1. Introduction	107
6.2. Material and Method	109
6.2.1. Materials	109
6.2.2. Enzyme preparation.....	109
6.2.3. Enzyme activity and protein concentration	110
6.2.4. Sequence Analysis.....	110
6.2.5. Experimental soil samples	111
6.2.6. Enzymatic degradation of contaminated soil with PAEs	112
6.2.7. Sample extraction	113
6.2.8. Analysis of PAEs.....	113
6.2.9. Degradation products.....	114
6.3. Results and Discussion.....	114
6.3.1. Enzyme assays	114
6.3.2. Kinetic parameters	115
6.3.3. Optimization of the solvent extraction	115
6.3.4. Enzymatic degradation in soil	117
6.3.5. Sequence Analysis.....	119
6.3.6. Degradation products.....	121
6.4. Conclusion.....	125
CHAPTER 7. CONCLUSION	126
CHAPTER 8. FUTURE PROJECTION.....	128
REFERENCES	129

APPENDICES

APPENDIX A. PERMISSION FOR REPRODUCING PUBLISHED ARTICLES.... 167
APPENDIX B. SUPPLEMENTARY INFORMATION FOR CHAPTER 2..... 169
APPENDIX C. SUPPLEMENTARY INFORMATION FOR CHAPTER 3..... 175
APPENDIX D. SUPPLEMENTARY INFORMATION FOR CHAPTER 4..... 179

LIST OF FIGURES

<u>Figure</u>	<u>Page</u>
Figure 1.1. (a) Primary metabolic pathway of PAEs to PA. (b) Aerobic metabolic pathway of PA. (c) Anaerobic metabolic pathway of PA.	12
Figure 2.1. 3D response surface and 2D contour plots: The effect on adsorption efficiency of (a-b) E/H and time, (c-d) temperature and pH.....	33
Figure 2.2. 3D response surface and 2D contour plots: The effect on the specific enzyme activity of (a-b) E/H and time; (c-d) temperature and pH.	34
Figure 2.3. Composite characterization: XRD analysis (a), SEM images (b), and TEM images of HNTs (c) and HNT-enzyme composite (d), FT-IR spectrum (e) and TGA curves (f) of HNT (black), esterase (red), and HNT-enzyme composite (blue).	39
Figure 2.4. DBP degradation efficiency in the presence of (a) free esterase and (b) HNT-enzyme composite.....	42
Figure 3.1. Multiple amino acid sequence alignment of esterase and palatase genes. ...	57
Figure 3.2. CD spectra of free palatase and HNTs-P composite.	61
Figure 3.3. DBP/DEHP degradation efficiency in the presence of HNTs-P composite..	64
Figure 3.4. LC-MS chromatograms of the samples before and after DBP/DEHP degradation experiment in the presence free palatase and HNTs-P.	65
Figure 4.1. Esterase activity under different conditions.	79
Figure 4.2. Time-dependent DBP (▪) and DEHP(•) concentration changes in the presence of free esterase (1 mg/mL).	80
Figure 4.3. Profile of concentrations of (a) DBP and (b) DEHP in their degradation by CTS-HNT-EST (▪) and ALG-HNT-EST (•).	85
Figure 4.4. Pollutants removal of (a) DBP and (b) DEHP operating in continuous under different volumetric flows in the presence of the CTS-HNT-EST (green) and ALG-HNT-EST (brown).	87
Figure 4.5. (a) Relative activity of the esterase immobilized on CTS-HNT-EST (▪) and ALG-HNT-EST (•) during the DBP degradation. (b) Relative activity of the esterase immobilized on CTS-HNT-EST and ALG-HNT-EST during the DEHP degradation.	89

<u>Figure</u>	<u>Page</u>
Figure 5.1. SDS-PAGE analysis of the collected fractions (a) before and (b) after purification step.	100
Figure 5.2. Esterase activity at different pH values (a) and temperatures (b).	101
Figure 5.3. Lineweaver Burk plot for pNPC-2 hydrolysis with recombinant esterase.	102
Figure 5.4. Degradation efficiency of DBP and DEHP with 50 and 100 mg/L in aqueous solution in the presence of recombinant esterase for 48h.	103
Figure 5.5. Degradation efficiency of DBP and DEHP with 25 mg/L in the presence of recombinant esterase for 168 h.	104
Figure 5.6. LC-MS chromatogram of the samples before (a) and after DBP degradation experiments in the presence of recombinant esterase (b).	105
Figure 5.7. LC-MS chromatogram of the samples before (a) and after DEHP degradation experiments in the presence of recombinant esterase (b).	106
Figure 6.1. Effect of different solvents on extraction efficiency of DBP from soil 1 (a) and soil 2 (b).	116
Figure 6.2. Effect of different solvents on extraction efficiency of DEHP from soil 1 (a) and soil 2 (b).	116
Figure 6.3. Degradation efficiency of DBP in (a) soil 1 and (b) soil 2 by <i>Bacillus subtilis</i> esterase and recombinant esterase.	117
Figure 6.4. Degradation efficiency of DEHP in (a) soil 1 and (b) soil 2 by <i>Bacillus subtilis</i> esterase and recombinant esterase.	118
Figure 6.5. Multiple amino acid sequence alignment of esterase from <i>Bacillus subtilis</i> and <i>Geobacillus</i> sp.	121
Figure 6.6. LC-MS chromatogram of the samples before (a) and after DBP degradation experiments conducted in soil 1 and soil 2 in the presence of <i>Bacillus subtilis</i> esterase (b and d) and recombinant esterase (c and e).	123
Figure 6.7. LC-MS chromatogram of the samples before (a) and after DEHP degradation experiments conducted in soil 1 and soil 2 in the presence of <i>Bacillus subtilis</i> esterase (b and d) and recombinant esterase (c and e).	124

LIST OF TABLES

<u>Table</u>	<u>Page</u>
Table 1.1. Physical and chemical properties of PAEs	4
Table 1.2. The concentration of PAEs in different media.	10
Table 6.1. Characteristics of soil 1 and soil 2.....	112

CHAPTER 1

INTRODUCTION

Endocrine disrupting chemicals (EDCs) are synthetic industrial pollutants that contaminate our environment and have been linked to abnormal developmental patterns, immunological issues, cancers, neurodevelopmental delays, and reproductive issues in the human population (WHO and UNEP, 2012). Every year, thousands of these chemicals are produced around the world, and most of them could potentially affect hormones.

Phthalate Esters or Phthalic Acid Esters (PAEs) are a group of widely utilized plasticizer chemicals that are environmentally pervasive. Many of PAEs interfere with the endocrine system of humans and mammals at extremely low concentrations (Hannon and Flaws, 2015). They are considered to be mutagenic, hepatotoxic, and carcinogenic agents. The current global production of PAEs is estimated at 300 million tons, and it is projected to increase to 500 million tons by 2050, with a massive portion of this production consisting of single-use products (Sardon and Dove, 2018). PAEs are easily released into the environment including atmosphere, lithosphere (soil and sediment), and hydrosphere (surface water, wastewater, etc.) through the large-scale production and wide commercial use due to their weak interactions (hydrogen bonds or van der Waals forces) with plastic matrix.

PAEs are among the most detected persistent organic pollutants (POPs) in the environment. Considering the hazards of PAEs and their large scale and worldwide use, six congeners of PAEs; dimethyl phthalate (DMP), diethyl phthalate (DEP), dibutyl phthalate (DBP), di-n-octyl phthalate (DnOP), diethylhexyl phthalate (DEHP), and butyl benzyl phthalate (BBP), have been listed as priority pollutants by United States Environmental Protection Agency, the European Union, and the China National Environmental Monitoring Center. The effective removal of PAEs in the environment poses a serious challenge because the global consumption of PAEs continues to rise.

1.1. Physical and chemical properties of PAEs

PAEs are chemical compounds that are synthesized by the esterification of phthalic anhydride with various alcohols. The physicochemical properties of PAEs can vary significantly based on their chemical structures and the length of their alkyl side chains (Tran et al., 2022a). PAEs are colorless or slightly yellowish liquids with no odor and a flavorless nature. They show a more fluid and oily structure as the length of the alkyl side chains increases (Staples, 2003). Most of PAEs have low volatility and poor solubility in water. Nevertheless, they are soluble in organic solvent and oils (Gani et al., 2017). They may exist in liquid form at a wide range of temperatures (25–50°C) and are chemically stable (Tran et al., 2021). Their boiling points range from 230°C to 486°C, whereas their melting points are often less than -25°C.

PAEs can be used for various purposes because of their different chemical and physical characteristics (Bornehag et al., 2005). They are divided into long chains (PAEs with 7 to 13 carbon chains) and short chains congeners (PAEs with 3 to 6 carbon chains). Long-chain phthalates including di(2-ethylhexyl) phthalate (DEHP), dioctyl phthalate (DnOP), di-iso-decyl phthalate (DiDP) and di-iso-nonyl phthalate (DiNP) are commonly used in PVC polymers. Short-chain phthalates including dibutyl phthalate (DBP), butyl benzyl phthalate (BBP), diethyl phthalate (DEP), dimethyl phthalate (DMP), and di-iso-butyl phthalate (DiBP) are frequently used in non-PVC applications (Wittassek et al., 2011).

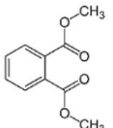
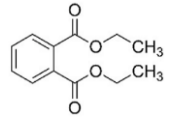
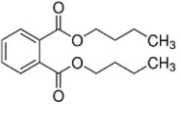
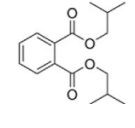
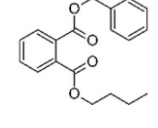
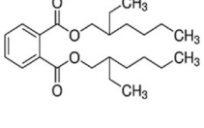
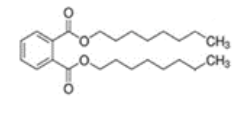
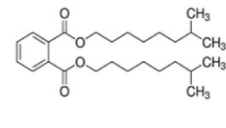
Solubility in both air and water decreases significantly by order of magnitude from the short alkyl side chain PAEs such as DMP to the long alkyl side chain PAEs such as DEHP. The octanol-water partition coefficient (K_{ow}), indicative of hydrophobicity, rises by order of magnitude as the alkyl side chain length increases (Cousins et al., 2003; Net et al., 2015). This increase is mainly controlled by the reduction in water solubility rather than an increase in octanol solubility. Cousins and Mackay (2000) highlighted that the sensitivity of solubilities in octanol to variations in molar volume is considerably lower compared to solubilities in water and air. The decrease in solubilities from DMP to Ditridecyl phthalate (DTDP) in octanol is only approximately one order of magnitude, whereas in water, it decreases by 11 orders of magnitude. Consequently, the observed increase in the K_{ow} with longer alkyl chain lengths can be attributed to the fact that

solubilities in water experience a more significant decrease per unit volume in molar volume than solubilities in octanol. However, vapor pressure at 25°C in mm Hg decreases with the increasing molecular mass (g/mol) or alkyl side chains. These properties play a significant role in the behavior, fate/transport, and degradation of PAEs in various environmental compartments, including the biosphere, hydrosphere, atmosphere, and lithosphere. They can significantly impact on PAEs' potential for persistence and bioavailability. High K_{OW} values of PAEs are strongly associated with particles in air and water and they result in the adsorption of PAEs to soil and sediment (Wu et al., 2019). Additionally, PAEs exhibit high hydrophobicity, which leads to their strong binding affinity to the organic matter in the soil. The air-water partition coefficient (K_{AW}) and octanol-air partition coefficient (K_{OA}) increase with increasing alkyl side chain length (Cousins et al., 2003; Net et al., 2015). The PAEs with lower molecular are quite volatile, but owing to their extremely low K_{AW} values they will volatilize fairly rapidly from the pure state but only very slowly from aqueous solution. Furthermore, PAEs with high K_{OA} in atmosphere will be appreciably sorbed to aerosol particles, soil and vegetation (Cousins et al., 2003). Table 1.1 shows physico-chemical data such as Log K_{OW} , Log K_{OA} , Log K_{AW} , and solubility for the most predominant PAEs (Cousins et al., 2003; Tran et al., 2022b; Kaur et al., 2023). The biological degradation of PAEs is also influenced by their structure. PAEs with a cyclic structure, particularly those containing a benzene ring along with long branched chains and electron-withdrawing groups tend to be resistant to biodegradation.

1.2. Main sources of PAEs

Anthropogenic activities, including residential, agricultural, and industrial processes are the primary sources of PAEs in the environment. Currently, there are approximately 60 different congeners of PAEs used in a variety of industries, including personal care products (e.g., cosmetics, hair sprays, gels), packaging materials, plastic manufacturing, lubricants, insecticides, paint additives, and adhesives (Eichler et al., 2019). Due to their low volatility, PAEs' interaction with the atmosphere may be limited. When waste is incinerated, PAEs are primarily released into the atmosphere. The primary

Table 1.1. Physical and chemical properties of PAEs (Cousins and Mackay, 2000; Cousins et al., 2003; Gani et al., 2017; Tran et al., 2022b).

Properties	PAEs							
	DMP	DEP	DBP	DiBP	BBP	DEHP	DnOP	DINP
Formula	C ₁₀ H ₁₀ O ₄	C ₁₂ H ₁₄ O ₄	C ₁₆ H ₂₂ O ₄	C ₁₆ H ₂₂ O ₄	C ₁₉ H ₂₀ O ₄	C ₂₄ H ₃₈ O ₄	C ₂₄ H ₃₈ O ₄	C ₂₆ H ₄₂ O ₄
Molecular weight (g/mol)	194.18	222.24	278.34	278.34	312.40	390.60	390.60	418.60
Log K _{OW}	1.64	2.50	4.27	4.27	4.73	7.73	7.73	8.60
Log K _{OA}	7.01	7.55	8.54	8.54	8.78	10.53	10.53	11.03
Log K _{AW}	-5.40	-5.01	-4.27	-4.27	-4.08	-2.80	-2.80	-2.43
Vapor pressure (mm Hg, 25 °C)	9.12 x 10 ⁻³	1.67 x 10 ⁻³	2.01 x 10 ⁻⁵	4.76 x 10 ⁻⁵	8.25 x 10 ⁻⁶	1.42 x 10 ⁻⁷	1 x 10 ⁻⁷	5.40 x 10 ⁻⁷
Solubility (mg/L, °C)	4,000	1,080	11.20	0.01	2.69	0.27	0.02	0.20
Melting point (°C)	5.5	-40.5	-35	-64	-35	-55	25	-43
Boiling point (°C, 760 mm Hg)	283.7	295	340	296	370	384	220	77.8
No. of C atom/chain	1	2	4	4	4, 6	8	8	9
Structure								

sources of atmospheric PAEs in urban areas are industrial emissions and vehicle exhaust (Gao et al., 2018). Agricultural activities such as irrigation, the use of agricultural film, mulching, pesticide and fertilizer, and sewage sludge discharge cause PAE pollution in the soil (Cai et al., 2007; Net et al., 2015; Tran et al., 2015; Lü et al., 2018). Residential activities can lead to the generation of urban dust, which can contribute to soil contamination by deposition. Both dry and wet deposition processes can contribute to the contamination of soil with PAEs, especially in highly industrialized areas where PAE emissions are more prevalent (Wu et al., 2015). Dry deposition involves the direct settling of particulate matter containing PAEs from the atmosphere onto the soil surface, when wet deposition occurs when PAEs are carried to the ground by precipitation, such as rain or snow. These processes can introduce PAEs into the soil, potentially leading to contamination.

1.3. PAE toxicity

1.3.1. Human toxicity

Exposure to PAEs can occur through various pathways, including ingestion, inhalation, skin absorption, or contact, and even intravenous injection. It can lead to detrimental impacts on human health (Braun et al., 2017; Chang et al., 2021). It is well-known that PAEs exhibit potent estrogenic effects on the human body. DEHP is the most concerning substance as it has been associated with a reduction in male sperm quality and testosterone levels (Oishi and Hiraga, 1980; Chang et al., 2021). Additionally, the presence of PAEs in soils results in their adsorption on sediment and has an adverse effect on human health. Many studies indicated the presence of PAEs in various food products and personal care products (Pereira et al., 2019b). Packaged food was found to account for most of the human exposure, up to 67% (Das et al., 2014). Plastic materials in food packages cause sensitivity to DEHP levels in humans (Tran and Kannan, 2015).

Exposure to them increases asthma symptoms, allergic respiratory diseases, and atopic disorders (Bertelsen et al., 2013; Bornehag et al., 2015). PAEs exhibit endocrine-disrupting characteristics. They can disrupt the development of the human nervous and

immune systems, potentially leading to physiological and psychomotor disorders as well as intellectual deficiencies in children (Kim et al., 2018; Radke et al., 2020). They have been associated with an increased risk of hypertension, alterations in thyroid hormone levels, and metabolic disorders (Zhang et al., 2021). PAEs can also induce alterations in liver structure or impair various liver functions (Tang et al., 2019). DEHP and BBP have even been classified as carcinogens by the International Agency for Research on Cancer. Consequently, several countries have imposed restrictions on the use of individual PAEs in certain products (Calafat et al., 2015; Wang et al., 2018). Studies conducted by USEPA have revealed that trace amounts of DEHP are highly carcinogenic.

PAEs may generally be shown to be acutely toxic with fatal dose (LD50) values of 1-30 g kg⁻¹ bodyweight (Kaur et al., 2023). The potential for human exposure to PAEs from different intake routes has been investigated. In the early 1990s, the daily DEHP intake levels for the infants in Canada were 9, 19, 14, and 6 µg kg⁻¹ body weight day⁻¹, respectively (Meek and Chan, 1994). As for the 2000s, in Germany DEHP intake levels in adults in relation to daily food consumption ranged from 1,000-4,200 ng kg⁻¹ body weight day⁻¹ (Fromme et al., 2007). Similarly, intake levels of DEHP (2,700-4,300 ng kg⁻¹ body weight day⁻¹), DBP (1,900-4,100 ng kg⁻¹ body weight day⁻¹), and BBP (290-430 ng kg⁻¹ body weight day⁻¹) were reported in Denmark (Petersen and Breindahl, 2000). Children are more likely to be exposed to PAEs than adults. Polymer toys containing PAEs have been identified as a significant source of exposure for infants and young children due to their mouthing behaviors. As a result of DEHP exposure through toys (via sucking or chewing) or other sources, children's intake levels are estimated to be up to 85 g kg⁻¹ body weight day⁻¹.

1.3.2. Ecological toxicity

Public concern regarding the toxicity of PAEs is increasing not only in human trials but also in animal testing. PAEs can accumulate in ecosystems over the long-term, resulting in exposure to PAEs. Many studies have been conducted to examine the harmful effects of PAEs on the environment. Environmental risk limits (ERL) for DBP and DEHP in water were 0.19 and 10 g/L, respectively (van Wezel et al., 2000). Weizhen et al. (2020)

investigated the risks associated with the levels of PAEs in aquatic organisms in sediments and water. They found that the levels of PAEs with long alkyl side chains, such as DEHP, DNOP, and DiNP exceeded ERL mainly in the water, while PAEs with short alkyl side chains like butyl methyl phthalate (BMP) and DiBP exceeded ERL primarily in the sediment. Freshwater and saltwater species of fish, invertebrates, and algae frequently suffer from both acute and chronic effects caused by DMP, DEP, and DBP (Kaur et al., 2023).

The presence of PAEs was associated with adverse estrogenic effects on wildlife (Tran et al., 2022a). Similarly, soils contaminated with PAEs have serious negative effects on soil fauna and flora. Additionally, PAEs in soil can be absorbed by plants and accumulate in their tissues. This accumulation is highly likely to adversely affect the quality of crops.

Due to their widespread occurrence and toxicity, several countries, including China, Korea, the United States, and the European Union (EU), have imposed restrictions on PAEs. According to the USEPA, several PAEs, including DEHP, BBP, DMP, DEP, DBP, and DnOP, have been identified as priority hazardous pollutants. In Korea, PAEs (such as DBP, BBP, and DEHP) are severely restricted in products marketed to children, and the regulations have been broadened to include DiDP, DiNP, and DnOP in medical equipment and cosmetics (Lee et al., 2020). Currently, the EU has prohibited the use of DBP, BBP, DEHP, DiNP, and DiDP in childcare items and children's toys. Similar regulations and guidelines are also implemented in many countries, including Türkiye, Greece, Mexico, Sweden, Norway, Sweden, Argentina, Austria, Denmark, Finland, etc. (Huang et al., 2018). In the case of DEHP, medical devices represent a significant source of exposure for community health. As a result, the use of DEHP tubes has been prohibited in hospitals. In the legal regulations implemented by Türkiye as well as other countries, PAEs' use has been limited and the maximum usage limit has been determined as 0.1 % by weight of the plasticized materials (Tran et al., 2022a). Tolerable Daily Intake (TDI) was determined to be 50g/kg of body weight/day for the PAEs. Additionally, the regulation specifies specific migration limits for PAEs, including DEHP with ≤ 1.5 mg/kg), DBP with ≤ 0.3 mg/kg), BBP with ≤ 30 mg/kg), and DIDP + DINP with 9 mg/kg (SGS, 2020; Tran et al., 2022a). The European Food Safety Authority has also emphasized that a daily dose of 50 $\mu\text{g}/\text{kg}\cdot\text{day}$ of PAEs may result in testicular toxicity, and the USEPA's reference dose of 20 $\mu\text{g}/\text{kg}\cdot\text{day}$ is considered to pose a significant health risk (Serrano Se Fau-Braun et al., 2014).

The World Health Organization (WHO) and the EU have established regulations and guidelines for PAE concentrations in drinking water. For instance, the maximum allowable DEHP concentration in drinking water has been regulated by the WHO (8 $\mu\text{g/L}$), the United States (6 $\mu\text{g/L}$), New Zealand (10 $\mu\text{g/L}$), Australia (9 $\mu\text{g/L}$), and Japan (100 $\mu\text{g/L}$) (WHO, 2011; Yousefi et al., 2019; Tran et al., 2022a). However, there is no regulation regarding the presence of PAEs in drinking water in Turkey. Environmental quality standards (EQSs) based on yearly average concentrations have been established for various PAEs, ranging from 20 $\mu\text{g/L}$ (for DEHP) to 800 $\mu\text{g/L}$ (for DMP) in aquatic environments.

1.4. Occurrence of PAEs in the environment

Due to the fact that PAEs don't have any chemical bond with plastic matrix, they can distribute in environment during manufacturing, employ, treatment and then degrade slowly under natural conditions and accumulate in air, freshwater, sediment, soil, wastewater and sewage sludge throughout world over time (Pirsaheb et al., 2009; Rodgers et al., 2014; Wei et al., 2016; Gani et al., 2017; Yang et al., 2018). The concentration of various congeners of PAEs in many environmental compartments is shown in Table 1.2.

1.5. Removal of PAEs in the environment

PAEs scarcely undergo natural environmental degradation due to their highly recalcitrant nature. The removal of PAEs in the environment has been a key research focus. The removal of PAEs from the environment can be accomplished through a variety of abiotic methods such as physical, chemical, advanced oxidation processes, and a combination of these. However, these techniques have several drawbacks, including the creation of secondary sludge, high process cost, and severe operating conditions. Removal and degradation of PAEs by abiotic processes (non-biological) such as hydrolysis and photodecomposition has been reported to be slow and insignificant

(Pirsaheb and Zinatizadeh, 2009; Huang et al., 2013; Ahmadi et al., 2015). For instance, the half-life of BBP was more than 100 days with aqueous photolysis and the half-lives of DMP and DEHP with hydrolysis at neutral pH were approximately 3 and 2,000 years, respectively (Staples et al., 1997; Gao et al., 2016). Biodegradation is more advantageous for PAEs' degradation when compared to physicochemical methods. It is a fast, promising, cost-effective, and environmentally friendly method that results in innocuous end products (Pirsaheb and Zinatizadeh, 2009; Huang et al., 2013; Ahmadi et al., 2015). As a result of the extensive plastic waste disposed of in landfills, water bodies, and various environmental areas, many new microorganisms have evolved to survive in the presence of PAEs in the contaminated environment. These microorganisms can carry out either the complete or partial degradation process on their own or as part of a consortium (Benjamin et al., 2015; Tang et al., 2020). As shown in Figure 1.1, the biodegradation of PAEs involves two basic mechanisms: (i) transforming PAEs to phthalic acid (PA) (upstream steps) and (ii) utilization of PA (downstream steps). The upstream steps draw the attention of researchers since they are crucial to the breakdown of PAEs. The upstream steps involve two different types of reactions: (1) Shortening of side chains. This step involves converting phthalate diesters (PDEs) into phthalate monoesters (PMEs). Examples are the conversion of DBP to DEP (β -oxidation) or the transesterification of DEP into ethyl methyl phthalate and the conversion of DEP into DMP (demethylation) (Amir et al., 2005). Decreasing the size of side chains towards smaller ones reduces the steric effect of longer chains. The latter one is (2) hydrolysis of ester bond which PME converts to PA. This is the common step for aerobic and anaerobic degradation of PAEs. PA is an intermediate product in the degradation of PAEs. In downstream steps, PA could be further used through ring-cleavage reactions and the metabolic pathways of PA differ under anaerobic and aerobic process conditions (Ren et al., 2018). In aerobic degradation, PA is converted to protocatechuate. The conversion processes vary among different strains in the presence of 4,5-dihydroxyphthalate or 3-4-dihydroxyphthalate. The ring-cleavage of protocatechuate was mediated by intradiol ring-cleavage dioxygenases or extradiol ring-cleavage dioxygenases, resulting in the production of 3-carboxymuconic acid or 4-carboxyl-2-hydroxymuconic semialdehyde, respectively. 3-carboxymuconic acid was transformed into β -ketoadipate and subsequently entered the β -ketoadipate pathway. 4-carboxy-2-hydroxymuconic semialdehyde was metabolized into oxaloacetate and pyruvate. As for anaerobic degradation, PA is first converted into benzoic acid by the decarboxylation process and then to adipic acid by β -oxidation (Kaur et al., 2023). Within

Table 1.2. Concentration of PAEs in different media.

Media/ Location	Unit	DMP	DEP	DBP	DEHP	Reference
<u>Soil</u>						
Brickearth, UK	µg/kg	0.10	0.20-0.90	7.90-8	22.2-75.8	Gibson et. al., 2005
Urban area, China		0.07-31.58	0.07-100	0.15-2583.5	0.15-1350.2	Xia et al., 2011 Kong et al., 2012
Suburban area, China		2-101	2-114	7-185	26-4170	
<u>Sewage Sludge</u>						
STP Finland	mg/kg dry weight	-	-	-	180	Martinen et al., 2003
WWTP, Taiwan		-	-	718	41	Ma and Lin, 2011
WWTP, Türkiye		1.4-2.7	1.1-2.8	0.6-6.2	18-490	Cifci et al., 2013
<u>Sediment</u>						
River, South Africa	mg/kg	0.22-12.8	2.48-44.8	57.1	3660	Sibali et al., 2013
Lakes, China		21.50-133	2.4-20	10.2-1114	83.5-5775	Zheng et al., 2014
<u>Freshwater</u>						
Marina, Canada	µg/L	0.002-0.005	0.05-0.35	0.05-0.244	0.17-0.44	Mackintosh et al.,2006
River, South Africa		0.01-0.1	0.05-0.21	0.21-0.53	0.32-0.78	Teil et al., 2007
River, France		0.04-0.56	0.08-0.39	0.79-3.65	0.49-5.58	Sibali et al., 2013
<u>Drinking Water</u>						
Various cities, USA	µg/L	-	-	-	86	Wypych, 2004
Well, USA		-	4.6	-	-	
Supplies USA		-	-	0.1-470	-	
<u>Air</u>						
River, Canada	ng/m ³	-	3.8-6.6	4.5-8	156-458	Hoff and Chan, 1987
Apartment, Kindergarten, Germany		-	-	1083-1183		Fromme et al., 2004
Urban Area, France		0.5	10.7	-	18.9	Teil et al., 2006
Urban Center, China		10.1	3.4	58.8	20.3	Wang et al., 2008

this process, several intermediates were detected, including 1-cyclohexene-1-carboxylic acid and 2-hydroxycyclohexanecarboxylic acid (Ren et al., 2018).

In numerous studies, biodegradation of PAEs have been investigated under aerobic or anaerobic conditions in various environmental media such as water (Fang et al., 2017; Huang et al., 2020), soil (Chao and Cheng, 2007; Fan et al., 2018; Bai et al., 2020), sludge (Zeng et al., 2004; Chang et al., 2007), sediment (Chang et al., 2005), landfill (Boonyaroj et al., 2012), etc. Different bacterial strains have been isolated in the environment to conduct the degradation studies of PAEs. Some of these bacterial strains are *Achromobacter* sp. (Jin et al., 2015), *Acinetobacter* sp. (Fang et al., 2017) *Pseudomonas* sp. (Feng et al., 2002; Xu et al., 2008), *Bacillus* sp. (Quan et al. 2005; Huang et., 2019), *Sphingomonas* sp. (Chang et al., 2004), *Arthrobacter* sp. (Vega and Bastide, 2003; Chatterjee and Dutta, 2008), *Rhodococcus* (Nalli et al., 2006), *Variovorax* sp. (Prasad and Suresh, 2012). They use PAEs as food and energy sources. Biodegradation studies on PAE comprise not only the use of bacterial strain but also that of hydrolase enzymes secreted by these bacterial strains. Numerous studies have demonstrated that esterase is responsible for PAEs' degradation (Hernandez-Sanchez et al., 2019). In particular, the involvement of esterase as a key enzyme in PAEs' biodegradation has been reported. The esterase enzymes from *Bacillus* sp. (Niazi et al., 2001), *Delftia* sp. TBKNP-05 (Patil et al., 2006), *Sphingobium* sp. SM42 (Sungkeeree et al., 2016), *Acinetobacter* sp. (Fang et al., 2017), *Bacillus megaterium* (Feng et al., 2018), *Bacillus subtilis* (Balci et al., 2023) have high PAEs degradation efficiency.

The enzymes, highly versatile natural catalysts with high selectivity and activity, reduce the number of reaction steps, cannot be modified due to their interaction with the environment and can be used repeatedly. Enzymes are environment friendly as they are not a pollutant in the products formed at the end of the reaction, and lowering cost in the applications where it is used (Zhai et al., 2010; Datta et al., 2013; Pandey et al., 2017; Cinar et al., 2017; Zdarta et al., 2018). Therefore, they exhibit great potential in many environmental applications as well as industries ranging from food to drug (Zhai et al., 2010; Datta et al., 2013; Zdarta et al., 2018). However, enzyme applications are hampered by the fact that generally enzymes are relatively unstable, have a short catalytic lifetime, difficulties in recovery from the reaction mixture after use (Katchalski-Katzir et al., 1971; Nasliyan, 2012). These issues are being solved by enzyme immobilization (Zhai et al., 2010; Nasliyan, 2012; Brena et al., 2013). With immobilization, enzymes are physically or chemically bound to an insoluble matrix in the reaction and can be easily removed

from the medium at the end of the reaction (Zaborsky, 1973; Worsfold, 1995; Cinar et al., 2017).

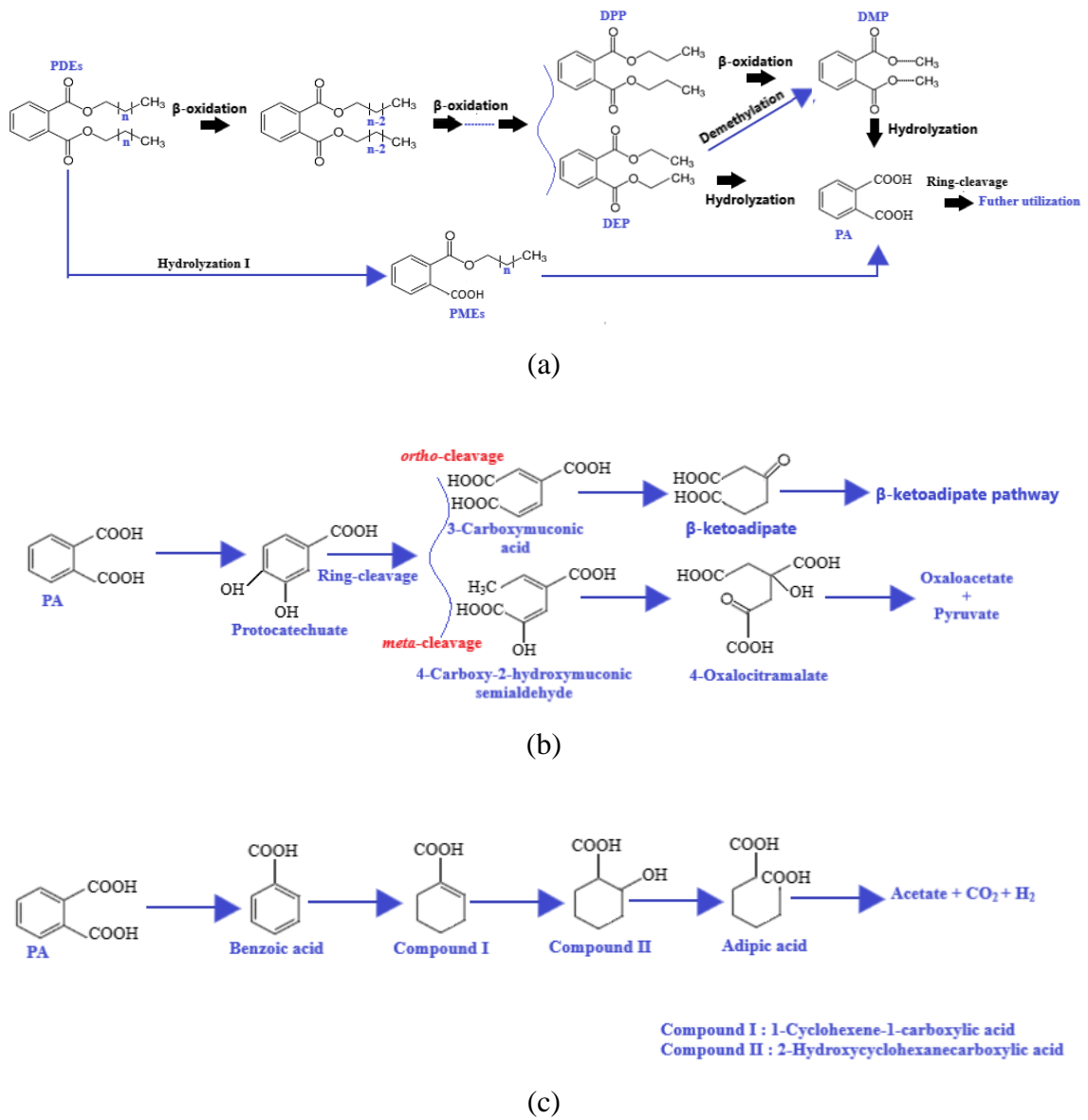


Figure 1.1. (a) Primary metabolic pathway of PAEs to PA. (b) Aerobic metabolic pathway of PA. (c) Anaerobic metabolic pathway of PA.

Immobilization increases the stability and half-life of the enzyme and maintains activity of the enzyme with increasing its resistance to changing environmental conditions such as pH and temperature. Furthermore, immobilization may increase the efficiency in many applications as it allows enzymes to be reused in the catalytic cycle (Nasliyan, 2012; Cinar et al., 2017; Zdarta et al., 2018). However, this efficiency depends on pH, technique

and duration of immobilization, surface curvature, and surface modification of support material (Guzik et al., 2014).

1.6. Immobilization

Generally, immobilization methods are classified under two main headings: physical and chemical methods. Physical methods include adsorption, encapsulation, and entrapment. Chemical methods include cross-linking, covalent and ionic binding (Twaig et al., 2017; Zdarta et al., 2018). Each of these methods has advantages and disadvantages in many applications (Nasliyan, 2012; Fernandez et al., 2013) It is especially important to protect the enzyme's active region and to know the enzyme's structure in the immobilization. Enzyme retention, enzyme stability, and cost of regeneration are very important factors in the selection of immobilization method. For instance, adsorption which is one of the simplest and economical method and no need of chemical use. Also, supports can be reused after their regeneration, in the case of inactivation of immobilized enzyme. Retention and stability of enzyme is high and enzyme leakage is low in the cross-linking method. Due to their mentioned properties, these two methods are particularly useful and preferable for immobilization compared to other methods (Nunes and Marty, 2006; Nasliyan, 2012). In immobilization, the choice of support material is very important. Distinctive immobilization method for each enzyme as well as universally defined support materials are not available. In the selection of the support material, the surface area and the particle size of the support, its hydrophobicity and hydrophilicity, its chemical, mechanical and thermal stability, its resistance to microbial attacks, and its economic value are crucial factors (Worsfold, 1995; Jesionowski et al., 2014). Support materials used for immobilization can be classified as organic and inorganic according to their chemical compositions (Brena et al., 2006; Nasliyan, 2012). Inorganic materials have high stability, resistance to microbial degradation and organic solvent and ease of reusability compared to organic materials (Zhai et al., 2010). Among these materials, natural minerals such as hydrotalcites, zeolites, and nanotubes (NT) are the most widely used support materials in immobilization. The zeolite and hydrotalcites are suitable for loading certain specific enzymes due to their pore diameters and surface areas being

limited. The access of large molecules to the microporous surface of the zeolite having a pore diameter in the range of 0.5 and 1.1 nm is limited. Despite these advantages of zeolites and other natural materials, nanotubes appear to be very attractive for enzyme immobilization due to their large pore diameter (especially in the adsorption method) (Zhai et al., 2010). Halloysite nanotubes (HNTs), are inorganic natural clay minerals with a large surface area, consist of two-layer aluminosilicates and has a length of between 400 and 1000 nm. They have negative outer surface containing silicon dioxide (SiO_2) with outer diameter between 50 and 70 nm, and positive inner surface containing aluminum hydroxide (AlOH_3) with a lumen diameter ranging between 15 and 20 nm (Tari et al., 1999; Chao et al., 2013). Maintaining of the counter-charged surfaces of HNTs between pH 3 and 10 constitutes a selectivity for the immobilization of the charged molecule (Kamble et al., 2012, Shutava et al., 2014). HNTs have a non-toxic, porous, and biocompatible structure compared to zeolite and other natural materials, and they are suitable materials since they are cheaper and easier to find than carbon nanotubes (Kamble et al., 2012, Yeniova-Erpek et al., 2015). Based on the mentioned information, HNTs have been selected support materials for immobilization of the enzyme in this study.

1.7. Research Objectives

PAEs are well-known for polluting the environment and their detrimental effects on the endocrine systems of both humans and animals. The main objective of this thesis is to investigate the degradation of two PAE congeners (DBP and DEHP) by obtaining an esterase enzyme from a thermophilic bacterium isolated from Balçova Geothermal Region in İzmir, Türkiye. To achieve the research objective, the following actions were taken:

- Expressing and purifying of esterase from *E.coli* strains that have esterase-producing gene of *Geobacillus* sp.
- Using the obtained recombinant esterase to degrade DBP and DEHP in water and soil.

- Comparing the PAE degradation abilities of commercial esterase/lipase obtained from various microorganisms with those of the recombinant enzyme.
- Overcoming the problem of short enzyme catalytic lifetime and low stability under changing environmental conditions, including pH and temperature fluctuations in the applications, through enzyme immobilization with adsorption and crosslinking method.

1.8. Thesis Overview

Each chapter of this thesis was written in article format and was described in detail below:

- Chapter 2: DBP-degrading abilities of lipase and esterase enzymes from various microorganisms were reported. The enzyme exhibiting the highest degradation performance was identified. By determining the optimal conditions, immobilization of this enzyme was carried out on a natural support material called HNTs. Immobilization efficiency and DBP degradation performance of the immobilized enzyme were then evaluated.
- Chapter 3: A novel bionanocomposite consisting of *Rhizomucor miehei* lipase immobilized on HNTs for the degradation treatment of specific PAE congeners (DBP and DEHP) was produced. After the enzyme immobilization, the changes in the secondary structure of the enzyme were clarified by using Circular Dichroism (CD) analysis.
- Chapter 4: To develop an environmentally friendly method for DBP and DEHP degradation, two bionanocomposites were prepared by immobilizing *Bacillus subtilis* esterase on HNTs supported with chitosan and alginate beads by the cross-linking method. Two fixed bed reactors filled with both bionanocomposites were operated in batch and continuous modes to degrade PAEs.

- d. Chapter 5: The recombinant esterase enzyme from *Geobacillus* sp. isolated from Izmir Balçova Geothermal area was expressed and purified to be used in the PAEs degradation study. DBP and DEHP degradation ability of the recombinant esterase was investigated.
- e. Chapter 6: Soil samples with different characteristic features were collected from the Urla district in Izmir to investigate the presence of DBP and DEHP in the soils. DBP and DEHP degrading performance of recombinant esterase and *Bacillus subtilis* esterase in soil was evaluated.

1.9. Significance and Impact

The development of environmentally friendly alternatives to eliminate PAEs pollution is of great importance. Enzymatic degradation is vital in eliminating PAEs from contaminated sites, providing benefits such as high efficiency, cost-effectiveness, and environmental safety. It is known that hydrolase enzymes have a major role in initiating the first step of breaking down the ester bond of PAEs. In this thesis, commercial and recombinant esterase enzymes were examined in free and immobilized forms. Their congener-specific behavior, enzyme dynamics, and ability to degrade short- and long-chain PAEs in water and soil were investigated. The findings of this study could provide a fundamental framework for utilizing immobilized enzymes on HNTs across various environmental compartments to facilitate the degradation of PAEs. Moreover, it opens up opportunities for diverse applications of immobilized enzymes, including environmental treatment, food, pharmaceutical, industrial sectors, and so on.

CHAPTER 2

IMMOBILIZATION OF ESTERASE FROM *BACILLUS SUBTILIS* ON HALLOYSITE NANOTUBES AND APPLICATIONS ON DIBUTYL PHTHALATE DEGRADATION

2.1. Introduction

Over the past few decades, the number of synthetic chemicals found in pharmaceutical and manufacturing additives as well as metal, personal and household care products has increased to supply the needs of modern society. The production volume of phthalic acid esters (PAEs) is over 8 million metric tons per year in the world (Seyoum and Pradhan, 2019; Balci et al., 2022). PAEs are ubiquitous and recalcitrant compounds that can be released into the environment during their manufacturing and use. Thus, they are degraded slowly under natural conditions and accumulate in the air, surface water, wastewater, sediment, and soil over time (Scholz et al., 1997; Pirsahab and Zinatizadeh, 2009; Kong et al., 2018; Baloyi et al., 2021). Most PAEs can easily migrate to various water bodies and then enter a variety of aquatic organisms (Cao et al., 2018; Huang et al., 2021) and being accumulated in the food chain and cause health problems such as chronic health effects, cancer risks, and endocrine disruption. Additionally, they have significant adverse impacts on mammalian reproduction, development, and the nervous system (Wang et al., 2023). Among the various types of PAEs, dimethyl phthalate (DMP), diethyl phthalate (DEP), dibutyl phthalate (DBP), butyl benzyl phthalate (BBP), di-n-octyl phthalate (DnOP), diethylhexyl phthalate (DEHP) have been categorized as priority pollutants by The United States Environmental Protection Agency

This chapter has been published as:

Balci, E., Rosales, E., Pazos, M., Sofuoglu, A., Sanroman, M.A. 2023. Immobilization of esterase from *Bacillus subtilis* on Halloysite nanotubes and applications on dibutyl phthalate degradation. *Environmental Technology & Innovation*, 30, 103113.

(USEPA) and its counterparts in European Union countries.

Different available methods include photolysis and hydrolysis; however, biodegradation is considered safer, cleaner, and more environmentally friendly. Recently, there has been a significant increase in the use of enzymes in various industries such as biomedicine, food, and energy. The enzymes have a vital role in protecting the environment (Moreira et al., 2020; Bilal et al., 2022). Hydrolase enzymes such as esterase and lipase are highly effective on the ester bonds in the structure of PAEs (Sharma et al., 2019). There are several studies demonstrating that esterase from *Bacillus* sp. and lipase from *Candida cylindracea*, *Pseudomonas* sp. V21b and *Comamonas* sp. 51F exhibit the ability to degrade PAEs (Tanaka et al., 2000; Ding et al., 2015; Sungkeeree et al., 2017; Kumar et al., 2017). However, enzymes are relatively unstable losing their structural stability for the duration of any reaction and, thus, having a short catalytic lifetime (Brena et al., 2013; Sharma et al., 2021; Souza et al., 2022). The generation of a composite by immobilization of the enzyme enhances the kinetic and biochemical properties of enzymes enabling enzyme recycling and reuse and reducing its inhibition (Zhai et al., 2010; Monteiro et al., 2019; Cavalcante et al., 2021; Bilal et al., 2022). Adsorption is one of the simplest and most economical immobilization methods not requiring the use of chemicals and the generated composite can be reused multiple times (Sassolas et al., 2012). The choice of adequate support material is crucial, and several alternatives have been proposed in the literature, including the most expensive activated carbon and nanoparticles or cheaper natural minerals (Kamble et al., 2012; Yeniova-Erpek et al., 2015). Among the natural minerals with high abundance (zeolite, hydrotalcite, or nanotubes), only zeolite and hydrotalcite are suitable for loading certain specific enzymes due to their limited pore diameters and surface areas. Materials with nano-scale structures can greatly enhance the active surface available for enzyme adsorption (Zhao et al., 2017). Halloysite nanotubes (HNTs) have a non-toxic, porous, and biocompatible structure being suitable materials for the composite. In comparison with other nano-scale materials, they are easily obtainable and much more cost-effective than carbon nanotubes (CNTs) (Zhai et al., 2010). Besides, materials with HNTs have high mechanical strength compared to those with kaolinites (Gass et al., 2015). HNTs are inorganic natural clay minerals with a large surface area consisting of two-layer aluminosilicates and have a length of between 400 and 1,000 nm. They have a negative outer surface containing silicon dioxide (SiO₂) with an outer diameter between 50 and 100 nm, and a positive inner surface of aluminum hydroxide (Al(OH)₃) with a lumen diameter ranging between 15 and 20 nm (Tari et al.,

1999; Yeniova-Erpek et al., 2015). The maintenance of the counter-charged surfaces of HNTs between pH 3 and 10 constitutes a selectivity for the immobilization of the charged molecule (Kamble et al., 2012). Besides, the most obvious difference between HNTs and other aluminosilicate minerals is that HNTs have a unique nanotubular structure and biocompatibility (Ferrari et al., 2017). Due to all these properties, HNTs appear to be a very attractive matrix for the immobilization of various molecules such as drugs, antiseptics, corrosion inhibitors, and proteins (Abdullayev et al., 2009; Patel et al., 2016; Tully et al., 2016; Rao et al., 2018). Immobilization on HNTs improves enzyme stability, activity, selectivity, and specificity, and prevents enzyme inhibition, thus making enzymes reusable in continuous reactors.

Central composite design (CCD) is a statistical experimental design technique used to optimize and model a response variable, typically in the context of engineering, chemistry, or other scientific fields. It enables the investigation of the covariance of variables (independent factors) to achieve the optimal response (dependent factor) with a minimal number of experiments (Monteiro et al., 2019). In this context, CCD of the response surface methodology (RSM) was applied to determine the optimum values of process variables for the immobilization of the enzyme to HNTs in this study.

So far, a few studies have focused on the degradation of PAEs in the presence of a hydrolase enzyme in the literature. However, there are no studies on the immobilization of a hydrolase enzyme obtained from bacteria on HNTs and its subsequent use in the degradation of PAEs. In this sense, the study may form the basis for the use of the immobilized enzyme to HNTs in various environmental compartments for the degradation of PAEs. Furthermore, the potential uses of the immobilized enzyme (environmental treatment, food, pharmaceutical, industrial sectors, etc.) may expand.

In the present study, firstly, the ability of commercial lipase and esterase enzymes to degrade DBP, which is one of the most widely used and produced PAEs, was investigated. The enzyme exhibiting the highest DBP degrading ability was immobilized onto HNTs generating a composite. Then, the optimal conditions for the immobilization were determined by CCD. Next, the biocompatibility between the enzyme and HNTs in the composite was investigated and used to treat DBP. Finally, the generation of DBP metabolites and the reuse of the composite were investigated.

2.2. Material and Method

2.2.1. Materials

Pure halloysite (HNT) powder was provided by Esan, Eczacibasi Industrial Raw Materials Company (Istanbul, Turkey). Esterase enzymes (esterase from *Bacillus subtilis* (EC 3.1.1.1; ≥ 10 U/mg) and *Bacillus stearothermophilus* (EC 3.1.1.1; ≥ 0.2 U/mg)) were obtained from Sigma-Aldrich and lipase enzymes (lipozyme CALB from *Candida Antarctica B.* (EC 3.1.1.3; 5,000 LU/g), lipozyme TL 100 L from *Thermomyces lanuginosus* (EC 3.1.1.3; 100 KLU/g), and palatase 20,000 L from *Rhizomucor miehei* (EC 3.1.1.3; 20,000 LU/g)) were purchased from Novozymes (Denmark). Bovine serum albumin (BSA, >99%), DBP (99%), Methanol (99.8% ACS reagent), Tween-80 and p-nitrophenyl acetate (pNPC-2, esterase substrate >98%) were purchased from Sigma-Aldrich. Other chemicals were of laboratory reagent grade and used without any further purification.

2.2.2. DBP degradation in the presence of free enzymes

To investigate the DBP degrading ability of free enzymes, a DBP solution (1,000 mg/L) was prepared in methanol. To increase the solubility of DBP in the solution, Tween-80 was used as a solubilizing agent. The reaction mixture (1 mL) consisted of 0.1 mL of the free enzyme (1 mg/mL), 0.1 mL of 1,000 mg/L DBP in methanol, 0.1 mL of Tween-80 (1%, v/v), and 0.7 mL of phosphate buffer (0.1 M, pH 7). The reaction mixture was incubated for 15 min under optimum conditions determined by the manufacturers. After incubation of the reaction mixtures for an interval of a specific time, the samples were collected. 1 N HCl was added to the collected samples at a rate of 10% (v/v) to stop the enzymatic reaction (Saito et al., 2010). All samples were filtered through a 0.22 μ m PTFE syringe filter to remove particles prior to HPLC analysis.

2.2.3. Enzyme immobilization on HNT and optimization

2.2.3.1. HNT-enzyme composite

The enzyme immobilization by adsorption was conducted with minor modifications to the study of Wang et al. (2015a). Firstly, an enzymatic solution (1 mg/mL) in which the selected enzyme was dissolved in sodium phosphate buffer (0.1 M, pH 7) and stirred well was prepared. Next, 1 mL of this solution was added to the HNTs with an Enzyme/HNTs (E/H) ratio of 0.2. The obtained suspensions were vortexed for 5 min and stirred at 150 rpm in an incubator shaker for 195 min. Then, the Enzyme-HNTs were sonicated for 30 min to eliminate the agglomeration of HNTs. They were centrifuged at 8,000 rpm for 10 min. The supernatant phase was collected and then the HNT pellets with enzyme were washed twice with the buffer (1 mL) to remove excess protein/unbounded enzyme. Following this, the supernatant and washing solutions were stored at 4 °C for the activity measurement and determination of protein concentration.

2.2.3.2. Optimization of the parameters for the immobilization procedure

The optimization of the parameters affecting the enzyme immobilization was carried out using the RSM and more specifically, a central composite design face-centered (CCDFC) was selected for this purpose. This design was developed using the Design-Expert software 8.00 (Stat-Ease Inc., Minneapolis, USA) to explore the impact of the selected independent variables on the immobilization process (pH, adsorption time, E/H ratio, and temperature). These variables were labeled as X_1 , X_2 , X_3 , and X_4 , respectively. The adsorption efficiency (%) and the specific enzyme activity (U/mg) were taken as responses Y_1 and Y_2 , respectively. A CCDFC design 2^4 (2-levels-4 factors) was used to determine the optimum conditions of the variables considering the following ranges: pH (5–7), adsorption time (30–360 min), E/H ratio (0.02–0.2 mg enzyme/mg HNT), and

temperature (20–40 °C). In the CCDFC, the number of experimental tests (N=30) was calculated using Eq. (2.1) with 2^n factorial runs, n axial runs, and n_C central points.

$$N = 2^n + 2n + n_C \quad (2.1)$$

The statistical analysis of the model was carried out using analysis of variance (ANOVA) with Design Expert® 8.0.0 software. This analysis included the Fisher's F test (overall model significance), its associated probability values, and the coefficient of determination R^2 which measures the goodness of fit of the regression model (Rosales et al., 2012). The responses were expressed using a quadratic polynomial regression model to describe the correlation between responses and independent variables. The model Eq. (2.2) is as follows:

$$Y = \beta_0 + \sum_{i=1}^n \beta_i X_i + \sum_{i=1}^n \beta_{ii} X_i^2 + \sum_{i=1}^n \sum_{j=1}^n \beta_{ij} X_i X_j + \varepsilon \quad (2.2)$$

where Y represents the response of dependent variables; X_i and X_j are the independent variables; β_0 , β_i , β_{ii} , and β_{ij} are the mathematical model constants, the linearity coefficient of i factor, the quadratic coefficient of i factor, and the interaction coefficient between factors (i and j), respectively; ε is an experimental uncertainty (error) that indicates the various sources variability.

2.2.4. Characterization analysis

Before and after the adsorption experiments, numerous analyses were conducted to determine both the structure and the structural changes in raw HNTs and HNT-enzyme composite. Before the characterization analysis, raw HNTs and HNT-enzyme composite

were dried in a vacuum oven at 100 °C and 45 °C, respectively to eliminate their moisture content.

2.2.4.1. Structural characterization of the composite

The microstructure of HNTs was examined using an FEI QUANTA 250 FEG scanning electron microscopy (SEM) instrument-equipped secondary detector. To observe detailed surface characteristics of HNTs and HNT-enzyme composite, the analysis of transmission electron microscopy (TEM) was performed on MICRO JEOL JEM 1010 at 200 kV (Service of Electronic Microscopy, C.A.C.T.I., University of Vigo, Vigo, Spain). To determine the crystal structure of the HNTs, x-ray diffraction analysis (XRD) was carried out at $2\Theta=3-80^\circ$ using the Philips Xpert Pro XRD analyzer at a scanning rate of 0.02°/min.

2.2.4.2. Nanotextural and chemical characterization of the composite

The nanotextural and chemical characterization was performed by Brunner-Emmet-Teller (BET) analysis, Fourier transform infrared spectroscopy (FT-IR), and thermogravimetric analysis (TGA). BET was performed using Mikromeritics TriStar II Plus 3.00 to determine the surface area and micropore size distribution of HNTs and HNT-enzyme composite. FT-IR analysis was done using JASCO FT-IR 4100 (Jasco Inc., Easton, MD, USA) equipped with an attenuated total reflectance (ATR) accessory to examine functional groups in HNTs and HNT-enzyme composite between 4000 and 400 cm^{-1} . The samples were mixed with potassium bromide and pelletized. TGA was carried out using a Seteram thermogravimetric analyzer with a temperature range that started at room temperature and ended at 800°C at a heating rate of 10°C/min under 20 mL/min N_2 atmosphere to record the weight change and to indicate the thermal stability and heat resistance of the HNTs and HNT-enzyme composite.

2.2.5. Degradation studies in presence of the HNT-enzyme composite

In degradation experiments conducted using immobilized enzyme, HNT-enzyme composite (5 mg) was taken in a glass tube. Then, the reaction mixture containing 0.1 mL of DBP (1,000 mg/L), 0.1 mL Tween-80 (1%, v/v) solution, and 0.8 mL of phosphate buffer (0.1 M, pH 7) was added to the glass tube. During 1h-periods, the samples were put into an incubator shaker to degrade 100 mg/L DBP. At the end of each cycle consisting of 1h-periods, the samples were collected. They were vortexed for 30 seconds and centrifuged at 5,000 rpm for 10 min. After centrifugation, the supernatant phase was collected, and 1 N HCl was added to the supernatant at a rate of 10% (v/v) to stop the enzymatic reaction. Then, the supernatant was filtered through a 0.22 μ m PTFE syringe filter to remove particulate material from the samples. It was stored at 4°C for further analysis. At the end of each cycle, the pellet phase with the enzyme was fed with the reaction mixture. The relative activity was calculated after each catalytic cycle according to equation (2.3). The first measured activity of the immobilized enzyme was assumed to be 100% (He et al., 2015).

$$\text{Relative activity (\%)} = \frac{\text{Activity at the end of nth cycle}}{\text{Activity at the end of 1st cycle}} \times 100 \quad (2.3)$$

2.2.6. Analytical procedures

2.2.6.1. Determination of the enzyme activity and protein concentration

The enzyme activity was determined by hydrolysis of pNPC-2 according to Tekedar and Sanli-Mohamed (2011). The assay mixture (1 mL) consisted of 0.8 mL phosphate buffer (0.1 M, pH 7), 0.1 mL of 0.5 mM pNPC-2 dissolved in acetonitrile, and 0.1 mL of enzyme solution (1 mg/mL). This solution was incubated at optimum temperature for 5 min and then used to determine the catalytic activity. The absorbance was

spectrophotometrically measured at 400 nm. After the measurement of the absorbance, the activity calculation will be made according to the following equation (2.4).

$$\text{Enzyme activity (U/L)} = \frac{(\text{Absorbance at 400 nm/min}) \cdot (V_t) \cdot (DF)}{(\epsilon) \cdot (V_e) \cdot (d)} \quad (2.4)$$

where V_t : Test volume (mL), DF : Dilution factor, ϵ : molar extinction coefficient of 4-nitrophenol at 400 nm, V_e : Volume of enzyme used (mL), d : Lightpath (1 cm).

One unit (U) of activity is defined as the amount of enzyme releasing 1.0 μmol of 4-nitrophenol per minute at pH 7, optimum temperature, and using pNPC-2 as a substrate. The molar extinction coefficient of 4-nitrophenol in the buffer system is 17,215 $\text{M}^{-1} \cdot \text{cm}^{-1}$.

The protein concentration of the initial enzyme solution, supernatant, and washing solution was determined according to Bradford Method (Bradford, 1976). The amount of adsorbed enzyme was calculated based on a mass balance. Adsorption efficiency ((Ads. ef. (%)) and enzyme loading amount (Load. Amt. (mg/mg)) were calculated based on the quantity of unadsorbed protein according to the following equations (2.5-2.6):

$$\text{Ads. ef.} = \frac{\text{protein amount} - (\text{protein amount in the supernatant} + \text{washing solution})}{\text{Initial protein amount}} \times 100 \quad (2.5)$$

$$\text{Load. amt.} = \frac{\text{Initial protein amount} - (\text{protein amount in the supernatant} + \text{washing solution})}{\text{mass of HNT}} \quad (2.6)$$

2.2.6.2. Enzyme stability and reusability tests

Enzyme stabilization is a key objective of enzyme immobilization, as it enables the preservation of enzyme activity against changing conditions and allows for enzyme reuse in multiple reaction cycles (Cruz-Ortiz et al., 2011).

To perform the thermal stability tests, free esterase and HNT-enzyme composite were incubated in phosphate buffer (0.1 M, pH=7) at various temperatures ranging from 20 to 70°C. Following incubation, the samples were collected. After cooling, the activity was measured in the presence of 0.5 mM pNPC-2 substrate.

For the storage stability tests, both free esterase and the HNT-enzyme composite were stored for 7 days. Aliquots were taken for a predetermined period of time to measure the enzyme activity using 0.5 mM pNPC-2 substrate.

The enzyme activity of the HNT-enzyme composite was measured to determine the reusability of the composite. The same sample was used repeatedly for 7 cycles of enzyme catalysis. In each cycle, the sample was incubated with 0.5 mM pNPC-2 dissolved in acetonitrile for 5 min at 30°C. After incubation, the supernatant was separated to measure the enzyme activity. The difference between the enzyme activity of the sample before incubation and that of the supernatant after incubation was calculated for each cycle. The remaining activity was expressed as relative activity (%).

2.2.6.3. Determination of kinetic parameters

The kinetic parameters, including V_{max} and K_m , of both free esterase and HNT-enzyme composite, were determined by measuring enzyme activity at various concentrations of pNPC-2 (0-50 mg/L). The Lineweaver-Burk plots were used to estimate the kinetic parameters.

2.2.6.4. Analysis of DBP and its metabolites

DBP concentrations were determined under a reversed-phase using an Agilent 1260 Infinity series HPLC-DAD equipped with a column ZORBAX Eclipse XDB C-8 column (5 μ m particle size, 150 mm x 4.6 mm i.d.). The mobile phase consisting of acetonitrile:water (60:40, v/v) was used at a flow rate of 1 mL/min. For each injection,

the volume taken from samples was 20 μ L. The analysis was carried out together with a UV detector (224 nm) at room temperature.

DBP metabolites were identified using a trapped ion-mobility spectrometry time-of-flight mass spectrometer (TIMS-TOF-MS) (Bruker Daltonics, Bremen Germany). Ionization was performed using an electrospray (ES) source with a voltage of 3.5 kV applied to the needle and an endplate offset of 500 V. Using both positive and negative scan modes, ES spectral data was obtained. Data was acquired using Bruker Otof Control Software version 5.1 and processed with the Data analysis software version 5.1 from Bruker Daltonics.

2.3. Results and Discussion

2.3.1. Determination of the most suitable enzyme for DBP degradation

Before enzymatic degradation experiments, the optimal temperature for each enzyme was evaluated based on the optimum conditions determined by the manufacturers (Figure B.1a.). The results confirmed the optimal conditions specified by the manufacturers. The degradation experiments by free enzymes were performed under optimum conditions for each enzyme (Figure B.1b.). Esterase from *Bacillus subtilis* degraded 100% of DBP at 30°C within 15 min, however, esterase from *Bacillus stearothermophilus* was able to degrade 3.7 \pm 0.9% of DBP at 60°C at the same time. As for degradation experiments conducted using lipase enzymes for 15 min, whereas Lipozyme CALB and Lipozyme TL 100 degraded 17.6 \pm 1.17% and 35.2 \pm 0.2% of DBP at 50°C, respectively, palatase degraded 95.2 \pm 0.7% of DBP at 40°C.

The esterase from *Bacillus subtilis* exhibited the best result with the highest DBP degradation efficiency (100%) in a short time. According to equation (4), the activity of free esterase was determined to be 521.2 U/L at 30 °C. In the literature, there are various studies on the effective use of esterase for the degradation of most PAEs. Saito et al. (2010) investigated the ability of bovine pancreatic cholesterol esterase (CEase) to degrade DBP, DEP, di-n-propyl phthalate (DprP), di-n-pentyl phthalate (DpeP), dihexyl

phthalate (DHP), and DEHP. They found that CEase completely degraded all PAEs (5 μmol) within 15 min. Zhang et al. (2014) investigated the degradation of 10 μmol PAEs (DEP, DPrP, DBP, DPeP, DHP, DEHP, dicyclohexyl phthalate (DCHP), and BBP) using esterase obtained from *Sulfobacillus acidophilus*. They reported that the esterase has a high degradation rate on PAEs with short alkyl side chains, especially DBP. While the esterase was able to degrade 35% to 82% of PAEs (10 mM) within 2 min, it degraded all PAEs within 24 h. Esterase from *Bacillus* sp. K91 was reported to degrade 100% of diisobutyl phthalate (DiBP) (10 mM) over a long duration of time (Ding et al., 2015). Similar to the results of the aforementioned studies, esterase from *Bacillus subtilis* displayed a high ability to degrade DBP in this study. Therefore, this study focused on the immobilization of esterase obtained from *Bacillus subtilis* as the major enzyme responsible for DBP degradation.

2.3.2. Esterase Immobilization

The increase of the enzyme activity and stability and also facilitating the recovery and reuse of the enzyme is a matter of interest and the immobilization of enzymes is a tool commonly applied to fulfill these objectives. In this study, enzyme immobilization was performed by physical adsorption on a nanoclay support (HNTs).

Initially, the enzyme immobilization was studied considering an adsorption time of 360 min, pH 7, E/H 0.02, and temperature of 20°C, and the results demonstrated that the immobilized enzyme had significant activity and adsorption efficiency. The loading efficiency and specific enzyme activity are different depending on several variables such as pH, adsorption time and temperature, and E/H ratio. Thus, the study of the influence of the selected variables on enzyme adsorption during the immobilization process was then tackled with both composite adsorption efficiency and the activity as the responses (Table B.1.).

2.3.2.1. HNT-enzyme composite adsorption efficiency

The response surface analysis by ANOVA was performed (Table B.2.) and the constructed regression model was determined to be significant ($p < 0.05$). Besides, the model F-value was found to be 63.14, and this large F-value related to the p-value showed that the experiment can be modeled with less error (Sadukhan et al., 2016). All the considered variables, the interaction terms between X_1 and X_4 , X_3 and X_4 , and the quadratic terms of the X_1 , and X_4 were significant for the esterase adsorption efficiency. The final model equation (2.7) avoiding the insignificant terms led to a reduction in the equation representing the relationship between the independent variables and the efficiency of enzyme adsorption as follows:

$$Y_1 = 86.06 - 16.11 X_1 + 3.45 X_2 + 2.17 X_3 - 8.70 X_4 - 9.27 X_1 X_4 + 4.75 X_3 X_4 - 8.39 X_1^2 - 21.82 X_4^2 \quad (2.7)$$

Among them, X_2 , and X_3 , an interaction term between X_3 and X_4 exhibited a positive effect on the efficiency of enzyme adsorption. However, X_1 , X_4 , the interaction term between X_1 and X_4 , and the quadratic terms of X_1 and X_4 showed a negative effect on the adsorption efficiency of esterase. To evaluate the quality of curve fitting, the coefficient of determination (R^2) and the adjusted coefficient of determination ($\text{Adj-}R^2$) was found to be 0.98 and 0.96, respectively. These values showed that the model has a high capability to predict the responses. Furthermore, the predicted R^2 ($\text{Pred-}R^2$) of 0.90 was in reasonable agreement with the $\text{Adj-}R^2$. Adequate Precision (Adeq. Precision) is known to be a test that measures the signal-to-noise ratio (Dritsa et al., 2009). This ratio is used to compare the range of the predicted values at design points to the average of the prediction error. If the ratio is higher than 4, it is considered acceptable. For the adsorption efficiency, it was found to be 28.06. This also can be concluded in the model is significant. The value associated with the Adeq. Precision suggests that obtained model can be used to navigate the design space. The coefficient of variance (C.V.) of 5.29% indicated that the experiment had a very high precision and good reliability. The 3D response surface

and 2D contour plots showing the effect of some independent parameters on the enzyme adsorption efficiency are given in Figure 2.1.

As can be seen in Figures. 2.1a and 2.1b, the maximum adsorption efficiency (95.4%) was obtained when the adsorption time and the E/H ratio were at 360 min and 0.2 mg/mg with temperature and pH considered in the middle points, respectively. The adsorption efficiency improved with the increase in the E/H ratio and the prolonged adsorption time. The adsorption efficiency tends to increase along with the rise in the amount of adsorbent and enzyme (Wang et al., 2015a; Mohammadi et al., 2020). Wang et al. (2015a) observed a decrease in adsorption efficiency when the E/H ratio was reduced by two-fold. Ilgu et al. (2011) reported that there was almost no change in the immobilization efficiency of the enzyme when the amount of their support material was increased from 1.5 to 3 mg. Similarly, increasing the amount of HNTs did not make a significant difference in the adsorption efficiency in this study. This may be because a low amount of HNTs is sufficient for the adsorption of a low amount of the enzyme. Moreover, a high E/H ratio should be chosen to minimize oversaturated HNTs which can cause inappropriate and non-specific chemical adsorption (Wang et al., 2015a).

In Figures. 2.1c and 2.1d, the maximum adsorption efficiency was determined at the center points where the temperature was 30°C and the pH was 6. While the pH value did not have a significant effect on the adsorption efficiency, the temperature had a positive effect on the adsorption efficiency up to a certain temperature and then the efficiency began to decrease with the increase in the temperature. This may be due to the weakening of electrostatic interactions between enzyme and support at high temperatures (You et al., 2015). Twaig et al. (2017) reported that the amount of active sites on the surface of HNTs increases with increasing temperature and adsorption efficiency hereby increases. They observed a decrease in the adsorption capacity over 35°C and suggested that this decrease may be related to the conformational change on the enzyme surface or distortion of the HNT structure. Based on this information, it may be more appropriate to set the adsorption temperature below 40°C for enzyme immobilization.

2.3.2.2. HNT-enzyme composite specific activity

The analysis by ANOVA of the results attained in the design of experiments concerning this response showed that the model is significant (p-value <0.05 and F value 1254.63) (Table B.3). The specific activity of esterase was significant (p<0.05) and model equation (2.8) with the significant terms was given as follows:

$$Y_2 = 7.27 + 13.79 X_1 + 0.45 X_2 + 1.74 X_4 - 0.50 X_1X_3 + 1.19 X_1X_4 + 0.55 X_2X_4 + 0.25 X_3X_4 + 9.16 X_1^2 \quad (2.8)$$

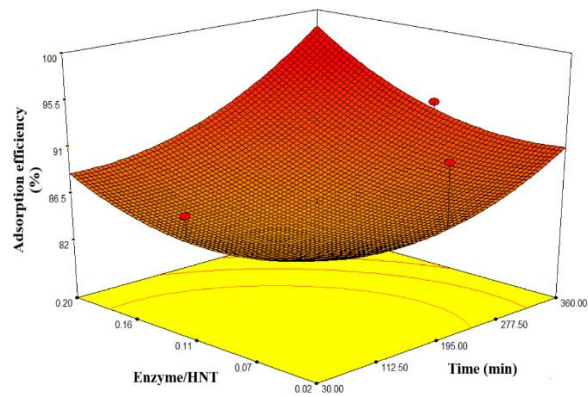
X_1 , X_2 , and X_4 , the interaction terms between X_1 and X_3 , X_1 and X_4 , X_2 and X_4 , X_3 and X_4 , the quadratic term of X_1 played a significantly important role in the specific enzyme activity. The interaction term between X_1 and X_3 displayed a negative effect on the specific enzyme activity. X_1 was the most significant factor affecting the specific enzymatic activity (F=14842.97). Both the R^2 and the Adj- R^2 were found to be 0.99. These results indicated a great connection between the predicted values and the actual values obtained as a result of the experiment. Besides, the Pred- R^2 was determined to be 0.99. It was in reasonable agreement with the value of the Adj- R^2 . The F-value of the model with 1254.63 implied that the model was significant. The Adeq. Precision value was obtained as 90.79. This value indicated the constructed model was usable for navigating the design space. The C.V. (3.80%), which had a very low value, showed a very high degree of precision and good reliability of the experiment. The 3D response surface and 2D contour plots showing the interaction of the model-independent parameters on the specific enzyme activity are given in Figure 2.2. As shown in Figures 2.2a and 2.2b, the highest specific enzyme activity was achieved when the E/H ratio and the adsorption time were 0.2 mg/mg and 360 min, respectively. With a rise in the E/H ratio and adsorption time, the enzyme-specific activity increased. However, the E/H ratio and the adsorption time had no significant effect on the enzyme-specific activity in this study. Wang et al (2015a) reported that the amount of loaded enzyme and enzyme activity increased when the incubation time was prolonged and then they reached an equilibrium.

In this study, enzyme activity decreased with the high amount of HNTs (Low E/H) and increased with the high amount of enzyme (high E/H) and then it plateaued. Wang et al. (2010) studied laccase immobilization on silica nanoparticles and reported a similar trend for the laccase enzyme. Mohammadi et al. (2020) investigated the effects of the amount of HNTs and enzyme on specific enzyme activity. They reported that enzyme activity decreased at a high amount of HNTs and enzyme. Besides, Wang et al. (2015a) reported that the amount of adsorbed lipase enzyme and enzyme activity increased with the increase in the enzyme concentration and then reached a plateau. Lee et al. (2009) adsorbed a commercial porcine pancreas lipase on the surface of modified nano-sized magnetite particles and observed that increased lipase concentration had an optimum concentration because more than optimum value caused a decrease in specific enzyme activity due to protein-protein interaction hindrance (Jiang et al., 2009).

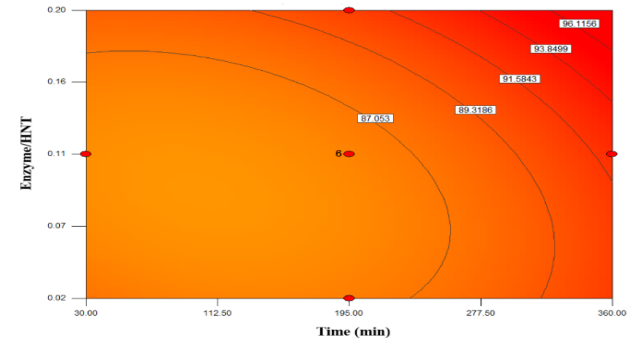
As seen in Figures 2.2c and 2.2d, the pH and adsorption temperature at which the enzyme has the highest specific activity were determined to be 7 and 40°C, respectively. The specific enzyme activity increased when pH and adsorption temperature rose and then reached a plateau in this study. Generally, the temperature has a positive effect on the enzyme activity up to a certain temperature and then the activity begins to decrease as the temperature increases (Osho et al., 2016).

2.3.2.3. Optimization of the conditions for the enzyme immobilization

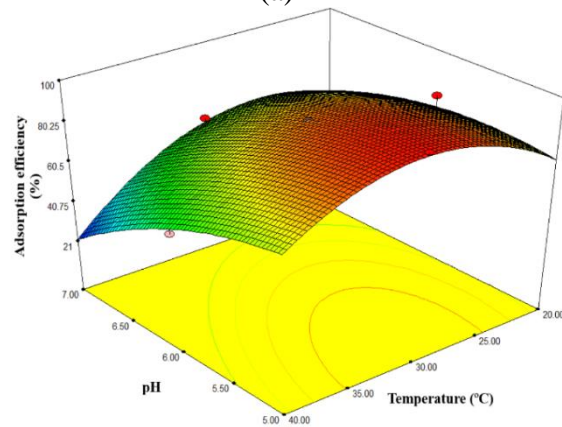
Based on the obtained results, the optimization of the variables was carried out considering simultaneously both responses studied. To maximize both responses, Design Expert 8 software was used. The optimum conditions for esterase immobilization were determined to be the pH of 7, the adsorption time of 360 min, the E/H ratio of 0.2 and the adsorption temperature of 30°C, and the adsorption efficiency and the specific enzyme activity predicted with the model were 73.15% and 29.05 U/mg, respectively, with a desirability value of 0.796. After immobilization, the relative activity of the esterase was determined to be 82.7%. These results were validated experimentally, and the attained results were quite similar to the predicted (71.86%, 28.5 U/mg). Under the optimal conditions, the loaded amount of enzyme on HNTs was determined to be 1.922 mg/mg.



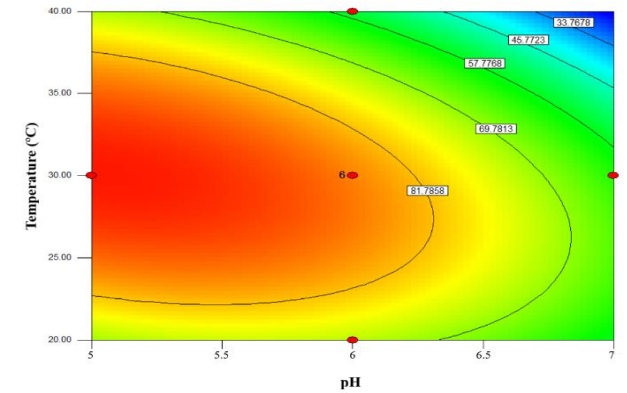
(a)



(b)

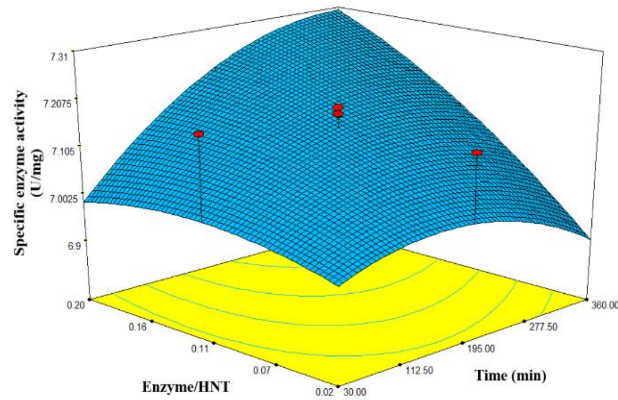


(c)

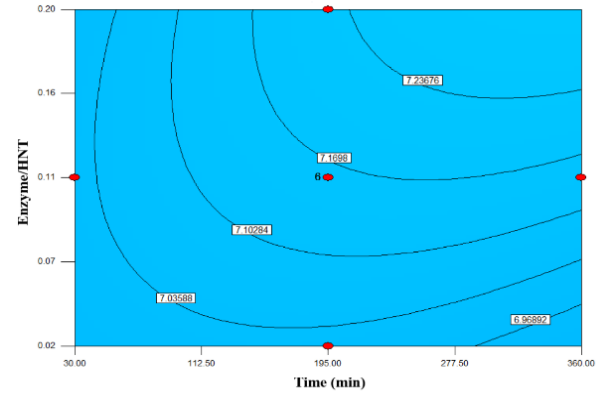


(d)

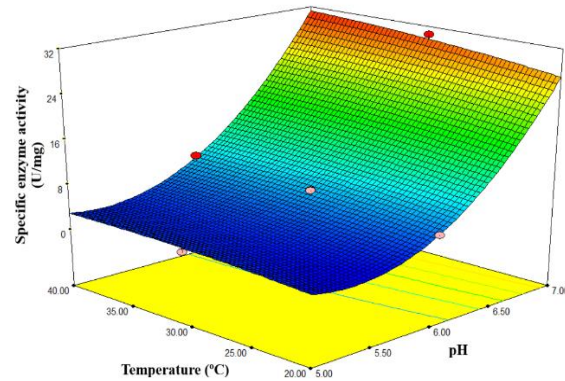
Figure 2.1. 3D response surface and 2D contour plots: The effect on adsorption efficiency of (a-b) E/H and time, (c-d) temperature and pH.



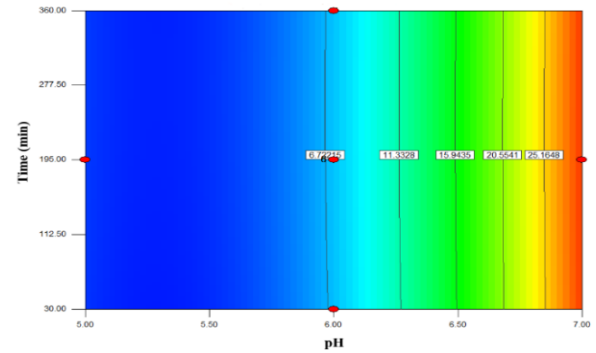
(a)



(b)



(c)



(d)

Figure 2.2. 3D response surface and 2D contour plots: The effect on the specific enzyme activity of (a-b) E/H and time; (c-d) temperature and pH.

Ilgu et al. (2011) immobilized the thermophilic recombinant esterase on chitosan nanoparticles. They found the loading amount of the esterase on the nanoparticles as 0.85 mg/mg. Thörn et al. (2011) reported the loading amount of feruloyl esterase on mesoporous silica materials (MPS-5D and MPS-9D) and non-porous silica as 0.034, 0.073, and 0.031 mg/mg, respectively. Bonzom et al. (2018) determined the maximum loading amount of the esterase on MPS to be 0.022 ± 0.03 mg enzyme/mg MPS. Compared to the other studies, the loaded amount of esterase on HNTs in this study (1.922 mg/mg) is noticeable and it can be attributed to the structure of HNTs due to specific sites in and out of the lumen.

2.3.3. Characterization Analysis

Once the optimal conditions were determined, the composite was characterized, and its structural and morphological properties were evaluated.

2.3.3.1. Structural characterization of HNTs and HNT-enzyme composite

The characterization of the composite structure was performed using XRD, SEM, and TEM microscopy (Figure 2.3a-d). The observed diffraction peaks are indexed to the hexagonal structure of HNT ($\text{Al}_2\text{Si}_2\text{O}_5(\text{OH})_4$) based on the reported values of Halloysite 7Å which complies with lattice constants: $a=b=5.13$, $c=7.16$ (JCPDS 00-029-1487). Bragg's law (2.9) is used to determine the d-spacing (the interlayer distance between the layers of HNT).

$$\lambda = 2 d \cdot \sin \theta \quad (2.9)$$

λ is the wavelength of the X-ray sent on the samples, and θ is the diffraction angle.

HNTs showed the first diffraction peak (001) at 12.1° corresponding to a basal spacing of 0.73 nm. A second diffraction peak (100) at 20.1° attributed to 0.44 nm indicates the tubular structure of HNTs. Also, other diffraction peaks at 24.5° (002), 35° (110), 37.9° (003), 54.5° (210), and 62.5° (300) with lower intensity are ascribed to Halloysite 7Å (Zhai et al., 2013).

The three-dimensional structure of pure HNTs and their surface was studied using SEM. The average length of the HNTs varies between 0.4 and 1 μm and its external diameter ranges from 70 to 100 nm. Additionally, its internal diameter is found to be more or less 30 nm, and its average wall thickness is 10 nm.

TEM images of the pure HNTs (Figure 2.3c) and HNT-enzyme composite (Figure 2.3d) showed that HNTs have a hollow tubular structure, and their two ends are open. Thus, after adsorption, esterase may be immobilized to the lumen and surface of HNTs. After enzyme immobilization, small irregular formations were observed in the lumen and surface of the HNTs, confirming the adsorption of esterase to the HNTs. Similar results are reported in the literature by Tully et al. (2016) who immobilized lipase enzymes to HNTs.

2.3.3.2. Nanotextural and chemical characterization of HNT-enzyme composite

N₂ adsorption-desorption analysis was performed to determine the adsorption efficiency according to the changes in Braun-Emmet-Teller (BET) surface area, pore volume, and pore diameter. BET surface area and pore volume of pure HNTs were calculated to be 66.064 m²/g and 0.002772 cm³/g, respectively. When the enzyme is immobilized on the support material, the surface area of HNTs decreases (Rodrigues et al., 2008). When the HNTs showed a decrease in BET surface area from 66.064 m²/g to 37.8918 m²/g (42.64% decrease) after the esterase adsorption, the micropore volume of HNTs diminished from 0.002772 to 0.001632 cm³/g (41.12% decrease). When the average pore diameter of the HNT-enzyme composite was found to be 107,931 Å, that of HNTs was 90,325 Å. Following the enzyme adsorption, the decrease in the surface area and pore volume and

the increase in pore diameter of HNTs could be implications for enzyme immobilization on HNTs. The structure of the nanotextured composite was investigated by the FT-IR spectrum of HNTs and esterase (Figure 2.3e). The infrared spectrum of pure HNT characteristic peaks shows the O-H stretching of water at 3696 cm^{-1} , the OH deformation of water at 3625 cm^{-1} , and in-plane Si-O stretching at 1033 cm^{-1} . In addition, the peaks at 910 cm^{-1} and 693 cm^{-1} are caused by deformation vibrations of hydroxyl groups. Lastly, the peaks at 754 cm^{-1} and 540 cm^{-1} could be attributed to perpendicular stretching of Si-O and deformation of Al-O-Si, respectively. The amide I (1630 cm^{-1}) and amide II (1535 cm^{-1}) bands are the two most prominent vibrational bands of the protein backbone. It is apparent that both the amide bands and characteristic peaks of HNTs in the spectrum of HNT-enzyme composite are observed. There are significant differences between the peaks of HNTs and HNT-enzyme composite. Several researchers have attempted to immobilize lipase on HNTs. They have obtained similar results demonstrating that the adsorption method is a practicable method for enzyme immobilization on the HNTs (Wang et al., 2015a; Mohammadi et al., 2020).

TGA was performed to prove that proteins adsorb onto HNTs (Figure 2.3f). It is shown that HNTs have undergone dehydration of the physically adsorbed water at $30\text{ }^{\circ}\text{C}$ and interlayer water molecules bound by hydrogen bonds at 250°C , and the dehydroxylation process at 470°C . It is known that the decomposition of protein under air flow shows a maximum mass loss in the range of $300\text{ }^{\circ}\text{C}$ and $350\text{ }^{\circ}\text{C}$ (Duce et al., 2017). In addition, a shoulder forms at $245\text{ }^{\circ}\text{C}$ due to the polypeptide chain thermal decomposition of esterase. At $450\text{ }^{\circ}\text{C}$ and $650\text{ }^{\circ}\text{C}$, esterase undergoes the decomposition of aggregates as well as the carbonizing and ashing of the hard residues of the proteins (Duce et al., 2017). Compared to the HNT-enzyme composite, the free esterase displayed rapid decomposition with the increasing temperature due to enzyme denaturation. The pure HNTs and the free esterase displayed a mass loss of 17.53% and 87.27% , respectively in the range of $20\text{ }^{\circ}\text{C}$ and $800\text{ }^{\circ}\text{C}$. As for the HNT-enzyme composite, the weight loss percentage was determined to be 20.05% within the same temperature range. These results exhibited that the enzyme adsorption on HNTs significantly improved the thermal resistance of the enzyme.

2.3.4. Stability test

2.3.4.1. Thermal stability

With the increase in temperature, the HNT-enzyme composite showed a 17.5% loss in activity at 70°C while the free esterase enzyme only maintained about 5.7% of its original activity at the same temperature (Figure B.2a). The enzyme immobilization resulted in enhanced thermal stability at higher temperatures, which is attributed to an increase in rigidity achieved during the immobilization process. This rigidity helps to prevent conformational changes in the enzyme's tertiary structure (Hartmeier, 1988; Zhai et al., 2010). Consequently, immobilized enzymes have the potential to be used in a wide range of industrial applications (Hu et al., 2007).

2.3.4.2. Storage stability

As shown in Figure B.2b, at the end of storage time for 14 days, free esterase lost almost 80% of its original activity, whereas the HNT-enzyme composite still retained 92% of its initial activity. Zhai et al. (2010) reported that the immobilized urease and α -amylase on HNT retained %90 and 94% of their initial activities, respectively after 15 days of storage time. Wang et al. (2015a) conducted a test to evaluate the stability of immobilized lipase on HNTs. They reported that the immobilized lipase maintained more than 80% of the initial activity at the end of 14 days storage, while free lipase lost almost all of the original activity at the same time. This fact indicates that HNTs can offer a conducive environment for immobilized enzymes, resulting in significantly improved storage stability.

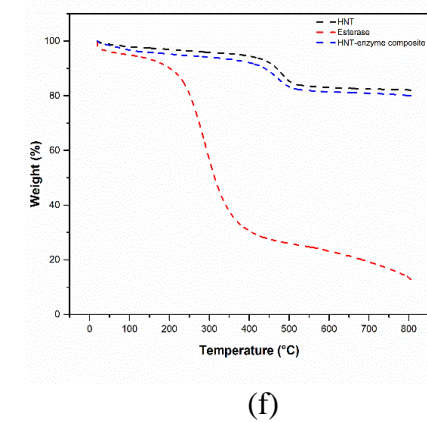
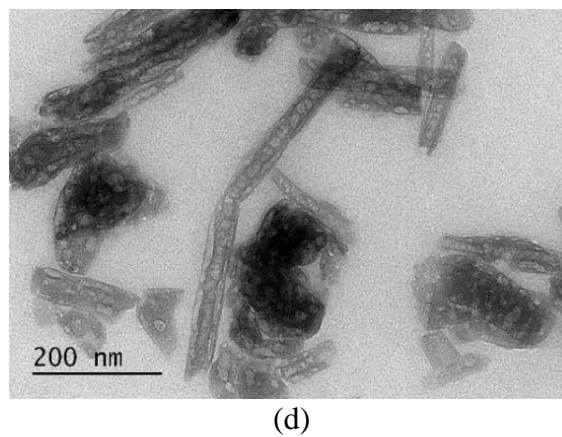
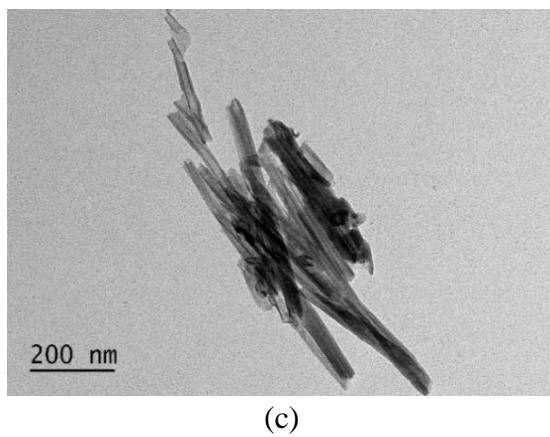
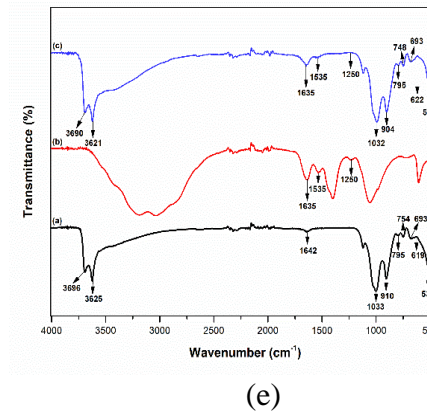
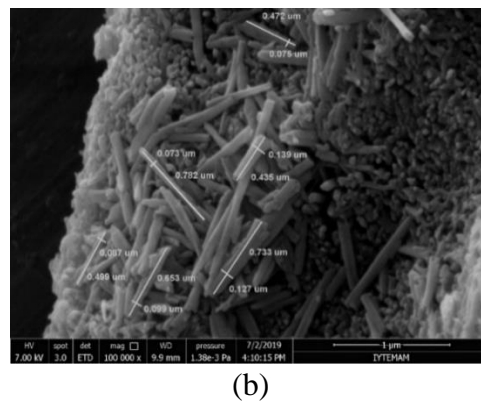
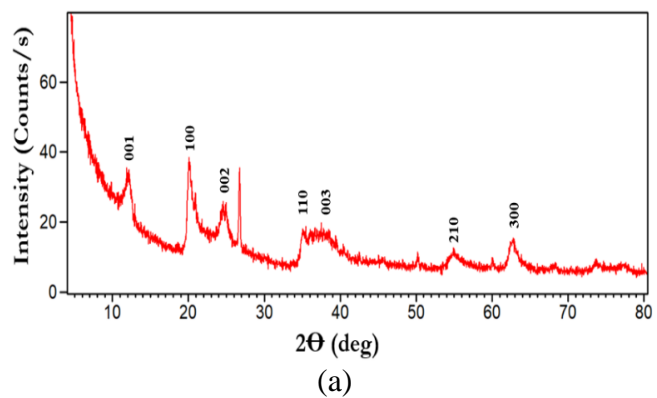


Figure 2.3. Composite characterization: XRD analysis (a), SEM images (b), and TEM images of HNTs (c) and HNT-enzyme composite (d), FT-IR spectrum (e) and TGA curves (f) of HNT (black), esterase (red), and HNT-enzyme composite (blue).

2.3.4.3. Reusability of HNT-enzyme composite

Enzymes that have been immobilized on supports can be readily recovered and reused multiple times, which is not possible with free enzymes that are difficult to separate from the reaction mixture. In the literature, the relative enzyme activities after 7 repeated uses following the immobilization of α -amylase (Zhai et al., 2010), urease (Zhai et al., 2010), and lipase (Mohammadi et al., 2020) onto HNTs were reported as 56.2%, 65%, and 70%, respectively. In this study, the HNT-enzyme composite exhibited significant stable activity even after 7 continuous cycles of the enzymatic reaction and it retained almost 75% of its initial activity (Figure B.3). This result demonstrated much better reusability of HNT-esterase composite compared to other immobilized enzymes on HNTs. This may be attributed to biocompatibility between enzyme and HNTs. Additionally, the loss in activity can be due to enzyme inactivation resulting from its repeated use (Zhai et al., 2010).

2.3.5. Determination of kinetic parameters

K_m and V_{max} of the free esterase and HNT-esterase composite were determined using the Lineweaver-Burk plots (data not shown). The Lineweaver-Burk plots demonstrated a linear relationship within the tested concentration range. When the K_m and V_{max} of free esterase were 0.673 μM and 35.461 $\mu\text{M}/\text{min}$, respectively, these values of the HNT-enzyme composite were determined to be 1.76 μM and 52.6 $\mu\text{M}/\text{min}$, respectively. The K_m value for the HNT-esterase composite was found to be higher than that of free esterase, indicating that the HNT-enzyme composite had a lower affinity for the substrate and a lower tendency to interact with it. Similar results were reported in the literature (Pereira et al., 2019a; Mohammadi et al., 2020) which the HNT-enzyme composite exhibited a higher K_m value than free esterase. Furthermore, the V_{max} value of the HNT-enzyme composite was 1.5-fold higher than that of free esterase. The immobilization process can lead to changes in the structure of the enzyme and alter its accessibility to the substrate, which can affect the kinetic parameters. Therefore, differences in the K_m and V_{max} values between free and immobilized enzymes can be

attributed to these changes (Akgöl et al., 2001; Tutar et al., 2009). In addition, the increase in the V_{max} value of the HNT-enzyme composite, despite the increase in the K_m value, may be attributed to a decrease in enzyme inhibition (Rodrigues et al., 2013). The K_m and V_{max} values obtained in this study may be lower than those obtained in the literature (Tekedar and Sanli-Mohamed, 2011; Mohammadi et al., 2020). The enzyme with low K_m and V_{max} indicates better enzyme-substrate binding (Sudo, 1995; Saganuwan, 2021). This fact shows that the esterase enzyme used in the study has a high affinity with its substrate.

2.3.6. DBP degradation study by HNT-enzyme composite

The results of the degradation experiment showed that the free esterase enzyme (1 mg/mL) completely degraded DBP (100 mg/L) within 15 minutes (Figure 2.4a), and the HNT-enzyme composite continued the degradation of DBP until the end of the 3rd cycle with a 100% efficiency (Figure 2.4b). Moreover, the HNT-enzyme composite was able to degrade almost 70% of 100 mg/L DBP at the end of the 7th cycle. It can be used in long cycles for DBP degradation although the free esterase could not be used repeatedly due to the need to separate from the reaction mixture. This may be because only a part of the HNT-enzyme composite comes into contact with DBP. Therefore, the HNT-enzyme composite exhibits good degradation capability even after repeated use. In recent years, a few studies have focused on the degradation of DBP in the presence of an enzyme immobilized on various materials. Dulazi and Liu (2011) immobilized lipase enzyme on chitosan beads to degrade different types of PAEs (15 mg/L). They reported that the lipase immobilized on chitosan beads degraded 73.05% of DBP in a solution consisting of a mixture of different types of PAEs. Sungkeeree et al. (2017) conducted a DBP degradation study using an immobilized esterase obtained from *Sphingobium* sp. SM42 on amine-functionalized supports. They reported that the immobilized esterase degraded 99% of 10 mM DBP and 30% of 100 mM DBP within 18 h. In this study, the HNT-enzyme composite with high activity exhibited high degradation efficiency in long cycles. It may be related to the biocompatibility between the esterase and HNTs. Because the

reusability of the immobilized enzyme depends on the support material and the substrate (Zhai et al., 2010).

Contrary to the free esterase, the HNT-enzyme composite could be separated easily in the reaction mixture and subsequently reused. At the end of each degradation cycle, the activity of the composite was assayed again. Free esterase enzyme could not be reused in degradation experiments. During the degradation experiments with the 7 cycles of 1h-periods, the relative activity and the mass percentage of the esterase immobilized on HNTs were given (data not shown).

The mass percent of the esterase on HNTs was 71% at the 3rd cycle and this percentage was determined to be 48% at the end of the experiment. It was understood that approximately 50% of the esterase immobilized on HNTs was released at the end of the experiment. Furthermore, while the esterase immobilized on HNTs retained 70% of its initial activity in the 3rd cycle in the degradation experiment, it lost 55% of initial activity at the end of the 7th cycle. This decrease in the activity of the HNT-enzyme composite can be attributed to the accumulation of metabolites that covers the enzyme and has an effect on the next degradation cycles (Zhai et al., 2013).

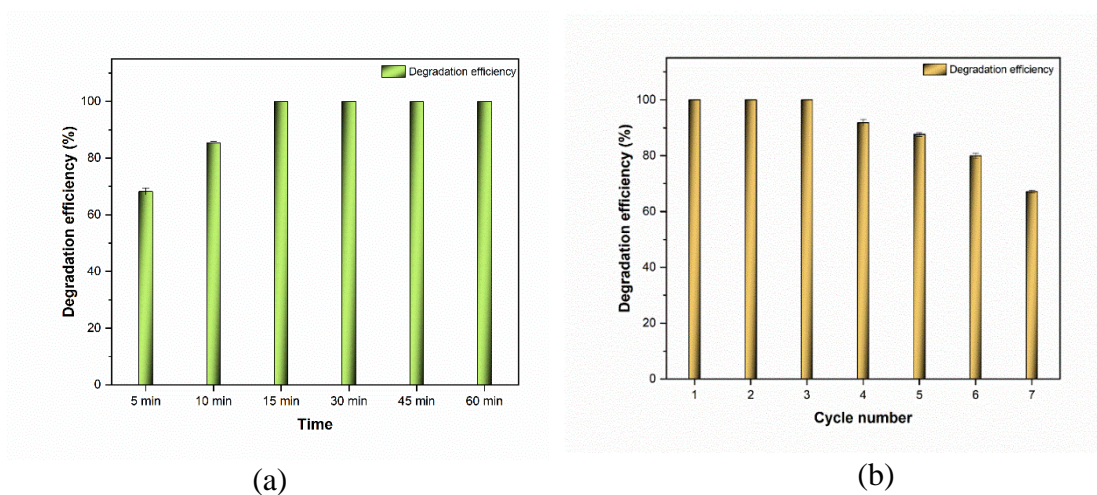


Figure 2.4. DBP degradation efficiency in the presence of (a) free esterase and (b) HNT-enzyme composite.

2.3.7. Investigation of DBP metabolites

After the degradation experiments, the metabolites of DBP were identified based on mass spectra at a particular retention time (RT) as shown in Figure B.4. DBP solution without the esterase was used as the control sample in HPLC-MS analysis (Figure B.4a). The obtained m/z ratios by mass spectrometry were compared to those of compounds in the literature. The m/z ratio for DBP was 279.15 (RT 22.6 min). After degradation experiments in the presence of free esterase, phthalic anhydride (M1; m/z 149.02; RT 2.8 min), DMP (M2; m/z 163.0388; RT 6.9 min), mono butyl phthalate (MBP; M3; m/z 223.0961; RT 9.7 min) and butyl methyl phthalate (BMP; M4; m/z 259.039; RT 15.4 min) were detected as the metabolites of DBP (m/z) in the presence of methanol (Figure B.4b). MBP, BMP, and DMP are likely to be formed by transesterification reaction in the presence of methanol as a result of the DBP degradation experiments (Kim and Lee, 2005; Ahn et al., 2006; Kumar et al., 2017). Besides, Okamoto et al. (2011) reported that PAEs undergo transesterification which is the process of exchanging the alkyl group of an ester with the alkyl group of an alcohol. Phthalic acid (PA) which is formed by the de-esterification reaction of PMEs was reported in many studies as a metabolite of PAEs via bacterial (Feng et al., 2002) or enzymatic degradation (Saito et al., 2010; Dulazi and Liu, 2011). Then, phthalic anhydride is formed as a result of the dehydration of PA. In this study, the other peaks observed in the chromatograms were determined to be polymers. Kim and Lee (2005) studied the degradation of DBP by free esterase and cutinase. They identified three metabolites: 1,3 isobenzofurandione (IBF), DMP, and BMP. In the study, firstly, DBP was converted to 1,3 isobenzofurandione (IBF) at the end of 7.5 h in the presence of cutinase and then, the amount of BMP began to increase as that of IBF decreased after the 3rd day. It was reported that BMP was the major metabolite of DBP degradation conducted using the esterase. IBF was not detected in this study. This is because the formation of the metabolites significantly depends on the enzyme used in the study. IBF is a major degradation product in the DBP degradation study in the presence of cutinase (Ahn et al., 2006). Fang et al. (2010) conducted a study on DBP degradation using a bacteria (*Enterobacter* sp. T5) isolated from municipal solid waste, and they reported that the major DBP metabolites were MBP and PA. Kumar et al. (2017) conducted a study on the biodegradation of DBP using two isolated bacteria

(*Pseudomonas* sp. V21b and *Comamonas* sp. 51F) from municipal solid waste. They identified MBP and PA to be the metabolites of DBP. Fang et al. (2017) investigated the biodegradation of DBP in the presence of *Acinetobacter* sp. strain LMB-5 isolated from soil. There were four metabolites of DBP, 1,2 benzenedicarboxylic acid, butyl methyl ester, DMP, and PA during DBP degradation. Generally, most DBP metabolites identified in the literature were found as a result of DBP degradation in the presence of the esterase in this study. It is apparent from Figure B.4c that MBP, BMP, DMP, and phthalic anhydride appeared in the HPLC chromatogram at the end of the degradation experiment conducted using the HNT-enzyme composite for 1h. PAEs and their metabolites tend to be adsorbed in the support materials (Dulazi and Liu, 2011). Compared to Figure B.4b and 4.4c, there were differences in the peak areas of metabolites that occurred in the presence of free enzyme and HNT-enzyme composites. This fact may be due to the adsorption of some PAE metabolites on the HNT-enzyme composite. For this reason, the peak area may be visible at a lower intensity. As seen in the HPLC-MS chromatograms, all metabolites that appeared in the presence of free esterase during DBP degradation were found in the presence of the HNT-enzyme composite. As a result of this study, it is understood that the HNT-enzyme composite metabolizes DBP to phthalic anhydride. This may be an indication that the esterase does not lose its characteristic properties after immobilization and can be used as an effective degrader during long cycles of degradation experiments.

2.4. Conclusion

In this study, the ability of esterase and lipase enzymes obtained from various microorganisms to degrade DBP was investigated. Esterase from *Bacillus subtilis* displayed the highest DBP degradation ability and then it was immobilized on halloysite nanotubes (HNTs) with the adsorption method under optimal conditions. The HNT-enzyme composite was repeatedly used in the DBP degradation over time, retaining most of its initial activity. Whereas the free esterase revealed a high ability to degrade DBP in a short time, the immobilized esterase could be used with a high degradation ability during long cycles. It has been confirmed that HNTs are a desirable natural support material to

overcome the limitation of enzyme catalytic activity, and also the esterase obtained from *Bacillus subtilis* is an effective degrader of DBP. All these results support the fact that the HNT-enzyme composite can be more suitable for future practical applications in the remediation of PAEs in different environments.

CHAPTER 3

DEGRADATION OF DIBUTYL AND DIETHYLHEXYL PHTHALATES BY *RHIZOMUCOR MIEHEI* LIPASE: SUBSTRATE SPECIFICITY, IMMOBILIZATION, CATALYTIC PERFORMANCE

3.1. Introduction

Phthalic Acid Esters (PAEs) are synthetic chemicals that are produced on massive scales and widely used in various industrial processes and products. They are commonly used as plasticizers and added to materials to boost flexibility, durability, and workability. They are linked to the plastic matrix with hydrogen bonds and van der Waals forces and thus they can easily enter the surrounding environment such as the atmosphere, water bodies, soil, etc. Thereafter, they can accumulate in living organisms, including plants, animals, and humans (Sun et al., 2015; Mu et al., 2017). Moreover, they are of increasing interest because they may cause cancer (Medellin-Castillo et al., 2013), reproductive and neurophysiological disorders (Wu et al., 2013; Ren et al., 2018), organ damage, birth defects (Tumay-Ozer et al., 2012; Tsai et al., 2018) and developmental problems, and they can also exhibit endocrine-disruptive properties (Tumay-Ozer and Gucer, 2012; Sheikh et al., 2016).

Dibutyl phthalate (DBP) and diethylhexyl phthalate (DEHP), detected in the environment, are typical representatives of PAEs with short and long chains, respectively. They have been ranked as priority pollutants by regulatory agencies in the United States and the European Union countries (EC, 1997). Thus, the widespread use and potential hazards of PAEs on the ecosystem and public health have led to a need for a method to remove them from the environment. Even though photodegradation and hydrolysis can occur for PAEs through natural abiotic conditions, their degradation rate is very low (Ren

et al., 2018). Additionally, some of the PAEs are resistant to hydrolysis and photolysis (Bai et al., 2020). Biodegradation is generally perceived as a safer, cleaner, and more environmentally friendly option compared to other methods such as photolysis and hydrolysis. There is no secondary pollution after the biological degradation of PAEs (Huang et al., 2019). The search for an environmentally friendly degradation method, especially for contaminated sites, is still active. Therefore, the biodegradation of PAEs in the environment by enzymes is recognized as a promising method as it can occur relatively rapidly (Yastrebova et al., 2019; Savinova et al., 2022). PAEs toxicity is related to the ester bonds present in their chemical structure (Heindel and Powell, 1992). Lipase, one of the hydrolase enzymes, has shown notable effectiveness in breaking down the ester bonds within the structure of PAEs and facilitating their biodegradation (Sharma et al., 2019). Earlier studies have demonstrated that the lipase from *Candida cylindracea* (Tanaka et al., 2000), *Pseudomonas* sp. V21b (Kumar et al., 2017), *Comamonas* sp. 51F (Kumar et al., 2017), and *Candida lipolytica* (Sun et al., 2022b) can degrade PAEs. Despite that, free lipases exposed to harsh environments including high temperatures, persistent reactions, and organic solvents are generally unstable, meaning they can lose their structural stability during a reaction and have a relatively short catalytic lifetime. An effective strategy to address these challenges is to immobilize the enzyme onto a support material. This approach can increase the enzyme's stability and half-life and maintain the enzyme activity under varying environmental conditions, including fluctuations in pH and temperature (Puri et al., 2013). Adsorption that does not require the use of chemicals is a simple and economical method for the immobilization of enzymes. Adsorbed enzyme can easily be separated from the mixture and its repeated use for applications is possible. However, conformational changes in the enzyme's secondary structure and protein refolding, which can also reduce enzyme activity and stability may occur (Collins et al., 2011; Mohamad et al., 2015). These changes can take place due to the interaction between the enzyme and the immobilization matrix, or the confinement of the enzyme within the matrix. Demonstrating these changes could be important in the development of sophisticated biocatalysts for biotechnological applications.

Due to their high surface area, a strong surface binding capability, high biocompatibility, and high mechanical properties nanostructured materials such as nanoparticles, nanofibers, nanotubes, and nanocomposites are widely used as a matrix to immobilize and stabilize enzymes by improving biocatalytic efficiency (Asuri et al., 2006; Verma et al., 2013; Puri et al., 2013). Halloysite nanotubes (HNTs,

$\text{Al}_2\text{Si}_2\text{O}_5(\text{OH})_4 \cdot 2\text{H}_2\text{O}$), which is one of the natural materials, have recently received attention as outstanding support materials for enzyme immobilization due to their distinctive tubular structure, cost-effectiveness, favorable biocompatibility, and being environmentally friendly material.

The main objective of the present study is to comprehensively investigate the ability of *Rhizomucor miehei* (*R.miehei*) lipase (palatase) as free and immobilized form onto HNTs (HNTs-P composite) in terms of the degradation of PAEs with short and long chains (DBP and DEHP). This study has a different perspective from the literature on enzymatic degradation, considering substrate specificity, enzyme selectivity, amino acid sequences, binding pocket shapes, and DBP/DEHP degradation products. Furthermore, in the literature, only a few studies have addressed alterations in the secondary structures of enzymes following immobilization to HNTs. With this study, circular dichroism (CD) spectroscopy analysis was performed to clarify the changes in the secondary structure of the enzymes after immobilization. Lastly, the degradation products of DBP and DEHP, and the reusability of the composites in the experiments were investigated. The study can contribute to the broader application of immobilized enzymes not only in persistent organic contaminant treatment but also in prospective applications in the food, pharmaceutical, and industrial areas.

3.2. Material and Method

3.2.1. Materials

Pristine halloysite nanotubes (HNTs) were kindly donated by Esan, Eczacibasi Industrial Raw Materials Co. (Türkiye). *R. miehei* lipase (EC 3.1.1.3; 20,000 LU/g) known as palatase was supplied from Novozymes (Denmark). Bovine serum albumin (BSA), DBP and DEHP solution (%99) and p-nitrophenyl acetate (pNPC-2) were products of Sigma-Aldrich. All other chemicals have reagent-grade quality, and they were utilized as received.

3.2.2. Enzyme immobilization onto HNTs

Since palatase was in liquid form, it was directly used as an enzyme solution in adsorption experiments. The immobilization study was conducted according to the procedure reported by Balci et al. (2023).

3.2.3. Enzyme characteristic properties

The enzymatic activity was assessed through the hydrolysis of pNPC-2, based on the method described by Tekedar and Sanli-Mohamed (2011). The activity was subsequently determined using the following equation (3.1).

$$\text{Activity (U/L)} = \frac{(\text{Abs at 400 nm/min}) \cdot (V_t) \cdot (DF)}{(\epsilon) \cdot (V_e) \cdot (d)} \quad (3.1)$$

Where V_t : Test volume (mL), DF: Dilution factor, ϵ : molar extinction coefficient of paranitrophenol (p-nitrophenol) at 400 nm, V_e : Volume of used enzyme (mL), d : Lightpath (1 cm).

One unit (U) of enzyme activity is defined as the quantity of enzyme capable of liberating 1.0 μmol of p-nitrophenol per min, under assay conditions, using 0.5 mM pNPC-2 as the substrate. The extinction coefficient for p-nitrophenol in the buffer system is determined to be $17,215 \text{ M}^{-1} \text{ cm}^{-1}$.

The protein content of the enzyme solution, supernatant, and washing solution was measured using the Bradford Method with Bovine Serum Albumin (BSA) as the model protein (Bradford, 1976). The absorbance of the solutions was recorded at 595 nm using a UV-Visible spectrophotometer (Genesys-150). Adsorption efficiency (Ads. eff. (%)) and enzyme loading amount (Load. amount (mg/mg)) were calculated by considering the quantity of enzyme that remained unadsorbed, using the following equations (3.2-3.3):

$$\text{Ads. eff.} = \frac{\text{Total enzyme amount} - (\text{enzyme amount in the supernatant and washing solution})}{\text{Total protein amount}} \times 100 \quad (3.2)$$

$$\text{Load. amount} = \frac{\text{Total enzyme amount} - (\text{enzyme amount in supernatant and washing solution})}{\text{mass of HNTs}} \times 100 \quad (3.3)$$

3.2.4. Material characterization

Transmission Electron Microscopy (TEM) and Fourier Transform Infrared Spectroscopy (FT-IR) were utilized to analyze and characterize the structure of HNTs before and after palatase immobilization. With thermogravimetric (TG) analysis, the thermal stability of these materials was evaluated. Before the characterization analyses, HNTs and HNTs-P were kept in a vacuum oven at 100°C and 45°C, respectively.

The detailed surface morphology of HNTs and HNTs-P was examined using a MICRO JEOL JEM 1010 Transmission electron microscopy (TEM) with an accelerating voltage of 200 kV.

FT-IR spectra of the HNTs and HNTs-P were collected on a JASCO FT-IR 4100 spectrometer (Jasco Inc., Easton, MD, USA) to analyze their respective functional groups. All data was obtained by scanning in the range of 4000 and 400 cm^{-1} at a resolution of 2 cm^{-1} .

The thermal stability of both HNTs and HNTs-P were examined using a Setaram thermogravimetric analyzer. The analysis was conducted in the temperature range of 30°C to 800°C at a heating rate of 10°C/min under high-purity nitrogen flow (20 mL/min). The mass loss with heat was recorded to assess the thermal stability of the materials.

3.2.5. Sequence analysis

The specific amino acid sequence of palatase (P19515) was retrieved from the protein databases available at UniProt with the corresponding accession numbers and compared to that of *Bacillus subtilis* esterase (O32232) with high PAEs degrading ability.

The Basic Local Alignment Search Tool (BLAST) program from National Center for Biotechnology Information (NCBI) and Clustal Omega (Clustal O(1.2.4)) program from European Bioinformatics Institute were utilized to conduct sequence similarity searches. The binding properties of the active site for enzymes were investigated using the ScanProsite program.

3.2.6. Circular Dichroism (CD) Analysis

Circular dichroism (CD) is an excellent method used to rapidly assess changes in protein conformation, enzyme stability, binding characteristics, and folding/unfolding transitions under various conditions, such as changes in temperature, pH, and the presence of ligands or other environmental factors. The far UV (200-260 nm) CD spectra are indicative of α -helices, β -sheets, β -turn, and random coils in the protein secondary structure (Roberts et al., 1989).

In this study, a CD analysis was carried out using a Jasco Spectropolarimeter (J-815, Tokyo, Japan) to demonstrate the conformational changes in the secondary structure of the palatase before and after immobilization in the range of 200-260 nm at 0.1 nm intervals. The CD spectra were obtained at room temperature using a quartz cuvette with a cell length of 1 cm. For all samples, the spectra data were obtained as an average of three scans, and a blank spectrum devoid of protein was subtracted. The CD raw data were directly given as ellipticity values in millidegrees (mdeg). Considering the mean residue ellipticity at about 216 nm, the relative structure percentage (%) was calculated using the following equation (3.4).

$$\text{Relative structure (\%)} = \frac{\theta_{IE}}{\theta_E} \times 100 \quad (3.4)$$

where θ represents ellipticity at 216 nm, θ_{IE} and θ_E for the free and immobilized enzymes, respectively.

3.2.7. Stability tests

Stability experiments were expressed by the relative activity (%) and the initial lipase activity was assumed to be 100%.

Temperature stability tests for both free palatase and HNTs-P were performed with incubation of samples in a phosphate buffer (0.1 M, pH 7) at different temperatures between 20°C and 70°C. The samples were taken and subsequently cooled to room temperature (Jafarian et al., 2018) and their relative activity was measured using pNPC-2 (0.5 mM) in acetonitrile.

To assess storage stability, both the free palatase and HNTs-P were kept for 14 days at 4°C. Samples were periodically taken during the predetermined time interval to measure relative enzyme activity using a 0.5 mM pNPC-2 substrate.

To test the pH effect on the stability, the pH of the samples was adjusted at various values (3, 5, 7, and 9) using a phosphate buffer (0.1 M) at the optimal temperature for the enzyme. Following the incubation period, the activity was assessed with 0.5 mM pNPC-2 substrate present.

3.2.8. Degradation assays

3.2.8.1. Degradation assay by free palatase

The degradation experiments with free palatase were conducted using a procedure reported by Balci et al. (2023). Firstly, a concentrated 1,000 mg/L DBP and DEHP solution was prepared in methanol separately. Tween-80 was added as a solubilizing agent to enhance the solubility of PAEs in the solution. 0.1 mL of the palatase, 0.1 mL of 1,000 mg/L DBP/DEHP in methanol, 0.1 mL of Tween-80 (1%), and 0.7 mL of phosphate buffer (0.1 M, pH 7) made up the reaction mixture. The mixture was kept for 1 h under optimal conditions specified by the manufacturers. After a specific time-interval, the samples were periodically taken and subsequently, the enzymatic reaction was terminated

by adding 1 N HCl to the samples at a rate of 10% (v/v) (Saito et al., 2010). Prior to HPLC analysis, the samples were filtered through a 0.22 µm PTFE syringe filter to eliminate particle materials.

3.2.8.2. Degradation assay by HNTs-P composite

0.8 mL of phosphate buffer (0.1 M, pH 7), 0.1 mL of Tween-80 (1%), and 0.1 mL DBP/DEHP (1,000 mg/L) in methanol were added to the glass tube containing 5 mg of HNTs-P. For 1h-periods, samples were placed in an incubator shaker. At the end of each period, they were taken, vortexed for 30 sec, and then centrifuged at 5,000 rpm for 10 min. The supernatant phases were taken to measure enzyme activity and protein concentration. 1 M HCl (10% (v/v)) was added to the remaining supernatant phase to terminate the reaction and then the samples were analyzed using an HPLC device to measure the concentration of DBP/DEHP. After each cycle, the pellet phase with palatase was supplemented with the reaction mixture (1 mL) containing 0.1 mL of DBP/DEHP solution (1,000 mg/L) and 0.9 mL of phosphate buffer (0.1 M, pH 7).

3.2.9. Analysis of PAEs and their metabolites

HPLC (Agilent 1260 Infinity) was used for the quantification of DBP in the samples. The HPLC system consisted of a quaternary pump, an autosampler, a ZORBAX Eclipse XDB C-8 column (5 µm particle size, 150 mm × 4.6 mm i.d), and a diode array detector (DAD). The mobile phase which was acetonitrile:water (60:40, v/v) for DBP analysis was used in isocratic mode at a flow rate of 1 mL/min with 20 µL sample injection. For the analysis of DEHP in gradient elution, the ratio of mobile phase (acetonitrile: water) was adjusted over time periods as follows: 0 to 3 min 80:20, 3 to 9 min 95:5, 9 to 12 min 100:0 and 12 to 22 minutes 80:2. The flow rate was maintained at 0.5 mL/min throughout the analysis with 10 µL sample injection. The analyses were performed at room temperature, using a UV detector set at 224 nm. The Bruker Elute LC

system coupled with a Trapped Ion-Mobility Spectrometry Time-of-Flight Mass Spectrometer (TIMS-TOF-MS) from Bruker Daltonics (Bremen, Germany) was utilized to identify the degradation products of DBP and DEHP. Ionization was carried out by an electrospray (ES) source, where the needle was subjected to a voltage of 3.5 kV and an endplate offset of 500 V. ES spectral data were acquired in both positive and negative scan modes. The Bruker Otof Control Software version 5.1 was used to obtain the data, which were subsequently processed with the Data analysis software version 5.1 from Bruker Daltonics.

3.3. Results and Discussion

3.3.1. Enzyme immobilization and characterization

Following immobilization, the adsorption efficiency and relative enzyme activity of the obtained supernatants and washing solutions were measured. These values for HNTs-P were found to be 80.3% and 87.8%, respectively. They were expressive compared to other studies in literature. Balci et al. (2023) reported that the adsorption efficiency and enzyme activity for immobilized esterase to HNTs (HNTs-E) were 73.2% and 82.7%. Wang et al. (2015a) underlined that more than 85% of lipase enzyme was immobilized to HNTs. Mohammadi et al. (2020) conducted a study on immobilization of lipase onto HNTs, resulting in an enzyme adsorption efficiency of approximately 70%. These results can be attributed to the prolonged immobilization process and the compressional deformation of enzymes on HNTs (Yang et al., 2019). These differences in the adsorption values can be related to the effect of enzymes isoelectric point (pI) value on immobilization. Another reason for this could be the biocompatibility that exists between the enzymes and HNTs.

3.3.1.1. Morphological properties

The hollow tubular structure of HNTs with a transparent central area and its lumen with two open ends were clearly visible in TEM images (Figure C.1a). After the immobilization of the palatase onto HNTs, the difference in morphological structure of the HNTs (Figure SM1b) was observed as small irregular formations inside the lumen and on the surface of HNTs. These observed formations are related to the presence of the enzyme. Notably, there is a slight increase in the outer diameter of the HNTs-P and a decrease in their inner diameter. This fact can be attributed to the pI of the enzyme affecting immobilization. Since the pI of the palatase is about 3.8 in the phosphate buffer (0.1 M, pH 7) (Rodrigues and Fernandez-Lafuente, 2010), the palatase, which is an anionic protein, is mostly driven into the lumen of HNTs with a positive charge (Tully et al., 2016). All these results demonstrated that the palatase was successfully adsorbed on the HNTs.

3.3.1.2. Physical and chemical properties

The adsorption of palatase on the HNTs was analyzed with an FT-IR study (Figure C.2a). For HNTs, the FT-IR spectrum indicated a characteristic absorption peak at 3696 cm^{-1} and 3626 cm^{-1} which was attributed to the O-H stretching of water and OH deformation of water within HNTs. Additionally, a strong peak at 1032 cm^{-1} originated from in-plane Si-O stretching. The peaks at 910 cm^{-1} and 693 cm^{-1} were due to the deformation vibrations of Al-OH. Lastly, the perpendicular stretching of Si-O at 754 cm^{-1} and the deformation bonding of Al-O-Si at 540 cm^{-1} were caused by vibrations of Al-O-Si. In the spectra of the proteins, the bands at 1630 cm^{-1} (amide I) and 1535 cm^{-1} (amide II) are two prominent vibrational bands of proteins that give information about the secondary structure of the polypeptide chain. The presence of amide bands and HNT characteristic peaks observed in the FT-IR spectra of HNTs-P implies immobilization of lipase onto HNTs.

TG analysis was conducted to investigate the decomposition temperature of the enzyme. Figure C.2b indicated the mass loss trends of HNTs and HNTs-P from 30°C to 800°C. Firstly, HNTs underwent the dehydration of the physically adsorbed water on the external surfaces of HNTs at 30°C, and water molecules in the HNT structural layer were released at 250°C. Next, HNTs went through the dehydroxylation process of the hydroxyl groups in the structural layer of HNTs above 480°C. Maximum mass loss in protein decomposition under airflow was observed between 300°C and 350°C (Duce et al., 2017). The shoulder at 245°C was due to thermal degradation of the polypeptide chain of enzymes. Enzymes typically undergo processes involving the breakdown of aggregates as well as the carbonization, and ashing of the hard residues of the proteins. The free enzymes have more rapid decomposition than the HNTs-P with the increasing temperature owing to enzyme denaturation. HNTs-P composite had a higher weight loss in the range from 250°C to 420°C. This was due to the loss of water and denaturation of the enzymes by heat, followed by the destruction of the protein structure. The mass loss of HNTs-P began at 420°C as a result of the combined breakdown of the HNTs and enzymes. Between 30°C and 800°C, HNTs and HNTs-P experienced losses of 82.06% and 67.41%, respectively. This indicated that palatase was successfully immobilized on HNTs, and the thermal resistance of the enzymes significantly improved with the immobilization process.

3.3.2. Sequence analysis

The sequence analysis study was conducted to understand the effectiveness of enzymes owing to relatively formed differences in enzymatic degradation. The BLAST and Clustal Omega searches of the deduced amino acid sequence revealed significant differences between esterase that was used in previous work (Balci et al., 2023) and palatase (Figure 3.1). The encoded esterase consists of 246 amino acids in length with a calculated mass of 28.193 kDa. As for the encoded palatase, it contains 363 amino acids in length and has a calculated molecular mass of 39.602 kDa. The α/β hydrolase fold family is one of the most extensive groups of structurally related proteins, encompassing a broad range of catalytic and non-catalytic functions (Carr and Ollis, 2009). In general,

lipase and esterase enzymes exhibit a similar folding pattern known as the α/β hydrolase fold (Ollis et al., 1992). In many α/β hydrolases, the active site comprises a catalytical triad consisting of a nucleophilic residue, a catalytic acid that is not directly involved in catalysis, and a histidine residue (Eggert et al., 2000). The active site of hydrolases such as esterase and palatase typically comprises serine, aspartate or glutamate, and histidine. The active site triad for palatase consists of Ser238, Asp297, and His351 while it is Ser93, Asp192, and His222 for esterase. Typically, the Ser-His-Asp triad of α/β hydrolases plays a crucial role in the hydrolysis of ester bonds (Fan et al., 2018).

sp 032232 EST_BACSU	-----	0
sp P19515 LIP_RHIMI	MVLKQRANYLGF LIVFFTAFLVEAVPIKRQSNSTVDSLPLIPSRTSAPSSSPSTTDPEA	60
sp 032232 EST_BACSU	--MKVVTPKP-----FTFKGG-----	14
sp P19515 LIP_RHIMI	PAMSRNGPLPSDVETKYGMALNATSYPDSVVQAMSIDGGIRAATSQEINELTYTTLSAN	120
	*. * * : : : **	
sp 032232 EST_BACSU	-----DKAVLLLHGFTGNTADV	31
sp P19515 LIP_RHIMI	SYCRTVIPGATWDCIHCDATEDLKI IKTWSTLIYDTNAMVARGDSEKTIYIVFRGSSSIR	180
	*. : * * : :	
sp 032232 EST_BACSU	RMLG-----RYLNERGYTCHAPQYEGHGVPEELVHTGPEDWKNVMDGYEYLKSEGY	84
sp P19515 LIP_RHIMI	NWIADLTFVPVSYPPVSGTKVHKGF LDSYGEVQNELVA-----TVLDQFKQ---YPS	229
	. : . * * * . * : : * : * * * . * : * : :	
sp 032232 EST_BACSU	ESIAACGLSLGGVFSLKLGYTVPIKGI VPMCAPMHIKSEEV-MYQGVLSYARNYKFFEGK	143
sp P19515 LIP_RHIMI	YKVAVTGHS LGGATALL-----CALDLYQRE EGLSSSNLFLYTQGG-----	270
	. : * . * * * * . : * * * : * * . : : : * : :	
sp 032232 EST_BACSU	SPEQIEEEMKEFE---KTPMNTL KALQDLIADVRNNVMDIYSPTFV VQARHDMINTESA	200
sp P19515 LIP_RHIMI	-PRVGDPAFANYV VSTGIPYRRTVNERDIVPH-----LPPAAF GF-----	309
	*. : : : * . : * : : . : * .	
sp 032232 EST_BACSU	NIIYNEVETDDKQLKWEESG----HVITL DKERDLVHQDVYEFLE---KLDW-----	246
sp P19515 LIP_RHIMI	-----LH--AGEEY WITDNSPETVQVCTSDLETSDCSNSIVPFTSVLDHLSYFGINTGL	361
	: . : * : . . : * * * * . : : * . : * : :	
sp 032232 EST_BACSU	-- 246	
sp P19515 LIP_RHIMI	CT 363	

Figure 3.1. Multiple amino acid sequence alignment of esterase and palatase genes.

Due to seeing similar degradation but not to reach phthalic acid (PA) step led us to investigate structural differences of enzymes. To compare the similarities and differences between these two enzymes: palatase (this study) and esterase from the previous work (Balci et al, 2022), the sequence information for esterase and lipase has been utilized to

identify potential sequence motifs. Most of the lipase and esterase have the consensus sequence Gly-X-Ser-X-Gly motif (Mala and Takeuchi, 2008; Keun et al., 2012). The lipase from *Candida rugosa*, *Geotrichum candidum*, and *Yarrowia lipolytica* and esterase have this conserved sequence motif surrounding the central active site serine residue (Fojan et al., 2000; Keun et al., 2012). The motif is typically situated in a position between a β -strand and an α -helix and assumes an extremely sharp turn known as nucleophilic elbow (Ollis et al., 1992; Keun et al., 2012). It provides information about the classification of an amino acid sequence. The same motif is detected in palatase according to the results of the ScanProsite tool. The amino acids in the active site, the substrate binding site of enzymes, use many chemical mechanisms that convert the substrate to the product. That is, enzymatic reactions occur in the enzymes' active sites. The substrate specificity of the enzyme depends on the characteristic properties of the active site region. It is determined by the specific arrangement of amino acids within the active site and the structure of the substrates. Different substrate specificity can arise from identical active sites due to the influence of substrate and enzyme dynamics (Gade et al., 2021). For instance, *B. subtilis* esterase and *B. stearothermophilus* esterase with 74.8% similarity have the same active site triad. However, the DBP degradation ability of *B. stearothermophilus* esterase is much lower than that of *Bacillus subtilis* esterase (Balci et al., 2023). Unlike this, whilst *R. miehei* lipase and *Candida* sp. lipase do not show significant similarity in amino acid sequences, both have very high PAEs degradation ability (Dulazi and Liu, 2011; Balci et al., 2023). This can be attributed to their difference in substrate specificity. Not only substrate specificity but also other properties are also important for selectivity. The substitution of amino acids in the entrance region of enzyme active sites can alter the selectivity of the enzyme towards its substrate (Albayati et al., 2020). Enzyme specificity and selectivity in catalyzing different substrates are determined by the complementarity between the substrate and the enzyme, as well as the specific interactions that occur between the substrate and residues of the enzyme (Albayati et al., 2020). Additionally, selectivity can also be observed in terms of the fatty acid chain lengths, including short, medium, or long-chain fatty acids, as well as the degree of unsaturation. These variations contribute to different selectivity types exhibited by enzymes in their interaction with substrates. Whereas lipase effectively catalyzes the hydrolysis of ester bonds in a broader spectrum of fatty acids, esterase displays a higher substrate specificity for short and medium-chain fatty acid residues ($C \leq 12$) (Fojan et al., 2000; Samoylova et al., 2018; Ding et al., 2022). The physical characteristics of the

substrate are likely to play a significant role in determining the enzyme's substrate specificity. Long-chain fatty acids generally exhibit a low solubility, often forming emulsions. Therefore, lipase possesses the ability to recognize and interact with insoluble or highly aggregated substrates. Esterase activity is highest when acting on substrates that are more soluble in water (Fojan et al., 2000). The shape of the enzyme's binding site, along with the specific amino acid sequences that form the binding site, are vital factors in determining the preference of lipase for different sizes of acyl groups (Albayati et al., 2020). These factors are the main determinants that control the substrate specificity and selectivity of lipase towards acyl groups of varying sizes. The shape of the acyl binding site plays a critical role in determining substrate specificity. The specific shape and arrangement of amino acids within the binding site contribute to the enzyme's ability to recognize and accommodate particular substrates, thereby influencing its substrate specificity. By complementing the shape of the acyl group, the binding site enables the enzyme to selectively interact with and catalyze reactions involving specific substrates. Lipases typically possess a hydrophobic, elongated binding site for the scissile fatty acid. This binding site is situated within the binding pocket, which can be described as a wall of a binding funnel or a tunnel-like structure (Albayati et al., 2020). This unique arrangement allows lipase to effectively accommodate and interact with the fatty acid substrates, facilitating the catalytic hydrolysis or synthesis of ester bonds. Esterase enzymes have a small acyl binding pocket compatible with their substrate. The diverse characteristics of enzymes cause variations in their capacity to degrade the PAEs. These differences arise from variations in their substrate specificities, active site structures, and binding pocket shapes, which collectively influence their ability to degrade and interact with specific compounds. Consequently, the varying enzymatic properties between *R. miehei* lipase and *B. subtilis* esterase and can result in distinct efficiencies and capabilities for degrading the pollutants.

3.3.3. Conformational change in the enzyme structure

The enzyme's activity is substantially influenced by changes in its conformation, primarily due to the structural impact on the binding affinity of diverse substrates to the

consistently reactive sites (Figure 3.2). Collins et al. (2011) suggested that palatase formed 48% α -helices and 32% β -sheet. Figure 3.2 show CD spectra of free palatase and HNTs-P in phosphate buffer (0.1 M, pH 7). There were two negative peaks at about 208 and 216 nm in the CD spectra of free palatase. The α -helix has two negative peaks with a similar magnitude between 208 and 220 nm (Greenfield, 2006; Correa et al., 2009; Ernest et al., 2014). Additionally, it has a positive band in the range of 195 and 200 nm (Kikani and Singh, 2015). It is obvious that a positive peak associated with α -helix tends to form from 190 nm to 200 nm (Figure 3.2). These peaks in the CD spectra of free palatase can be attributed to the characteristic of α -helix structure. Upon the immobilization of the enzymes to HNTs, the CD spectra of palatase demonstrated a decrease in the intensity of the two negative peaks observed at 208 and 216 nm, indicating a potential decrease in the α -helix structure. It may be related to the β -sheet conformation of the enzyme due to the fact that the β -sheet protein exhibits a negative spectrum between 210 and 220 nm (Rigos et al., 2003). The trends may imply an alteration in the α -helix and the β -sheet of enzyme. Consequently, after the palatase immobilization, a decrease in α -helix structures and an increase in β -sheet structures were obvious. Similar findings were reported in the literature (Ernest et al. 2014; Chen et al., 2021a). Collins et al. (2011) immobilized palatase to bare and glutaraldehyde-functionalized chitosan. They observed some changes in the conformation of the enzyme after immobilization of both chitosan and glutaraldehyde-functionalized chitosan and detected a decrease in the α -helix and an increase in β -sheet. Ernest et al. (2014) studied the interaction of amylase with silver nanoparticles (AgNPs). They reported a decrease from 63.5% to 60.3% in α -helix structure after AgNP treatment. They underlined that the band at 222 nm related to the α -helix structure shifted to 215 nm. Yang et al. (2019) reported that the intensity of negative peaks in the free horseradish peroxidase (HRP) enzyme decreased after enzyme immobilization at 208 and 222 nm. This fact may imply a conformational transformation in the structure of enzymes on HNTs.

The relative structure percentage of HNTs-P at 216 nm were found to be approximately 83% and respectively. The relative structure percentage of the immobilized palatase on the HNTs showed slight change, indicating that the secondary structure of the enzyme was mostly preserved (Verma et al., 2013). This preservation of the secondary structure demonstrated that the HNTs-P retained most of enzyme's catalytic activity before immobilization. These results suggested that the HNTs-P exhibited a higher stability, as the structural integrity of the enzyme was maintained. Not

only immobilization but also the presence of many substances in the environment can cause changes in the conformational structure of the enzyme. Hou et al. (2020) studied the conformational change of protein tyrosine phosphatase in the presence of sodium dodecyl sulfate (SDS). They reported that the peak at 222 nm in CD data exhibited an increase with the progressive rise in SDS concentration from 0 to 0.7 mM. Consequently, the presence of PAEs in the environment can also make changes in the secondary structure of the enzymes before or after immobilization in implication of induced active site when the substrates bind.

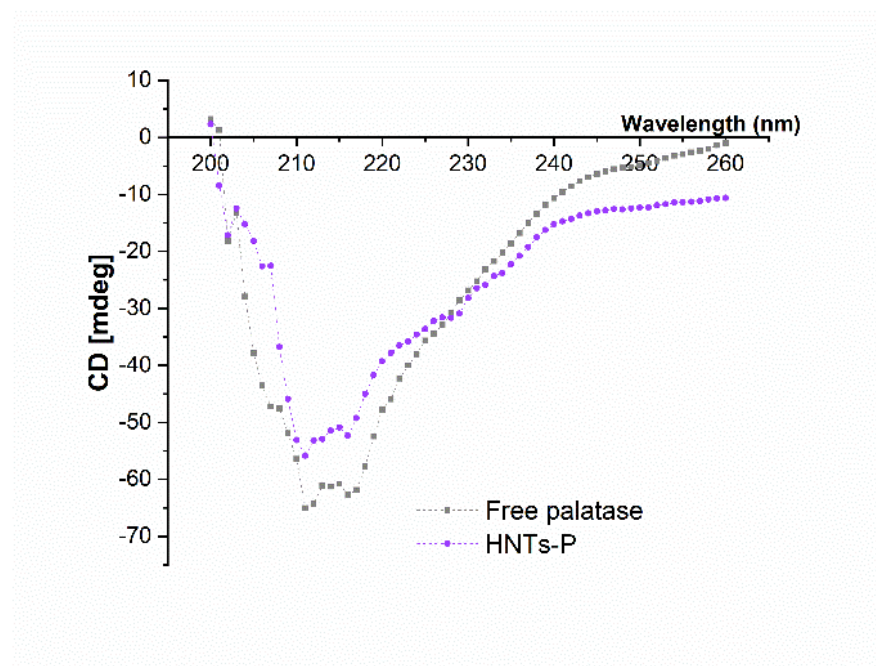


Figure 3.2. CD spectra of free palatase and HNTs-P composite.

3.3.4. Stability test assays

3.3.4.1. Temperature stability

The thermal stability of both free palatase and HNTs-P was evaluated at various temperatures ranging from 20°C to 70°C (Figure C.3). The response of free palatase and HNTs-P to heat exposure exhibited noticeable differences. At temperatures above 40°C,

free palatase activity was greatly reduced compared to HNTs-P due to enzyme denaturation. As the temperature increased, the HNTs-P composite experienced a 10.7% reduction in activity at 70°C, whereas the free palatase only retained approximately 40.3% of initial activity at the same temperature. It is noteworthy that when compared to free esterase (Balci et al., 2023), free palatase can still maintain some of its activity at high temperatures. The optimal temperature of palatase was 40°C as specified by the manufacturer. The immobilization of the enzyme results in improved thermal stability at higher temperatures due to the enhanced rigidity achieved during immobilization. This can avoid conformational changes in the enzyme structure (Hartmeier, 1988; Zhai et al., 2010). This property of immobilized enzymes makes them promising for use in various industrial applications (Hu et al., 2007).

3.3.4.2. Storage stability test

The activities of free palatase and HNTs-P after a 14-day storage period at 4°C has revealed that the immobilization process has improved the stability of the enzyme. The findings of the storage stability test at 4°C are depicted in Figure C.4. After the 14-day storage period, although the free palatase experienced a decline of 78% in its original activity, HNTs-P maintained 95% of its initial activity. The results indicated that the immobilization enhanced the stability of palatase, leading to a prolonged duration of activity. Zhai et al. (2010) reported that HNTs with urease and α -amylase maintained 90% and 94% of their original activities, respectively, even after being stored for 15 days. Similarly, Wang et al. (2015a) conducted a study on immobilized lipase on HNTs and found that it maintained over 80% of its initial activity after 14 days of storage, while the free lipase lost nearly all of its initial activity during the same time period. Balci et al. (2023) immobilized *Bacillus subtilis* esterase on HNTs and reported that the immobilized esterase retained nearly 80% of its initial activity at the end of 14 days-storage. These findings highlight that HNTs provide a favorable environment for immobilized enzymes which leads to a substantial improvement in their storage stability.

3.3.4.3. pH stability test

The effect of various buffer pH values on the enzyme activity of both free palatase and HNTs-P can be seen in Figure C.5. The activity curves of both the free palatase and HNTs-P at different pH values exhibited similarities. The maximum values of relative activity for free palatase and HNTs-P were obtained at pH 7. The enzyme activity of HNTs-P declined as the pH values deviated from the optimum range. However, this reduction was more pronounced in the case of free enzymes. When the pH value was increased to over 7, a decrease in enzyme activity was observed for both free palatase and HNTs-P. However, this decrease is relatively minor compared to the reductions observed at lower pH values. The optimal pH range for palatase specified by the manufacturer company was between 7 and 10. It is obvious that the immobilization of palatase on HNTs improved the stability of the enzymes against pH changes (Figure C.5).

3.3.5. DBP degradation by free palatase and HNTs-P composites

The degradation assays using free palatase were conducted under optimal conditions. Palatase was able to completely degrade DEHP (100 mg/L) within 15 min at 40°C, while it could degrade 95.2 ± 0.7% of DBP (100 mg/L) for same duration. Sun et al. (2022b) studied DEHP degradation at 5 mg/L concentration in the presence of lipase and reported that the lipase enzyme could be degraded %94.8 of DEHP at within 3 h. This variability is attributed to the substrate specificities of lipase and esterase enzymes. When lipase exhibits a higher substrate specificity on long-chain PAEs such as DEHP, esterase is effective on short and medium-chain PAEs. The performance of HNTs-P was investigated during continuous degradation cycles. HNTs-P also exhibited a good degradation ability with high DBP and DEHP concentration (100 mg/L) in long degradation cycles. The results indicated that the HNTs-P was able to degrade to all DBP and DEHP within 1st cycle (Figure 3.3). At the end of the 7th cycle, HNTs-P was able to degrade 63.3% of DBP and 72.8% of DEHP. The gradual deterioration of a portion of the enzyme structure over the continuous cycle had an impact on the activity of the HNTs-P. This observation suggests that HNTs-P maintained a relatively stable degradation

efficiency through continuous cycles and exhibited good reusability in DBP and DEHP degradation without losing all its characteristic properties. This can be attributed the biocompatibility between HNT and palatase. Dulazi and Liu (2011) studied the immobilization of lipase enzyme to chitosan beads with EDC activation and subsequently, they used the beads with the enzyme to degrade DBP and DEHP at 15 mg/L. The immobilized enzyme was able to degrade 55.2% of DBP and %100 of DEHP. Sungkeeree et al. (2017) reported that an immobilized esterase enzyme (from *Sphingobium* sp. SM42) on amine-functionalized supports was able to degrade 99% of 10 mM DBP and 30% of 100 mM DBP within 18 h. Sun et al. (2022a) performed a study on the DBP (1 mg/L) degradation by using of lipase and esterase in water. At the end of 48 h the esterase almost entirely degraded DBP while the lipase was achieved a DBP degradation rate of 95.9%. It is clear that both enzymes exhibit significant selectivity in catalytically degrading PAE congeners with diverse substituent groups.

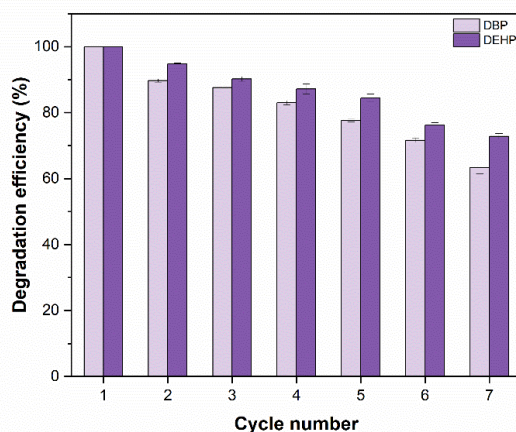


Figure 3.3. DBP/DEHP degradation efficiency in the presence of HNTs-P composite.

Unlike free palatase, the HNTs-P was separated from the reaction mixture and reused in subsequent degradation cycles. HNTs-P's relative activity and mass percentage were assessed once again following each degradation cycle (data not shown). Its mass percentage at the 3rd and 7th cycles of DBP degradation experiment was 76% and 53%, respectively. As for the same cycles of DEHP degradation experiment, it was 78% and 56%, respectively. This indicated that following the 7-cycle degradation experiments, approximately 55% of the enzymes from both HNTs-P were released. The HNTs-P had

75% of its original activity after the 3rd cycle of DBP degradation but experienced a decline, losing 63% of its initial activity by the end of the 7th cycle. As for HNTs-P, it retained 66% of its initial activity after the 7th cycle of DEHP degradation. This reduction in activity could be ascribed to the accumulation of metabolites that covered the enzyme, potentially affecting subsequent degradation cycles, as reported by Zhai et al. (2013).

3.3.6. Degradation metabolites

The metabolites produced during DBP and DEHP degradation by palatase enzyme (Figure 3.4.) and the compound ratios obtained through mass spectrometry were verified against those of the same compounds reported in the literature and LC-MS analysis was carried out for detection.

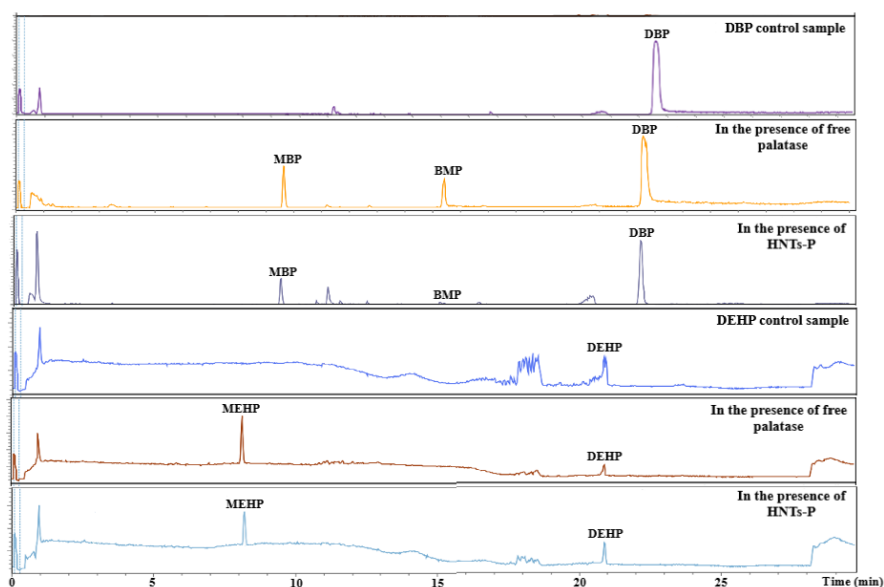


Figure 3.4. LC-MS chromatograms of the samples before and after DBP/DEHP degradation experiment in the presence free palatase and HNTs-P.

DBP and DEHP solution without the addition of any enzymes was employed as a control sample. DBP and DEHP exhibited a retention time of 22.6 and 20.9 min,

respectively. The MS spectrum was generated through the fragmentation of the molecular ions that were protonated under positive electrospray ionization. The resulting DBP and DEHP fragment ions were identified at m/z 279.15 and 391.28, respectively. At the end of the degradation experiments conducted by using free palatase and HNTs-P, new peaks appeared along with DBP and DEHP. The MS spectra of the newly formed peaks were obtained through the fragmentation of the protonated molecular ions under negative electrospray ionization.

PAEs tend to undergo hydrolysis by two enzymes (esterase and lipase), resulting in the formation of the respective mono-phthalate esters (MPEs) and PA (Sun et al., 2022a). Subsequently, the mineralization process concludes with the degradation of PA and CO_2 , and/or CH_4 by microorganisms. The DBP degradation experiments resulted in the formation of monobutyl phthalate (MBP; m/z 163.0388; RT 6.9 min), butyl methyl phthalate (BMP; m/z 259.039; RT 15.4 min) through a transesterification reaction in the presence of methanol (Kim and Lee, 2005; Ahn et al., 2006; Kumar et al., 2017; Balci et al., 2023). Numerous studies have reported PA as a metabolite (Saito et al., 2010; Dulazi and Liu, 2011) as a result of the de-esterification of PMEs. Phthalic anhydride, DMP, MBP, and BMP were detected as the metabolite of DBP in the presence of methanol in degradation experiments conducted using free esterase (Balci et al., 2023). Compared with these findings, there were only MBP and BMP in the presence of free palatase. The degradation metabolites of DBP in the presence of free palatase were the same as those in the presence of HNTs-P. The metabolites that emerge as a result of the degradation of DEHP were monoethyl hexyl phthalate (MEHP) and PA (Saito et al., 2010; Nahurira et al., 2017; Yang et al., 2018; Lamraoui et al., 2020). As can be seen from Figure 3.4, the palatase converted DEHP to MEHP (m/z : 277; RT 8.3 min). PA metabolite was not found in the presence of free palatase and HNTs-P. It might be connected to the steric hinderance of MEHP, which has carboxyl groups that prevent the enzyme from binding to the substrate (Liang et al., 2008; Singh et al., 2017). In other words, MEHP's side ester chain interferes with the hydrolytic enzyme's ability to connect to it. As a result, MEHP's hydrolysis reaction is blocked. This fact suggested palatase enzyme could not catalyze the hydrolysis of PME into phthalic anhydride. Balci et al. (2022) underlined that *Bacillus subtilis* esterase degraded DBP and DEHP to PA. Hence, it is likely that a prolonged degradation time might be necessary compared to the research findings in the presence of esterase enzyme. Consequently, degradation mechanism of PAEs begins in the presence

of palatase. Different hydrolase enzymes and microorganisms may take part to complete the final mechanism of PAEs degradation (Staples et al., 1997).

There were discrepancies in the peak areas of metabolites observed in the presence of free palatase and HNTs-P (Figure 3.4). It is reported that PAEs and their metabolites have a tendency to be adsorbed into the support materials (Dulazi and Liu, 2011). The adsorption of some PAE metabolites onto the HNTs-P could be reason for a lower intensity of the peak area.

The group of enzymes that have the ability to break down ester bonds in side chains, such as esterase, phthalate ester hydrolase, and lipase, can be categorized into three distinct groups (I, II, and III) based on their properties of hydrolyzing ester bonds (Song et al., 2022). The group-I enzymes have the ability to transform PAEs into MPEs while the group-II enzymes can convert MPEs into PA. The group-III enzymes are able to convert PAEs into PA, giving them a distinct advantage over the other two groups (Song et al., 2022). However, these group-III enzymes are still not widely available in significant quantities (Xu et al., 2021). *Bacillus subtilis* esterase degraded DBP to phthalic anhydride (Balci et al., 2023) while palatase enzyme was able to degrade DBP to MBP and BMP. In accordance with all this information, *Bacillus subtilis* esterase can be included in the group-III enzymes, while palatase can be included in the group-I enzyme.

3.4. Conclusion

The study investigated the DBP and DEHP degradation capability of *R. miehei* lipase (palatase) with free and immobilized forms for potential environmental applications by considering the substrate specificity, amino acid chain, and degradation products. Palatase was immobilized to HNTs and formed HNTs-P composites showed a high DBP and DEHP degrading ability during long cycles, indicating the stability and effectiveness of the composite.

Palatase has the ability to degrade DBP and DEHP in a short time. There is a difference between the PAEs degradation end products in the presence of palatase. This can be attributed to the fact that variability stems from differences in substrate specificities, active site structures, and binding pocket shapes, which collectively impact

their interactions and degradation capabilities towards specific compounds. Despite this, the palatase is very effective in the hydrolyzation of ester bonds that causes the toxicity of PAEs and converts PAEs into PMEs.

After immobilization, the enzymes retained their secondary structure significantly. The analysis of the CD spectra proved that the immobilized enzyme retained its structural integrity and maintained a high catalytic activity compared to the free enzyme. This observation suggested that the immobilized enzymes exhibited a higher stability since the secondary structure of the enzyme was mostly maintained, which is a promising outcome. This indicates that the immobilization of the enzymes onto HNTs may be a viable approach to enhance the stability and catalytic performance of the enzymes, potentially making it suitable for practical applications in various environmental remediation processes.

CHAPTER 4

CONTINUOUS TREATMENT OF DIETHYLHEXYL AND DIBUTYL PHTHALATES BY FIXED-BED REACTOR: COMPARISON OF TWO ESTERASE BIONANOCOMPOSITES

4.1. Introduction

Phthalic acid esters (PAEs) are one of the widely used synthetic chemicals in the plastic industry to supply the needs of modern society. Increasing demand for plastics has led to a significant increase in the global production of PAEs around the world. Today, PAEs have an annual production volume of over 80 million metric tons in the world (Weizhen et al., 2020). Owing to the fact that they do not have any covalent bond to the plastic matrix, they can be released into the environment during their manufacturing, use, and disposal. Once released, they reach almost all environmental media through geochemical processes, subsequently degrade very slowly under natural conditions, and lastly accumulate in the air surface water, wastewater, sediment, soil, sewage sludge, and biota over time (Clark et al., 2003; Das et al., 2014). Dibutyl phthalate (DBP) and Diethylhexyl phthalate (DEHP) are among the most abundant PAEs detected in the environment (Gao et al., 2020). They exhibit mutagenic, and carcinogenic properties even at low concentrations. Due to their high production volume, widespread distribution, and possible toxic effects, DBP and DEHP have been declared environmental priority pollutants by the United States Environmental Protection Agency (USEPA) and the European Union (EU). Besides, some nations in the EU and United States of America have limited or prohibited their production and use. Therefore, the efficient removal of

This chapter has been published as:

Balci, E., Rosales, E., Pazos, M., Sofuoglu, A., Sanroman, M.A. 2022. Continuous treatment of diethyl hexyl phthalates and dibutyl phthalates by fixed-bed reactor: Comparison of two esterase bionanocomposites. *Bioresource Technology*, 263, 127990.

DBP and DEHP in the contaminated environment is great of importance. Various methods such as biodegradation and physical-chemical methods (photolysis, chemical hydrolysis, and oxidation) have been used to degrade DBP and DEHP in the environment. The biodegradation process has a major role in the removal of these pollutants. This is because it is a faster process than photolysis and hydrolysis, and results in innocuous end products. Biodegradation studies on PAEs comprise not only using bacterial strains but also using enzymes from these bacterial strains. Earlier reports also revealed that esterase is a major enzyme that acts on the ester bonds in the structure of PAEs. The esterase from *Bacillus sp.* (Niazi et al., 2001) and the esterase from *Bacillus sp.* K91 (Ding et al., 2015) were reported to be highly effective to degrade PAEs. Saito et al. (2010) underlined that pancreatic cholesterol esterase enzymes (50 U) completely degraded DBP and DEHP (5 μmol) within 15 min. Sun et al. (2022a) reported that carboxyl esterase (0.1 U) was able to degrade more than 90% of DBP and DEHP (1 mg/L) in an aqueous solution within 288 h. The esterase appeared capable of degrading PAEs to their corresponding monoester and phthalic acid (PA) (Ding et al., 2015; Saito et al., 2010). Although there is information in the literature on the degradation of PAEs in the presence of the esterase enzyme obtained from various sources, no study was found on the use of the enzyme obtained from *Bacillus subtilis* in the degradation studies of PAEs.

Immobilization on a support material increases the stability and half-life of the enzyme and improves the resistance of the enzyme to changing environmental conditions such as pH, and temperature (Handayani et al., 2012; Wei, et al., 2022). Enzymes can be bound by a support material using various immobilization methods such as adsorption, crosslinking, encapsulation, and entrapment. Among these methods, crosslinking is a very useful and preferable immobilization method. This is because it has various advantages over the stability and retention rate of enzyme on support. Furthermore, the leakage of enzyme on support is low level. In enzyme immobilization, different support materials such as chitosan (Dulazi and Liu, 2011; Olshansky et al., 2018), alginate (Ramsay et al., 2005), silica (Chen and Lin, 2007) as well as alumina are used. Support materials must be water-insoluble and must have thermal, mechanical, and chemical stability as well as resistance to microbial attack. At the same time, these materials must be low cost and must have biodegradability to harmless products. Among many supports, chitosan (CTS) and alginate (ALG) are the materials of interest in enzyme immobilization due to their wide availability and having most of the above-mentioned properties (Choo et al., 2016; Hurmuzlu et al., 2021). Furthermore, the reactive amino and hydroxyl groups of CTS that

are effective on enzyme binding reactions provide a higher protein loading and higher activity (Hung et al., 2003; Dulazi and Liu, 2011). However, it needs to improve its mechanical properties before an immobilization study (Peng et al., 2015; Choo et al., 2016). As for ALG, its use can be limited in various applications due to its swelling and degradation behavior in the water (Bhagyaraj and Krupa, 2020). To be used in many applications, it is necessary to minimize its swelling and improve its mechanical properties, that is, to extend its service life (Bhagyaraj and Krupa, 2020). It is possible to form composite beads with the addition of nano clay, carbon nanotubes (CNTs), and titanium dioxide to reinforce the mechanical properties of CTS and ALG. Among these materials, CNTs exhibit the potential to enhance the mechanical properties of support material. However, there are no studies about the esterase immobilization on CTS-HNT and ALG-HNT beads and their capability for the degradation of PAEs.

In this study, the main focus is the continuous degradation of DBP and DEHP by two bionanocomposites based on CTS-HNT and ALG-HNT beads. For this purpose, the amount of esterase immobilized on both bionanocomposites was analyzed, the enzyme immobilization efficiency and stability were compared, and the feasibility of systems was tested by DBP and DEHP degradation in fixed-bed reactors operating in continuous mode.

4.2. Material and method

4.2.1. Materials

Pure HNT powder was provided by Esan, Eczacibasi Industrial Raw Materials Company (Istanbul, Turkey). Chitosan from crab shells, Bovine Serum Albumin (BSA), and Glutaraldehyde (GTA) were supplied from Sigma-Aldrich (USA). Sodium Alginate was purchased from Quimipur, S.L.U. All other chemicals were of laboratory reagent grade and used without further purification. Esterase from *Bacillus subtilis* was obtained from Sigma-Aldrich. Before the immobilization study, HNT and CTS were dried in a

vacuum oven at 100 °C and 40 °C, respectively to eliminate their moisture content and to make them ready for use. The esterase was stored at -20 °C until its use.

4.2.2. Immobilization study

4.2.2.1. Preparation of chitosan-halloysite beads

CTS-HNT beads were prepared with minor modifications to the previous studies (Choo et al., 2016; Hurmuzlu et al., 2021). Briefly, the procedure is described as follows: Firstly, 2 g of CTS were dissolved in 100 mL acetic acid solution (2.5%, v/v). The mixture was stirred magnetically for 24 h at room temperature. Then 1 g of HNT was added to the CTS solution and mixed for 24 h. Following this, the solution was sonicated for 1 h at ambient temperature to obtain a homogenous dispersion of CTS-HNT. The resultant solution was pumped into 125 mL of deionized water containing 15 g NaOH and 25 mL of 95% ethanol through a needle (diameter 1.2 mm) at a flow rate of 1 mL/min under stirring. Thereafter, the CTS-HNT spheres were formed instantaneously and washed with deionized water until neutral pH was reached. Subsequently, the beads were kept at -20 °C in the fridge overnight and then dried using a freeze dryer (lyophilizer) under vacuum conditions for 24 h at -50 °C (Telstar Cryodos).

4.2.2.2. Preparation of alginate-halloysite beads

3 g of sodium alginate were dissolved in 100 mL at 25 °C by mechanically stirring. 0.5 g of HNT was added to the sodium alginate solution. The solution was mixed until HNT was dispersed in an alginate solution at 300 rpm. After that, it was placed in an ultrasonicator for 1 h at room temperature. The obtained solution was dropped at a flow rate of 1mL/min into calcium chloride solution (1 M) through a syringe needle with a diameter of 1.2 mm under continuous stirring. The calcium chloride solution was kept at

4 °C before its use. The formed beads were taken from the solution and then washed with deionized water several times until the pH of the beads became neutral. Lastly, ALG-HNT beads were stored at -20 °C and then dried using a freeze dryer under vacuum conditions for 24 h at -108 °C. The dried CTS-HNT and ALG-HNT beads were stored until further use.

4.2.2.3. Immobilization of esterase on chitosan-halloysite and alginate-halloysite beads

In this study, GTA was used as a crosslinking agent to immobilize the esterase enzyme on the beads. In previous studies, the amount of GTA in the solution required for the enzyme immobilization on beads has been used in the range of 0.072 mL (0.15%) and 0.36 mL (0.75%) and the optimal amount of GTA was determined to be 0.072 mL in the solution for 0.4 g of beads (Mondal et al., 2015). To prepare the crosslinked beads with GTA, 0.15% GTA solution (v/v) was added to 0.4 g of each bead (Mondal et al., 2015). To prepare the crosslinked beads with mixed for 4 h at 25 °C and 150 rpm in an incubator shaker. To remove the non-crosslinked agent with beads, the beads were rinsed with deionized water three times. Thereafter, 1 mL of the enzyme (2 mg/mL) was added to the crosslinked beads and mixed on a test tube shaker at 25 °C, 80 rpm for 1 h. At the end of this period, the beads were filtered and washed with deionized water three times to remove the unbounded enzyme. After the immobilization process, the supernatant and washing solution was kept at 4 °C to determine the enzyme immobilization efficiency.

As a result of these procedures, two different bionanocomposites were synthesized: CTS-HNT-EST and ALG-HNT-EST.

4.2.3. Protein determination

To determine the protein concentration of free and beads immobilized enzyme, the Bradford method was implemented. Firstly, a standard curve was created using Bio-Rad

dye reagent and BSA as model protein. The absorbance of the solutions was measured using a UV-Visible spectrophotometer (Genesys-150) at the wavelength of 595 nm (Bradford, 1976). The protein concentration in the solutions was estimated using a calibration curve. Then, the amount of immobilized enzyme on the beads was calculated according to the mass balance. Immobilization efficiency (Imm. eff. (%)) and enzyme loading amount (Load. amt (mg/mg)) were calculated using the following equations (4.1-4.2).

$$\text{Im eff.} = \frac{\text{Initial protein amount} - (\text{protein amount in the supernatant} + \text{washing solution})}{\text{Initial protein amount}} \times 100 \quad (4.1)$$

$$\text{Load. amt} = \frac{\text{Initial protein amount} - (\text{protein amount in the supernatant} + \text{washing solution})}{\text{mass of HNT}} \quad (4.2)$$

4.2.4. Enzyme activity assay

The enzyme activity of free and immobilized esterase was determined spectrophotometrically by hydrolysis of 4-nitrophenyl acetate (pNPC-2) according to Tekedar and Sanli-Mohamed (2011). For free esterase, the assay mixture (1 mL) consisted of 0.8 mL phosphate buffer (100 mM, pH=7), 0.1 mL of 0.5 mM pNPC-2 dissolved in acetonitrile, and 0.1 mL of free enzyme solution (1 mg/mL). The activity of the immobilized enzyme was determined according to the activity measurement of the free enzyme. Instead of free enzyme solution, 0.1 mL of supernatant and/or washing solution was added to assay mixture. Then, the assay mixture was incubated at optimum temperature for 5 min and initial rates were estimated by measuring the increase in absorbance at 400 nm as a function of time. The activity of the immobilized enzyme was determined depending on the calculated activity of the free enzyme. The enzyme activity (U/L) was calculated according to the following equation (4.3).

$$\text{Enzyme activity (U/L)} = \frac{(\text{Absorbance at 400 nm}) \cdot (V_t) \cdot (DF)}{(t) \cdot (\epsilon) \cdot (V_e) \cdot (d)} \quad (4.3)$$

Vt: total sample volume (mL), DF: Dilution factor, t: reaction time, ϵ : paranitrophenol molar extinction coefficient at 400 nm ($17,215 \text{ M}^{-1} \cdot \text{cm}^{-1}$), Ve: enzyme volume (mL), d: light path (1 cm).

Besides, after each day of degradation experiments, the activity of the immobilized enzyme was measured and then expressed as relative activity (He et al., 2015).

4.2.5. Material characterization

Before and after enzyme immobilization, HNT, CTS-HNT, and ALG-HNT were structurally characterized by Scanning Electron Microscopy (SEM), Transmission Electron Microscopy (TEM), Fourier Transform Infrared Spectroscopy (FT-IR). To investigate the thermal resistance of these materials, a Thermogravimetric Analysis (TGA) was conducted. These analyses were done by the external services of CACTI (University of Vigo).

4.2.5.1. Scanning Electron Microscopy analysis

The microstructure of pure HNT, CTS-HNT, and ALG-HNT beads and the beads with esterase was examined using an FEI QUANTA 250 FEG Scanning Electron Microscopy (SEM) instrument equipped secondary detector. Before SEM analysis, the samples were dried, and their surface was coated with gold in argon to eliminate the charging of the beam.

4.2.5.2. Transmission Electron Microscopy analysis

The morphological properties of HNT, CTS-HNT, and ALG-HNT beads were investigated using a MICRO JEOL JEM 1010 Transmission electron microscopy (TEM) with an accelerating voltage of 200 kV. Before TEM analysis, both HNT and the beads

with HNT were dispersed in ethanol solution using an ultrasonic bath. Subsequently, a drop of each dispersion was deposited on a 400-mesh carbon-coated copper grid. The sample grids were kept at room temperature to evaporate ethanol.

4.2.5.3. Fourier-Transform Infrared spectroscopy analysis

Before FTIR analysis, the samples were mixed with potassium bromide (KBr) and pelletized. FT-IR spectra of HNT, CTS-HNT, ALG-HNT, CTS-HNT with esterase, and ALG-HNT with esterase were recorded on a JASCO FT-IR 4100 spectrometer (Jasco Inc., Easton, MD, USA) to examine functional groups. All spectra were scanned in the range of 4000-400 cm^{-1} at a resolution of 2 cm^{-1} .

4.2.5.4. Thermogravimetric analysis

The thermal behavior of CTS-HNT with esterase and ALG-HNT with esterase was investigated using a Seteram thermogravimetric analyzer a temperature range that started at the room temperature and ended at 800°C at a heating rate of 10 °C/min under nitrogen atmosphere (20 mL/min).

4.2.6. Degradation assay

4.2.6.1. Assays with free esterase

For the experiment on DBP and DEHP (100 mg/L) degradation, a reaction mixture (1 mL) containing 0.1 mL of free esterase solution (1 mg/mL), 0.1 mL of DBP/DEHP (1000 mg/L) in DMSO, 0.1 mL of Tween 80 (1%, v/v) and 0.7 mL of phosphate buffer

(0.5 mM, pH=7) was prepared. Tween 80 was used as a solubility agent to increase the solubility of DBP and DEHP in the solution. Under optimum conditions, the samples containing the reaction mixture were incubated at certain time intervals for 1 h and subsequently were collected. All samples were filtrated with a 0.22 μm PTFE syringe filter to remove particulate material from the samples before HPLC analysis. Subsequently, 1 M HCL (10% v/v) was added to the samples to stop the enzymatic reaction and the samples were stored at 4 °C until the analysis.

4.2.6.2. Assays with bionanocomposites

Enzymatic experiments were conducted in two column systems filled with CTS-HNT-EST and ALG-HNT-EST. 0.4 g of beads containing esterase were placed in the column. Initially, the batch experiments were performed by filling the column with DBP or DEHP solution with an initial concentration of 100 mg/L.

For the continuous process, the systems were fed with the DBP solution with a concentration of 100 mg/L under different volumetric flows (0.015-0.045 mL/min). After DBP degradation experiments were completed using each bead with esterase, DEHP degradation experiments were performed under the same conditions. During continuous operation, samples were collected in the system to determine the enzyme and pollutants concentration. All samples were filtered through a 0.22 μm PTFE syringe filter to remove particulate material prior to High-Performance Liquid Chromatography (HPLC) analysis. To terminate the enzymatic reaction, 1 M HCL (10%, v/v) was added to the samples, which were then stored at 4 °C in a fridge.

4.2.6.3. Analysis of PAEs and their metabolites

After degradation experiments, the quantification of DBP and DEHP was analyzed under a reversed-phase using HPLC Agilent 1260 Infinity connected to a DAD equipped with ZORBAX Eclipse XDB C-8 column (5 μm particle size, 150 mm x 4.6 mm i.d.).

The mobile phase consisting of acetonitrile:water (60:40, v/v) was used at a flow rate of 1 mL/min for DBP analysis. As for DEHP analysis, the mobile phase composition (acetonitrile:water) in gradient elution was varied over time as follows: 0 to 3 min 80:20, 3 to 9 min 95:5, 9 to 12 min 100:0, 12 to 22 min 80:20 and the flow rate was set at 0.5 mL/min. For each injection, the volume taken from samples in DBP and DEHP analysis was 20 μ L and 10 μ L, respectively. The analysis was carried out together with a UV detector (224 nm) at room temperature. DBP and DEHP degradation metabolites were identified using a Bruker Elute LC system connected to a Trapped Ion-Mobility Spectrometry Time-of-Flight Mass Spectrometer (TIMS-TOF-MS) (Bruker Daltonics, Bremen Germany). Ionization was performed using electrospray (ES) source with a voltage of 3.5 kV applied to the needle and endplate offset of 500 V. Using both positive and negative scan modes, ES spectral data was obtained. The data were obtained using Bruker Otof Control Software version 5.1 and processed with the Data analysis software version 5.1 from Bruker Daltonics.

4.3. Results and Discussion

4.3.1. Assays with free enzymes

4.3.1.1. Effect of the operational condition on the esterase activity

In this study, an esterase obtained from *Bacillus subtilis* was selected to evaluate its efficiency in the removal of PAEs. Although it is a mesophilic enzyme, the effect of temperature on the enzyme activity was measured in a wide temperature range from 20 °C to 70 °C and examined for a solution pH between 5 and 7.

As shown in Figure 4.1, the activity of the esterase increased with the temperature rising to 30 °C in the presence of pNPC-2 substrate. However, the increase above 40 °C caused a sharp decrease in the activity of the esterase. These results are in accordance with the reported in the literature where it is noted that temperature above 30 °C are likely

to cause a decrease in the activity of the enzyme (Fitter et al., 2001). Besides, the importance of pH on the enzyme activity was probed to be quite high at pH 7 compared to the more acidic investigated pH values. Therefore, the optimum temperature and pH for the esterase were determined to be 30 °C and 7, respectively. Once the optimal operational conditions were evaluated the degradation capacity of the enzyme for two different PAEs (DEHP and DBP) was studied.

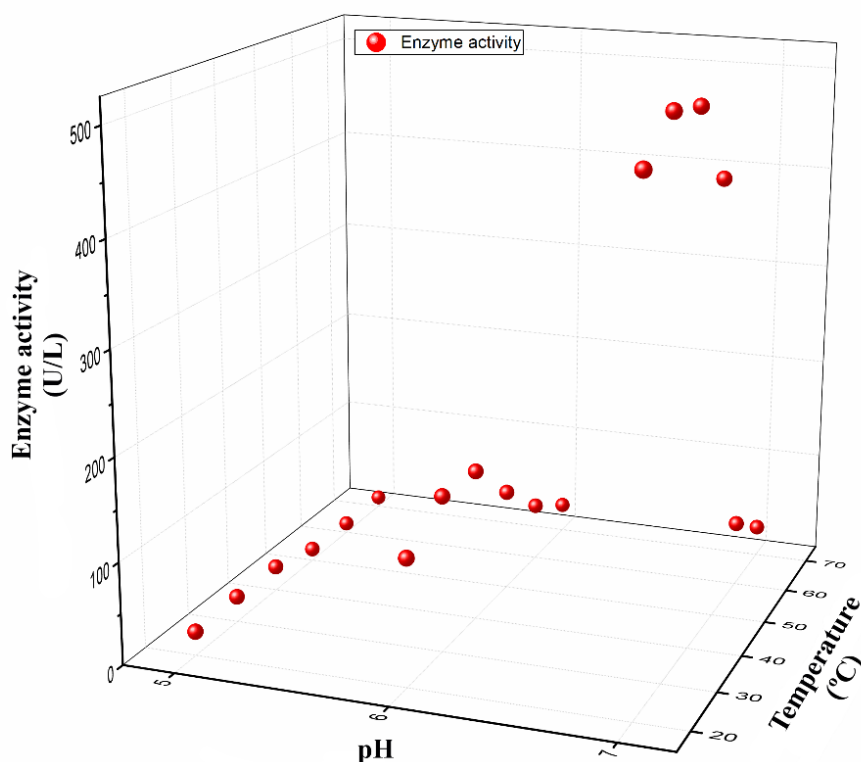


Figure 4.1. Esterase activity under different conditions.

4.3.1.2. Degradation assays

Enzymatic degradation experiments of DBP and DEHP (100 mg/L) were performed using free esterase enzyme (1 mg/mL) under optimum conditions. Figure 4.2. shows the change of DBP and DEHP concentration over time in presence of the esterase. While the esterase was able to completely degrade DBP for 15 min, it could not exhibit the same degradation ability on DEHP within same time. At the end of 15 min, DEHP

concentration was approximately 80.13 mg/L. It is apparent from Figure 4.2. that the free esterase can degrade DEHP more slowly. It is known that PAEs with lower molecular weight such as DBP are more easily degraded compared to those with high molecular weight such as DEHP (Dulazi and Liu, 2011). Zhang et al. (2014) conducted a study on the degradation of different PAEs types using the esterase enzyme obtained from *Sulfobacillus acidophilus* DSM10332. They reported that six PAEs (Diethyl phthalate (DEP), Dipropyl phthalate (DPrP), DBP, Dipentyl phthalate (DPeP), Dihexyl phthalate (DHP), and Benzyl butyl phthalate (BBP)) were completely degraded to their monoesters within 24 h, but two PAEs, namely DEHP and Dicyclohexyl (DCHP), could not be degraded in same period. Many studies have highlighted that the degradation rate of PAEs may decrease with the increase of the molecular weight (Ren et al., 2016). For this reason, the degradation of DEHP may take a longer time than that of DBP in this study. As can be seen from Figure 4.2, DEHP was completely degraded within 8 h in the presence of the esterase.

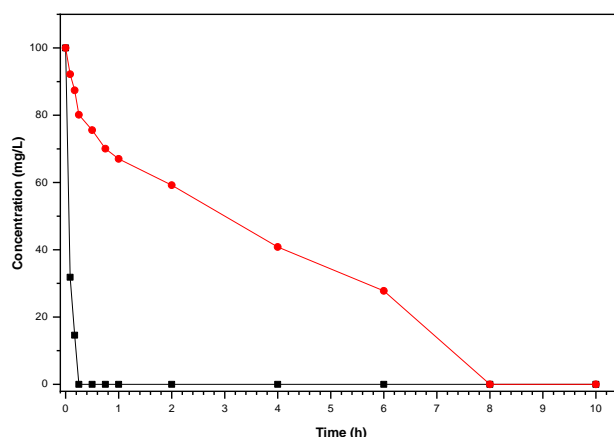


Figure 4.2. Time-dependent DBP (▪) and DEHP(•) concentration changes in the presence of free esterase (1 mg/mL).

4.3.2. Characterization of bionanocomposites

The free enzyme proved to be a viable alternative for the treatment of PAEs. However, the enzyme's resistance to changing environmental conditions and allowing its use in a continuous treatment system needs to be developed. This purpose can be achieved

by its immobilization in a suitable matrix. The immobilization of the enzyme in clay support such as HNT by crosslinking allows to achieve the anchoring of the enzyme, but for an application, in continuous treatment, the generation of a powder is discouraged by the operational problems generated in these treatment systems. Thus, the combination of the HNT with immobilized enzyme generating both CTS and ALG based beads was carried out. The enzyme immobilization efficiency of the esterase in CTS-HNT-EST and ALG-HNT-EST was evaluated attaining 89.2% and 95.2% efficiency (Eq. (1)) respectively. Moreover, the loss rate of enzyme activity in the immobilized process on CTS-HNT and ALG-HNT is 17.83% and 18.66%, respectively. The prepared bionanocomposites (CTS-HNT and ALG-HNT beads) were characterized in order to determine their morphological and chemical properties.

The three-dimensional tubular structure of pure HNT and its surface was recognized in the SEM images (Figure D.1a). The length of the HNT is not uniform and ranges from 0.4 to 1 μm . The diameter of HNT is more or less 30 nm and its outer surface is between 70 and 100 nm. Additionally, its average wall thickness is approximately 10 nm. SEM images of CTS-HNT and ALG-HNT beads (Figure D.2a-d) before and after enzyme immobilization at different magnifications show that the beads containing HNT have a rough, dense, and compact structure. Similar observations have been reported in previous studies (Zhai et al., 2013; Hurmuzlu et al., 2021). Zhai et al. (2013) underlined that after modification of HNT with CTS, the surface of the CTS-HNT composite is rougher than that of pure HNT. The roughness of the surface increases the enzyme immobilization efficiency when creating a new surface on material for enzymes (Zhai et al., 2013). HNT in the beads is not visible, however, it can be seen that HNT was covered by CTS and ALG, respectively. Esterase immobilized on CTS-HNT and ALG-HNT formed new regions by partially reducing the roughness on the surfaces of the beads. On the other hand, esterase immobilization changed the surface morphology of the beads. Consequently, this implies that enzyme immobilization has been successfully performed.

TEM images of the pure HNT revealed that the HNT has a hollow cylindrical structure with a transparent central area and two open ends (Figure D.1b). Before and after enzyme immobilization, TEM images of CTS-HNT and ALG-HNT beads were taken and the tube structure of HNT is visible on both beads (Figure D.2.e-h).

After enzyme immobilization, the presence of esterase is observed in TEM images of CTS-HNT and ALG-HNT beads. There is a slight increase in the outer diameter of the nanotubes in the beads with esterase. Zhai et al. (2013) stated that the HNT with enzyme

is rougher and thicker than pure HNT. This result shows that the enzyme is loaded on CTS-HNT and ALG-HNT beads.

The infrared spectrum of pure HNT shows the O-H stretching of water at 3696 cm^{-1} , and the OH deformation of water at 3625 cm^{-1} . The sharp peak at 1033 cm^{-1} originated from in-plane Si-O-Si stretching vibration (Luo et al., 2010). The peaks correspond to the deformation vibrations of inner surface hydroxyl groups at 910 cm^{-1} and 693 cm^{-1} . Besides, the peaks observed at 754 cm^{-1} and 540 cm^{-1} could be attributed to perpendicular stretching of Si-O and deformation of Al-O-Si, respectively (Luo et al., 2010). It can be observed that CTS-HNT samples (Figure D.3a) exhibited some new peaks at 1639 and 1650 cm^{-1} (amide I) and 1529 - 1535 cm^{-1} (amide II) compared to pure HNT. The amide I (1630 cm^{-1}) and amide II (1535 cm^{-1}) bands are the two most prominent vibrational bands of the protein backbone (Jang et al., 2015). In addition, the spectra of CTS-HNT composite samples appear to contain characteristic peaks of both HNT and CTS. These results demonstrate that HNT has been successfully combined with CTS in this study. With the addition of GTA to CTS-HNT beads, three prominent peaks of GTA (1708 , 1654 , and 1562 cm^{-1}) are observed. After the immobilization of esterase, there is a small modification in the FT-IR spectrum of CTS-HNT-EST implying the immobilization of esterase.

The FT-IR spectrum of ALG (Figure D.3b) contains a broad band centered at approximately 3250 cm^{-1} due to the stretching of hydroxyl groups. The band at 2900 cm^{-1} is assigned to $-\text{CH}_2$ groups. The two peaks at 1610 cm^{-1} and 1417 cm^{-1} arise due to the asymmetric and symmetric stretching modes of carboxylate salt groups ($-\text{COONa}$), respectively. The vibrations in the range of 1200 cm^{-1} and 1000 cm^{-1} come from the glycoside bonds in the polysaccharide (C-O-C stretching). The spectrum of EST crosslinked on ALG-HNT beads indicated the characteristic peaks of ALG, HNT, and EST. After the immobilization of enzymes, the intensity of the peak attributed to the asymmetric stretching of carboxylate salt groups decreased. This result implies the esterase has been successfully immobilized on the ALG-HNT beads.

TGA results were determined for studying the degradation trend of the prepared beads (Figure D.4). The decomposition of protein under air flow shows a maximum mass loss between $300\text{ }^\circ\text{C}$ and $350\text{ }^\circ\text{C}$ (Duce et al., 2017). In addition, a shoulder is observed at $245\text{ }^\circ\text{C}$ due to the polypeptide chain thermal decomposition of esterase (Duce et al., 2013). At $450\text{ }^\circ\text{C}$ and $650\text{ }^\circ\text{C}$, esterase undergoes the decomposition of aggregates as well as the carbonizing and ashing of the hard residues of the protein (Duce et al., 2017).

Thermal degradation of CTS-HNT-EST and ALG-HNT-EST is observed in two stages. In the first stage, the thermal degradation of CTS-HNT-EST in the range of 25 °C and 100 °C is caused by the loss of the physically adsorbed water molecules (Lisuzzo et al., 2020). As for ALG-HNT-EST, the weight loss between 70 °C and 90 °C can be attributed to the evaporation of loosely bound moisture. In the second stage, while degradation of CTS-HNT-EST, vaporization and elimination of volatile compounds occurred between 170 °C and 500 °C (Hurmuzlu et al., 2021). The reduction of ALG-HNT-EST in the range of 190 °C-280 °C can be attributed to the evaporation of glycerol and the thermal degradation of biopolymer (Bhagyaraj and Krupa, 2020). As a result, the bionanocomposites obtained by immobilization of esterase on CTS-HNT and ALG-HNT beads significantly improved the thermal resistance of the enzyme.

4.3.3. Batch degradation assays with bionanocomposites

The use of enzymes on a large scale demands operational stability from the bionanocomposite as a key factor in the processes and also to decrease operational costs.

Based on the promising previous results, the ability of the bionanocomposites for the degradation of DBP was ascertained in a batch system and the attained results are shown in Figure 4.3. A significant difference between them suggests that the enzyme is more available when CTS-HNT-EST was used with complete removal of the pollutant in only 1 h. The process is slower in ALG-HNT-EST attaining less than 70% of removal after 4 h.

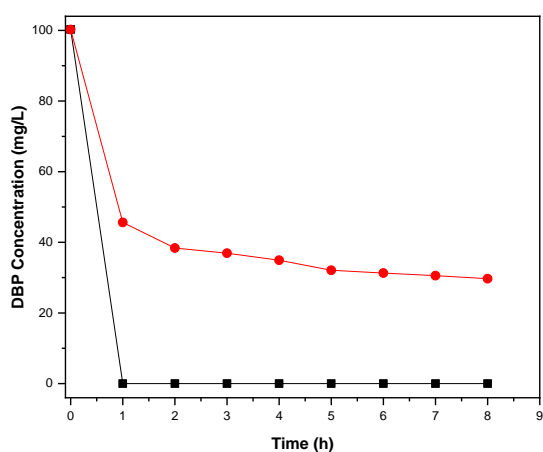
The good results achieved in the DBP degradation suggested that the system could be applied for the removal of a more complex compound such as DEHP and the study of the effect of the chain length in the biocomposites degradation of the pollutants was performed. According to the results, it can be assumed that a rapid degradation process occurs in the first hour, followed by a significant reduction in the degradation rate after the sixth hour. No complete degradation is achieved with any of the bionanocomposites, meaning that the length of the pollutant chain affects the treatment process. They present a higher degradation ability for PAEs with lower molecular weights. This is in accordance

with the reported in the literature by Dulazi and Liu (2011) who reported similar behavior for lipase immobilized in chitosan beads.

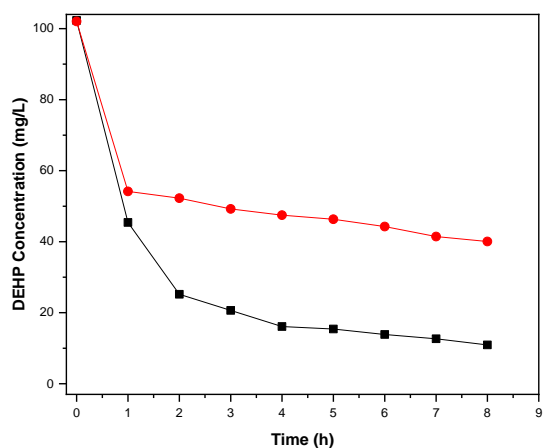
As conclusion from the batch assays, it can be suggested that there are two plausible mechanisms involved in the process: (i) direct degradation by the immobilized enzyme and (ii) the combination of adsorption and degradation in the process. For this reason, the possible generation of metabolites during the treatment process was ascertained confirming the degradation process is taking place.

The metabolites, generated during the degradation processes, were identified using LC-MS and the ratios of the compounds obtained by mass spectrometry were confirmed with the ratios of the same compounds in the literature (Figure D.5). DBP solution without enzyme was used as control sample in the analysis. Initially, DBP was identified and at the end of the degradation experiment in the presence of the esterase for 15 min. There was a signal showing the presence of phthalic anhydride ($C_8H_4O_3$), which is a product formed due to the dehydration of PA. According to the literature, it is known that the biodegradation mechanism of PAEs begins with the hydrolyzation of the ester bond in the presence of esterase. PAE is converted to its monoesters and then to PA and corresponding alcohol (Wang and Gu, 2016). Lastly, the mineralization mechanism ends with the decomposition of PA and CO_2 and/or CH_4 by microorganisms (Staples et al., 1997). Mono butyl phthalate (MBP), Dimethyl phthalate (DMP), and PA products have been also detected as intermediates in the actual degradation assays. Generally, butyl methyl phthalate (BMP), MBP, DMP, and PA are detected as the potential metabolites of DBP that occur via transesterification and/or de-esterification reaction in the presence of methanol (Kim and Lee, 2005; Ahn et al., 2006; Kumar et al., 2017). Kim and Lee (2005) conducted a study on the enzymatic degradation of DBP. They reported that BMP was the major metabolite to appear in DBP degradation conducted using the esterase. Fang et al. (2017) focused on the degradation of DBP using a bacterium (*Enterobacter* sp. T5) which was isolated from municipal solid waste. They underlined MBP and PA as major metabolites of DBP in the study. In a study by Fang et al. (2017), 1,2 benzenedicarboxylic acid, butyl methyl ester, DMP, and PA were among the metabolites detected as an indicator of DBP degradation. Wang et al. (2017) conducted a study on DBP degradation using a bacterial consortium (LV-1). They identified three major metabolites (MBP, monoethyl phthalate (MEP), and PA) at the end of DBP degradation experiments. In another study on DBP degradation, DBP was degraded to PA after the formation of MBP MEP, and monomethyl phthalate (MMP) (Ahuactzin-Perez et al., 2018). However, most

of the above-mentioned metabolites may not have appeared in this study due to the use of DMSO, an organic solvent to dissolve PAEs. This is because in the absence of methanol, PAEs undergo transformation only via the sequential hydrolysis of ester and the esterification of the carboxylic acid in the monoester forms does not occur (Okamoto et al., 2011). It is apparent from LC chromatograms that DBP was degraded to phthalic anhydride by esterase immobilized on CTS-HNT and ALG-HNT.



(a)



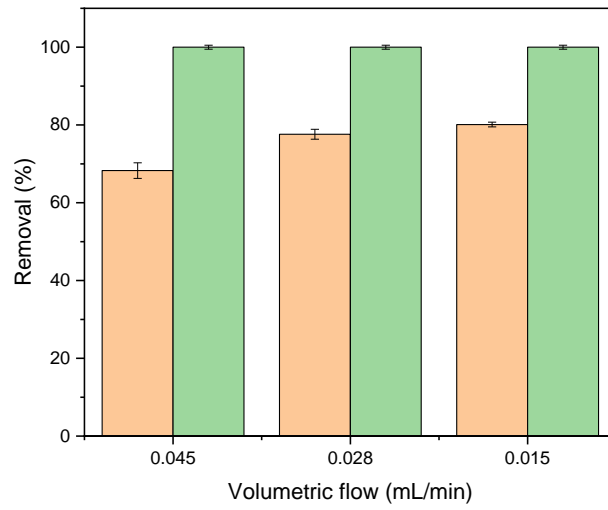
(b)

Figure 4.3. Profile of concentrations of (a) DBP and (b) DEHP in their degradation by CTS-HNT-EST (■) and ALG-HNT-EST (●).

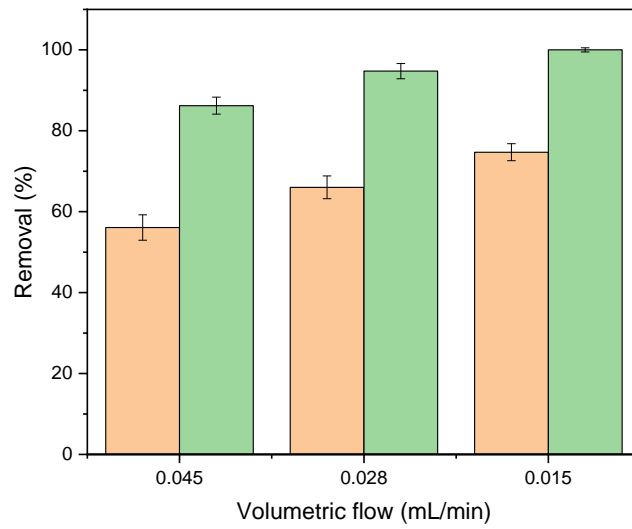
Phthalic anhydride that appeared in the presence of free esterase during DBP degradation was also found in the presence of the esterase immobilized on CTS-HNT and

ALG-HNT beads. These results demonstrate that both free esterase and immobilized esterase degraded DBP to phthalic anhydride and imply that after immobilization, the esterase has the potential to be used as an effective degrader in long cycles without losing all of its characteristics.

Similarly, DEHP as well as three degradation products, 1,3-isobenzofurandione (IBF), phthalic anhydride, and mono-2-ethylhexyl phthalate (MEHP), were identified when metabolites related to DEHP degradation were investigated. During this degradation process, DEHP was converted to IBF by diester hydrolysis. The formation of MEHP and PA was also reported as the result of enzymatic or bacterial degradation of DEHP (Saito et al., 2010). Besides, Fang et al. (2002) conducted a study on DEHP biodegradation using a bacterium (*Pseudomonas fluorescens* FS1) isolated from the activated sludge at a petrochemical factory. MEHP, benzene dicarboxylic acid, benzoic acid, and phenol were identified as the major metabolites of DEHP in the study. Yang et al. (2018) studied DEHP degradation using *Rhodococcus ruber* YC-YT1 and reported that DEHP was hydrolyzed to PA through the formation of MEHP. Subsequently, the bacterium converted PA to benzoic acid for cell proliferation in the study. DEHP metabolites which were defined based on the information compiled from the literature were also found in this study. The signal at 11.2 min observed in the chromatogram belongs to the polymer. When the chromatograms related to DBP and DEHP degradation are examined, the retention time of PA is different for each chromatogram. The reason for this is the use of different methods in LC-MS analysis of the two PAEs. While the immobilized esterase on CTS-HNT and ALG-HNT was able to degrade DEHP to phthalic anhydride, the free esterase enzyme was incubated in DEHP solution for 8 h, and it degraded DEHP to MEHP. It may be related to the steric hindrance of MEHP which has carboxyl groups inhibiting free enzymes to bind substrates (Liang et al., 2008). That is, the side chain of MEHP hampers the binding site of hydrolytic enzymes (Liang et al., 2008; Singh et al., 2017). Therefore, the hydrolysis of MEHP is hindered and thus the hydrolysis of MEHP is hindered and thus the hydrolysis reaction is inhibited. There are some studies where the steric hindrance near the ester bonds inhibits the rate of hydrolysis. Singh et al. (2017) studied DMP and DEHP degradation using *Arthrobacter* sp. C21. They reported that the degradation efficiency of DMP (99.5%) was higher than that of DEHP (51.4%) and underlined that this is due to the steric hindrance caused by the side ester chain of DEHP.



(a)



(b)

Figure 4.4. Pollutants removal of (a) DBP and (b) DEHP operating in continuous under different volumetric flows in the presence of the CTS-HNT-EST (green) and ALG-HNT-EST (brown).

4.3.4. Continuous degradation

Once the efficiency of the degradation of the pollutants and their mineralization has been proved, the proposed treatments have been evaluated in a continuous flow system

for the removal of both pollutants (DBP and DEHP).

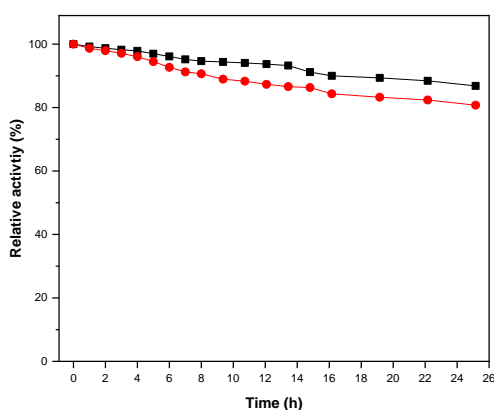
4.3.4.1. Dibutyl phthalate bionanocomposite degradation

Figure 4.4a shows the stationary DBP concentrations attained in continuous degradation experiments in the presence of the CTS-HNT-EST and ALG-HNT-EST bionanocomposites at different volumetric flows.

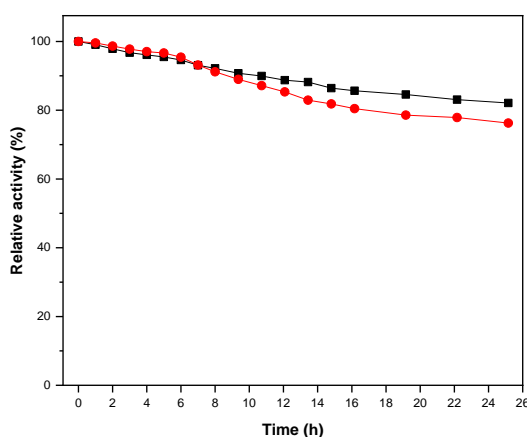
Operating at a flow rate of 0.045 mL/min, it can be observed that the alginate bionanocomposite reduced DBP significantly until values close to 30 mg/L. However, the selection of chitosan bionanocomposite led to the complete removal of DBP. This fact can be due to differences in the enzyme activity. The chitosan bionanocomposite resulted in a lower loss of activity and, thus, higher degradation capability in comparison with alginate composite (ALG-HNT-EST) which lost two-folds the relative activity. The reduction of the volumetric flow to 0.030 mL/min (led to an improvement in the efficiency of the removal with ALG-HNT-EST attaining a DBP concentration value of 21 mg/L and degradation level of around 80%. As can be expected according to the previous results, CTS-HNT-EST bionanocomposite was able to remove all the DBP. After the degradation tests were completed, it was observed that DBP was completely degraded in the presence of the CTS-HNT-EST bionanocomposite when the volumetric flask was still decreased (0.015 mL/min). However, no total degradation was detected for ALG-HNT-EST bionanocomposite with a concentration found to be 19.11 mg/L. This fact can be related to the enzymatic activity retained after the treatment. The degradation efficiency of DBP in the presence of ALG-HNT-EST at a flow rate of 0.045, 0.028, and 0.015 mL/min was 70%, 80%, and 81%, respectively. Thus, reducing the volumetric flow prolonged the contact time of DBP with bionanocomposites. This fact may be the reason for the increased degradation efficiency of DBP in column experiments.

Figure 4.5a shows the relative activity of the esterase crosslinked on the bionanocomposites. In all the evaluated flows, ALG-HNT-EST bionanocomposite presented a higher decrease in the enzyme activity with values 5% lower than the detected within CTS-HNT-EST bionanocomposite. At the end of the experiments, ALG-HNT-EST retained 79% of its initial activity while CTS-HNT-EST retained over 85% of its

initial activity indicating that they have good operational stability operating in a continuous way. The values are in good agreement with the reported by Tercan et al. (2021) in the esterase entrapment using chitosan/calcium/alginate-blended beads with more than 70% of the enzyme activity after three subsequent cycles. Yoo et al. (2020) also reported good operational stability (70%) by using crosslinked enzyme aggregate (CLEA) for twenty cycles. Accordingly, at the end of DBP degradation experiments, the enzyme mass (%) on CTS-HNT and ALG-HNT was found to be 86.48% and 80.2%, respectively.



(a)



(b)

Figure 4.5. (a) Relative activity of the esterase immobilized on CTS-HNT-EST (▪) and ALG-HNT-EST (•) during the DBP degradation. (b) Relative activity of the esterase immobilized on CTS-HNT-EST and ALG-HNT-EST during the DEHP degradation.

4.3.4.2. Diethylhexyl phthalate bionanocomposite degradation

The profiles of DEHP concentration during the treatment with the bionanocomposites at different flow rates in the presence of esterase immobilized on CTS-HNT-EST and ALG-HNT-EST beads are shown in Figure 4.4b.

Similarly, and as reported in previous section, the bionanocomposite containing esterase immobilized on the CTS-HNT-EST presented the highest value of degradation, but no complete removal of DEHP was achieved (≈ 11 mg/L DEHP). The bionanocomposite of esterase immobilized on the ALG-HNT-EST was not able to completely degrade DEHP reaching a concentration of around 40 mg/L. It suggests that availability of the immobilized enzyme for the degradation of the PAEs and their complexity are key factors in the degradation process. The analysis of the morphology of bionanocomposites by SEM images (Figure D.2) could explain some of the causes of the different behavior being related to the distribution of HNT-EST in the composite. These images showed a higher availability of HNT containing enzyme on the surface of the CTS bionanocomposite in comparison with alginate and with a higher surface. Thus, when the volumetric flow was decreased and thus the residence time increased, DEHP concentration was found to be zero in the presence of CTS-HNT-EST bionanocomposite. The steady state was reached in all evaluated volumetric flows. Thus, the DEHP concentration was 27 mg/L for the column filled with ALG-HNT-EST bionanocomposite at 0.030 mL/min, while the value decreased 23.6 mg/L when a lower volumetric flow was chosen (0.015 mL/min). As well as the reduction of the compound, the relative activity during the treatment process is an important factor to consider (Figure 4.5b). At the end of the operation in continuous, CTS-HNT-EST bionanocomposite retained 81% of its initial activity, while ALG-HNT-EST bionanocomposite was able to maintain approximately 75% of its initial activity (Figure 4.5b). Moreover, the enzyme mass (%) on CTS-HNT and ALG-HNT was found to be 85.48% and 79.2%, respectively. This may be because an amino group of CTS that is unreacted with GTA in the immobilization with the crosslinking method can adsorb PAEs and their metabolites (Dulazi and Liu, 2011).

In addition, although CTS-HNT beads did not break or deform, ALG-HNT beads showed deformations upon completion of the experiment. This may be related to alginate having fast swelling behavior. Throughout the experiment, the solution with PAEs

diffuses into the beads, thereby increasing the osmotic pressure inside the beads. The ALG-HNT beads may swell increasing their size, and eventually, the bead may collapse (Roquero et al., 2022). This may be the reason why ALG-HNT with esterase exhibits less degradation efficiency when compared to CTS-HNT with esterase.

4.4. Conclusion

Bionanocomposite beads based on esterase enzyme immobilized in halloysite nanotubes and natural polymers (chitosan and alginate) were successfully prepared and proved an improvement of the catalytic activity and other properties of the enzyme. The results demonstrated that they maintained their activity for a long period and the enzymatic degradability of PAEs is affected by the length of alkyl side chain in their structures. CTS-HNT-EST is a more effective and robust support material for the degradation of the pollutants in batch and continuous treatment. Both of them may act as strong candidates for the remediation of PAEs.

CHAPTER 5

CHARACTERIZATION AND EXPRESSION OF RECOMBINANT THERMOALKALOPHILIC ESTERASE FROM *GEOBACILLUS* SP. AND PAES' DEGRADATION

5.1. Introduction

Environmental pollution caused by human activity is currently a major issue on a global scale. Phthalic acid esters (PAEs), which are a group of synthetic chemicals, are pervasive environmental pollutants. They are frequently utilized as plasticizers on massive scales with the purpose of improving the flexibility and workability of plastic products. Additionally, they are used in many applications as additives in the production of adhesives, paints, varnishes, cardboard, cosmetics, and various other products. They have weak interactions with the plastic matrix therefore they have the potential to leach into the environment. Their low solubility in water causes them to remain stable in the environment for long periods of time (Vikelsee et al., 2002; Huang et al., 2008). They can accumulate in the food chain and cause chronic health problems, endocrine disruption, and cancer (Hahladakis et al., 2018; Groh et al., 2019). Among all PAEs, particularly, dibutyl phthalate (DBP) and diethylhexyl phthalate (DEHP) are the most widely utilized and frequently encountered PAEs in the environment. These PAEs have been listed as top priority pollutants by both the European Union and US Environmental Protection Agency (USEPA). There is a pressing need to develop a feasible and efficient approach for the removal of PAEs from the environment to avoid the effects of PAEs on the environment and living organisms. Biodegradation has a significant role in the elimination of PAEs from contaminated sites, offering advantages such as high efficiency, cost-effectiveness, and environmental safety. Numerous bacteria capable of degrading PAEs have been isolated and identified (Chen et al., 2015; Tang et al., 2016). However, only a few had an application potential and an exceptional adaptability to

various environmental conditions (Ren et al., 2018). Many whole genomes of bacteria that break down PAEs have been sequenced and annotated due to advances in gene sequencing technology. As a result, a database for gene screening and functional gene identification has been formed to facilitate research on important metabolic enzymes. (Chen et al., 2021b).

Enzymatic degradation has recently gained extensive attention as a method of removing PAEs. The esterase enzyme, which is a hydrolase enzyme, has an essential role in degrading PAEs. Previous studies indicated the esterases from *Norcardia erythropolis* (Kurane et al., 1980), *Pseudomonas fluorescences* FS1 (Zeng et al., 2004), *Bacillus* sp. K91 (Ding et al., 2015), *Bacillus velezensis* SYBC H47 (Huang et al., 2020), *Fusarium* sp. DMT53 (Luo et al., 2012), *Gordonia* strain (Huang et al., 2019) have the ability to degrade PAEs. To date, the majority of enzymes used in studies have been secreted from mesophilic organisms. Although they offer many advantages in applications, their use has been limited by their low stability under various conditions (temperature, pH, and ionic strength). Thus, there has been a growing interest in microorganisms that thrive in extreme environments. Enzymes from thermophilic microorganisms are of great interest in demanding industrial and biotechnological processes. High-temperature environments contaminated by PAEs are quite common. For instance, the temperature of the soil under a mulch film that widely contains PAEs can reach 50°C or higher during the summer. Another well-known method involves composting, which is frequently employed to treat pollutants found in both lagoons and activated sludges. The process is typically conducted at relatively high temperatures to maintain the efficiency of the reaction.

Prior to this study, *Geobacillus* sp. had been isolated from Balçova (Agamemnon) Geothermal Region in İzmir, Turkey (Yavuz et al., 2004). Following this, its esterase-producing gene was cloned in pET-28a (+) by Tekedar and Sanli-Mohamed (2011). In this study, the expression of recombinant enzyme in *E. coli* and its purification were performed. The obtained pure esterase with stability against the changes of pH and temperature was used to degrade PAEs with short (DBP) and long (DEHP) alkyl chains. The metabolites occurring as a result of degradation of these PAE congeners were examined.

5.2. Material and Method

5.2.1. Materials

DBP, DEHP, monobutyl phthalate (MBP), dimethyl phthalate (DMP), monoethyl hexyl phthalate (MEHP), and phthalic acid (PA) standard grades were supplied from Sigma Aldrich (USA). p-nitrophenyl acetate (pNPC-2) and tween-80 were purchased from Sigma-Aldrich. All other chemicals and solvents were of reagent grade. Bacterial cells were grown on solid and liquid Luria Bertani (LB) medium with kanamycin. DBP and DEHP stock solutions of 5,000 mg/L concentration were prepared in methanol.

5.2.2. Enzyme preparation

The strain in the glycerol stock stored at -86°C was streaked in an LB plate containing 30 µg/mL kanamycin and incubated at 37°C for 17 h. After the incubation, a single colony selected from the plates was inoculated overnight in 10 mL LB media containing 30 µg/mL kanamycin at 37°C, with constant shaking at 200 rpm. Then, the cultures were diluted (1:10) into 100 mL media and grown under the same conditions. At the point where the optical density (OD) of bacterial cultures reached about 1 at 600 nm corresponding to the mid-logarithmic phase, they were induced with the addition of 1mM IPTG, and their growth was allowed at 28°C, 200 rpm for 4 h more to express the esterase-producing gene. Before and after the addition of IPTG, the samples were collected. The cultures were centrifuged at 8,000 rpm and 4°C for 10 minutes to remove the supernatant which was formed by cell precipitation. The obtained pellets were stored at -20°C until the purification process. The expression and purification of esterase were evaluated using sodium dodecyl sulfate polyacrylamide gel electrophoresis (SDS-PAGE).

5.2.3. Recombinant esterase' molecular mass

An SDS-12% polyacrylamide gel was prepared according to the Laemmli Method (Laemmli, 1970). The gel contains 10% (w/v) SDS and 30% acrylamide mixture, 1.5 M Tris-HCl buffer (pH=8.8), 10% (w/v) ammonium persulfate and tetramethylethylenediamine (TEMED). During the preparation of the resolving gel, polymerization began with the addition of TEMED. The resolving mixture was poured into the thin gap between two glass plates and tertamyl alcohol was added to the resolving mixture in order to avoid bubble formation on the gel. The polymerization was achieved in 30 minutes. This step was followed by the preparation of stacking gel. After the preparation of stacking gel, the mixture was poured into the polymerized resolving gel, and a comb which had 10 holes was placed on the gel before the polymerization process. At the end of the polymerization of the stacking gel, the comb was removed from the top of the gel. The gel was placed in a tank filled with 1x Tris-Glycine-SDS run buffer. The protein samples were mixed with the sample buffer containing distilled water, 0.5 M Tris-HCl at pH 6.8, glycerol, 10% SDS, mercaptoethanol, and 0.5 (w/v) bromophenol blue at a ratio of 4:1 (v/v). After that, all samples were heated at 100 °C in a water bath for 10 minutes. A protein molecular marker containing β -galactosidase (116.0 kDa), bovine serum albumin (68 kDa), ovalbumin (45 kDa), lactase dehydrogenase (35 kDa), rease Bsp 981 (25 kDa), and β -lactoglobulin (18.40 kDa) served as a reference. The samples and the molecular marker were loaded into the gel in the tank. Electrophoresis was performed with a vertical mini-gel system (Bio-Rad, mini protean Tetra) by applying 100 volts for 2 h. Electrophoresis was finished at the point where the blue dye reached the bottom of the gel, and the gel was removed from the tank. It was washed with distilled water after the staining process. Then, it was placed in a destaining solution containing 13% trichloroacetic acid, 5% methanol, and 82% distilled water. After the destaining process, the gel was washed with distilled water carefully and a photo of the gel was taken using a gel imaging system (Bio-Rad, Versadoc 4000 MP).

5.2.4. Affinity chromatography

The frozen pellets were thawed and dissolved in 10x weight: volume of 50 mM sodium phosphate buffer at pH 7. Subsequently, the obtained samples were lysed by a sonicator (Bendelin UW 2070) for 5 min. To discard insoluble materials, the samples were centrifuged at 10,000 rpm for 30 min. The supernatant phase was retained for further purification. To purify the esterase protein, a His-tag Nickel Affinity Column with 2.5 x 10 cm was used. Before the supernatant was loaded onto the column, the column was equilibrated with 50 mM sodium phosphate buffer at pH 7. This column was washed with 100 mL sodium phosphate buffer containing 0.3 M NaCl to remove unbound protein and then elution of the esterase enzyme was performed using 250 mM imidazole in 50 mM phosphate buffer (pH=7) including 0.1 M NaCl. The eluted enzyme was fractionated as 20 drops in each collection tube. The fractions collected from the column were analyzed by using a UV-vis spectrophotometer (Shimadzu 2600) at the wavelength of 280 nm to determine the approximate concentration of protein. The collected samples were pooled and dialyzed against a 0.5 mM phosphate buffer at pH 7 overnight to remove imidazole from the solution. Then, the success of the purification was examined using SDS-PAGE. After the purification, the obtained liquid enzyme was lyophilized under vacuum conditions for 24 h at -50°C (Telstar Cryodos).

5.2.5. Protein concentration and enzyme activity

The protein content of the enzymes was determined using the Pierce BCA Protein Assay Kit (ThermoFisher) according to the bicinchoninic acid (BCA) method. Bovine serum albumin (BSA) was used as a reference protein. Firstly, the reagent mixture was prepared by the addition of 10 mL of Reagent A and 200 µL of Reagent B. BSA stock (2 mg/mL) in the ampule was used to prepare a set of diluted standards within the working range (0-2000 µg/mL). The assay was run on a 96-well U plate. 10 µL of the was added to the wells. Then, 200 µL of the reagent mixture was added to each well. To avoid light, the 96-well plate was covered with aluminum foil and incubated at 37.5°C for 30 minutes.

The absorbances were measured spectrophotometrically at 562 nm as two replicates. A standard curve was created using the absorbance of the diluted BSA standards. Subsequently, the protein concentration of samples was determined using the calibration curve.

To determine the enzyme's optimal working conditions, various tests were conducted in different temperatures (25°C-95°C) and pH ranges (4-13). The enzyme activity was determined by hydrolysis of pNPC-2. The assay mixture (1 mL) consisted of 0.8 mL phosphate buffer (0.1 M) at different pH values, 0.1 mL of 0.5 mM pNPC-2 dissolved in acetonitrile, and 0.1 mL of enzyme solution (10 mg/mL). This mixture was incubated at different temperatures for 5 min. Afterwards, the absorbance of mixture was spectrophotometrically measured at 400 nm. Activity calculation was made according to the equation below (5.1).

$$\text{Enzyme activity (U/L)} = \frac{(\text{Absorbance at 400 nm}) \cdot (\text{Vt}) \cdot (\text{DF})}{(\text{t}) \cdot (\epsilon) \cdot (\text{Ve}) \cdot (\text{d})} \quad (5.1)$$

Vt: total sample volume (mL), DF: Dilution factor, t: reaction time, ϵ : p-nitrophenol molar extinction coefficient at 400 nm ($17,215 \text{ M}^{-1} \cdot \text{cm}^{-1}$), Ve: enzyme volume (mL), d: light path (1 cm).

One unit of activity is defined as the amount of enzyme releasing $1.0 \mu\text{mol}$ of p-nitrophenol per minute under optimal conditions using pNPC-2 as a substrate. The molar extinction coefficient of p-nitrophenol in the buffer system is $17,215 \text{ M}^{-1} \cdot \text{cm}^{-1}$.

5.2.6. Kinetic parameters of enzyme

The kinetic parameters, specifically the maximum rate (V_{max}) and Michaelis-Menten constant (K_m), for the esterase enzyme were determined by assessing enzyme activity in the presence of pNPC-2 (0-400 mg/L). They were calculated using the Lineweaver Burk plots.

Additionally, to determine the enzyme kinetics for the hydrolysis of DBP and DEHP, the enzyme (10 mg/1 mL) was incubated with various concentrations of DBP and DEHP (25-100 mg/L) for 1 h. After the incubation, enzyme activity was spectrophotometrically measured using pNPC-2 substrate at 55°C.

5.2.7. Enzymatic degradation experiments

Firstly, 10 mg of lyophilized esterase was solved in 1 mL phosphate buffer (0.1 M, pH=8). DBP/DEHP solution with 1,000 mg/L was prepared in methanol. Then the enzyme solution was added to the reaction mixture (1 mL) containing the phosphate buffer, Tween-80 (%1, v/v) and DBP/DEHP solution. Degradation experiments were conducted during 168 h under the enzyme's optimal conditions.

5.2.8. Chromatographic analysis of PAEs

After degradation experiments, the quantification of DBP and DEHP was investigated under a reversed-phase using an Agilent 1260 Infinity II LC system connected to a Diode Array Detector (DAD) equipped with an ODS-3 column (5 µm particle size, 250 mm x 4.6 mm i.d.) a RESTEC RAPTOR-C18 column (2.7 µm particle size, 100 mm x 4.6 mm i.d.), respectively. The mobile phase consisting of methanol:water (75:25, v/v) was used at a flow rate of 1 mL/min for DBP analysis. As for DEHP analysis, the mobile phase composition (acetonitrile:water) in gradient elution was varied over time as follows: 0 to 3 min 80:20, 3 to 9 min 95:5, 9 to 12 min 95:5, 12 to 18 min 100:0, 18 to 23 min 60:40, 23 to 24 60:40, 24 to 26 80:20 and the flow rate was set at 0.7 mL/min. For each injection, the volume taken from samples in both DBP and DEHP analysis was 20 µL. The analyses were carried out together with a UV detector (230 nm) at room temperature.

The analysis of the PAEs' degradation products was conducted using an Agilent Technology 1260 Infinity series high performance liquid chromatograph connected to an

accurate mass quadrupole time-of-flight 6550 iFunnel Q-TOF mass spectrometer equipped with a Jet Stream ion source. The analysis was conducted in positive mode over the range of m/z 50–950 (Agilent Technologies, Santa Clara, CA, USA). The chromatographic separation was carried out using a Poroshell 120 SB-C18 column (3.0×100 mm, particle size 2.7 μm) with a gradient mixture of 0.1% formic acid in water (A) and 0.1% formic acid in acetonitrile (B) at the flow rate of 0.4 mL/min. The gradient program was as follows: 0–1 min, 40% B; 1–20 min, 40%–95% B; 20–27 min, 95% B; 27–30 min, 40% B. The injection volume was 10 μL and column temperature was maintained at 40°C. Data acquisition was managed using Agilent MassHunter Acquisition Software Ver. A.09.00, and data processing was done with MassHunter Qualitative Software Ver. B.07.00.

5.3. Results and discussion

5.3.1. Expression and purification of esterase enzyme

Before the enzyme purification process, an SDS-PAGE analysis was conducted to observe whether the esterase-producing gene in the pET28 (+) expression vector which was recombined to the BL21(DE3) *E.coli* host was induced by IPTG for the production of a 28 kDa esterase protein. The SDS bands of the protein in the samples before (1,2,3, and 5) and after IPTG addition (4 and 6) and marker (M) are shown in Figure 5.1a. Protein bands at 28 kDa were faintly visible prior to IPTG addition. However, after the addition of IPTG, the protein bands at 28 kDa belonging to the esterase enzyme could be seen very clearly. That is, this level of expression indicated that the major proteins in the induced cells were esterase. The purification process of the esterase was performed using His-tag nickel affinity chromatography to obtain a nearly homogenous protein. After the purification process, the fractions collected from the column were analyzed by using a UV-vis spectrophotometer. Then, an SDS-PAGE analysis was performed to evaluate the homogeneity of the esterase. It showed that the purification process had been carried out successfully (Figure 5.1b).

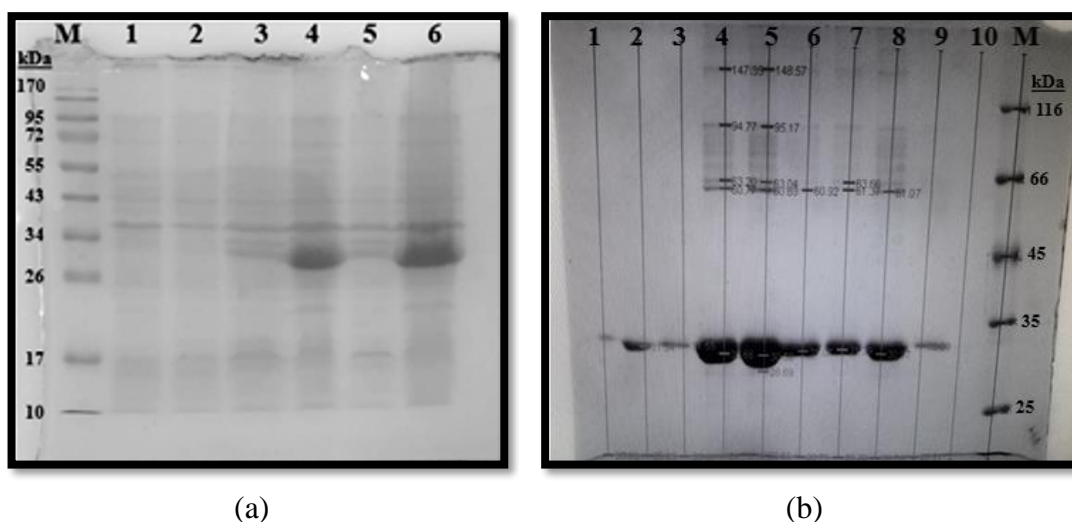


Figure 5.1. SDS-PAGE analysis of the collected fractions (a) before and (b) after purification step.

5.3.2. Enzyme activity assay

To determine the optimal pH value for the esterase enzyme, enzyme activity was measured in the presence of 0.1 M phosphate buffer at various pH values ranging from 4 to 13 by an increment of 1. As can be seen in Figure 5.2a, while the enzyme activity was quite low at pH values below 7, no major changes were observed between 7 and 12 pH values. The pH value with the highest enzyme activity was determined to be 8. Like the esterase from *Geobacillus* sp., *Sorghum bicolor* esterase (Gasparin et al., 2020) and soybean esterase (De Barros and Macedo, 2011) which were alkaline enzymes exhibited highest activity at pH 8.

To determine the optimum temperature for the esterase enzyme, the activity was measured at temperatures between 25°C and 95°C, and the results were shown in Figure 5.2b. With the increasing temperature, the activity of the enzyme increased up to 55°C in the presence of pNPC-2 substrate. There was no significant change in the enzyme activity between 55°C and 75°C. However, increases in temperature above 75°C caused a decrease in the activities of the enzyme. That is, the enzyme could not maintain its three-dimensional structure by thermal unfolding or thermal inactivation above 75°C. Therefore, the optimum temperature for the activity of the esterase enzyme was determined to be 55°C.

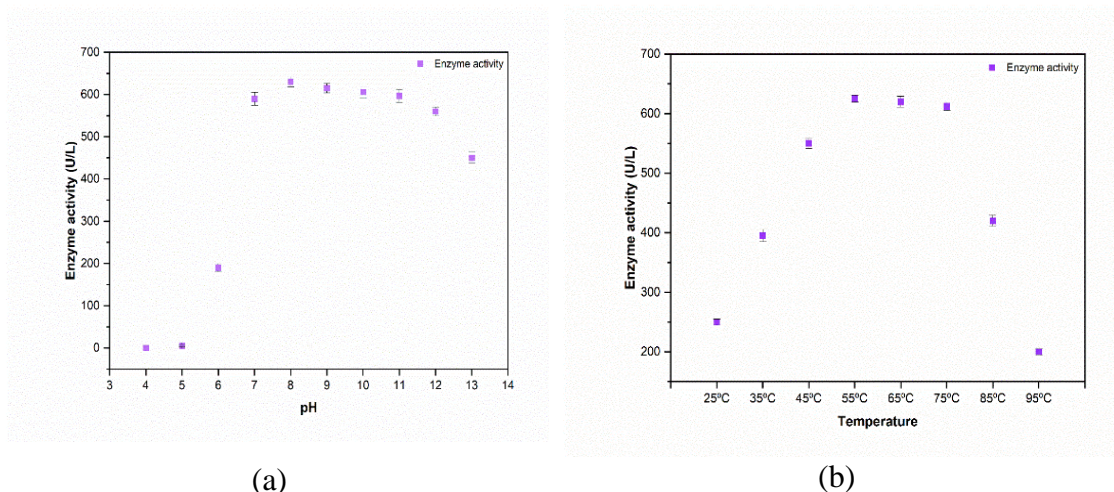


Figure 5.2. Esterase activity at different pH values (a) and temperatures (b).

5.3.3. Enzyme kinetics

The kinetic parameters for enzymatic hydrolysis of pNPC-2 were calculated using Lineweaver Burk plots (Figure 5.3). The Lineweaver-Burk plots exhibited a linear relationship ($R^2=0.986$) across the range of concentrations tested. V_{max} and K_m of esterase with pNPC-2 as substrate were determined to be 35.98 $\mu\text{M}/\text{min}$ and 0.684 μM . K_m is a parameter that quantifies the affinity of an enzyme for a specific substrate. The K_m and V_{max} values obtained in this study may appear lower than those reported in the literature (Tekedar and Sanli-Mohamed, 2011; Mohammadi et al., 2020). Low K_m and V_{max} suggest stronger enzyme-substrate binding (Sudo, 1995; Saganuwan, 2021). Furthermore, a low K_m means that only a small amount of the substrate is required to saturate the enzyme with high affinity for the substrate. This indicates that the esterase enzyme utilized in the study exhibits a high affinity for its substrate.

Enzyme kinetics were calculated using the Lineweaver-Burk plot for the hydrolysis of DBP and DEHP by recombinant esterase (not shown). V_{max} of enzymatic hydrolysis reaction for DBP and DEHP was determined to be 72.3 $\mu\text{M}/\text{min}$ and 75.2 $\mu\text{M}/\text{min}$, respectively. For the enzymatic hydrolysis reaction of DBP and DEHP, the K_m values were 3.1 μM and 3.4 μM , respectively. The K_m value for DEHP was higher than that calculated for DBP. This means the affinity of the esterase enzyme for DBP was higher than that for DEHP.

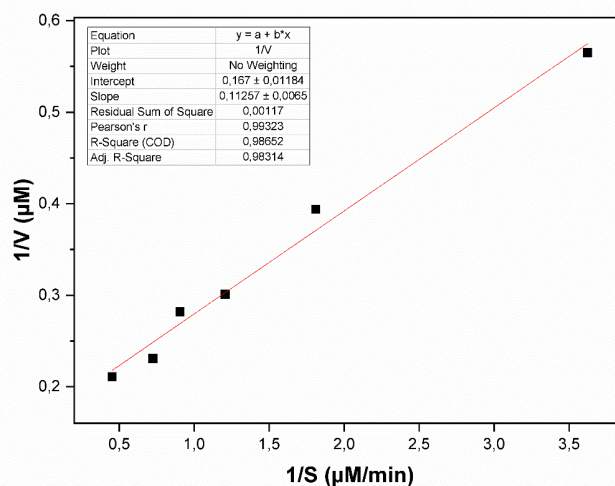


Figure 5.3. Lineweaver Burk plot for pNPC-2 substrate hydrolysis with recombinant esterase.

5.3.4. Degradation experiments

The degradation experiments at different DBP and DEHP concentrations with 50 and 100 mg/L in aqueous solution were performed in the presence of recombinant esterase for 48 h under the optimal conditions (Figure 5.4). The degradation efficiency of DBP with 50 and 100 mg/L in the presence of recombinant esterase for 48 h was determined to be approximately $27.6\% \pm 1.3$ and $19.8\% \pm 1$, respectively. As for DEHP degradation experiment results, these values were found to be $12.2\% \pm 0.9$ and $17.5\% \pm 0.98$, respectively. Saito et al. (2010) studied DBP and DEHP (5 μmol) degradation by bovine pancreatic cholesterol esterase and reported conversion of DBP and DEHP into corresponding monoesters within 15 min. Zhang et al. (2014) performed the DBP and DEHP degradation experiments within *Sulfobacillus acidophilus* esterase. They observed that while the esterase enzyme degraded 100% of DBP within 1 h, it was not able to degrade DEHP within 24 h. Balci et al. (2022) conducted a study on the degradation of DBP and DEHP (100 mg/L) by *Bacillus subtilis* esterase. They reported that the esterase enzyme fully degraded DBP and DEHP with 100 mg/L for 0.25 h and 8 h, respectively. Sun et al. (2022a) reported that *Rhizopus oryzae* esterase was able to degrade 95% of DBP (1 mg/L) and 85% of DEHP (1 mg/L). Compared to the findings in the literature,

recombinant esterase was not able to display the high performance on DBP and DEHP degradation. However, given enzyme dosage and PAE concentrations, these degradation rates can be considered to be normal.

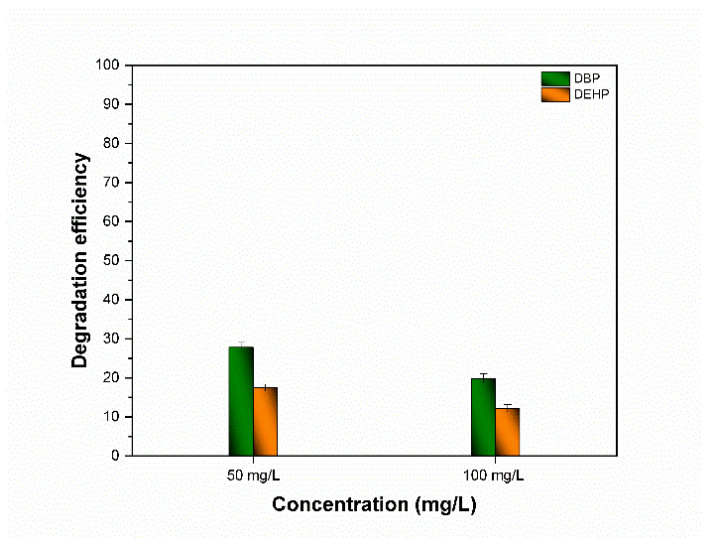


Figure 5.4. Degradation efficiency of DBP and DEHP with 50 and 100 mg/L in aqueous solution in the presence of recombinant esterase for 48h.

Decreasing the concentration and extending the degradation time up to 168 h during the degradation of the congeners resulted in 40% and 30% degradation of DBP and DEHP, respectively (Figure 5.5). The esterase enzyme exhibited a notable degradation performance in the degradation of PAEs with a concentration of 25 mg/L compared to high PAEs concentrations. It is noteworthy that the esterase demonstrated a higher performance in degrading DBP (a PAE with short-chain) than it did in degrading DEHP (a PAE with long-chain). When compared to PAEs with short alkyl side chains, it is more difficult for PAEs with long alkyl side chains to bind with enzyme active sites. This fact is due to steric hindrance of PAEs with long alkyl side chains (Rivera-Hoyos et al., 2013). The catalytic degradation of PAEs by esterase typically relies on the length of the alkyl side chain of PAEs and their molecular configurations.

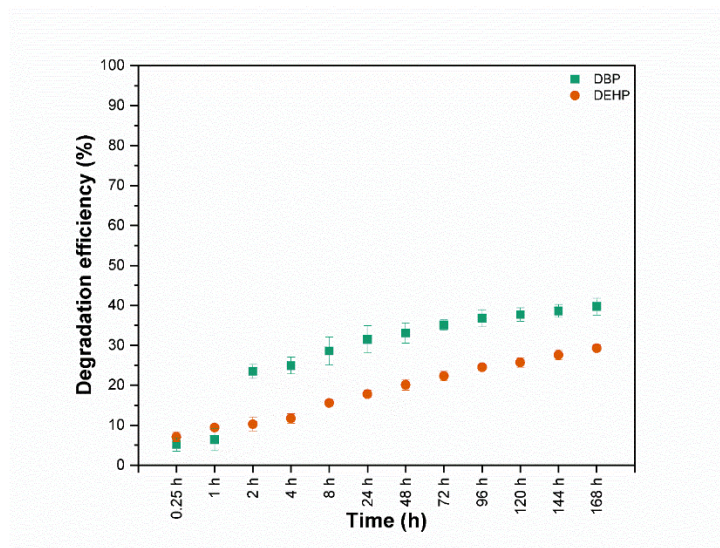


Figure 5.5. Degradation efficiency of DBP and DEHP with 25 mg/L in the presence of recombinant esterase for 168 h.

5.3.5. Degradation products of PAEs

PAEs are typically degraded by enzymes initially into monoesters and subsequently into phthalic acid (PA). DBP and DEHP degradation products at the end of 168 h were identified by taking into account the mass spectra (m/z) of potential products at a particular retention time (RT) in the literature. In LC-MS analysis, DBP and DEHP solutions containing no enzyme were used as the control samples. The m/z ratio for DBP and DEHP was 279.15 (RT 8.5 min) and 391 (RT 11.5 min), respectively (Figures 5.6a and 5.7a). As seen from Figures 5.6b and 5.7b, the recombinant esterase degraded DBP to MBP (m/z 222, RT 7.7 min) and DEHP to MEHP (m/z 277, RT 8.7 min). Although it specifically hydrolyzed DBP and DEHP to their corresponding monoalkyl PAEs, it was not able to monoalkyl PAEs hydrolyze to PA which is a main metabolite in the biodegradation of PAEs. Only one of the ester bonds can be hydrolyzed by the majority of esterases (Akita et al., 2001; Maruyama et al., 2005; Ding et al., 2015). In a study conducted by Niazi et al. (2005), *Bacillus* sp. esterase degraded DMP up to monomethyl phthalate (MMP) without further degradation step. Saito et al. (2010) underlined that Bovine pancreatic cholesterol esterase degraded DBP and DEHP up to monoalkyl PAEs. Similarly, Luo et al. (2012) reported that *Fusarium* sp. DMT 5-3 esterase degraded only

dimethyl terephthalate (DMT) to monomethyl terephthalate (MMT). The esterase could only break down the initial carboxylic ester bond of DMT and did not possess the capability to hydrolyze the second bond. Balci et al. (2022) underlined that *Bacillus subtilis* esterase fully degrade DBP and DEHP to phthalic anhydride. It was obvious that esterases are a group of enzymes with diverse roles in the cleavage of carboxylic ester linkages of PAEs. In addition to all these, the recombinant enzyme from *Geobacillus* sp. is a soil-derived enzyme. For this reason, it may not have exhibited a high performance in the PAE congeners' degradation experiments carried out in aqueous media.

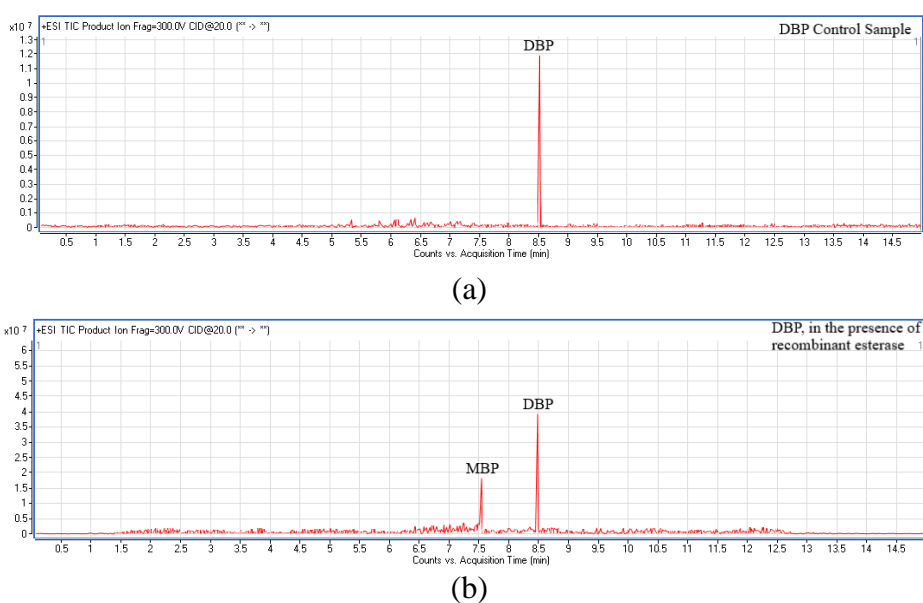


Figure 5.6. LC-MS chromatogram of the samples before (a) and after DBP degradation experiments in the presence of recombinant esterase (b).

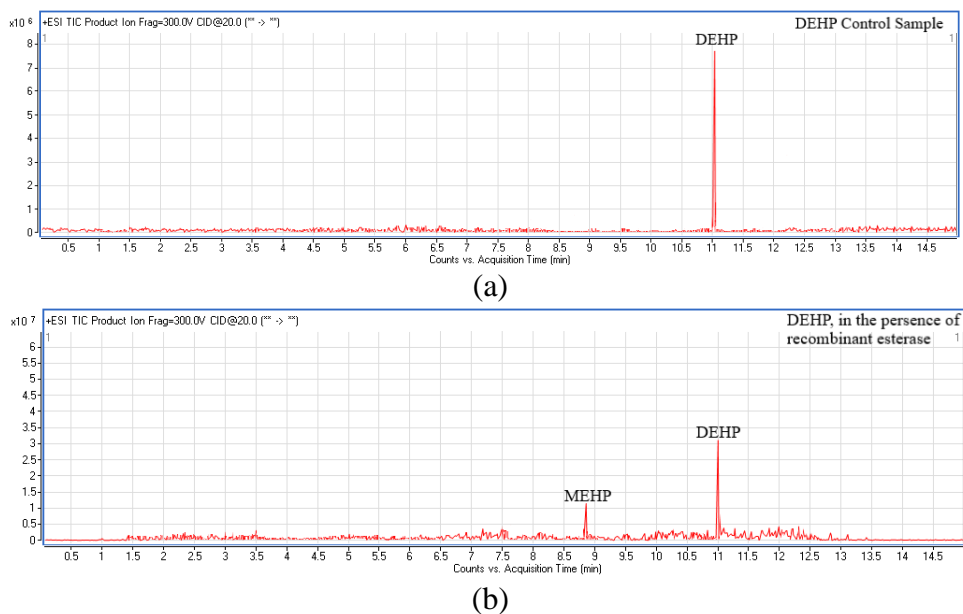


Figure 5.7. LC-MS chromatogram of the samples before (a) and after DEHP degradation experiments in the presence of recombinant esterase (b).

5.4. Conclusion

This study investigated the DBP and DEHP degradation performance of the thermoalkalophilic recombinant esterase. The esterase partially degraded DBP, whereas it had little effect on DEHP degradation. The degradability of PAE congeners showed a negative correlation with the length of the alkyl chain. Generally, although recombinant esterase was generally unable to completely degrade PAEs, it exhibited a notable degradation performance. In future studies, mutation strategy and promoter engineering can be combined to provide a basis for improving the enzyme's activity and enhancing its degradation ability, subsequently being used efficiently in applications. Furthermore, the degradation performance of this enzyme could potentially be enhanced through the presence of ions and agents known to positively influence enzyme activity. This could potentially expand the applications of this enzyme in agriculture, biotechnology, the treatment of pollutants as well as various industries.

CHAPTER 6

ENZYME-MEDIATED DEGRADATION OF PHTHALATE ESTERS IN SOIL

6.1. Introduction

Phthalate esters (PAEs) are frequently used in the production of plastics to increase plastics' flexibility and robustness. Due to the widespread usage of plastics, PAEs have been found in numerous industrial, residential, and even agricultural regions all over the world. Today, as global plastic production exceeds 150 million tons each year, the annual consumption of PAEs is estimated to be over 8 million metric tons in the world (Weizhen et al., 2020). Due to their widespread use and resulting environmental impacts, PAEs have been detected in all environmental media, including soil, sediment, water, and even air. Owing to their high hydrophobicity which leads to their strong binding affinity to the organic matter in the soil, PAE contamination is primarily observed in soil (Wei et al., 2020). PAEs that are loosely attached to plastics are easily released into the environment and subsequently, they have an impact on the soil ecosystem under the effect of UV radiation, temperature, oxygen content, soil acidity and alkalinity, and the presence of soluble organic matter (Chen et al., 2021b). The major source of soil PAEs is mostly the excessive use of agricultural chemicals (e.g., pesticides, fertilizers, and plastic mulch film), leachate from landfills, and sewage and wastewater irrigation. Among these sources, the employment of plastic mulch film for the cultivation of vegetables is usually considered to be the main contributor (Bai et al., 2020). Residential activities have the potential to generate urban dust, which can lead to soil contamination through the process of deposition. Both dry and wet deposition mechanisms play a role in the contamination of soil with PAEs, particularly in areas with a high level of industrialization (Wu et al., 2015). PAEs can exhibit long half-lives in soil under natural conditions, ranging from 3 to 2,000 years (Gao and Wen, 2016). PAEs in soil can be absorbed by plants and

accumulate in their tissues. This accumulation has the potential to adversely affect the quality of crops, including vegetables in various ways and thereby entering the food chain. Because of the bioaccumulation of PAEs, humans are primarily exposed to them through food consumption. This exposure can potentially lead to endocrine disruption, metabolic disorders, and reproductive toxicity (Schettler, 2006; Wang et al., 2023). Prolonged exposure to PAEs, even at low levels, can have teratogenic, mutagenic, and carcinogenic effects on humans. Consequently, the U.S. Environmental Protection Agency (EPA) has identified six major PAEs as priority pollutants that require regulation and monitoring (Deblonde et al., 2011). Considering their detrimental effects on the environment and living organisms, it is crucial to eliminate PAEs from all environmental media in eco-friendly ways.

The elimination of PAEs from the environment can be accomplished through various methods including physical-chemical degradation, advanced oxidation processes, and biodegradation. Among these methods, biological degradation is a prominent approach due to its environmental friendliness and cost-effectiveness. Importantly, it does not harm soil fertility or ecological functions (Gong et al., 2012). Numerous studies have been conducted on the biodegradation of PAEs in soil using various bacterial strains (Chao and Cheng 2007; Hu et al., 2022). Microorganisms capable of degrading PAEs become gradually acclimated in soils contaminated by PAEs over extended periods, and these bacteria can act either individually or in groups based on their tolerance to PAEs and their degradation capabilities (Chen et al., 2021b). While many strains capable of degrading PAEs have been isolated and characterized from various environmental sources, only a few of them possess the ability for complete degradation, exhibit strong environmental adaptability, and show potential for practical applications. Hydrolase enzymes secreted by these strains have a major role for PAEs degradation in environmental media. However, there is limited information available regarding the selectivity and specificity of the biodegradation of PAEs in the presence of various enzymes. The lack of information in this area hinders the establishment of application parameters for the use of free enzymes in the remediation of soils contaminated by PAEs.

In this study, two soil samples with different characteristics were collected from an agricultural area and a forest area. The presence of the dibutyl phthalate (DBP) and diethylhexyl phthalate (DEHP) in the soil, which are the most common PAEs in the environment, was investigated. To evaluate the effect of PAEs' chemical structures on specificity and selectivity of enzymes, the degradation experiments of DBP (PAEs with

a short alkyl side chain) and DEHP (PAEs with a long alkyl side chain) in soils were conducted in the presence of *Bacillus subtilis* esterase and recombinant esterase expressed from *E.coli* strains which have esterase-producing gene of *Geobacillus* sp. isolated from Balçova Geothermal region. Furthermore, the degradation time, enzyme activity, and soil characteristics were investigated in enzymatic bioremediation experiments.

6.2. Material and Method

6.2.1. Materials

Bacillus subtilis esterase (EC 3.1.1.1; ≥ 10 U/mg) was obtained from Sigma-Aldrich. DBP (>99% purity), DEHP (>99% purity), methanol (99.8% ACS reagent), and p-nitrophenyl acetate (pNPC-2, esterase substrate >98%) were purchased from Sigma-Aldrich. Other chemicals were of laboratory reagent grade and used without any further purification. Deionized water was prepared using a Milli-Q Plus water purification process (Millipore Corp, Molsheim, France). The enzyme solutions were freshly prepared in phosphate buffer solution (0.1 M, pH=7 and 8) before all enzymatic remediation experiments.

6.2.2. Enzyme preparation

Thermoalkalophilic esterase from *Geobacillus* sp. had been isolated from Balçova (Agamemnon) Geothermal Region in İzmir, Turkey by Yavuz et al., 2004. Subsequently, its esterase-producing gene was cloned in pET-28a (+) by Tekedar and Sanli-Mohamed (2011). In this study, the expression of recombinant enzyme in *E.coli* and purification were performed according to a procedure reported by Tekedar and Sanli-Mohamed (2011). The obtained purified esterase enzyme was lyophilized under vacuum conditions for 24 h at -50 °C (Telstar Cryodos). Before degradation experiments, enzyme solutions

containing *Bacillus subtilis* esterase and recombinant esterase (*Geobacillus* sp. esterase) were dissolved in phosphate buffer (0.1 M) at pH=7 and pH=8, respectively.

6.2.3. Enzyme activity and protein concentration

The enzyme activity for the esterases was determined by hydrolysis of pNPC-2 according to the procedure reported by Tekedar and Sanli-Mohamed (2011). The assay mixture (1 mL) consisted of 0.8 mL phosphate buffer (0.1 M, pH 7), 0.1 mL of 0.5 mM pNPC-2 dissolved in acetonitrile, and 0.1 mL of enzyme solution (1 mg/mL). This solution was incubated at optimum temperature for 5 min and then used to determine the catalytic activity. The absorbance was spectrophotometrically measured at 400 nm. After the measurement of the absorbance, the activity calculation will be made according to the following equation (1).

The protein concentration of the enzymes was determined using the Pierce BCA Protein Assay Kit (Thermofisher) according to the bicinchoninic acid (BCA) assay. Bovine serum albumin (BSA) was used as a standard protein. A standard calibration curve was constructed using BSA protein.

6.2.4. Sequence Analysis

The precise amino acid sequences of the esterases produced by *Geobacillus* sp. (Q06174) and *Bacillus subtilis* (O32232) were compared by obtaining from the protein databases at UniProt using the respective accession numbers. Sequence similarity searches were carried out using the Basic Local Alignment Search Tool (BLAST) program from the National Center for Biotechnology Information (NCBI) and the Clustal Omega (Clustal O(1.2.4)) program provided by the European Bioinformatics Institute. Using the ScanProsite tool, the binding characteristics of the active site for enzymes were examined.

6.2.5. Experimental soil samples

Two typical sites were selected for soil sampling. The soil samples were taken from the top layer (0-20 cm) of the agricultural area (soil 1, 38° 19' 42.8" N, 26° 55' 23.5" E) where almonds are cultivated and the forest area (soil 2, 38° 18' 49.1" N, 26° 39' 49" E) where pine trees are present. The samples were collected as composite samples in an area of 100 m². They were mixed and sieved with a 2 mm mesh screen to remove plant residues and large particles. Afterward, they were incubated at 28°C for two days before the physico-chemical analyses were carried out. The background concentration of the soil was analyzed and no PAE congeners were detected in the soil samples.

The concentration of PAEs in the soil is related to soil physicochemical properties and soil microorganisms (Zhou et al., 2020). According to the spatial distribution data of soils in the literature, there were notable regional differences in the PAEs contamination of soils (Gennaro et al., 2005; Chai et al., 2014). Soil chemical properties such as pH, humidity, and total organic carbon (TOC) affect the adsorption and degradation behavior of organic pollutants in soil (Zeng et al., 2008; Wang et al., 2015b). The adsorption of PAEs to soil may be impacted by the TOC concentration of the soil (Yang et al., 2013). The relationship between PAEs and pH is still a controversial issue. An et al. (2010) revealed that pH has an effect on the adsorption of PAEs to soil organic matter. Yang et al. (2013) reported that increases in pH lead to a decrease in the sorption capacity of DEP and DMP. However, Zhou et al. (2020) did not find any correlation between pH and PAEs. In this study, soil samples with different characteristics were studied to determine whether the physicochemical properties of the soil influence the enzymatic degradation of PAE congeners (Table 6.1).

The pH of the soils was measured by mixing and vortexing the soil with distilled water at a ratio of 1:5 (w:v) (Li et al., 2016). The electrical conductivity of the soil was determined using Hach HQD portable meter. Total organic carbon content was determined using a TOC analyzer (Shimadzu TOC-VCPH). The concentrations of Na⁺, K⁺, Ca²⁺, Mg²⁺, Fe²⁺, and Al³⁺ cations were determined using ICP-OES according to standard methods.

Table 6.1. Characteristics of soil 1 and soil 2.

Measured parameters	Soil 1	Soil 2
pH	6.5	8.3
Electrical conductivity (dS/m)	14.3	8.4
Total organic carbon (mg/g)	28.1	2.4
Na ⁺ (mg/L)	57.7	57.3
K ⁺ (mg/L)	64.6	55.2
Ca ⁺² (mg/L)	791	1,918
Mg ⁺² (mg/L)	103.3	97.9
Fe ⁺³ (mg/L)	3.8	1.4
Al ⁺³ (mg/L)	7	27.5

6.2.6. Enzymatic degradation of contaminated soil with PAEs

The soils were intentionally contaminated with DBP and DEHP. Laboratory batch experiments were performed with contaminated soil in water suspension (soil slurry system). DBP and DEHP stock solutions (3,000 mg/L) were prepared in methanol separately. They were stored in the amber glass at -4 °C before use. 5 grams of the soils were taken in an amber glass (40 mL) and sterilized using an autoclave at 121°C for 1 h (Singh et al., 2017). The sterilized soils were contaminated with 100 µL of DBP or DEHP stock solutions (3,000 ppm). 1 mg of *Bacillus subtilis* esterase and 10 mg of recombinant esterase were dissolved in 3 mL of phosphate buffer (0.1 M) prepared at pH 7 and pH 8, respectively. While determining the amount of enzymes to be added to the soil, care was taken to ensure that the specific activities of the enzymes were approximately the same. The soils were incubated with the enzymes at 0.25 h, 1 h, 2 h, 4 h, 8 h, 24 h, 48 h, 72 h, 96 h, and 168 h. A control test was performed under the same conditions, but without adding any enzymes, in order to observe how efficiently PAEs degraded in the presence of enzymes. During degradation experiments, the soil moisture was maintained using

sterilized distilled water. At certain time intervals, samples were collected, and the enzymatic reaction was terminated by adding the 1 N HCl (10%, v/v).

6.2.7. Sample extraction

Three different solvents (Ethyl acetate, Acetone: n-Hexane (ACN:HXN=1:1, v/v), and Dichloromethane (DCM)) were tested to determine the most suitable solvent for the extraction of DBP and DEHP from the soils. DBP and DEHP were spiked in the soils. Extraction efficiency was calculated as the percentage of extraction recovery based on the HPLC peak areas.

After the enzymatic degradation experiments, the soils were ultrasonically extracted three times with 10 mL of the solvent with a best extraction efficiency and centrifuged.

The clear supernatants were combined and concentrated using a rotary evaporator at 40°C and finally transferred into acetonitrile (1 mL). The samples were filtered through a 0.22 µm PTFE syringe filter to remove particulate material prior to High-Performance Liquid Chromatography (HPLC) analysis. Then, the samples were stored at 4°C until HPLC analysis.

6.2.8. Analysis of PAEs

The quantification of DBP and DEHP was investigated under a reversed-phase using an Agilent 1260 Infinity II LC system connected to a Diode Array Detector (DAD) equipped with an ODS-3 column (5 µm particle size, 250 mm x 4.6 mm i.d.) a RESTEC RAPTOR-C18 column (2.7 µm particle size, 100 mm x 4.6 mm i.d.), respectively. The mobile phase consisting of methanol:water (75:25, v/v) was used at a flow rate of 1 mL/min for DBP analysis. As for DEHP analysis, the mobile phase composition (acetonitrile:water) in gradient elution was varied over time as follows: 0 to 3 min 80:20, 3 to 9 min 95:5, 9 to 12 min 95:5, 12 to 18 min 100:0, 18 to 23 min 60:40, 23 to 24 60:40,

24 to 26 80:20 and the flow rate was set at 0.7 mL/min. For each injection, the volume taken from samples in both DBP and DEHP analysis was 20 μ L. The analyses were carried out together with a UV detector (230 nm) at room temperature.

6.2.9. Degradation products

To identify the products resulting from enzymatic degradation of DBP and DEHP, an Agilent Technologies 1260 Infinity series high performance liquid chromatograph coupled with an accurate mass quadrupole time-of-flight 6550 iFunnel Q-TOF mass spectrometer. Jet Stream ion source was operated in positive scan mode over the range of m/z 50–950 (Agilent Technologies, Santa Clara, CA, USA). For the chromatographic separation, a Poroshell 120 SB-C18 column (3.0 \times 100 mm, particle size 2.7 μ m) was used with a gradient mixture of 0.1% formic acid in water (A) and 0.1% formic acid in acetonitrile (B) at a flow rate of 0.4 mL/min. The gradient program included 0–1 min, 40% B; 1–20 min, 40%–95% B; 20–27 min, 95% B; 27–30 min, 40% B. The temperature of the column was kept at 40°C, and the injection volume was 10 μ L. Agilent MassHunter Acquisition Software Ver. A.09.00 was used to control data acquisition, and MassHunter Qualitative Software Ver. B.07.00 was used for data processing.

6.3. Results and Discussion

6.3.1. Enzyme assays

optimum conditions of pH 8 and temperature 55°C for recombinant esterase, enzyme activity was measured as 650 U/L in the presence of 0.5 mM pNPC-2 as substrate. As for *Bacillus subtilis* esterase, the activity at pH 7 and 30°C was found to be 550 U/L. Based on the protein concentration calculations, the specific enzyme activity for

recombinant esterase and *Bacillus subtilis* esterase were calculated to be 9.84 U/mg and 27.5 U/mg.

6.3.2. Kinetic parameters

Lineweaver Burk plots were used to calculate the kinetic parameters of the recombinant esterase and *Bacillus subtilis* esterase (data not shown) based on the original substrate of enzymes. Each enzyme had a simple Michaelis-Menten kinetics. Over the investigated concentration range, Lineweaver Burk plots demonstrated a linear response. When the K_m and V_{max} of *Bacillus subtilis* esterase were $0.673 \mu\text{M}$ and $35.461 \mu\text{M}/\text{min}$, respectively, these values of the recombinant esterase composite were determined to be $0.684 \mu\text{M}$ and $35.98 \mu\text{M}/\text{min}$, respectively. These slight differences can be attributed to the structural changes in enzymes affecting the enzyme-substrate binding (Gulay and Sanli-Mohamed, 2012). Generally, the K_m and V_{max} values of both enzymes were low compared to the values in the literature (Tekedar and Sanli-Mohamed, 2011; Mohammadi et al., 2020). Indeed, low K_m and V_{max} values demonstrated a robust interaction between the enzymes and their substrate (Sudo, 1995; Saganuwan, 2021). As a result, the esterase enzymes had a high affinity for their substrate.

6.3.3. Optimization of the solvent extraction

The best solvent for the extraction of DBP and DEHP from soils were determined to be ethyl acetate as shown in Figures 6.1 and 6.2. While the extraction recovery for DBP from soil 1 with ethyl acetate, ACN:H2N, and DCM was $95\% \pm 6.4$, $45\% \pm 7$, and $62\% \pm 9$ respectively, that from soil 2 was $96\% \pm 4.6$, $58\% \pm 2.1$, and $65\% \pm 4.9$, respectively. As for the extraction efficiency of DEHP from the soil, it was found to be $88\% \pm 6.3$, $32.3\% \pm 5.9$, and 64.7 ± 3.8 in the presence of ethyl acetate, ACN:H2N, and DCM from soil 1, respectively. This efficiency from soil 2 in the presence of the same solvents was $94.6\% \pm 5.7$, $43.7\% \pm 7.8$, and $64.2\% \pm 5.4$, respectively. Zhang et al. (2020) used ethyl

acetate as a solvent to extract DEHP from the soil. Similarly, Pietrogrande et al. (2003) highlighted that ethyl acetate was the best solvent for the extraction of PAEs.

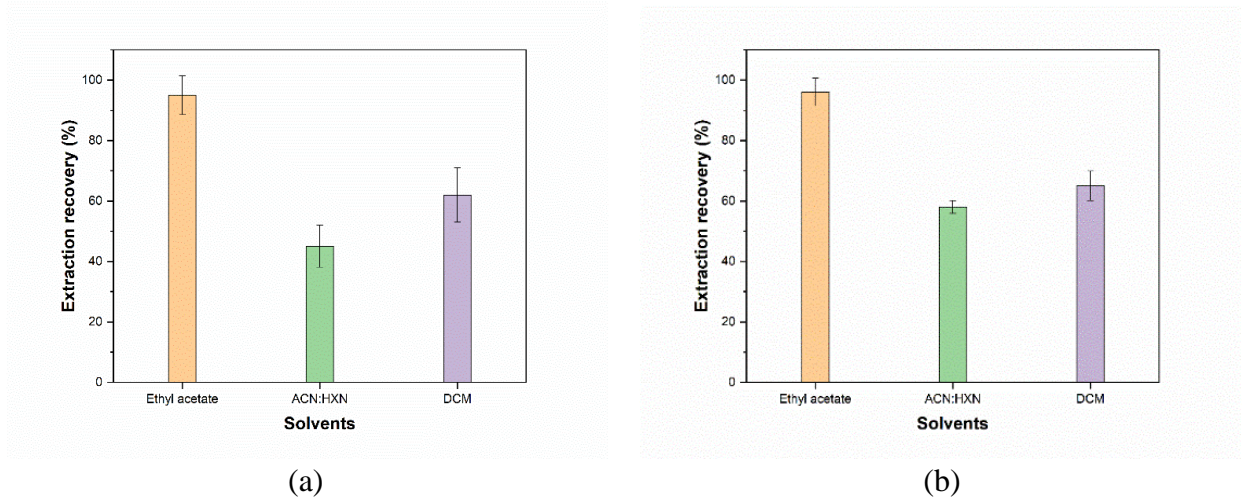


Figure 6.1. Effect of different solvents on extraction efficiency of DBP from soil 1 (a) and soil 2 (b).

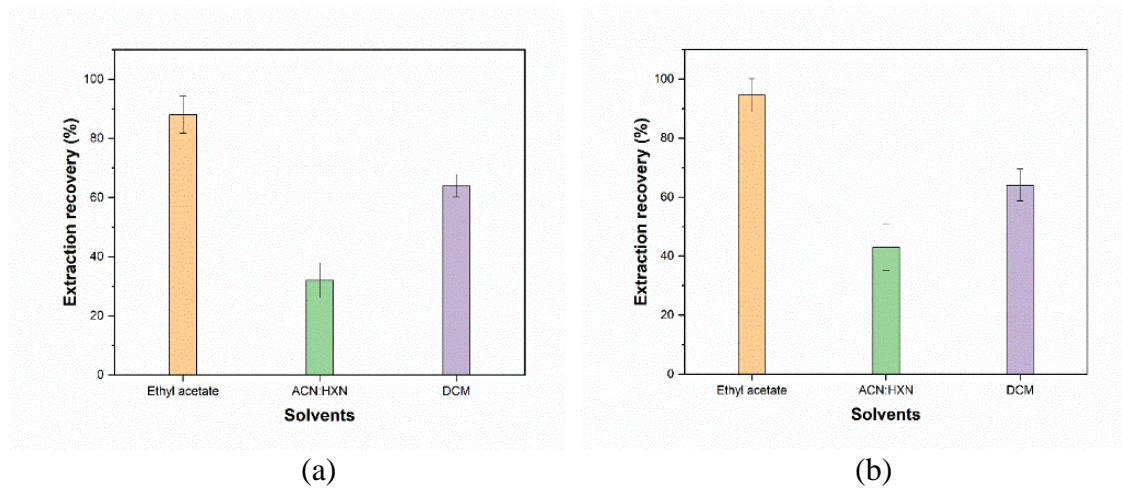


Figure 6.2. Effect of different solvents on extraction efficiency of DEHP from soil 1 (a) and soil 2 (b).

6.3.4. Enzymatic degradation in soil

Before the degradation experiments, the presence of PAEs in the soil was investigated and no residue of PAEs was found in either soil. The degradation experiments of DBP and DEHP with 100 mg/L added in the soil by *Bacillus subtilis* esterase and recombinant esterase were performed under optimum conditions for 168 h. Figures 6.3 and 6.4 demonstrate the degradation efficiency of DBP and DEHP in both soil in the presence of esterase enzymes, respectively. Continuous decreases in the concentration of DBP and DEHP were observed throughout the entire incubation period in the presence of esterase enzymes. The data in Figure 6.3 indicated that while *Bacillus subtilis* esterase completely degraded DBP in soil 1 and soil 2 within 72 h, recombinant esterase could degrade 50% and 82% of DBP in soil 1 and soil 2, respectively, at the end of 168 h. As seen in Figure 6.4, while the esterase enzymes degraded almost 35% of DEHP in soil 1, they could degrade approximately 38% of DEHP in soil 2. That is, both esterase enzymes could not fully degrade DEHP in soil 1 and soil 2. Sun et al. (2022a) reported that when carboxylesterase from *Rhizopus oryzae* could degrade almost 85% of DBP with 1 mg/L in soil within 168 h, it was able to degrade approximately 35% of DEHP (1 mg/L) in soil for the same duration. Compared to the literature, at higher DBP and DEHP concentrations as *Bacillus subtilis* esterase and recombinant esterase exhibited similar or higher degradation efficiency.

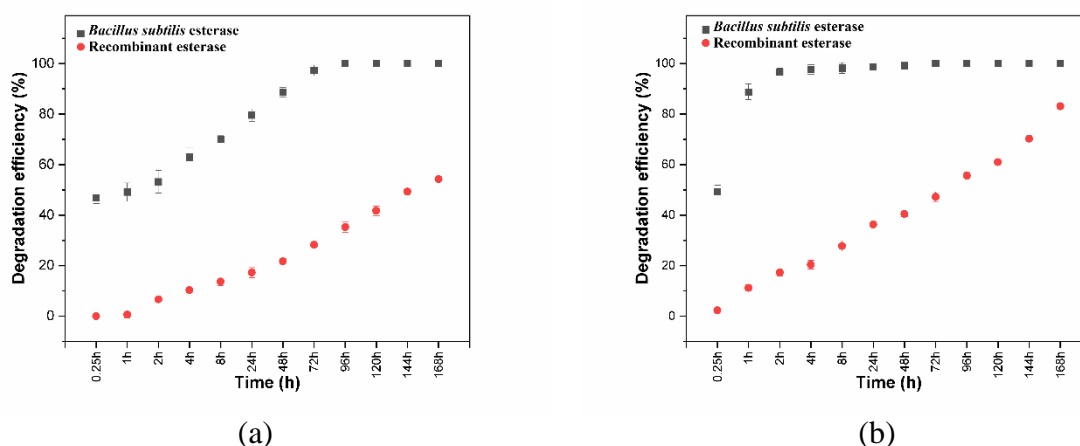


Figure 6.3. Degradation efficiency of DBP in (a) soil 1 and (b) soil 2 by *Bacillus subtilis* esterase and recombinant esterase.

Comparing the enzymatic degradation efficiencies for DBP and DEHP at the same concentration in both soils, both esterase enzymes effectively degraded DBP in soil 2. It is obvious that the characteristic properties of both soils have effects on the enzyme activity in this study. The activity of enzymes is generally affected by various factors such as temperature, humidity, metal ions, nutrient availability, pH, and the content of organic matter etc. (Bueis et al., 2018). Tekedar and Sanli Mohamed (2011) investigated the effect of the ions on the activity of the recombinant esterase. They noted that while Ca^{+2} and Zn^{+2} and Na^{+} positively affected the activity, in the presence of other ions (Mg^{+2} , Mn^{+2} , K^{+} , Fe^{+3}), esterase activity was inhibited at a low rate. Rao et al. (2013) reported that metal ions (Co^{+2} , Ni^{+2} , and Fe^{+3}) have minor inhibition effects on the activity of esterase from *Bacillus pseudofirmus* OF4, while the original activity of enzyme reached 109% and 114% in the presence of Ca^{+2} and Mg^{+2} , respectively. Soil 1 and soil 2 used in this study contain many soil ions such as K^{+} , Na^{+} , Ca^{+2} , Mg^{+2} , Fe^{+3} , and Al^{+3} . The results of the remediation experiments indicated that ions present in the soil can have a noticeable impact on the enzyme activity. For this reason, the degradation efficiency of PAEs in soil 2 was higher than that in soil 1.

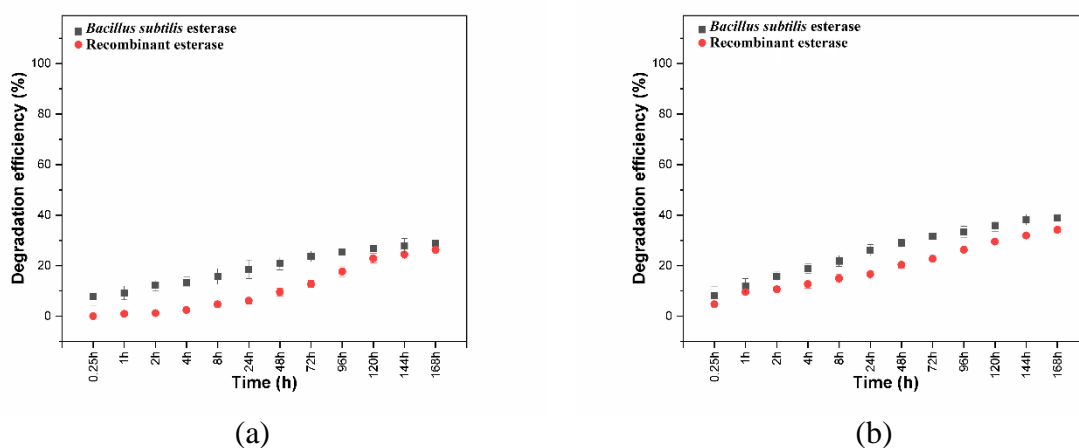


Figure 6.4. Degradation efficiency of DEHP in (a) soil 1 and (b) soil 2 by *Bacillus subtilis* esterase and recombinant esterase.

Esterase enzyme displays a higher substrate specificity for short and medium-chain fatty acid residues ($\text{C} \leq 12$) (Fojan et al., 2000; Samoylova et al., 2018; Ding et al., 2022). Additionally, PAEs with short alkyl side chains such as DMP, DBP, and DEP were most easily degradable among other PAE congeners (Sun et al., 2022a). PAEs with long chains

(DiNP, DnOP, DEHP) and those with benzene ring side chains (BBP) are very difficult to degrade due to steric hindrance (Liang et al., 2008; Ren et al., 2016). Different PAE isomers exhibit different rates of biodegradation, and phthalate hydrolyzing enzymes are structurally specific (Liang et al., 2008). Zhang et al. (2014) performed a study on the degradation of different PAEs types in the presence of the esterase enzyme from *Sulfobacillus acidophilus* DSM10332. They reported that six PAEs (diethyl phthalate (DEP), dipropyl phthalate (DPrP), DBP, dipentyl phthalate (DPeP), diphenyl phthalate (DHP), and BBP) were completely degraded to their phthalate monoesters within 24 h. However, two PAEs (DEHP and dicyclohexyl phthalate (DCHP)) could not be degraded in the same period. In this study, while both esterase enzymes were able to degrade DBP with high efficiency in soil 1 and soil 2, they could not exhibit the same degradation ability on DEHP in both soil at the same time. It is apparent from Figure 6.4 that the esterase degraded DEHP more slowly. Numerous studies have highlighted that the degradation rate of PAEs tends to decrease as the molecular weight increases (Dulazi and Liu, 2011; Ren et al., 2016; Balci et al., 2022; Sun et al., 2022a). Therefore, it is likely that the degradation of DEHP may take a longer time compared to that of DBP, considering their respective molecular weights.

6.3.5. Sequence Analysis

The BLAST and Clustal Omega searches of the deduced amino acid sequence unveiled notable similarities, accounting for approximately 74.5%, between *Bacillus subtilis* esterase and *Geobacillus* sp. esterase, as illustrated in Figure 6.5. These encoded esterase proteins are both comprised of 246 amino acids. *Bacillus subtilis* esterase has a mass of 28.193 kDa, while *Geobacillus* sp. esterase has a slightly higher mass of 28.256 kDa.

One of the largest families of structurally similar proteins, the α/β hydrolase fold family includes both catalytic and non-catalytic functions (Carr and Ollis, 2009). The α/β hydrolase fold is a common folding pattern shared by lipase and esterase enzymes (Ollis et al., 1992). A catalytic triad made up of a nucleophilic residue, a catalytic acid that is not directly involved in catalysis, and a histidine residue makes up the active site of

several α/β hydrolases (Eggert et al., 2000). Serine, aspartate, or glutamate, as well as histidine, are commonly found in the active sites of hydrolases like esterase. The active site triads for both esterase enzymes consist of Ser93, Asp192, and His222.

The consensus sequence Gly-X-Ser-X-Gly is present in the majority of esterase enzymes (Mala and Takeuchi, 2008; Keun et al., 2012). The nucleophilic elbow, which characterizes the motif, is often located where a strand and a helix meet (Ollis et al., 1992; Keun et al., 2012). It offers details on how an amino acid sequence is categorized. The ScanProsite tool's findings show that the same motif is found in both esterase. The amino acids in the active site, which is the substrate binding site of enzymes, use many chemical mechanisms that convert the substrate to the product. That is, enzymatic reactions occur in the enzymes' active sites. The substrate specificity of the enzyme depends on the characteristic properties of the active site region. It is determined by the arrangement of amino acids within the active site and the structure of the substrates. Different substrate specificity can arise from identical active sites due to the influence of substrate and enzyme dynamics (Gade et al., 2021). *Bacillus subtilis* esterase and recombinant esterase (*Geobacillus* sp.) have the same active site triad. However, the DBP and DEHP degradation ability of recombinant esterase is much lower than that of *Bacillus subtilis* esterase. This can be attributed to their difference in substrate specificity. Substrate specificity is crucial, but other enzyme properties also play a role in enzyme's selectivity. For instance, the substitution of amino acids in the entrance region of an enzyme's active site can modify its selectivity towards specific substrates (Albayati et al., 2020). The specificity and selectivity of enzymes when catalyzing various substrates are determined by the extent of complementarity between the substrate and the enzyme. Additionally, specific interactions that occur between the substrate and the enzyme's residues play a crucial role in this process (Albayati et al., 2020).

CLUSTAL O(1.2.4) multiple sequence alignment

```

sp|O32232|EST_BACSU      MKVVTPKPFTEKGGDKAVLLHGFNTADVRLGRYLNERGYTCHAPQYEGHGVPEE
sp|Q06174|EST_GEOSE     MKIVPPKPFTEFAGERAVLLHGFNTGNSADVRLGRFLESKGYTCHAPIYKGGHGVPEE
                        *: *  ***  *.:*.:*****:*****:*.:.***** *:*****
sp|O32232|EST_BACSU      VHTGPEDWVKNVMDGYEYLNKSEGYESIAACGLSLGGVFLKLGTVPIKGIIVMPCAPMH
sp|Q06174|EST_GEOSE     VHTGPDDWVQDVMNGYEFLNKNGYEKIAVAGLSLGGVFLKLGTVPIEGIVTMCAPMY
                        *****:***:.*:***:*.:.***.*.*****:*** *****;
sp|O32232|EST_BACSU      KSEEVMYQGVLSYARNYKKFEGKSPEQIEEEMKEFEKTPMNTLKALQDLIADVRNNVDM
sp|Q06174|EST_GEOSE     KSEETMYEGVLEYAREYKKREGKSEEQIEQEMEKFKQTPMNTLKALQELIADVRDHLDL
                        ****.*:***.***:*** ***** *****:*.:.***:*****:*****:.*:
sp|O32232|EST_BACSU      YSPTFVVQARHDMINTESANIIYNEVETDDKQLKWYEESGHVITLDKERDLVHQDVVE
sp|Q06174|EST_GEOSE     YAPTFVVQARHDEMINDSANIIYNEIESPVKQIKWYEQSGHVITLDQEKDQLHEDIYA
                        *:*****.*** :*****:*: **:*:*****:*:* :*:*:
sp|O32232|EST_BACSU      LEKLDW 246
sp|Q06174|EST_GEOSE     LESLDW 246
                        **.***

```

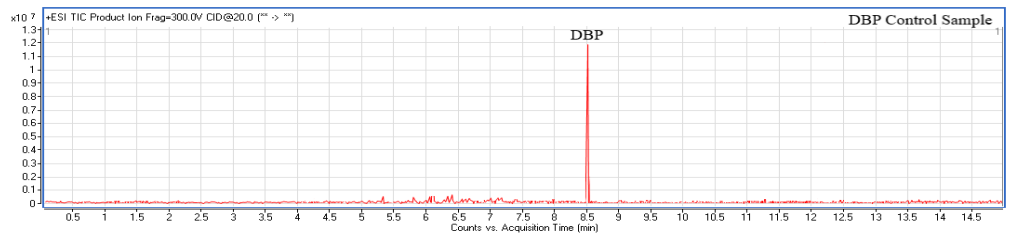
Figure 6.5. Multiple amino acid sequence alignment of esterase from *Bacillus subtilis* and *Geobacillus* sp.

6.3.6. Degradation products

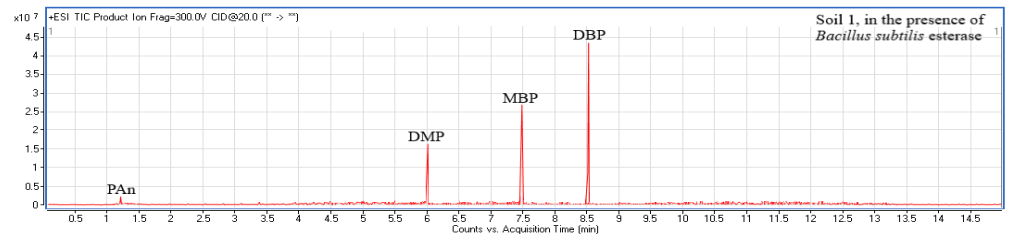
Degradation products of DBP and DEHP by *Bacillus subtilis* esterase and recombinant esterase were discovered by comparing the mass spectra at a retention time (RT) with the mass spectra (m/z) from database in the literature. Figure 6.6 and Figure 6.7 represent the LC-MS chromatogram of identified products of DBP and DEHP. DBP and DEHP standard solution in the absence of esterase was used as the control samples. The m/z ratio of DBP was determined to be 279.15 at 8.5 min (Figure 6.6a). Previous studies reported that DMP, MBP, phthalic acid (PA), corresponding alcohol, and phthalic anhydride (PAn) were metabolites occurring during DBP degradation by microorganisms or enzymes (Kim and Lee, 2005; Fang et al., 2010; Tang et al., 2016; Bope et al., 2019). During the DBP degradation experiments conducted in soil by *Bacillus subtilis* esterase and recombinant esterase, PAn (m/z 149.02, RT 1.3 min), DMP (m/z 163.038 RT 6.1 min), and MBP (m/z 222, RT 7.7 min) were explored to be DBP's products. However, PAn was not only detected in soil 1 in the presence of recombinant esterase enzyme. The DBP degradation experiments result in the formation of MBP and DMP through a transesterification reaction in the presence of methanol (Kim and Lee, 2005; Ahn et al.,

2006). The identified intermediate products can subsequently metabolize to PA by hydrolysis of ester group and demethylation (Tang et al., 2016). Under appropriate conditions, PA can convert PAn (Bope et al., 2019).

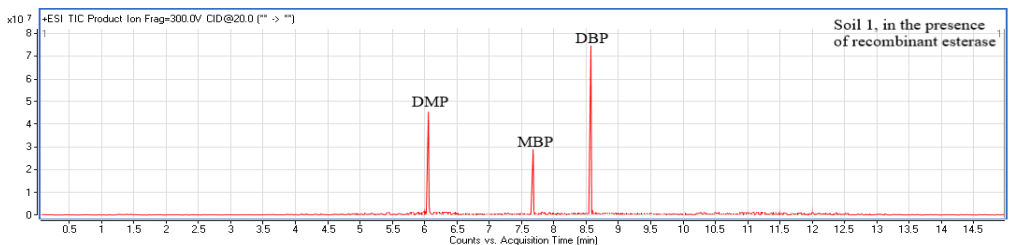
As for LC-MS chromatogram of DEHP, the m/z ratio of DEHP was 391 at 11.5 min (Fig 6.7a). At the end of DEHP degradation by both esterase in soil 1 and soil 2, new peaks appeared along with DEHP. The metabolites that emerge as a result of the degradation of DEHP are identified MEHP (m/z 277, RT 8.7 min) and PAn. The retention time of MEHP and PAn was less than that of DEHP. This is due to the fact that their polarity was higher than that of DEHP (Li et al., 2019). Via de-esterification reaction, an ester bond of DEHP can be attacked by an active amino acid residue on enzyme. Therefore, DEHP can be hydrolyzed to MEHP. The other ester bond on MEHP can be hydrolyzed to PA which is a key metabolite in the biodegradation of DEHP (Sun et al., 2022b). The presence of PA was not observed in the chromatogram of LC-MS analysis conducted after enzymatic degradation of DBP and DEHP in soil 1 and soil 2. Because PA can dehydrate to form PAn under MS conditions (Comak, 2008). Furthermore, it may be due to the conversion of all unreacted acids to the corresponding anhydride. As seen in Figures 6.6c and 6.7c, at DBP and DEHP degradation experiments in soil 1, recombinant esterase could not degrade PAEs to PAn. However, it was able to degrade PAEs up to PAn in soil 2 (Figures 6.6e and 6.7e). This can be attributed to the effect of soil characteristics on the PAE degradation ability of recombinant esterase. Despite all this, *Bacillus subtilis* esterase degraded DBP and DEHP to PAn in both soil 1 and soil 2 (Figures 6.6 and 6.7). These results indicate that *Bacillus subtilis* esterase was much more effective in the degradation of PAEs in soils compared to *Geobacillus* sp esterase. However, both enzymes have a very high potential to degrade PAEs in soil. The formation of MPEs and PAn as a result of PAEs degradation by enzymes is a critical step for microbial degradation (Liang et al., 2008). Therefore, it can be concluded that the presence of both esterase would significantly enhance the microbial degradability of PAEs. These enzymes can be used for the remediation of PAE contamination.



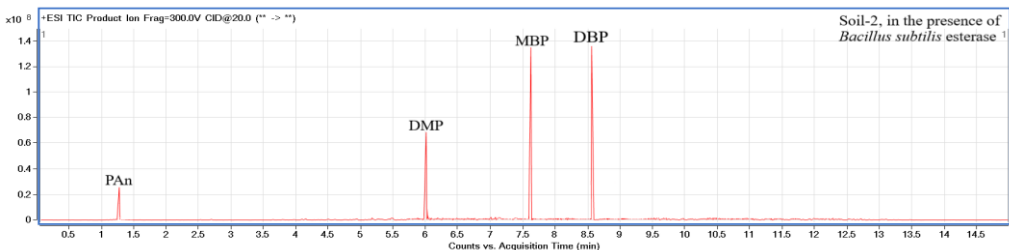
(a)



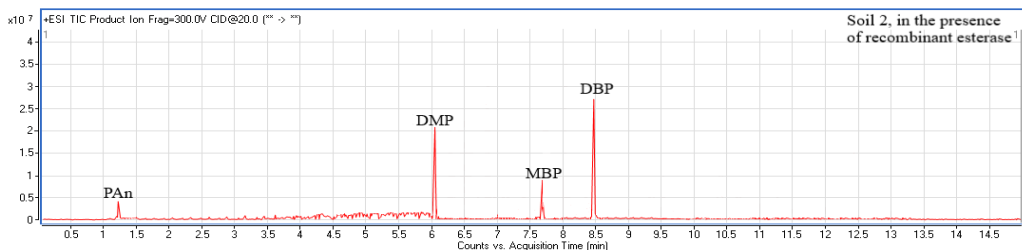
(b)



(c)



(d)



(e)

Figure 6.6. LC-MS chromatogram of the samples before (a) and after DBP degradation experiments conducted in soil 1 and soil 2 in the presence of *Bacillus subtilis* esterase (b and d) and recombinant esterase (c and e).

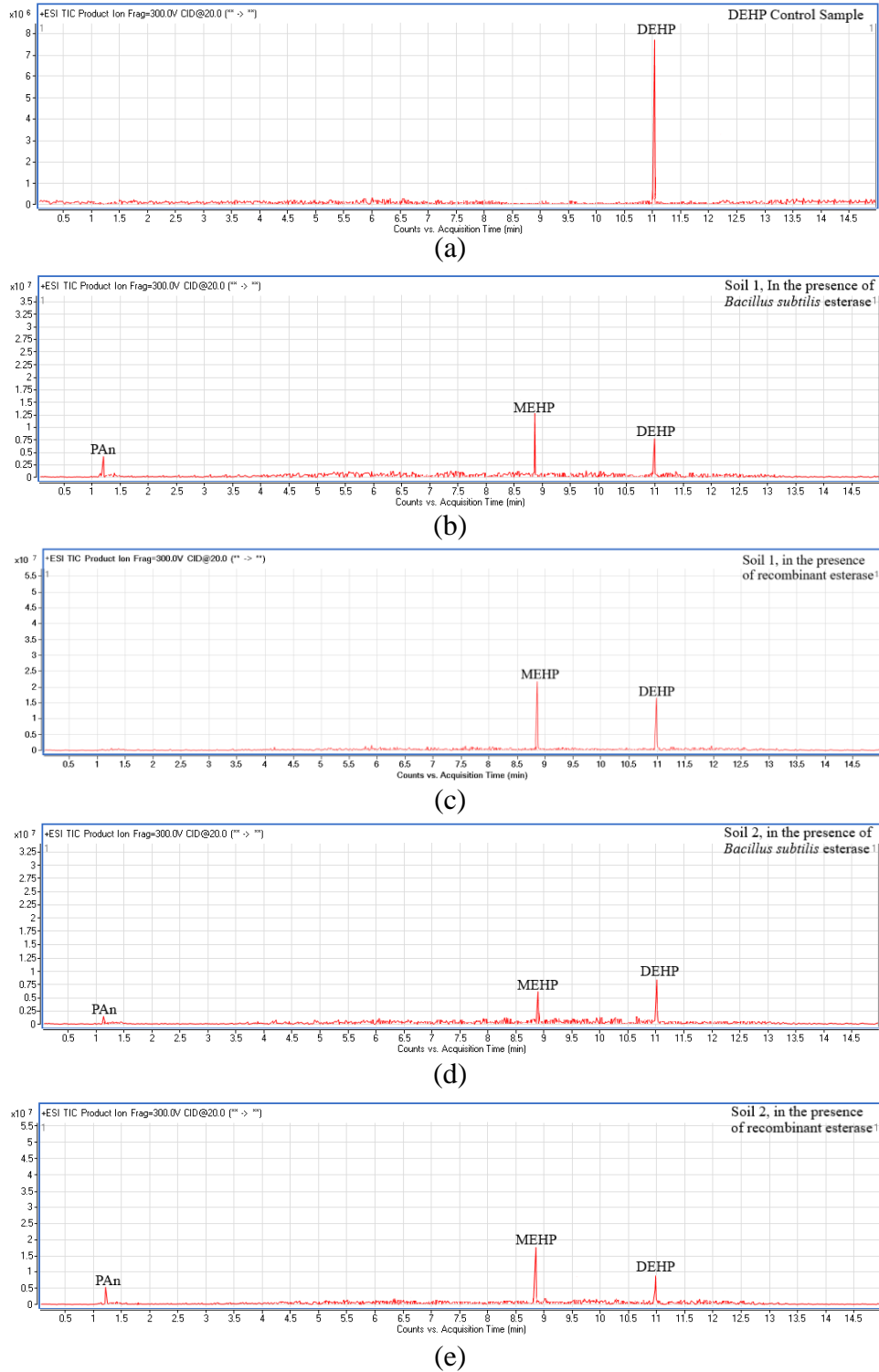


Figure 6.7. LC-MS chromatogram of the samples before (a) and after DEHP degradation experiments conducted in soil 1 and soil 2 in the presence of *Bacillus subtilis* esterase (b and d) and recombinant esterase (c and e).

6.4. Conclusion

This study investigated the enzymatic degradation of DBP and DEHP in two types of soil. *Bacillus subtilis* esterase could effectively degrade DBP and DEHP, whereas recombinant esterase had less effect on DBP and DEHP degradation. Although the *Bacillus subtilis* esterase and recombinant esterase have the same active site triad, they exhibited different substrate specificity owing to the effects of substrate characteristics and enzyme dynamics. It was observed that DEHP degradation needed a long time in soil media. The degradability of PAEs negatively correlated with the alkyl side chain. The variation in the biodegradability of PAEs can be attributed to the steric effects of the side ester chains of PAEs. These ester chains hinder the binding of hydrolytic enzymes to PAEs, subsequently impeding their hydrolysis. In the enzymatic degradation experiments of PAEs in soil, the esterase enzymes were not particularly effective in the degradation of DEHP. This is because the characteristic properties of soil have effects on the enzyme activity. This can affect the PAE-degrading ability of the esterase enzyme. The results obtained in this study are expected to guide the application of esterase in the remediation of waterbody and soil contaminated by various PAEs. Furthermore, the procedure and results of this study will offer both experimental and theoretical insights for the development of in situ enzymatic remediation of PAE-contaminated soils.

CHAPTER 7

CONCLUSION

This thesis focused on the enzymatic degradation of phthalic acid esters (PAEs) congeners, which possess both short (Dibutyl phthalate; DBP) and long alkyl (Diethylhexyl phthalate; DEHP) side chains in water and soil. These compounds are known to act as endocrine disruptors, mutagens, hepatotoxic agents, and carcinogens. The main objective is to develop a practical, effective, and eco-friendly pathway on the removal of PAEs from the contaminated environment, mitigating their adverse impact on ecosystems and living organisms. In this regard, recombinant esterase enzyme originating from *Geobacillus* sp. was successfully expressed and purified to degrade PAE congeners in water and soil. To compare the PAE-degrading abilities of commercial enzymes from various microorganisms with those of the recombinant enzyme, experiments were conducted in the presence of commercial esterase and lipase enzymes. The most important findings of this thesis study are as follows:

- Both recombinant and commercial enzymes degraded DBP and DEHP to a reasonable extent. While commercial enzymes exhibited over 90% degradation efficiency of PAE congeners, the recombinant enzyme degraded these congeners to a limited extent in water.
- Immobilization of enzymes to HNTs by adsorption method did not significantly affect the activity of commercial enzymes. The formed enzyme composites could be reused for 7 degradation cycles, keeping a remarkable catalytic activity.
- In other immobilization method (crosslinking), two bionanocomposites (CTS-HNT and ALG-HNT) were prepared by immobilizing commercial enzyme (*Bacillus subtilis* esterase) to HNTs modified with chitosan (CTS) and alginate (ALG). The bionanocomposite with CTS showed the best degradation levels in batch tests, attaining complete degradation of DBP and around 90% of DEHP.
- In the studies conducted to treat intentionally contaminated soil with DBP and DEHP in the presence of *Bacillus subtilis* esterase and recombinant esterase, recombinant esterase had a less significant effect on the degradation of DBP and

DEHP than *Bacillus subtilis* esterase. Whereas both *Bacillus subtilis* esterase and recombinant esterase have the same active site triad, their substrate selectivity can vary depending on the properties of the substrate and the dynamics of the enzyme. Besides, the soil characteristics had an impact on the enzymes' activity and degradation performance.

In conclusion, enzymatic degradation, which is an economical, safe, and environmentally friendly method, was successfully carried out to remove PAEs, which have negative effects on living things and the environment. With immobilization methods such as adsorption and cross-linking, the activity and stability of the enzymes were largely preserved throughout long-term degradation experiments. The findings of this thesis are anticipated to provide valuable guidance for the use of both immobilized and free enzymes in the remediation of environments contaminated with various PAEs.

CHAPTER 8

FUTURE PROJECTION

In future research endeavors, we advocate for the efficient utilization of both *Bacillus subtilis* esterase and recombinant esterase in addressing environmental pollutants containing ester bonds. While the thermophilic variant of the recombinant enzyme exhibited diminished performance, identifying, and overcoming the limitations highlighted in this study is crucial for further exploration. Employing a dual strategy involving mutation and promoter engineering holds promise for enhancing the enzymatic activity of the recombinant esterase in degrading PAEs and improving overall efficiency.

Simultaneously, our findings propose that the enzymatic hydrolysis of PAEs makes them susceptible to microbial influence for further degradation. Consequently, this study's methodology can be adapted for other congeners of PAEs, shedding light on their interactions with enzymes. This versatility opens the door to a range of applications in areas where phthalic acid esters are present, establishing a foundation for deploying the recombinant esterase enzyme with heightened PAE-degrading capabilities across various contexts.

REFERENCES

- Abdullayev, E., Price, R., Shchukin, D., Lvov, Y., 2009. Halloysite tubes as nanocontainers for anticorrosion coating with benzotriazole. *ACS Applied Materials & Interfaces*. 1(7), 1437-1443. <https://doi.org/10.1021/am9002028>.
- Ahmadi, E., Gholami, M., Farzadkia, M., Nabizadeh, R., Azari, A., 2015. Study of moving bed biofilm reactor in diethyl phthalate and diallyl phthalate removal from synthetic wastewater. *Bioresource Technology*. 183, 129-135. <https://doi.org/10.1016/j.biortech.2015.01.122>.
- Ahn, Y.J., Kim, Y.H., Min, J., Lee, J., 2006. Accelerated degradation of dipentyl phthalate by *Fusarium oxysporum* f. sp. *pisi* cutinase and toxicity evaluation of its degradation products using bioluminescent bacteria. *Current Microbiology*. 52(5), 340-344. <https://doi.org/10.1007/s00284-005-0124-9>.
- Ahuactzin-Perez, M., Tlecuitl-Beristain, S., Garcia-Davila, J., Santacruz-Juarez, E., Gonzalez-Perez, M., Gutierrez-Ruiz, M.C., Sanchez, C., 2018. Kinetics and pathway of biodegradation of dibutyl phthalate by *Pleurotus ostreatus*. *Fungal Biology* 122, 991-997. <https://doi.org/10.1016/j.funbio.2018.07.001>.
- Akgöl, S., Kacar, Y., Denizli, A., Arica, M., 2001. Hydrolysis of sucrose by invertase immobilized onto novel magnetic polyvinylalcohol microspheres. *Food Chemistry*. 74 (3), 281-288. [https://doi.org/10.1016/S0308-8146\(01\)00150-9](https://doi.org/10.1016/S0308-8146(01)00150-9).
- Akita, K., Naitou, C., Maruyama, K., 2001. Purification and characterization of an esterase from *Micrococcus* sp. YGJ1 hydrolyzing phthalate esters. *Bioscience, Biotechnology, and Biochemistry*. 65 (7), 1680-1683. <https://doi.org/10.1093/jb/mvi004>.
- Albayati, S.H., Masomian, M., Ishak, S.N.H., Ali, M.S.B.M., Thean, A.L., Sharif, F.B.M., Noor, N.D.B.M., Rahman, R.N.Z.R.A., 2020. Main structurally targets for engineering lipase substrate specificity. *Catalysts*, 10 (7), 747. <https://doi.org/10.3390/catal10070747>.

- Amir, S., Hafidi, M., Merlina, G., Hamdi, H., Jouraiphy, A., El Gharous, M., Revel, J.C., 2005. Fate of phthalic acid esters during composting of both lagooning and activated sludges. *Process Biochemistry*. 40(6), 2183-2190. <https://doi.org/10.1016/j.procbio.2004.08.012>.
- An, C.J., Huang, G.H., Yu, H., Wei, J., Chen, W., Li, G.C., 2010. Effects of short chain organic acids and pH on the behaviors of pyrene in soil-water system. *Chemosphere*. 81, 1423-1429. <https://doi.org/10.1016/j.chemosphere.2010.09.012>.
- Asuri P., Karajanagi S.S., Sellitto E., Kim, D.Y., Kane, R.S., Dordick, J.S., 2006. Water-soluble carbon nanotube-enzyme conjugates as functional biocatalytic formulations. *Biotechnology and Bioengineering*. 95 (5), 804– 811. <https://doi.org/10.1002/bit.21016>.
- Bai, N., Li, S., Zhang, J., Zhang, H., Zhang, H., Zheng, X., Lv, Z., 2020. Efficient biodegradation of DEHP by CM9 consortium and shifts in the bacterial community structure during bioremediation of contaminated soil. *Environmental Pollution*. 266, 115112. <https://doi.org/10.1016/j.envpol.2020.115112>.
- Balci, E., Rosales, E., Pazos, M., Sofuoglu, A., Sanroman, M.A., 2022. Continuously treatment of diethyl hexyl and dibutyl phthalates by fixed-bed reactor: Comparison of two esterase bionanocomposites. *Bioresource Technology*. 363. 127990. <https://doi.org/10.1016/j.biortech.2022.127990>.
- Balci, E., Rosales, E., Pazos, M., Sofuoglu, A., Sanroman, M.A., 2023. Immobilization of esterase from *Bacillus subtilis* on halloysite nanotubes and applications on dibutyl phthalate degradation. *Environmental Technology & Innovation* 30, 103113. <https://doi.org/10.1016/j.eti.2023.103113>.
- Baloyi, N.D., Tekere, M., Maphangwa, K.W., Masindi, V., 2021. Insights into the prevalence and impacts of phthalate esters in aquatic ecosystems. *Frontiers in Environmental Science*. 9, 684190. <https://doi.org/10.3389/fenvs.2021.684190>.
- Benjamin, S., Pradeep, S., Josh, M.S., Kumar, S., Masai, E. 2015., A monograph on the remediation of hazardous phthalates. *Journal of Hazardous Materials*. 298, 58-72. <https://doi.org/10.1016/j.jhazmat.2015.05.004>.

- Bertelsen, R.J., Carlsen, K.C.L., Calafat, A.M., Hoppin, J.A., Haland, G., Mowinckel, R., Lovik, M., 2013. Urinary biomarkers for phthalates associated with asthma in Norwegian children. *Environmental Health Perspectives*. 121 (2),251-256. <https://doi.org/10.1289/ehp.1205256>.
- Bhagyaraj S. and Krupa, I., 2020. Alginate-Halloysite Nanocomposite Aerogel: Preparation, Structure, and Oil/Water Separation Applications. *Biomolecules*. 10, 1632. <https://doi.org/10.3390/biom10121632>.
- Bilal, M., Rashid, E.U., Zdart, J., dos Santos, J.C.S., Fernandes, P.C.B., Cheng, H., Jesionowski, T., 2022. Engineering magnetic nanobiocatalytic systems with multipurpose functionalities for biocatalysis, biotechnology and bioprocess applications. *Sustainable Chemistry and Pharmacy*. 30, 100866. <https://doi.org/10.1016/j.scp.2022.100866>.
- Bonzom, C., Schild, L., Gustafsson, H., Olsson, L., 2018. Feruloyl esterase immobilization in mesoporous silica particles and characterization in hydrolysis and transesterification. *BMC Biochemistry*. 19(1), 1-12. <https://doi.org/10.1186/s12858-018-0091-y>.
- Bornehag, C. G., Lundgren, B., Weschler, C. J., Sigsgaard, T., Hagerhed-Engman, L., Sundell, J., 2005 Phthalates in indoor dust and their association with building characteristics. *Environmental Health Perspectives*. 113 (10), 1399–1404. <https://doi.org/10.1289/ehp.7809>.
- Bornehag, C.G., Carlstedt, F., Jönsson, B.A., Lindth, C.H., Jensen, T.K., Bodin, A., Swan, S.H., 2015. Prenatal phthalate exposures and anogenital distance in Swedish boys. *Environmental Health Perspectives*. 123, 101-107. <https://doi.org/10.1289/ehp.1408163>.
- Boonyaroj, V., Chiemchaisri, C., Chiemchaisri, W., Yamamoto, K., 2012. Removal organic micro-pollutants from solid waste landfill leachate in membrane bioreactor operated without excess sludge discharge. *Water Science & Technology*. 66,1774-1780. <https://doi.org/10.2166/wst.2012.324>.

- Bope, A., Haines, S.R., Hegarty, B., Weschler, C.J., Peccia, J., Dannemiller, K.C. 2019. Degradation of phthalate esters in floor dust at elevated relative humidity. *Environmental Science Processes & Impacts*. 21, 1268-1279. <https://doi.org/10.1039/C9EM00050J>.
- Bradford, M.M., 1976. A rapid and sensitive method for the quantitation of microgram quantities of protein utilizing the principle of protein-dye binding. *Analytical Biochemistry*. 72 (1-2), 248-254. [https://doi.org/10.1016/0003-2697\(76\)90527-3](https://doi.org/10.1016/0003-2697(76)90527-3).
- Braun, J.M., 2017. Early-life exposure to EDCs: role in childhood obesity and neurodevelopment. *Nature Reviews Endocrinology*. 13, 161–173. <https://doi.org/10.1038/nrendo.2016.186>.
- Brena, B., González-Pombo, P., Batista-Viera F., 2013. Immobilization of enzymes: A literature survey. *Immobilization of Enzymes and Cells*. 1051, 15-31. https://doi.org/10.1007/978-1-62703-550-7_2.
- Bueis, T., Turrion, M.B., Bravo, F., Pando, V., Muscolo, A., 2018. Factors determining enzyme activities in soils under *Pinus halepensis* and *Pinus sylvestris* plantations in Spain: a basis for establishing sustainable forest management strategies. *Annals of Forest Science*. 75, 34. <https://doi.org/10.1007/s13595-018-0720-z>.
- Cai, Q.Y., Mo, C.H., Wu, Q.T., Zeng, Q.Y., Katsoylannis, A., 2007. Occurrence of organic contaminants in sewage sludges from eleven wastewater treatment plants, China. *Chemosphere*. 68 (9), 1751-1962. <https://doi.org/10.1016/j.chemosphere.2007.03.041>.
- Calafat, A.M., Valentin-Blasini, L., Ye, X., 2015. Trends in exposure to chemicals in personal care and consumer products. *Current Environmental Health Reports*. 2, 348–355. <https://doi.org/10.1007/s40572-015-0065-9>.
- Cao, J., Mo, J., Sun, Z., Zhang, Y., 2018. Indoor particle age, a new concept for improving the accuracy of estimating indoor airborne SVOC concentrations, and applications. *Building and Environment*. 136, 88-97. <https://doi.org/10.1016/j.buildenv.2018.03.028>.

- Carr, P. D., Ollis, D.L., 2009. Alpha/beta hydrolase fold: an update. *Protein & Peptide Letters* 16, 1137–1148. <https://doi.org/10.2174/092986609789071298>.
- Cavalcante, F.C.T.T., Falcao, I.R.A., Souza, J.E.S., Rocha, T.G., de Sousa, I.G., Cavalcante, A.L.G., de Oliveira, A.L.B., de Sousa, M.C.M., dos Santos, J.C.S., 2021. Designing of nanomaterials-based enzymatic biosensors: Synthesis, properties, and applications. *Electrochemistry*. 2 (1), 149-184. <https://doi.org/10.3390/electrochem2010012>.
- Chai, C., Cheng, H., Ge, W., Ma, D., Shi, Y., 2014. Phthalic acid esters in soils from vegetable greenhouses in Shandong Peninsula, East China. *PLOS ONE*. 9(4), e95701. <https://doi.org/10.1371/journal.pone.0095701>.
- Chang, B.V., Yang, C.M., Cheng, C.H., Yuan, S.Y., 2004. Biodegradation of phthalate esters by two bacterial strains. *Chemosphere*. 55 (4), 533-538. <https://doi.org/10.1016/j.chemosphere.2003.11.057>.
- Chang, B.V., Liao, C.S., Yuan, S.Y., 2005. Anaerobic degradation of diethyl phthalate, di-n-butyl phthalate, and di-2(ethylhexyl) phthalate from river sediment in Taiwan, *Chemosphere*. 58, 1601-1607. <https://doi.org/10.1016/j.chemosphere.2004.11.031>.
- Chang, B.V., Wang, T.H., Yuan, S.Y., 2007. Biodegradation of four phthalate esters in sludge. *Chemosphere*. 69 (7), 1116-11123. <https://doi.org/10.1016/j.chemosphere.2007.04.011>.
- Chang, W.H., Herianto, S., Lee, C.C., Hung, H., Chen, H.L., 2021. The effects of phthalate ester exposure on human health: a review. *Science of Total Environment*. 786, 147371. <https://doi.org/10.1016/j.scitotenv.2021.147371>.
- Chatterjee, S., Dutta, T.K., 2008. Metabolic cooperation of *Gordonia* sp. strain MTCC 4818 and *Arthrobacter* sp. strain WY in the utilization of butyl benzyl phthalate effect of a novel co-culture in the degradation of a mixture of phthalates. *Microbiology*. 154 (11), 3338-3346. <https://doi.org/10.1099/mic.0.2008/021881-0>.
- Chao, C., Liu, J., Wang, J., Zhang, Y., Zhang, B., Zhang, Y., Xiang, X., Chen, R., 2013. Surface modification of halloysite nanotubes with dopamine for enzyme

- immobilization. *Applied Materials & Interfaces*. 5 (21), 10559-10564. <https://doi.org/10.1021/am4022973>.
- Chao, W.L., Cheng, C.Y., 2007. Effect of introduced phthalate-degrading bacteria on the diversity of indigenous bacterial communities during di-(2-ethylhexyl) phthalate (DEHP) degradation in a soil microcosm. *Chemosphere*. 67(3), 482-488. <https://doi.org/10.1016/j.chemosphere.2006.09.048>.
- Chen, B., Wang, X., Gao, X., Jiang, J., Hu, M., Li, S., Zhai, Q., Jiang, Y., 2021a. DNA directed immobilization of horseradish peroxidase on phase-transitioned lysozyme modified TiO₂ for efficient degradation of phenol in wastewater. *Materials and Design* 201, 109643. <https://doi.org/10.1016/j.matdes.2021.109463>.
- Chen, F., Chen, Y., Chen, C., Feng, C., Feng, L., Dong, Y., Chen, J., Lan, J., Hou, H., 2021b. High-efficiency degradation of phthalic acid esters (PAEs) by *Pseudarthrobacter defluvii* E5: Performance, degradative pathway, and key genes. *Science of the Total Environment*. 794, 148719. <https://doi.org/10.1016/j.scitotenv.2021.148719>.
- Chen, J.P., Lin, Y.S., 2007. Decolorization of azo dye by immobilized *Pseudomonas luteola* entrapped in alginate-silicate sol-gel beads, *Process Biochemistry*. 42, 934–942, <https://doi.org/10.1016/j.procbio.2007.03.001>.
- Chen, X., Zhang, X., Yang, Y., Yue, D., Xiao, L., Yang, L., 2015. Biodegradation of an endocrine-disrupting chemical di-n-butyl phthalate by newly isolated *Camelimonas* sp. and enzymatic properties of its hydrolase. *Biodegradation*. 26 (2), 171-182. <https://doi.org/10.1007/s10532-015-9725-6>.
- Choo, C.K., Kong, X.Y., Goh, T.L., Ngoh, G.C., Horri, B.A., Salamatina, B., 2016. Chitosan/Halloysite beads fabricated by ultrasonic-assisted extrusion-dripping and a case study application for copper ion removal. *Carbohydrate Polymers*. 138, 16-26. <https://doi.org/10.1016/j.carbpol.2015.11.060>.
- Clark, K., Cousins, I.T., MacKay, D., Yamada, K., 2003. Observed concentrations in the environment. In: Staples, C.A. (Ed.), *Handbook of Environmental Chemistry*. Springer, Berlin, Heidelberg, 125–177. <https://doi.org/10.1007/b11465>.

- Collins, S.E., Lassalle, V., Ferreira, M.L., 2011. FTIR-ATR characterization of free *Rhizomucor miehei* lipase (RML), Lipozyme RM IM and chitosan-immobilized RML. *Journal of Molecular Catalysis B: Enzymatic* 72 (3-4), 220-228. <https://doi.org/10.1016/j.molcatb.2011.06.009>.
- Comak, G., 2008. The synthesis of phthalate derivatives in high-pressure, high-temperature water. (Doctoral dissertation, University of Çukurova, Adana). Retrieved from <http://library.cu.edu.tr/tezler/6825>.
- Correa, D., and Ramos, C.H.I., 2009. The use of circular dichroism spectroscopy to study protein folding form and function. *African Journal of Biochemistry Research*. 3 (5), 167-173.
- Cousins, I., Mackay, D., 2000. Correlating the physical-chemical properties of phthalate esters using the “three solubility” approach. *Chemosphere*. 41(9), 1389-1399. [https://doi.org/10.1016/S0045-6535\(00\)00005-9](https://doi.org/10.1016/S0045-6535(00)00005-9).
- Cousins, I.T., Mackay, D., Parkerton, T.F., 2003 Physical-chemical properties and evaluative fate modelling of phthalate esters. In: *Handbook of Environmental Chemistry*. Springer, Berlin, Heidelberg, pp. 57–84. Available from: <https://link.springer.com/chapter/10.1007/b11463>. (accessed 17 March 2022).
- Cruz-Ortiz, B.R., Rios-Gonzalez, L.J., Garza Garcia, Y., Rodrigues de la Garza, J.A., Rodrigues-Martinez, J., 2011. Immobilization of *Thermomyces lanuginosus* lipase in PVA-alginate beads. *Journal of the Mexican Chemical Society*. 55(3), 176-188. <https://doi.org/10.29356/jmcs.v55i3.817>.
- Cifci, D.I., Kinaci, C., Arikan, O.A., 2013. Occurrence of phthalates in sewage sludge from three wastewater treatment plants in Istanbul, Turkey. *Clean-Soil, Air, Water*. 41(9), 851-855.
- Çinar, E., Ercan, S., Gulesci, N., 2017. Immobilization of urease in lewattite particle. *Batman University Journal of Life Science*. 7(2), 124-136.
- Das, M.T., Ghosh, P., Thakur, I.S., 2014. Intake estimates of phthalate esters for the South Delhi population based on exposure media assessment. *Environmental Pollution*. 189, 118–125. <https://doi.org/10.1016/j.envpol.2014.02.021>.

- Datta, S., Christena, L.R., Rajaram, Y.R.S., 2013. Enzyme immobilization: An overview on techniques and support materials. *3 Biotech.* 3 (1), 1-9. <https://doi.org/10.1007/s13205-012-0071-7>.
- De Barros, M., Macedo, G.A., 2011. Biochemical characterization of esterase from soybean (*Glycine max* L.). *Food Science and Biotechnology.* 20 (5), 1195-1201. <https://doi.org/10.1007/s10068-011-0165-8>.
- Deblonde, T., Cossu-Leguille, C., Hartemann, P., 2011. Emerging pollutants in wastewater: A review of the literature. *International Journal of Hygiene and Environmental Health.* 214 (6), 442-448. <https://doi.org/10.1016/j.ijheh.2011.08.002>.
- Ding, J., Wang, C., Xie, Z., Li, J., Yang, Y., Mu, Y., Tang, X., Xu, B., Zhou, J., Huang, Z., 2015. Properties of a newly identified esterase from *Bacillus* sp. K91 and its novel function in diisobutyl phthalate degradation. *PLoS ONE.* 10 (3), e0119216. <https://doi.org/10.1371/journal.pone.0119216>.
- Ding, Y., Nie, L., Yang, X.C., Li, Y., Huo, Y.Y., Li, Z., Gao, Y., Cui, H.L. Xu, X.W., 2022. Mechanism and structural insights into a novel esterase, E53, isolated from *Erythrobacter longus*. *Frontiers in Microbiology* 12, 798194. <https://doi.org/10.3389/fmicb.2021.798194>.
- Dritsa, V., Rigas, F., Doulia, D., Avramides, E.J., Hatzianestis, I., 2009. Optimization of culture conditions for the biodegradation of lindane by the polypore fungus *ganoderma australe*. *Water, Air, & Soil Pollution.* 204, 19-27. <https://doi.org/10.1007/s11270-009-0022-z>.
- Duce, C., Bramanti, E., Ghezzi, L., Bernazzani, L., Bonaduece, I., Colombini, M.P., Spepi, A., Biagi, S., Tine, M.R., 2013. Interactions between inorganic pigments and proteinaceous binders in reference paint reconstructions. *Dalton Transactions.* 42, 5975-5984. <https://doi.org/10.1039/C2DT32203J>.
- Duce, C., Porta, V.D., Bramanti, E., Campanella, B., Spepi, A., Tine, M.R., 2017. Loading of halloysite nanotubes with BSA, α -Lac, and β -Lg: A fourier transform infrared spectroscopic and thermogravimetric study. *Nanotechnology.* 28. <https://doi.org/10.1088/1361-6528/28/5/055706>.

- Dulazi, A.A., Liu, H., 2011. Removal of phthalate esters from water using immobilized lipase on chitosan beads. *Environmental Technology*. 32 (13), 1443-1451. <https://doi.org/10.1080/09593330.2010.538932>.
- E.C., 1997. Concerning the third list of priority substances as foreseen under Council Regulation (EEC) No 793/93. *Official Journal of European Communities*. 25, 13-14.
- Eggert, T., Pencreach, G., Douchet, I., Verger, R., Jaeger, K.E., 2000. A novel extracellular esterase from *Bacillus subtilis* and its conversion to monoacylglycerol hydrolase. *European Journal of Biochemistry*. 267, 6459-6464. <https://doi.org/10.1046/j.1432-1327.2000.01736.x>.
- Eichler, C.M., Hubal, E.A.C., Little, J.C., 2019. Assessing human exposure to chemicals in materials, products, and articles: The international risk management landscape for phthalates. *Environmental Science & Technology*. 53 (23), 13583-13597. <https://doi.org/10.1021/acs.est.9b03794>.
- Ernest, V., Sekar, G., Mukherjee, A., Chandrasekaran, N., 2014. Studies on the effect of AgNP binding on α -amylase structure of porcine pancreas and *Bacillus subtilis* by multi-spectroscopic methods. *Journal of Luminescence*. 146, 263-268. <https://doi.org/10.1016/j.jlumin.2013.09.065>.
- Fan, S., Wang, J., Yan, Y., Wang, J., Jia, Y., 2018. Excellent degradation performance of a versatile phthalic acid esters-degrading bacterium and catalytic mechanism of monoalkyl phthalate hydrolase. *International Journal of Molecular Sciences*. 19 (9), 2803. <https://doi.org/10.3390/ijms19092803>.
- Fang, C.R., Yao, J., Zheng, Y.G., Jiang, C.J., Hu, L.F., Wu, Y.Y., Shen, D.S., 2010. Dibutyl phthalate degradation by *Enterobacter* sp. T5 isolated from municipal solid waste in landfill bioreactor. *International Biodeterioration & Biodegradation*. 64 (6), 442-446. <https://doi.org/10.1016/j.ibiod.2010.04.010>.
- Fang, Y., Zhang, L., Wang, J., Zhou, Y., Ye, B., 2017. Biodegradation of phthalate esters by a newly isolated *Acinetobacter* sp. strain LMB-5 and characteristics of its

- esterase. *Pedosphere*. 27(3), 606-65. [https://doi.org/10.1016/S1002-0160\(17\)60355-2](https://doi.org/10.1016/S1002-0160(17)60355-2).
- Feng, N.X., Yu, J., Mo, C.H., Zhao, H.M., Li, Y.W., Wu, B.X., Cai, Q.Y., Li, H., Zhou, D.M., Wong, M.H., 2018. Biodegradation of di-n-butyl phthalate (DBP) by a novel endophytic *Bacillus megaterium* strain YJB2. *Science of the Total Environment*. 616-617, 117-127. <https://doi.org/10.1016/j.scitotenv.2017.10.298>.
- Feng, Z., Kunyan, C., Jiamo, F., Guoying, S., Huifang, Y., 2002. Biodegradability of di (2-ethylhexyl) phthalate by *Pseudomonas fluorescens* FS1. *Water, Air, & Soil Pollution*. 140(1), 297-305. <https://doi.org/10.1023/A:1020108502776>.
- Fernandez-Fernandez, M., Sanroman, M.A., Moldes, D., 2013. Recent developments and applications of immobilized laccase. *Biotechnology Advances*. 31(8), 1808-1825. <https://doi.org/10.1016/j.biotechadv.2012.02.013>.
- Ferrari, P.C., Araujo, F.F., Pianaro, S.A., 2017. Halloysite nanotubes-polymeric nanocomposites: characteristics, modifications, and controlled drug delivery approaches. *Ceramica*. 63, 423-431. <http://dx.doi.org/10.1590/0366-69132017633682167>.
- Fitter, J., Hermann, R., Dencher, N.A., Blume, A., Hauss, T., 2001. Activity and stability of a thermostable α -amylase compared to its mesophilic homologue: Mechanism of Thermal Adaptation. *Biochemistry*. 40 (35), 10723-10731. <https://doi.org/10.1021/bi010808b>.
- Fojan, P., Jonson, P.H., Petersen, M.T.N., Petersen, S.F., 2000. What distinguishes an esterase from a lipase: A novel structural approach. *Biochimie*. 82 (11). 1033-1044. [https://doi.org/10.1016/S0300-9084\(00\)01188-3](https://doi.org/10.1016/S0300-9084(00)01188-3).
- Fromme, H., Gruber, L., Schlummer, M., Waltz, G., Böhmer, S., Angerer, J., Mayer, R., Liebl, B., Bolte, G., 2007. Intake of phthalates and di(2-ethylhexyl) adipate: Results of the integrated exposure assessment survey based on duplicate diet sample and biomonitoring data. *Environment International*. 33 (8), 1012-1020. <https://doi.org/10.1016/j.envint.2007.05.006>.

- Gade, M., Tan, L.L., Damry, A.M., Sandhu, M., Brock, J.S., Delaney, A., Villar-Briones, A., Jackson, C.J., Laurino, P., 2021. Substrate dynamics contribute to enzymatic specificity in human and bacterial methionine adenosyltransferases. *JACS Au*. 1, 2349-2360. <https://doi.org/10.1021/jacsau.1c00464>.
- Gani, K.M., Tyagi, V.K., Kazmi, A.A., 2017. Occurrence of phthalates in aquatic environment and their removal during wastewater treatment processes: A review. *Environmental Science and Pollution Research*. 24, 17267-17284. <https://doi.org/10.1007/s11356-017-9182-3>.
- Gao, D., Li, Z., Wang, H., Liang, H., 2018. An overview of phthalate acid ester pollution in China over the last decade: Environmental occurrence and human exposure. *Science of the Total Environment*. 645(15), 1400-1409. <https://doi.org/10.1016/j.scitotenv.2018.07.093>.
- Gao, D.W., Wen, Z.D., 2016. Phthalate esters in the environment: A critical review of their occurrence, biodegradation, and removal during wastewater treatment processes. *Science of the Total Environment*. 541, 986-1001. <https://doi.org/10.1016/j.scitotenv.2015.09.148>.
- Gao, M., Dong, Y., Song, Z., 2020. Effect of dibutyl phthalate on microbial function diversity and enzyme activity in wheat rhizosphere and non-rhizosphere soils. *Environmental Pollution*. 265-114800. <https://doi.org/10.1016/j.envpol.2020.114800>.
- Gasparin, F.G.M., De Barros, M., Macedo, G.A., 2020. Partial purification and biochemical characterization of an alkaline esterase from *Sorghum bicolor*. *Acta Scientiarum Biological Sciences*. 42, e52115. <https://doi.org/10.4025/actascibiolsci.v42i1.52115>.
- Gass, S.E., Sandoval, M.L., Talou, M.H., Martinez, A.G.T., Camerucci, M.A., Gregorova, E., Pabst, W., 2015. High temperature mechanical behavior of porous

- cordierite based ceramic materials evaluated using 3-point bending. *Procedia Materials Science*. 9, 254-261. <https://doi.org/10.1016/j.mspro.2015.04.032>.
- Gennaro, P.D., Collina, E., Franzetti, A., Lasagni, M., Luridiana, A., Pitea, D., Bestetti, G., 2005. Bioremediation of Diethylhexyl phthalate contaminated soil: A feasibility study in slurry-and solid phase reactors. *Environmental Science & Technology*. 39, 325-330. <https://doi.org/10.1021/es035420d>.
- Gibson, R., Wang, M.J., Padget, E., Beck, A.J., 2015. Analysis of 4-nonylphenols, Phthalates and Polychlorinated Biphenyls in Soils and Biosolids. *Chemosphere*. 61(9), 1336-1344. <https://doi.org/10.1016/j.chemosphere.2005.03.072>.
- Gong, J.S., Lu, Z.M., Li, H., Shi, Z.S., Zhou, Z.M., Xu, Z.H., 2012. Nitrilases in nitrile biocatalysis: Recent progress and forthcoming research. *Microbial Cell Factories*. 11 (1), 142. <https://doi.org/10.1186/1475-2859-11-142>.
- Greenfield, N.J., 2006. Using circular dichroism spectra to estimate protein secondary structure. *Nature protocols* 1 (16), 2876-2890. <https://doi.org/10.1038/nprot.2006.202>.
- Groh, K.J., Backhaus, T., Carney-Almroth, B., Geueke, B., Inostroza, P.A., Lennquist, A., Leslie, H.A., Maffini, M., Slunge, D., Trasande, L., Warhurst, A.M., 2019. Overview of known plastic packaging-associated chemicals and their hazards. *Science of the Total Environment*. 651 (2), 3253-3268. <https://doi.org/10.1016/j.scitotenv.2018.10.015>.
- Gulay, S., Sanli-Mohamed G., 2012. Immobilization of thermoalkalophilic recombinant esterase enzyme by entrapment in silicate coated Ca-alginate beads and its hydrolytic properties. *International Journal of Biological Macromolecules*. 50 (3), 545-551. <https://doi.org/10.1016/j.ijbiomac.2012.01.017>.
- Guzik, U., Hupert-Kocurek, K., Wojcieszynska, D., 2014. Immobilization as a strategy for improving enzyme properties-application to oxidoreductases. *Molecules*. 19 (7), 8995-9018. <https://doi.org/10.3390/molecules19078995>.

- Hahladakis, J.N., Velis, C.A., Weber, R., Lacovidou, E., Purnell, P., 2018. An overview of chemical additives presents in plastics: Migration, release, fate and environmental impact during their use, disposal, and recycling. *Journal of Hazardous Materials*. 344, 179-199. <https://doi.org/10.1016/j.jhazmat.2017.10.014>.
- Handayani, N., Loss, K., Wahyuningrum, D., Zulfikar, M.A., 2012. Immobilization of *Mucor miehei* lipase onto macroporous polyethersulfone membrane for enzymatic reactions. *Membranes*. 2, 198-213. <https://doi.org/10.3390/membranes2020198>.
- Hannon, P.R., Flaws, J.A., 2015. The effects of phthalates on the ovary. *Frontiers in Endocrinology*. 6(8), 1-19. <https://doi.org/10.3389/fendo.2015.00008>.
- Hartmeier, W., 1988. *Immobilized biocatalysts-an introduction*, New York, Springer-Verlag.
- He, H., Zhang, S., Liu, X., 2015. Immobilization of feruloyl esterases on magnetic nanoparticles and its potential in production of ferulic acid. *Journal of Bioscience and Bioengineering*. 120 (3), 330-334. <https://doi.org/10.1016/j.jbiosc.2015.01.006>.
- Heindel, J.J., Powell, C.J., 1992. Phthalate ester effects on rat Sertoli cell function in vitro: Effects of phthalate side chain and age of animal. *Toxicology and Applied Pharmacology*. 115 (1), 116-123. [https://doi.org/10.1016/0041-008X\(92\)90374-2](https://doi.org/10.1016/0041-008X(92)90374-2).
- Hernandez-Sanchez, B., Diaz Godinez, R., Luna-Sanchez, S., Sanchez, C., 2019. Esterase production by microorganisms: Importance and industrial application. *Mexican Journal of Biotechnology*. 4(1), 25-37. <http://doi.org/10.29267/mxjb.2021.6.1.165>.
- Hoff, R.M., Chan, K.W. 1987. Measurement of polycyclic aromatic hydrocarbons in the air along the Niagara River. *Environmental Science & Technology*. 21(6), 556-561. <https://doi.org/10.1021/es00160a005>.

- Hou, H., He, H., Wang, Y., 2020. Effects of SDS on the activity and conformation of protein tyrosine phosphatase from *thermos thermophiles* HB27. Scientific Reports 10, 3195. <http://doi.org/10.1038/s41598-020-60263-4>.
- Hu, T., Yang, C., Hou, Z., Liu, T., Mei, X., Zhang, L., Zhang, W., 2022. Phthalate esters metabolic strain *Gordonia* sp. GZ-YC7, a potential soil degrader for high concentration di-(2-ethylhexyl) phthalate. Microorganisms. 10 (3), 641-656. <https://doi.org/10.3390/microorganisms10030641>.
- Hu, X., Zhao, X., Hwang, H.M., 2007. Comparative study of immobilized *Trametes versicolor* laccase on nanoparticles and kaolinite. Chemosphere. 66(9), 1618-1626. <https://doi.org/10.1016/j.chemosphere.2006.08.004>.
- Huang, H., Zhang, X.Y., Chen, T.L., Zhao, Y.L., Xu, D.S., Bai, Y.P., 2019. Biodegradation of structurally diverse phthalate esters by a newly identified esterase with catalytic activity toward di(2-ethylhexyl) phthalate. Journal of Agricultural and Food Chemistry. 67 (31), 8548-8558. <https://doi.org/10.1021/acs.jafc.9b02655>.
- Huang, J., Nkrumah, P.N., Li, Y., Appiah-Sefah, G., 2013. Chemical behavior of phthalates under abiotic conditions in landfills. In: Whitacre, D. (eds) Reviews of Environmental Contamination and Toxicology, vol 224. Springer, New York, NY. https://doi.org/10.1007/978-1-4614-5882-1_2.
- Huang, L., Meng, D., Tian, G., Yang, S., Deng, H., Guan, Z., Cai, Y., Liao, X., 2020. Characterization of novel carboxylesterase from *Bacillus velenzeis* SYBC H47 and its application in degradation of phthalate esters. Journal of Bioscience and Bioengineering. 129 (5), 588-594. <https://doi.org/10.1016/j.jbiosc.2019.11.002>.
- Huang, L., Zhu, X., Zhou, S., Cheng, Z., Shi, K., Zhang, C., Shao, H., 2021. Phthalic acid esters: Natural sources and biological activities. Toxins. 13 (7), 495. <https://doi.org/10.3390/toxins13070495>.
- Huang, P.C., Liao, K.W., Chang, J.W., Chan, S.H., Lee, C.C., 2018. Characterization of phthalates exposure and risk for cosmetics and perfume sales clerks. Environmental Pollution. 233, 577-587. <https://doi.org/10.1016/j.envpol.2017.10.079>.

- Huang, P.C., Tien, C.J., Sun, Y.M., Hsieh, C.Y., Lee, C.C., 2008. Occurrence of phthalates in sediment and biota; relationship to aquatic factors and the biota-sediment accumulation factor. *Chemosphere*. 73 (4), 539-544. <https://doi.org/10.1016/j.chemosphere.2008.06.019>.
- Hung, T.C., Giridhar, R., Chiou, S.H., Wu, W.T., 2003. Binary immobilization of *Candida rugose* lipase on chitosan. *Journal of Molecular Catalysis B: Enzymatic*. 26, 69-78. [https://doi.org/10.1016/S1381-1177\(03\)00167-X](https://doi.org/10.1016/S1381-1177(03)00167-X).
- Hurmuzlu, R., Okur, M., Saracoglu, N., 2021. Immobilization of *Trametes versicolor* laccase on chitosan/halloysite as a biocatalyst in the removal RR dye. *International Journal of Biological Macromolecules*. 192, 331-341. <https://doi.org/10.1016/j.ijbiomac.2021.09.213>.
- Ilgü, H., Turan, T., Sanlı-Mohammed, G., 2011. Preparation, characterization, and optimization of chitosan nanoparticles as carrier for immobilization of thermophilic recombinant esterase. *Journal of Macromolecular Science Part A: Pure and Applied Chemistry*. 48 (9), 713-721. <https://doi.org/10.1080/10601325.2011.596050>.
- Jafarian, F., Bordbar, A-K., Zare, A., Khorospour, A., 2018. The performance of immobilized *Candida rugosa* lipase on various surface modified graphene oxide nanosheets. *International Journal of Biological Macromolecules*. 111, 1166-1174. <https://doi.org/10.1016/j.ijbiomac.2018.01.133>.
- Jang, H., Yang, S., Kong, J., Dong, A., Yu, S., 2015. Obtaining information about protein secondary structures in aqueous solution using Fourier transform IR spectroscopy. *Nature Protocols*. 10 (3), 382-396. <https://doi.org/10.1038/nprot.2015.024>.
- Jesionowski, T., Zdzarta, J., Krajewska, B., 2014. Enzyme immobilization by adsorption: A review. *Adsorption*. 20 (5-6), 801-821. <https://doi.org/10.1007/s10450-014-9623-y>.
- Jiang, Y., Guo, C., Xia, H., Mahmood, I., Liu, C., Liu, H., 2009. Magnetic nanoparticles supported ionic liquids for lipase immobilization: enzyme activity in catalyzing esterification. *Journal of Molecular Catalysis B-Enzymatic*. 58, 103-109. <https://doi.org/10.1016/j.molcatb.2008.12.001>.

- Jin, D., Kong, X., Li, Y., Bai, Z., Zhuang, G., Zhang, X., Deng, Y., 2015. Biodegradation of di-n-butyl phthalate by *Achromobacter* sp. isolated from rural domestic wastewater. *International Journal of Environmental Research and Public Health*. 12 (10), 13510-13522. <https://doi.org/10.3390/ijerph121013510>.
- Kamble, R., Ghag, M., Gaikawad, S., Panda, B.K., 2012. Halloysite nanotubes and applications: A review. *Journal of Advanced Scientific Research*. 3(2), 25-29.
- Katchalski-Katzir, E., Silman, I, Goldman, R., 1971. Effect of the microenvironment on the mode of action of immobilized enzyme. *Advances in Enzymology and Related Areas of Molecular Biology*. 34, 445-536. <https://doi.org/10.1002/9780470122792.ch7>.
- Kaur, R., Kumari, A., Rajput, V.D., Minkina, T., Kaur, R., 2023. Biodegradation of phthalates and metabolic pathways: an overview. *Environmental Sustainability* 6, 303–318. <https://doi.org/10.1007/s42398-023-00268-7>.
- Keun, K.M., Kang, T.H., Kim, J., Kim, H., Yun, H.D., 2012. Cloning and identification of a new group esterase (Est5S) from noncultured rumen bacterium. *Journal of Microbiology and Biotechnology*. 22 (8), 1044-1053. <https://doi.org/10.4014/jmb.1201.12070>.
- Kikani, B.A., Singh, S.P., 2015. Enzyme stability, thermodynamics, and secondary structures of α -amylase as probed by the CD spectroscopy. *International Journal of Biological Macromolecules*. 81, 450-460. <https://doi.org/10.1016/j.ijbiomac.2015.08.032>.
- Kim, S., Eom, S., Kim, H.J., Lee, J.J., Choi, G., Choi, S., Kim, S., Kim, S.Y., Cho, G., Kim, Y.D., Suh, E., Kim, S.K., Kim, S., Kim, G.H., Moon, H.B., Park, J., Kim, S., Choi, K., Eun, S.H., 2018. Association between maternal exposure to major phthalates, heavy metals, and persistent organic pollutants, and the neurodevelopmental performances of their children at 1 to 2 years of age- CHECK cohort study. *Science of the Total Environment*. 624, 377–384. <https://doi.org/10.1016/j.scitotenv.2017.12.058>.

- Kim, Y.H., Lee, J., 2005. Enzymatic degradation of dibutyl phthalate and toxicity of its degradation products. *Biotechnology Letters*. 27(9), 635-639. <https://doi.org/10.1007/s10529-005-3631-7>.
- Kong, S., Ji, Y., Liu, L., Chen, L., Zhao, X., Wang J., Bar, Z., Sun, Z., 2012. Diversities of phthalate esters in suburban agricultural soils and wasteland soil appeared with urbanization in China. *Environmental Pollution*. 170,161-168. <https://doi.org/10.1016/j.envpol.2012.06.017>.
- Kong, X., Jin, D., Jin, S., Wang, Z., Yin, H., Xu, M., Deng, Y., 2018. Responses of bacterial community to dibutyl phthalate pollution in a soil-vegetable ecosystems. *Journal of Hazardous Materials*. 352, 142-150. <https://doi.org/10.1016/j.jhazmat.2018.04.015>.
- Kumar, V., Sharma, N., Maitra, S.S., 2017. Comparative study on the degradation of dibutyl phthalate by two newly isolated *Pseudomonas* sp. V216 and *Comamonas* sp. 51F. *Biotechnology Reports*. 15, 1-10. <https://doi.org/10.1016/j.btre.2017.04.002>.
- Kurane, R., Suzuki, T., Takahara, Y., 1980. Induction of enzymes involved in phthalate esters metabolism in *Nocardia erythropolis* and enzymatic hydrolysis of phthalate esters by commercial lipases. *Agricultural and Biological Chemistry*. 44 (3), 529-536.
- Laemmli, U.K., 1970. Cleavage of structure proteins during the assembly of the head of bacteriophage T4. *Nature*. 227, 680-685. <https://doi.org/10.1038/227680a0>.
- Lamraoui, I., Eltoukhy, A., Wang, J., Lamraoui, M., Ahmed, A., Jia, Y., Lu, T., Yan, Y., 2020. Biodegradation of Di (2-Ethyl hexyl) Phthalate by a novel *Enterobacter* spp. strain YC-IL1 isolated from polluted soil, Mila, Algeria. *International Journal of Environmental Research and Public Health*. 17 (20), 7501. <https://doi.org/10.3390/ijerph17207501>.
- Lee, D.G., Ponvel, K.M., Kim, M., Hwang, S., Ahn, I.S., Lee, C.H., 2009. Immobilization of lipase on hydrophobic nano-sized magnetite particles. *Journal of Molecular Catalysis B-Enzymatic*. 57 (1-4), 62-66. <https://doi.org/10.1016/j.molcatb.2008.06.017>.

- Lee, G., Kim, S., Kho, Y., Kim, S., Lee, S., Chai, G., Park, J., Worakhunpiset, S., Moon, H.B., Okanurak, K., Geounuppakul, M., Tangtitawong, J., Wetsutthanon, K., Trisurat, D., Choi, K., 2020. Urinary levels of phthalates and DINCH metabolites in Korean and Thai pregnant women across three trimesters. *Science of the Total Environment*. 711, 134822. <https://doi.org/10.1016/j.scitotenv.2019.134822>.
- Li, K., Ma, D., Wu, J., Chai, C., Shi, Y., 2016. Distribution of phthalate esters in agricultural soil with plastic film mulching in Shandong, Peninsula, East China. *Chemosphere*. 164, 314-321. <https://doi.org/10.1016/j.chemosphere.2016.08.068>.
- Li, J., Zhang, J., Yadav, M.P., Li, X., 2019. Biodegradability and biodegradation pathway of di-(2-ethylhexyl) phthalate by *Burkholderia pyrrocinia* B1213. *Chemosphere*. 225, 443-450. <https://doi.org/10.1016/j.chemosphere.2019.02.194>.
- Liang, D.W., Zhang, T., Fang, H.H.P., He, J., 2008. Phthalates biodegradation in the environment. *Applied Microbiology and Biotechnology*. 80, 183-198. <https://doi.org/10.1007/s00253-008-1548-5>.
- Lisuzzo, L., Cavallaro, G., Milioto, S., Lazzara, G., 2020. Halloysite nanotubes coated by chitosan for the controlled release of khellin. *Polymers*. 12, 1766. <https://doi.org/10.3390/polym12081766>.
- Luo, P., Zhao, Y., Zhang, B., Liu, J., Yang, Y., Liu, J., 2010. Study on the adsorption of neutral red from aqueous solution onto halloysite nanotubes. *Water Research*. 44, 1489-1497. <https://doi.org/10.1016/j.watres.2009.10.042>.
- Luo, Z.H., Pang, K.L., Wu, Y.R., Gu, J.D., Chow, R.K.K., Vrijmoed, L.L.P., 2012. Degradation of phthalate esters by *Fusarium* sp. isolated from Mangrove sediments. *Progress in Molecular and Subcellular Biology*. 53, 299-328. https://doi.org/10.1007/978-3-642-23342-5_15.
- Luo, Z.H., Wu, Y.R., Chow, R.R.K., Luo, J.J., Gu, J.D., Vrijmoed, L.L.P., 2012. Purification and characterization of an intracellular esterase from a *Fusarium* species capable of degrading dimethyl terephthalate. *Process Biochemistry*. 47(5), 687-693. <https://doi.org/10.1016/j.procbio.2012.01.015>.

- Lü, H., Mo, C.H., Zhao, H.M., Xiang, L., Katsoyiannis, A., Li, Y.W., Cai, Q.Y., Wong, M.H., 2018. Soil contamination and sources of phthalates and its health risk in China: A review. *Environmental Research*. 164, 417-429. <https://doi.org/10.1016/j.envres.2018.03.013>.
- Ma, Y.S., Lin, J.G., 2011. Sono-alkalization pretreatment of sewage sludge containing phthalate acid esters.. *Journal of Environmental Science and Health, Part A*, 46(9), 980-988.
- Mackintosh, C.E., Maldonado, J.A., Ikonou, M.G., Gobas, F.A.P.C. 2006. Sorption of Phthalate Esters and PCBs in a Marine Ecosystem. *Environmental Science & Technology*. 40(11), 3481-3488. <https://doi.org/10.1021/es0519637>.
- Mala, J.G.S., Takeuchi, S., 2008. Understanding structural features of microbial lipases- an overview. *Analytical Chemistry Insights*. 3, 9-19. <https://doi.org/10.4137/ACI.S551>.
- Maruyama, K., Akita, K., Naitou, C., Yoshida, M., Kitamura, T., 2005. Purification and characterization of an esterase hydrolyzing monoalkyl phthalates from *Micrococcus* sp. YGJ1. *The Journal of Biochemistry*. 137 (1), 27-37. <https://doi.org/10.1093/jb/mvi004>.
- Marttinen, S.K., Kettunen, R.H., Sormunen, K.M., Rintala, J.A., 2003. Removal of bis (2-ethylhexyl) phthalate at a sewage treatment plant. *Water Research*. 37, 1385-1393. [https://doi.org/10.1016/S0043-1354\(02\)00486-4](https://doi.org/10.1016/S0043-1354(02)00486-4).
- Medellin-Castillo, N.A., Ocampo-Perez, R., Leyva-Ramos, R., Sanchez-Polo, M., Rivrera-Utrilla, J., Mendez-Diaz, J.D., 2013. Removal of diethyl phthalate from water solution by adsorption, photo-oxidation, ozonation, and advanced oxidation process (UV/H₂O₂, O₃/H₂O₂, and O₃/activated carbon). *Science of the Total Environment* 442, 26-35. <https://doi.org/10.1016/j.scitotenv.2012.10.062>.
- Meek, M.E., Chan, P.K.L., 1994. Bis(2-ethylhexyl) phthalate: Evaluation of risks to health from environmental exposure in Canada. *Journal of Environmental Science and Health, Part C*. 12 (2), 179-194. <https://doi.org/10.1080/10590509409373439>.

- Mohamad, N.R., Marzuki, N.H.C., Buang, N.A., Huyop, F., Wahab, R.A., 2015. An overview of technologies for immobilization of enzymes and surface analysis techniques for immobilized enzymes. *Biotechnology & Biotechnological Equipment* 29 (2), 205-220. <https://doi.org/10.1080/13102818.2015.1008192>.
- Mohammadi, N.S., Khiabani, M.S., Ghanbarzadeh, B., Mokarram, R.R., 2020. Enhancement of biochemical aspects of lipase adsorbed on halloysite nanotubes and entrapped in polyvinyl alcohol/alginate hydrogel strategies to reuse the most stable lipase. *World Journal of Microbiology and Biotechnology*. 36 (3), 1-15. <https://doi.org/10.1007/s11274-020-02817-2>.
- Mondal, S., Li, C., Wang, K., 2015. Bovine serum albumin adsorption on glutaraldehyde cross-linked chitosan hydrogels. *Journal of Chemical & Engineering Data*. 60, 2356-2362. <https://doi.org/10.1021/acs.jced.5b00264>.
- Monteiro, R.R.C., Neto, D.M.A., Fachine, P.B.A., Lopes, A.A.S., Gonçalves, L.R.B., dos Santos, J.C.S., de Souza, M.C.M., Fernandez-Lafuente, R.F., 2019. Ethyl butyrate synthesis catalyzed by lipases A and B from *Candida Antarctica* immobilized onto magnetic nanoparticles. Improvement of biocatalysts's performance under ultrasonic irradiation. *International Journal of Molecular Sciences*. 20 (22), 5807. <https://doi.org/10.3390/ijms20225807>.
- Moreira, K.S., Junior, L.S.M., Monteiro, R.R.C., de Oliveira, A.L.B., Valle, C.P., Freire, T.M., Fachine, P.B.A., de Souza, M.C.M., Fernandez-Lorente, G., Guisan, J.M., dos Santos, J.C.S., 2020. Optimization of the production of enzymatic biodiesel from residual babassu oil (*Orbignya* sp.) via RSM. *Catalysts*. 10 (4), 414. <https://doi.org/10.3390/catal10040414>.
- Mu, D., Gao, F., Fan, Z., Shen, H., Peng, H., Hu, J., 2017. Levels of phthalate metabolites in urine of pregnant women and risk of clinical pregnancy loss. *Environmental Science & Technology* 49 (17), 10651-10657. <https://doi.org/10.1021/acs.est.5b02617>.
- Nahurira, R., Ren, L., Song, J., Jia, Y., Wang, J., Fan, S., Wang, H., Yan, Y., 2017. Degradation of Di (2-Ethylhexyl) Phthalate by a Novel *Gordonia alkanivorans*

- Strain YC-RL2. *Current Microbiology* 74, 309-319.
<https://doi.org/10.1007/s00284-016-1159-9>.
- Nalli, S., Cooper, D.G., Nicell, J.A., 2006. Interaction of metabolites with *R. rhodochrous* during the biodegradation of diester plasticizers. *Chemosphere*. 65 (9), 1510-1517.
<https://doi.org/10.1016/j.chemosphere.2006.04.010>.
- Nasliyan, M.V., 2012. Isolation and immobilization of aldose reductase from different tissues. (Master of Thesis, Ankara University, Ankara). Retrieved from
https://tez.yok.gov.tr/UlusalTezMerkezi/tezDetay.jsp?id=7_IENrxBI8PYkrWXS0x9Tg&no=jPeBXPsrBvYXhjzbZPNfGg.
- Net, S, Sempere, R., Delmont, A., Paluselli, A., Ouddane, B., 2015. Occurrence, fate, behavior, and ecotoxicological state of phthalates in different environmental matrices. *Environmental Science & Technology*. 49 (7), 4019-4035.
<https://doi.org/10.1021/es505233b>.
- Niazi, J.H., Prasad, D.T., Karegoudar, T.B., 2001. Initial degradation of dimethylphthalate by esterases from *Bacillus* species. *FEMS Microbiology Letters*. 196 (2), 201-205. <https://doi.org/10.1111/j.1574-6968.2001.tb10565.x>.
- Nunes, G.S. and Marty, J.L., 2006. Immobilization of enzyme on electrodes. *Methods in Biotechnology: Immobilization of Enzymes and Cells*, Second Edition, Edited by: J. M. Guisan © Humana Press Inc., Totowa, NJ., Vol.21; pp.239–250.
- Oishi, S., Hiraga, K., 1980. Testicular atrophy induced by phthalic acid monoesters: effects of zinc and testosterone concentrations. *Toxicology*. 15 (3), 197-202.
[https://doi.org/10.1016/0300-483X\(80\)90053-0](https://doi.org/10.1016/0300-483X(80)90053-0).
- Okamoto, Y., Toda, C., Ueda, K., Hashizume, K., Kojima, N., 2011. Transesterification in microbial degradation of phthalate esters. *Journal of Health Science*. 57 (3), 293-299. <https://doi.org/10.1248/jhs.57.293>.
- Ollis, D.L., Cheah, E., Cygler, M., Dijkstra, B., Frolow, F., Franken, S.M., Harel, M., Remington, S.J., Silman, I., Schrag, J., Sussman, J.L., Verschueren, K.H.G., Goldman, A., 1992. The α/β fold hydrolase fold. *Protein Engineering, Design, and Selection* 5 (3), 197-211. <https://doi.org/10.1093/protein/5.3.197>.

- Olshansky, Y., Masaphy, S., Root, R. A., Rytwo, G., 2018. Immobilization of *Rhus vernicifera* laccase on sepiolite; effect of chitosan and copper modification on laccase adsorption and activity. *Applied Clay Science*. 152, 143-147. <https://doi.org/10.1016/j.clay.2017.11.006>.
- Osho, M.B., Popoola, T., Adeleye, T.M., Adetunji, M.C., 2016. Response surface methodology for optimal immobilization of *Aspergillus niger* ATCC 1015 lipase by adsorption method. *International Journal of Biological Research*. 4 (1), 56-63. <https://doi.org/10.14419/ijbr.v4i1.6008>.
- Pandey, G., Munguambe, D.M., Tharmavaram, M., Rawtani, D., Agrawal, Y.K., 2017. Halloysite nanotubes – An efficient ‘nano-support’ for the immobilization of α -amylase. *Applied Clay Science*. 136, 184-191. <https://doi.org/10.1016/j.clay.2016.11.034>.
- Patel, S., Jammalamadaka, U., Sun, L., Tappa, K., Mills, D.K., 2016. Sustained release of antibacterial agents from doped halloysite nanotubes. *Bioengineering*. 3 (1), 1. <https://doi.org/10.3390/bioengineering3010001>.
- Patil, N.K., Kundapur, R., Shouche, Y.S., Karegoudar, T.B., 2006. Degradation of plasticizer Di-n-butyl by *Delftia* sp. TBKNP-05. *Current Microbiology*. 52, 369-374. <https://doi.org/10.1007/s00284-005-5258-2>.
- Peng, Q., Liu, M., Zheng, J., Zhou, C., 2015. Adsorption of dyes in aqueous solutions by chitosan-halloysite nanotubes composite hydrogel beads. *Microporous and Mesoporous Materials*. 201, 190-201. <https://doi.org/10.1016/j.micromeso.2014.09.003>.
- Pereira, A.D.S., Diniz, M.M., De Jong, G., Gama Filho, H.S., dos Anjos, M.J., Finotelli, P.V., Fontes-Sant’Ana, G.C., Amaral, P.F., 2019a. Chitosan-alginate beads as encapsulating agents for *Yarrowia lipolytica* lipase: Morphological physico-chemical and kinetic characteristics. *International Journal of Biological Macromolecules*. 139, 621-630. <https://doi.org/10.1016/j.ijbiomac.2019.08.009>.
- Perreira, J., Selbourne, M.D.C., Poças, F., 2019b. Determination of phthalates in olive oil from European Market. *Food Control*. 98, 54-60. <https://doi.org/10.1016/j.foodcont.2018.11.003>.

- Petersen, J.H., Breindahl, T., 2000. Plasticizers in total diet samples, baby food and infant formulae. *Food Additives & Contaminants*. 17 (2), 133-141. <https://doi.org/10.1080/026520300283487>.
- Pietrogrande, M.C., Rossi, D., Paganetto, G., 2003. Gas chromatographic – mass spectrometric analysis of di(2-ethylhexyl) phthalate and its metabolites in hepatic microsomal incubations. *Analytica Chimica Acta*. 480 (1), 1-10. [https://doi.org/10.1016/S0003-2670\(02\)01652-5](https://doi.org/10.1016/S0003-2670(02)01652-5).
- Pirsaheb, M., Zinatizadeh, A.A., 2009. Kinetic evaluation and process performance of a fixed film bioreactor removing phthalic acid and dimethyl phthalate. *Journal of Hazardous Materials*. 167, 500-506. <https://doi.org/10.1016/j.jhazmat.2009.0.003>.
- Prasad, B., Suresh, S., 2012. Biodegradation of phthalate esters by *Variovorax* sp. *APCBEE Procedia*. 1, 16-21. <https://doi.org/10.1016/j.apcbee.2012.03.004>
- Puri, M., Barrow, C.J., Verma, M.L., 2013. Enzyme immobilization on nanomaterials for biofuel production. *Trends in Biotechnology*. 31 (4), 215-216. <https://doi.org/10.1016/j.tibtech.2013.01.002>.
- Quan, C.S., Liu, Q., Tian, W.J., Kikuchi, J., Fan, S.D., 2005. Biodegradation of an endocrine-disrupting chemical, di-2-ethylhexyl phthalate, by *Bacillus subtilis* No.66. *Applied Microbial and Cell Physiology*. 66, 702-710. <https://doi.org/10.1007/s00253-004-1683-6>.
- Radke, E.G., Braun, J.M., Nachman, R.M., Cooper, G.S., 2020. Phthalate exposure and neurodevelopment: A systematic review and meta-analysis of human epidemiological evidence. *Environment International*. 137, 105408. <https://doi.org/10.1016/j.envint.2019.105408>.
- Ramsay, J. A., Mok, W. H. W., Luu, Y. S., Savage, M., 2005. Decoloration of textile dyes by alginate-immobilized *Trametes versicolor*. *Chemosphere*, 61 (7), 956-964. <https://doi.org/10.1016/j.chemosphere.2005.03.070>.
- Rao, K.M., Kumar, A., Suneetha, M., Han, S.S., 2018. pH and near-infrared active; chitosan-coated halloysite nanotubes loaded with curcumin-Au hybrid

- nanoparticles for cancer drug delivery. *International Journal of Biological Macromolecules*. 112, 119-125. <https://doi.org/10.1016/j.ijbiomac.2018.01.163>.
- Rao, L., Xue, Y., Zeng, Y., Lu, J.R., Ma, Y., 2013. A novel alkaliphilic *Bacillus* esterase belongs to the 13th bacterial lipolytic enzyme family. *PloS One*. 8 (4), e60645. <https://doi.org/10.1371/journal.pone.0060645>.
- Ren, L., Jia, Y., Ruth, N., Qiao, C., Wang, J., Zhap, B., Yan, Y., 2016. Biodegradation of phthalic acid esters by a newly isolated *Mycobacterium* sp. YC-RL4 and the bioprocess with environmental samples. *Environmental Science and Pollution Research*. 23, 16609-16619. <https://doi.org/10.1007/s11356-016-6829-4>.
- Ren, L., Lin, Z., Liu, H., Hu, H., 2018. Bacteria-mediated phthalic acid esters degradation and related molecular mechanisms. *Applied Microbiology and Biotechnology*. 102, 1085-1096. <https://doi.org/10.1007/s00253-017-8687-5>.
- Rigos, C.F., Santos, H.D.L., Thedei, G., Ward, J.R., Ciancaglini, P., 2003. Influence of enzyme conformational changes on catalytic activity investigated by circular dichroism spectroscopy. *Biochemistry and Molecular Biology Education*. 31 (5), 329-332. <https://doi.org/10.1002/bmb.2003.494031050264>.
- Rivera-Hoyos, C.M., Moroles-Alvarez, E.D., Potou-Pinales, R.A., Pedroza-Rodriguez, A.M., Rodriguez-Vazquez, R. Delgado-Boada, J.M., 2013. Fungal laccases. *Fungal Biology Reviews*. 27 (3-4), 67-82. <https://doi.org/10.1016/j.fbr.2013.07.001>.
- Roberts, I.M., Jacobson, P., Cornette, J., 1989. Secondary structures of rat lipolytic enzymes: Circular dichroism studies and relation to hydrophobic moments. *Biochemical and Biophysical Research Communications*. 162 (1), 95-101. [https://doi.org/10.1016/0006-291X\(89\)91967-0](https://doi.org/10.1016/0006-291X(89)91967-0).
- Rodgers, K.M., Rudel, R.A., Just, A.C. 2014. Phthalates in Food Packaging, Consumer Products, and Indoor Environments. *Nanoparticles in Polymer Nanocomposite Food Contact Materials: Uses, Potential Release and Emerging Toxicological Concerns Book*, 31-59.

- Rodrigues, D.S., Cavalcante, G.P., Ferreira, A.L.O., Goncalves, L.R.B., 2008. Immobilization of *Candida antarctica* lipase type B by adsorption on activated carbon. *Chemical and Biochemical Engineering Quarterly*. 22(1), 125-133.
- Rodrigues, R.C., Fernandez-Lafuente, R., 2010. Lipase from *Rhizomucor miehei* as a biocatalyst in fats and oils modification. *Journal of Molecular Catalysis B: Enzymatic*. 66, 15-32. <https://doi.org/10.1016/j.molcatb.2010.03.008>.
- Rodrigues, R.C., Ortiz, C., Berenguer-Murcia, A., Torres, R., Fernandez-Lafuente, R., 2013. Modifying enzyme activity and selectivity by immobilization selectivity by immobilization. *Chemical Society Reviews*. 42, 6290-6307. <https://doi.org/10.1039/C2CS35231A>.
- Roquero, D.M., Othman, A., Melman, A., Katz, E., 2022. Iron (III)-crosslinked alginate hydrogels: a critical review. *Materials Advances*. 3, 1849-1873. <https://doi.org/10.1039/d1ma00959a/>.
- Rosales, E., Sanromán, M.A., Pazos, M., 2012. Application of central composite face-centered design and response surface methodology for the optimization of electro-Fenton decolorization of Azure B dye. *Environmental Science and Pollution Research*. 19, 1738–1746. <https://doi.org/10.1007/s11356-011-0668-0>.
- Sadukhan, B., Mondal, N.K., Chatteraj, S., 2016. Optimisation using central composite design (CCD) and the desirability function for sorption of methylene blue from aqueous solution onto *Lemna major*. *Karbala International Journal of Modern Science*. 2 (3), 145-155. <https://doi.org/10.1016/j.kijoms.2016.03.005>.
- Saganuwan, S.A., 2021. Application of modified Michaelis-Menten equations for determination of enzyme inducing and inhibiting drugs. *BMC Pharmacology and Toxicology*. 22 (57), 1-15.
- Saito, T., Tanabe, R., Nagai, K., Kato, K., 2010. Enzymatic hydrolysis of structurally diverse phthalic acid esters by porcine and bovine pancreatic cholestral esterases. *Chemosphere*. 81, 1544-1548. <https://doi.org/10.1016/j.chemosphere.2010.08.020>.

- Samoylova, Y.V., Sorokina, K.N., Romanenko, M.V., Parmon, V., 2018. Cloning, expression, and characterization of the esterase estU1 from *Ureibacillus thermosphaericus* which belongs to a new lipase family XVIII. *Extremophiles* 22, 271-285. <https://doi.org/10.1007/s00792-018-0996-9>.
- Sardon, H., Dove, A.R., 2018. Plastic recycling with a difference. *Science*. 360 (6381), 380-381. <https://doi.org/10.1126/science.aat4997>.
- Sassolas, A., Blum, L.J., Leca-Bouvier, B.D., 2012. Immobilization strategies to develop enzymatic biosensors. *Biochemistry Advances*. 30 (3), 489-511. <https://doi.org/10.1016/j.biotechadv.2011.09.003>.
- Savinova, O.S., Shabaev, A.V., Glazunova, O.A., Eremin, S.A., Fedorova, T.V., 2022. Biodestruction of phthalic acid esters by white rot fungi. *Applied Biochemistry and Microbiology* 58, 598-612. <https://doi.org/10.1134/S0003683822050143>.
- Schettler, T., 2006. Human exposure to phthalates via consumer products. *International Journal of Andrology*. 29, 134-139. <https://doi.org/10.1111/j.1365-2605.2005.00567.x>.
- Scholz, N., Diefenbach, R., Rademacher, I., Linneman, D., 1997. Biodegradation of DEHP, DBP, and DNP: poorly water soluble and widely used phthalate plasticizers. *Bulletin of Environmental Contamination and Toxicology*. 58, 527-534. <https://doi.org/10.1007/s001289900367>.
- Seyoum, A., Pradhan, A., 2019. Effect of phthalates on development, reproduction, fat metabolism and lifespan in *Daphnia magna*. *Science of the Total Environment*. 654, 969–977. <https://doi.org/10.1016/j.scitotenv.2018.11.158>.
- Serrano, S.E., Braun, J., Trasende, L., Dills, R., Sathyanarayana, S., 2014. Phthalates and diet: a review of the food monitoring and epidemiology data. *Environmental Health*. 13 (1), 43. <https://doi.org/10.1186/1476-069X-13-43>.

- SGS, 2020. Turkey Strengthens Regulation on Food Contact Plastics. <https://www.sgs.com/en/news/2020/01/safeguards-00620-turkey-strengthens-regulation-on-food-contact-plastics>. Accessed date: 13/10/2023.
- Sharma, A., Sharma, T., Sharma, T., Sharma, S., Kanwar, S.S., 2019. Role of microbial hydrolases in bioremediation, in: Kumar, A., Sharma, S. (Eds), *Microbes and Enzymes in Soil Health and Bioremediation*. Springer, Singapore, pp. 149-164. https://doi.org/10.1007/978-981-13-9117-0_7.
- Sharma, D., Bhardwaj, K.K., Gupta, R., 2021. Immobilization and applications of esterases. *Biocatalysis and Biotransformation*. 1-16. <https://doi.org/10.1080/10242422.2021.2013825>.
- Sheikh, I.A., Turki, R.F., Abuzenadah, A.M., Damanhour, G.A., Beg, M.A., 2016. Endocrine disruption: Computational perspectives on human sex hormone-binding globulin and phthalate plasticizers. *PLOS ONE* 11 (3), e0151444. <https://doi.org/10.1371/journal.pone.0151444>.
- Shutava, T.G., Fakhrullin, R.F., Lvov, Y.M., 2014. Spherical and tubule nanocarriers for sustained drug release. *Current Opinion in Pharmacology*. 18, 141-148. <https://doi.org/10.1016/J.COPH.2014.10.001>.
- Sibali, L.L., Okonkwo, J.O., McCrindle, R.I., 2013. Determination of selected phthalate esters compounds in water and sediments by capillary gas chromatography and flame ionization detector. *Journal of Environmental Science and Health, Part A: Toxic/Hazardous Substances and Environmental Engineering*. 48(11), 1365-1377. <https://doi.org/10.1080/10934529.2013.781884>.
- Singh, N, Dalal, V., Mahto, J.K., Kumar, P., 2017. Biodegradation of phthalic acid esters (PAEs) and in silico structural characterization of mono-2-ethylhexyl phthalate (MEHP) hydrolase on the basis of close structural homolog. *Journal of Hazardous Materials*. 338, 11-22. <https://doi.org/10.1016/j.jhazmat.2017.04.055>.

- Song, X., Zhang, Z., Dai, Y., Cun, D., Cui, B., Wang, Y., Fan, Y., Tang, H., Qiu, L., Wang, F., Qiu, D., 2022. Biodegradation of phthalate acid esters by a versatile PAE-degrading strain *Rhodococcus* sp. LW-XY12 and associated with genomic analysis. *International Biodeterioration & Biodegradation* 170, 105399. <https://doi.org/10.1016/j.ibiod.2022.105399>.
- Souza, J.E.S., de Oliveira, G.P., Alexandre, J.Y.N.H., Neto, J.G.L., Sales, M.G., Junior, P.G.S., de Oliveira, A.L.B., de Souza, M.C.M., dos Santos, J.C.S., 2022. A comprehensive review on the use of metal-organic frameworks (MOFs) coupled with enzymes as biosensors. *Electrochemistry*. 3 (1), 89-113. <https://doi.org/10.3390/electrochem3010006>.
- Staples, C.A., Peterson, D.R., Parkerton, T.F., Adams, W.J., 1997. The environmental fate of phthalate esters: A literature review. *Chemosphere*. 35 (4), 667-749. [https://doi.org/10.1016/S0045-6535\(97\)00195-1](https://doi.org/10.1016/S0045-6535(97)00195-1).
- Staples, C.A., 2003. Phthalate esters. *The handbook of Environmental Chemistry*. Springer-Verlag Heidelberg, Germany.
- Sudo, K., 1995. Enzyme kinetics for enzyme immunoassay. *Nihon rinsho. Japanese Journal of Clinical Medicine*. 53 (9), 2134-2139.
- Sun, J., Wu, X., Gan, J., 2015. Uptake and metabolism of phthalate esters by edible plants. *Environmental Science & Technology* 49, 8471-8478. <https://doi.org/10.1021/acs.est.5b01233>.
- Sun, J., Yendluri, R., Liu, K., Guo, Y., Lvov, Y., Yan, X., 2017. Enzyme-immobilized clay-nanotube-chitosan membranes with sustainable biocatalytic activities. *Physical Chemistry Chemical Physics*. 19 (1), 562-567. <https://doi.org/10.1039/C6CP07450B>.
- Sun, J., Zhu, H., Yang, X., Zheng, Y., Sun, T., Xu, H., Meng, J., Zhang, A., 2022a. Carboxylesterase and lipase-catalyzed degradation of phthalate esters in soil and

- water: Congener structure selectivity and specificity. *Environmental Technology & Innovation*. 28, 102571. <https://doi.org/10.1016/j.eti.2022.102571>.
- Sun, Y., Guo, M., Hu, S., Fang, X., Jin, Z., Wu, R., 2022b. Nanosurface-immobilized lipase and its degradation of phthalate wastewater. *Molecular Catalysis*. 529, 112522. <https://doi.org/10.1016/j.mcat.2022.112522>.
- Sungkeeree, P., Whangsuk, W., Dubbs, J., Mongkolsuk, S., Loprasert, S., 2016. Biodegradation of endocrine disrupting dibutyl phthalate by a bacterial consortium expressing *Sphingobium* sp. SM42 esterase. *Process Biochemistry*. 51 (8), 1040-1045. <https://doi.org/10.1016/j.procbio.2016.04.014>.
- Sungkeeree, P., Whangsuk, W., Sallabhan, R., Dubbs, J., Mongkolsuk, S., Loprasert, S., 2017. Efficient removal of toxic phthalate by immobilized serine-type aldehyde tagged esterase G. *Process Biochemistry*. 63, 60-65. <https://doi.org/10.1016/j.procbio.2017.09.009>.
- Tanaka, T., Yamada, K., Tonosaki, T., Konishi, T., Goto, H., Taniguchi, M., 2000. Enzymatic degradation of alkylphenols, bisphenol A, synthetic estrogen, and phthalic ester. *Water Science and Technology*. 42, 89-95. <https://doi.org/10.2166/wst.2000.0556>.
- Tang, J., Rong, X., Jin, D., Gu, C., Chen, A., Luo, S., 2020. Biodegradation of phthalate esters in four agricultural soils: main influencing factors and mechanisms. *International Biodeterioration & Biodegradation*. 147, 104867. <https://doi.org/10.1016/j.ibiod.2019.104867>.
- Tang, W.J., Zhang, L.S., Fang, Y., Zhou, Y., Ye, B.C., 2016. Biodegradation of phthalate esters by newly isolated *Rhizobium* sp. LMB-1 and its biochemical pathway of di-n-butyl phthalate. *Journal of Applied Microbiology*. 121 (1), 177-186. <https://doi.org/10.1111/jam.13123>.
- Tang, Z., Chai, M., Cheng, J., Wang, Y., Huang, Q., 2019. Occurrence and distribution of phthalates in sanitary napkins from six countries: Implication for women's

- health. *Environmental Science & Technology*. 53(23), 13919-13928. <https://doi.org/10.1021/acs.est.9b03838>.
- Tari, G., Bobos, I., Gomes, C.S.F., Ferreira, J.M.F., 1999. Modification of surface charge properties during kaolinite to halloysite-7Å transformation. *Journal of Colloid and Interface Science*. 210 (2), 360-366. <https://doi.org/10.1006/jcis.1998.5917>.
- Teil, M.J., Blanchard, M., Chevreuil, M., 2006. Atmospheric fate of phthalate esters in an urban area (Paris-France). *Science of Total Environment*. 354, 212-223. <https://doi.org/10.1016/j.scitotenv.2004.12.083>.
- Teil, M.J., Blanchard, M., Dargnat, C., Larcher-Tiphagne, K., Chevreuil, M., 2007. Occurrence of phthalate diesters in rivers of the Paris district (France). *Hydrological Processes*. 21(18), 2515-1525.
- Tekedar, H.C., Sanli-Mohamed, G., 2011. Molecular cloning, over expression, and characterization of thermoalkalophilic esterases isolated from *Geobacillus* sp. *Extremophiles*. 15, 203-211. <https://doi.org/10.1007/s00792-010-0344-1>.
- Tercan, Ç., Sürmeli, Y., Şanlı-Mohamed, G., 2021. Thermoalkalophilic recombinant esterase entrapment in chitosan/calcium/alginate-blended beads and its characterization. *Journal of Chemical Technology & Biotechnology*. 96, 2257-2264. <https://doi.org/10.1002/jctb.6750>.
- Thörn, C., Gustafsson, H., Olsson, L., 2011. Immobilization of feruloyl esterases in mesoporous materials leads to improved transesterification yield. *Journal of Molecular Catalysis B-Enzymatic*. 72 (1), 57-64. <https://doi.org/10.1016/j.molcatb.2011.05.002>.
- Tran, B.C., Teil, M.J., Blanchard, M., Alliot, F., Chevreuil, M., 2015. Fate of phthalates and BPA in agricultural and non-agricultural soils of the Paris area (France). *Environmental Science and Pollution Research*. 22, 11118-11126. <https://doi.org/10.1007/s11356-015-4178-3>.

- Tran, H.T., Lin, C., Bui, X.T., Hayama, T., Dang, B.T., Cheruiyot, N.K., Hoang, H.G., Vu, C.T., 2021. Bacterial community progression during food waste composting containing high dioctyl terephthalate (DOTP) concentration. *Chemosphere*. 265, 129064. <https://doi.org/10.1016/j.chemosphere.2020.129064>.
- Tran, H.T., Lin, C., Bu, X.T., Nguyen, M.K., Cao, N.D.T., Mukhtar, H., Hoang, H.G., Varjani, S., Ngo, H.H., Nghiem, L.D., 2022a. Phthalates in the environment: characteristics, fate and transport, and advanced wastewater treatment technologies. *Bioresource Technology*. 344, PartB, 126249. <https://doi.org/10.1016/j.biortech.2021.126249>.
- Tran, H.T., Nguyen, M.K., Hoang, H.G., Hutchison, J.M., Vu, C.T., 2022b. Composting and green technologies for remediation of phthalate (PAE) contaminated soil: Current status and future perspectives. *Chemosphere*. 307, 135989. <https://doi.org/10.1016/j.chemosphere.2022.135989>.
- Tran, T.M., Kannan, K., 2005. Occurrence of phthalate diesters in particulate and vapor phases in indoor air and implications for human exposure in Albany, New York, USA. *Archives of Environmental Contamination and Toxicology*. 68, 489-499. <https://doi.org/10.1007/s00244-015-0140-0>.
- Tsai, Y.A., Tsai, M.S., Hou, J.W., Lin, C.H., Chen, C.Y., Chang, C.H., Liao, K.W., Wang, S.L., Chen, B.H., Wu, M.T., Hsieh, C.J., Chen, M.L., 2018. Evidence of high di(2-ethylhexyl) phthalate (DEHP) exposure due to tainted food intake in Taiwanese pregnant women and the health effects on birth outcomes. *Science of the Total Environment*. 618, 635-644. <https://doi.org/10.1016/j.scitotenv.2017.07.175>.
- Tully, J., Yendluri, R., Lvov, Y., 2016. Halloysite clay nanotubes for enzyme immobilization. *Biomacromolecules*. 17 (2), 615-621. <https://doi.org/10.1021/acs.biomac.5b01542>.
- Tumay-Ozer, E., Gucer, S., 2012. Determination of di(2-ethylhexyl) phthalate migration from toys into artificial sweat by gas chromatography mass spectrometry after activated carbon enrichment. *Polymer Testing*. 31, 474-480. <https://doi.org/10.1016/j.polymertesting.2012.01.007>.

- Tumay-Ozer, E., Osman, B., Kara, A., Besirli, N., Gucer, S., Sozeri, H., 2012. Removal of diethyl phthalate from aqueous phase using magnetic poly(EGDMA-VP) beads. *Journal of Hazardous Materials*. 229-230, 20-28. <https://doi.org/10.1016/j.jhazmat.2012.05.037>.
- Tutar, H., Yilmaz, E., Pehlivan, E., Yilmaz, M., 2009. Immobilization of *Candida rugose* lipase on sporopollenin from *Lycopodium clavatum*. *International Journal of Biological Macromolecules*. 45 (3), 315-320. <https://doi.org/10.1016/j.ijbiomac.2009.06.014>.
- Twaig, F., Chang, K.X., Ling, J.Y.W., 2017. Adsorption of diastase over natural halloysite nanotubes (HNTs). *IOP Conference Series: Materials Science and Engineering*. 206.
- Van Wezel, A.P., van Vlaardingen, P., Pasthumus, R., Crommentuijn, G.H., Sijm, D.T.H.M., 2000. Environmental risk limits for two phthalates, with special emphasis on endocrine disruptive properties. *Ecotoxicology and Environmental Safety*. 46 (3), 305-321. <https://doi.org/10.1006/eesa.2000.1930>.
- Vega, D., Bastide, J., 2003. Dimethyl phthalate hydrolysis by specific microbial esterase. *Chemosphere*. 51 (8), 663-668. [https://doi.org/10.1016/S0045-6535\(03\)00035-3](https://doi.org/10.1016/S0045-6535(03)00035-3).
- Verma, M.L., Naebe, M., Barrow, C.J., Puri, M., 2013. Enzyme immobilization on amino-functionalised multi-walled carbon nanotubes: Structural and biocatalytic characterization. *PLoS One* 8 (9), e73642. <https://doi.org/10.1371/journal.pone.0073642>.
- Vikelsee, J., Thomsen, M., Carlsen, L., 2002. Phthalates and nonylphenols in profiles of differently dressed soils. *Science of the Total Environment*. 296 (1-3), 105-116. [https://doi.org/10.1016/S0048-9697\(02\)00063-3](https://doi.org/10.1016/S0048-9697(02)00063-3).
- Wang, F., Guo, C., Yang, L.R., Liu, C.Z., 2010. Magnetic mesoporous silica nanoparticles: Fabrication and their laccase immobilization performance. *Bioresource Technology*. 101 (23), 8931-8935. <https://doi.org/10.1016/j.biortech.2010.06.115>.

- Wang, H., Zhao, X., Wang, S., Tao, S., Ai, N., Wang, Y., 2015a. Fabrication of enzyme-immobilized halloysite nanotubes for affinity enrichment of lipase inhibitors from complex mixture. *Journal of Chromatography A*. 1392, 20-27. <https://doi.org/10.1016/j.chroma.2015.03.002>.
- Wang, J., Chen, G., Christie, P., Zhang, M., Luo, Y., Teng, Y., 2015b. Occurrence and risk assessment of phthalate esters (PAEs) in vegetables and soils of suburban plastic film greenhouses. *Science of the Total Environment*. 523, 129-137. <https://doi.org/10.1016/j.scitotenv.2015.02.101>.
- Wang, P., Ma, J., Wang, L., Li, L., Yan, X., Zhang, R., Cernava, T., Jin, D., 2023. Di-n-butyl phthalate stress induces in the core bacterial community associated with nitrogen conversion during agricultural waste composting. *Journal of Hazardous Materials*. 446, 130695. <https://doi.org/10.1016/j.jhazmat.2022.130695>.
- Wang, P., Wang, S.L., Fan, C.Q., 2008. Atmospheric distribution of particulate and gas-phase phthalic esters (PAEs) in a metropolitan city, Nanjing, East China. *Chemosphere*. 72(10), 1567-1572. <https://doi.org/10.1016/j.chemosphere.2008.04.032>.
- Wang, W., Leung, A., Chu, L.H., Wong, M.H., 2018. Phthalates contamination in China: status, trends, and human exposure-with an emphasis on oral intake. *Environmental Pollution*. 238, 771-782. <https://doi.org/10.1016/j.envpol.2018.02.088>.
- Wang, Y., Li, F., Ruan, Y., Song, J., Lv, L., Chai, L., Yang, Z., Luo, L., 2017. Biodegradation of di-n-butyl phthalate by bacterial consortium LV-1 enriched from river sludge. *PLOS One*. 12 (5): e0178213. <https://doi.org/10.1371/journal.pone.0178213>.
- Wang, Y.P. and Gu, J.D. 2006. Degradation of dimethyl isophthalate by *Variovorax paradoxus* strain T4 isolated from deep-ocean sediment of the South China sea. *Human and Ecological Risk Assessment: An International Journal*. 12, 236-247. <https://doi.org/10.1080/10807030500531521>.

- Wei, L., Li, Z., Sun, J., Zhu, L. 2020. Pollution characteristics and health risk assessment of phthalate esters in agricultural soil and vegetables in the Yangtze River Delta of China. *Science of the Total Environment*. 726, 137978. <https://doi.org/10.1016/j.scitotenv.2020.137978>.
- Wei, X., Shi, Y., Fei, Y., Chen, J., Lv, B., Chen, Y., Zheng, H., Juli, S., Zhu, L. 2016. Removal of Trace Phthalate Esters from Water by Thin-Film Composite Nanoiltration Hollow Fiber Membranes. *Chemical Engineering Journal*. 292, 382-388. <https://doi.org/10.1016/j.chemosphere.2008.04.032>.
- Weizhen, Z., Xiaowei, Z., Peng, G., Ning, W., Zini, L., Jian, H., Zheng, Z., 2020. Distribution and risk assessment of phthalates in water and sediment of the Pearl River Delta. *Environmental Science and Pollution Research*. 27, 12550e12565. <https://doi.org/10.1007/s11356-019-06819-y>.
- WHO, 2011. Guidelines for drinking-water quality. 4th ed. WHO, Geneva, Switzerland.
- WHO and UNEP, 2012. State of the science of endocrine disrupting chemicals-2012. Editors: Bergman A, Heindel JJ, Jobling S, Kidd KA, Zoeller RT editors. WHO Press, Geneva, Switzerland, 2012, pp 1–38.
- Wittassek, M., Koch, H. M., Angerer, J., Brüning, T., 2011 Assessing exposure to phthalates – the human biomonitoring approach. *Molecular Nutrition and Food Research*. 55 (1), 7–31. <https://doi.org/10.1002/mnfr.201000121>.
- Worsfold, P.J., 1995. Classification and Chemical Characteristics of Immobilized Enzymes (Technical Report). *Journal Pure and Applied Chemistry*. 67 (4), 597-600. <https://doi.org/10.1351/pac199567040597>.
- Wu, Q., Liu, H., Ye, L.S., Li, P., Wang, Y.H., 2013. Biodegradation of Di-n-butyl phthalate esters by *Bacillus* sp. SASHJ under simulated shallow aquifer condition. *International Biodeterioration & Biodegradation*. 76, 102-107. <https://doi.org/10.1016/j.ibiod.2012.06.013>.

- Wu, W., Hu, J., Wang, J., Chen, X., Yao, N., Tao, J., Zhou, Y.K., 2015. Analysis of phthalate esters in soils near an electronics manufacturing facility and from a non-industrialized area by gas purge microsyringe extraction and gas chromatography. *Science of the Total Environment*. 508, 445-451. <https://doi.org/10.1016/j.scitotenv.2014.11.081>.
- Wu, Y., Sun, J., Zheng, C., Zhang, X., Zhang, A., Qi, H., 2019. Phthalate pollution driven by the industrial plastics market: A case study of the plastic market in Yuyao City, China. *Environmental Science and Pollution Research*. 26 (11), 11224–11233. <https://doi.org/10.1007/s11356-019-04571-x>.
- Wypych, G., 2004. *Handbook of Plasticizer*. Toronto-New York: Chemtech Publishing.
- Xia, X.H., Yang, L.Y., Bu, Q.W., Liu, R.M., 2011. Levels, distribution, and health risk of phthalate esters in urban soils of Beijing, China. *Journal of Environmental Quality*. 40 (5), 1643-1651. <https://doi.org/10.2134/jeq2011.0032>.
- Xu, G., Li, F., Wang, Q., 2008. Occurrence and degradation characteristics of dibutyl phthalate (DBP) and di-(2-ethylhexyl) phthalate (DEHP) in typical agricultural soils of China. *Science of the Total Environment*. 393 (2-3), 333-340. <https://doi.org/10.1016/j.scitotenv.2008.01.001>.
- Xu, Y., Liu, X., Zhao, J., Huang, H., Wu, M., Li, X., Li, W., Sun, X., Sun, B., 2021. An efficient phthalate ester-degrading *Bacillus subtilis*: Degradation kinetics, metabolic pathway, and catalytic mechanism of the key enzyme. *Environmental Pollution* 273, 116461. <https://doi.org/10.1016/j.envpol.2021.116461>.
- Yang, J., Guo, C., Liu, S., Liu, W., Wang, H., Dang, Z., Lu, G., 2018. Characterization of a di-n-butyl phthalate-degrading bacterial consortium and its application in contaminated soil. *Environmental Science and Pollution Research*. 25, 17645-17653. <https://doi.org/10.1007/s11356-018-1862-0>.
- Yang, Q., Yan, Yang, X., Liao, G., Wang, D., Xia, H., 2019. Enzyme immobilization in cage-like 3D-network PVA-H and GO modified PVA-H (GO@PVA-H) with stable

- conformation and high activity. *Chemical Engineering Journal*. 372, 946-955.
<https://doi.org/10.1016/j.cej.2019.04.216>.
- Yang, F., Wang, M., Wang, Z., 2013. Sorption behavior of 17 phthalic acid esters on three soils: Effects of pH and dissolved organic matter, sorption coefficient measurement and QSPR study. *Chemosphere*. 93 (1), 82-89.
<https://doi.org/10.1016/j.chemosphere.2013.04.081>.
- Yang, T., Ren, L., Jia, Y., Fan, S., Wang, J., Wang, J., Nahurira, R., Wang, H., Yan, Y., 2018. Biodegradation of di (2-ethylhexyl) phthalate by *Rhodococcus ruber* YC-YT1 in contaminated water and soil. *International Journal of Environmental Research and Public Health*. 15, 964. <https://doi.org/10.3390/ijerph15050964>.
- Yastrebova, O.V., Pyankova, E.G., 2019. Phthalate-degrading bacteria isolated from an industrial mining area and the processing of potassium and magnesium salt. *Applied Biochemistry and Microbiology*. 55, 397-404.
<https://doi.org/10.1134/S000368381904015X>.
- Yavuz, E., Gunes, H., Harsa, S., Yenidunya, A.F., 2004. Identification of extracellular enzyme producing thermophilic bacilli from Balcova (Agamemnon) geothermal site by ITS rDNA RFLP. *Journal of Applied Microbiology*. 97 (4), 810-817.
<https://doi.org/10.1111/j.1365-2672.2004.02374.x>.
- Yeniova-Erpek, C.E., Ozkoc, G., Yilmazer, U., 2015. Effects of halloysite nanotubes on the performance of plasticized poly(lactic acid)-based composite. *Polymer Composite*. 37 (11), 3134-3148. <https://doi.org/10.1002/pc.23511>.
- Yoo, W., Kim, B., Jeon, S., Kim, K.K., Kim, T.D., 2020. Identification, characterization, and immobilization of a novel YbfF esterase from *Halomonas elongata*. *International Journal of Biological Macromolecules*. 165, 1139-1148.
<https://doi.org/10.1016/j.ijbiomac.2020.09.247>.
- Yousefi, Z., Ala, A., Babanezhad, E., Ali Mohammadpour, R.J.E.H.E., Journal, M., 2019. Evaluation of the exposure to phthalate esters through the use of various brands of

- drinking water bottled in PET containers under different storage conditions. *Environmental Health Engineering and Management. Journal.* 6 (4), 247-255. <https://doi.org/10.15171/EHEM.2019.28>
- You, Z., Bedrikovetsky, P., Badalyan, A., Hand, M., 2015. Particle immobilization in porous media: Temperature effects on competing electrostatic and drag forces. *Geophysical Research Letters.* 42 (8), 2852-2860. <https://doi.org/10.1002/2015GL063986>.
- Zaborsky, O.R., 1973. *Entrapment within Cross-Linked Polymers, Immobilized Enzymes*, Boca Raton: CRS Press. 83-91.
- Zdarta, J., Meyer, A.S., Jesionowski, T., Pinelo, M., 2018. A general overview of support materials for enzyme immobilization: Characteristics, properties, practically utility. *Catalysts.* 8 (2), 92. <https://doi.org/10.3390/catal8020092>.
- Zeng, F., Cui, K., Li, X., Fu, J., Sheng, G., 2004. Biodegradation kinetics of phthalate esters by *Pseudomonas fluorescences* FS1. *Process Biochemistry.* 39 (9), 1125-1129. [https://doi.org/10.1016/S0032-9592\(03\)00226-7](https://doi.org/10.1016/S0032-9592(03)00226-7).
- Zeng, F., Cui, K., Xie, Z., Wu, L., Liu, M., Sun, G., Lin, Y., Luo, D., Zeng, Z., 2008. Phthalate esters (PAEs): Emerging organic contaminants in agricultural soils in peri-urban areas around Guongzhou, China. *Environmental Pollution.* 156 (2), 425-434. <https://doi.org/10.1016/j.envpol.2008.01.045>.
- Zhai, R., Zhang, B., Liu, L., Xie, Y., Zhang, Y., Liu, J., 2010. Immobilization of enzyme biocatalyst on natural halloysite nanotube. *Catalysis Communications.* 12, 259-263. <https://doi.org/10.1016/j.catcom.2010.09.030>.
- Zhai, R., Zhang, B., Wan, Y., Li, C., Wang, J., Liu, J., 2013. Chitosan-halloysite hybrid nanotubes: Horseradish peroxidase immobilization and applications in phenol removal. *Chemical Engineering Journal.* 214, 304-309. <https://doi.org/10.1016/j.cej.2012.10.073>.

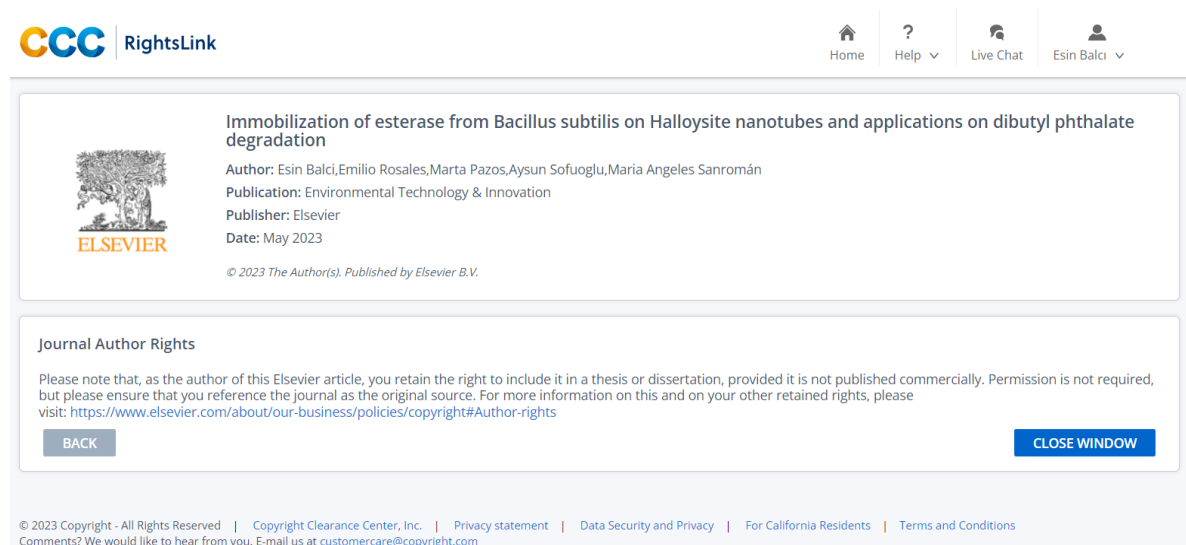
- Zhang, H., Lin, Z., Liu, B., Wang, G., Weng, L., Zhou, J., Hu, H., Huang, Y., Chen, J., Ruth, N., Li, C., Ren, L., 2020. Bioremediation of di-(2-ethylhexyl) phthalate contaminated red soil by *Gordonia terrae* RL-JC02: Characterization, metabolic pathway and kinetics. *Science of the Total Environment*. 733, 139138. <https://doi.org/10.1016/j.scitotenv.2020.139138>.
- Zhang, S., Zhang, W., Lin, L., 2021. Research progress on the removal of phthalic acid esters in water. *E3S Web of Conferences ICEMEE 2021*. 261 (4), 02041. <https://doi.org/10.1051/e3sconf/202126102041>.
- Zhang, X.Y., Fan, X., Qiu, Y.J., Li, C.Y., Xing, S., Zheng, Y.T., Xu, J.H., 2014. Newly identified thermostable esterase from *Sulfobacillus acidophilus*: Properties and performance in phthalate ester degradation. *Applied and Environmental Microbiology*. 80 (22), 6870-6878. <https://doi.org/10.1128/AEM.02072-14>.
- Zhao, W.W., Xu, J.J., Chen, H.Y., 2017. Photoelectrochemical enzymatic biosensors. *Biosensors and Bioelectronics*. 92, 294-304. <https://doi.org/10.1016/j.bios.2016.11.009>.
- Zheng, X., Zhang, B.T., Teng, Y., 2014. Distribution of phthalate acid esters in lakes of Beijing and its relationship with anthropogenic activities. *Science of the Total Environment*. 476(1),107-113. <https://doi.org/10.1016/j.scitotenv.2013.12.111>.
- Zhou, B., Zhao, L., Wang, Y., Sun, Y., Li, X., Xu, H., Weng, L., Pan, Z., Yang, S., Chang, X., Li, Y., 2020. Spatial distribution of phthalate esters and the associated response of enzyme activities and microbial community composition in typical plastic-shed vegetable soils in China. *Ecotoxicology and Environmental Safety*. 195, 110495. <https://doi.org/10.1016/j.ecoenv.2020.110495>

APPENDIX A

PERMISSION FOR REPRODUCING PUBLISHED ARTICLES

All permissions have been taken to reproduce the full text presented in Chapters 2 and 4 through the Copyright Clearance Center. All documentation of the approvals is listed on the following pages.


Chapter 2




The screenshot shows a web interface for RightsLink. At the top left is the CCC RightsLink logo. At the top right are navigation icons for Home, Help, Live Chat, and a user profile for Esin Balci. The main content area is divided into two sections. The first section, titled 'Immobilization of esterase from Bacillus subtilis on Halloysite nanotubes and applications on dibutyl phthalate degradation', includes the Elsevier logo, author names (Esin Balci, Emilio Rosales, Marta Pazos, Aysun Sofuoglu, Maria Angeles Sanromán), publication details (Environmental Technology & Innovation, Elsevier, May 2023), and a copyright notice. The second section, titled 'Journal Author Rights', contains a paragraph explaining that authors retain the right to use their work in theses or dissertations, provided they reference the journal as the original source. It includes a URL for more information and two buttons: 'BACK' and 'CLOSE WINDOW'. At the bottom of the page, there is a footer with copyright information and links to privacy and terms pages.

Figure A.1. Permission for the published article in Chapter 2.

Chapter 4

Home | Help | Live Chat | Esin Balci



Continuous treatment of diethyl hexyl and dibutyl phthalates by fixed-bed reactor: Comparison of two esterase bionanocomposites

Author: Esin Balci, Emilio Rosales, Marta Pazos, Aysun Sofuoglu, Maria Angeles Sanroman

Publication: Bioresource Technology

Publisher: Elsevier

Date: November 2022

© 2022 The Author(s). Published by Elsevier Ltd.

Creative Commons Attribution-NonCommercial-No Derivatives License (CC BY NC ND)

This article is published under the terms of the [Creative Commons Attribution-NonCommercial-No Derivatives License \(CC BY NC ND\)](#). For non-commercial purposes you may copy and distribute the article, use portions or extracts from the article in other works, and text or data mine the article, provided you do not alter or modify the article without permission from Elsevier. You may also create adaptations of the article for your own personal use only, but not distribute these to others. You must give appropriate credit to the original work, together with a link to the formal publication through the relevant DOI, and a link to the Creative Commons user license above. If changes are permitted, you must indicate if any changes are made but not in any way that suggests the licensor endorses you or your use of the work.

Permission is not required for this non-commercial use. For commercial use please continue to request permission via RightsLink.

[BACK](#)

[CLOSE WINDOW](#)

© 2023 Copyright - All Rights Reserved | [Copyright Clearance Center, Inc.](#) | [Privacy statement](#) | [Data Security and Privacy](#) | [For California Residents](#) | [Terms and Conditions](#)
Comments? We would like to hear from you. E-mail us at customer@copyright.com

Figure A.2. Permission for the published article in Chapter 4.

APPENDIX B

SUPPLEMENTARY INFORMATION FOR CHAPTER 2

Table B.1. CCDFC arrangement with 2^4 and the experimental responses for the esterase immobilization.

Run	X ₁ , pH	X ₂ , Time (min)	X ₃ , E/H	X ₄ , Temperature (°C)	Y ₁ , Adsorption efficiency (%)	Y ₂ , Specific enzyme activity (U/mg)
1	5	30	0.02	20	77.61	1.31
2	5	30	0.02	40	63.30	2.30
3	5	360	0.02	20	78.77	1.38
4	5	360	0.02	40	72.31	2.28
5	6	195	0.02	30	92.57	7.16
6	7	30	0.02	20	60.94	27.80
7	7	30	0.02	40	22.41	30.91
8	7	360	0.02	20	67.17	27.91
9	7	360	0.02	40	22.75	34.61
10	5	195	0.11	30	95.42	2.22
11	6	30	0.11	30	87.65	7.19
12	6	195	0.11	20	78.37	5.15
13	6	195	0.11	30	82.86	7.18
14	6	195	0.11	30	84.65	7.08
15	6	195	0.11	30	84.33	7.04
16	6	195	0.11	30	84.99	7.12
17	6	195	0.11	30	85.36	7.11
18	6	195	0.11	30	84.92	8.19
19	6	195	0.11	40	53.18	9.13
20	6	360	0.11	30	92.89	7.07
21	7	195	0.11	30	62.97	30.60
22	5	30	0.2	20	67.85	2.37
23	5	30	0.2	40	81.86	3.05
24	5	360	0.2	20	79.56	2.35
25	5	360	0.2	40	94.73	3.94
26	6	195	0.2	30	87.74	7.16
27	7	30	0.2	20	60.09	26.29
28	7	30	0.2	40	24.72	30.78
29	7	360	0.2	20	60.92	25.83
30	7	360	0.2	40	39.39	34.78

Table B.2. ANOVA results for the proposed model on the adsorption efficiency of HNTs with esterase.

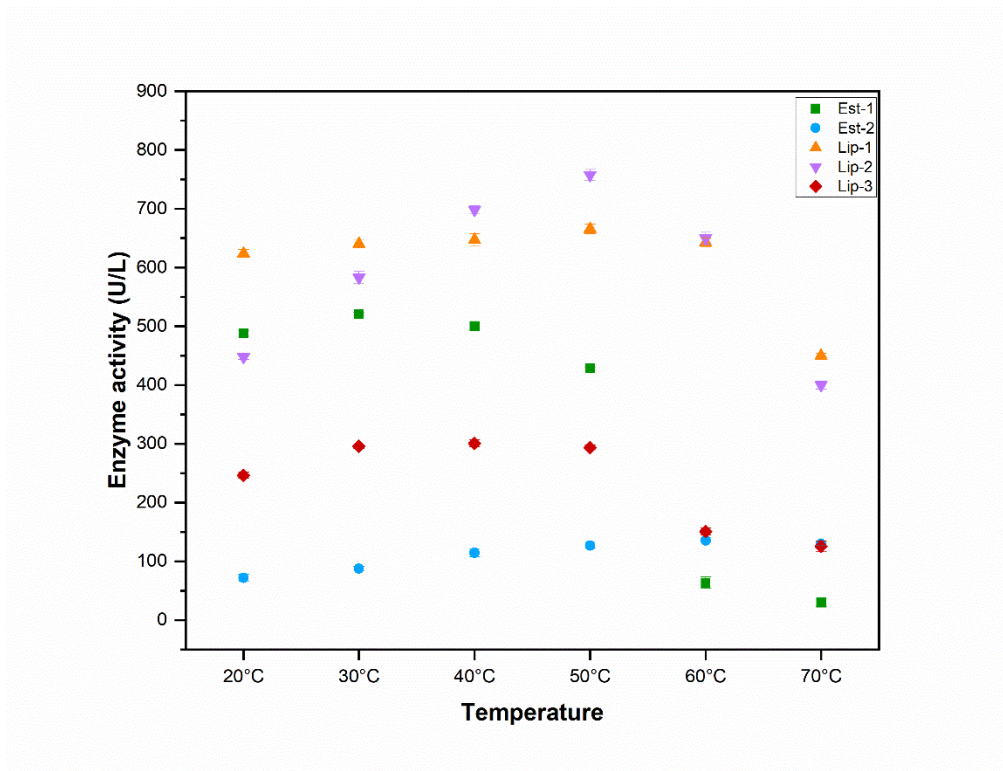
Source	Sum of squares	df	Mean square	F-value	Prob > F
Model	12518.56	14	894.18	63.14	< 0.0001
X ₁ -pH	4673.99	1	4673.99	330.06	< 0.0001
X ₂ -Adsorption Time	214.04	1	214.04	15.11	0.0015
X ₃ -Enzyme/HNT	84.67	1	84.67	5.98	0.027
X ₄ -Adsorption temperature	1362.93	1	1362.93	96.25	< 0.0001
X ₁ X ₂	10.01	1	10.01	0.71	0.413
X ₁ X ₃	25.42	1	25.42	1.79	0.200
X ₁ X ₄	1373.91	1	1373.91	97.02	< 0.0001
X ₂ X ₃	34.10	1	34.10	2.41	0.141
X ₂ X ₄	17.98	1	17.98	1.27	0.277
X ₃ X ₄	360.99	1	360.99	25.49	0.0001
X ₁ ²	182.47	1	182.47	12.89	0.0027
X ₂ ²	18.62	1	18.62	1.31	0.269
X ₃ ²	17.08	1	17.08	1.21	0.289
X ₄ ²	1233.33	1	1233.33	87.09	< 0.0001
Residual	212.41	15	14.16		
Lack of Fit	208.50	10	20.85	26.65	0.001
Pure Error	3.91	5	0.78		
Cor Total	12730.97	29			
	Std. Dev.	3.76	R ²	0.983	
	Mean	71.08	Adj. R ²	0.968	
	C.V. (%)	5.29	Pred. R ²	0.902	
	R ²	0.983	Adeq.	28.066	
			Precision		

P < 0.05 significant; P > 0.05 not significant

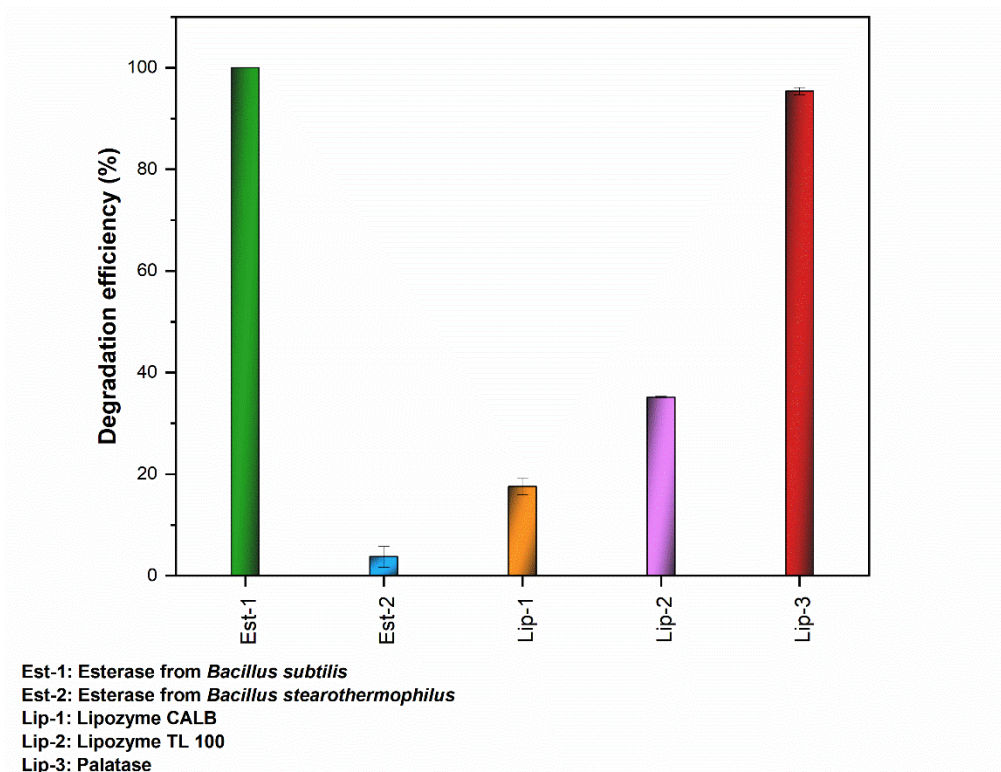
Table B.3. ANOVA results for the model on the specific activity of HNTs with esterase.

Source	Sum of squares	df	Mean square	F-value	Prob > F
Model	3828.25	14	273.45	1254.63	< 0.0001
X ₁ -pH	3235.03	1	3235.03	14842.97	< 0.0001
X ₂ -Adsorption Time	0.07	1	0.07	0.32	0.5780
X ₃ -Enzyme/HNT	0.20	1	0.20	0.91	0.3563
X ₄ -Adsorption Temperature	30.35	1	30.35	139.25	< 0.0001
X ₁ X ₂	0.02	1	0.02	0.098	0.7585
X ₁ X ₃	3.05	1	3.05	14.00	0.0020
X ₁ X ₄	9.13	1	9.13	41.89	< 0.0001
X ₂ X ₃	0.15	1	0.15	0.68	0.4229
X ₂ X ₄	0.22	1	0.22	1.01	0.3317
X ₃ X ₄	1.57	1	1.57	7.22	0.0169
X ₁ ²	219.67	1	219.67	1007.90	< 0.0001
X ₂ ²	0.01	1	0.01	0.075	0.7885
X ₃ ²	4.11E-003	1	4.11E-003	0.019	0.8926
X ₄ ²	0.81	1	0.81	3.73	0.0726
Residual	3.27	15	0.22		
Lack of Fit	3.25	10	0.32	75.04	< 0.0001
Pure Error	0.02	5	4.33E-003		
Cor Total	3831.52	29			
	Std. Dev.	0.47	R ²	0.999	
	Mean	12.28	Adj. R ²	0.998	
	C.V. (%)	3.80	Pred. R ²	0.994	
	R ²	0.999	Adeq.	90.79	
			Precision		

P < 0.05 significant; P > 0.05 not significant

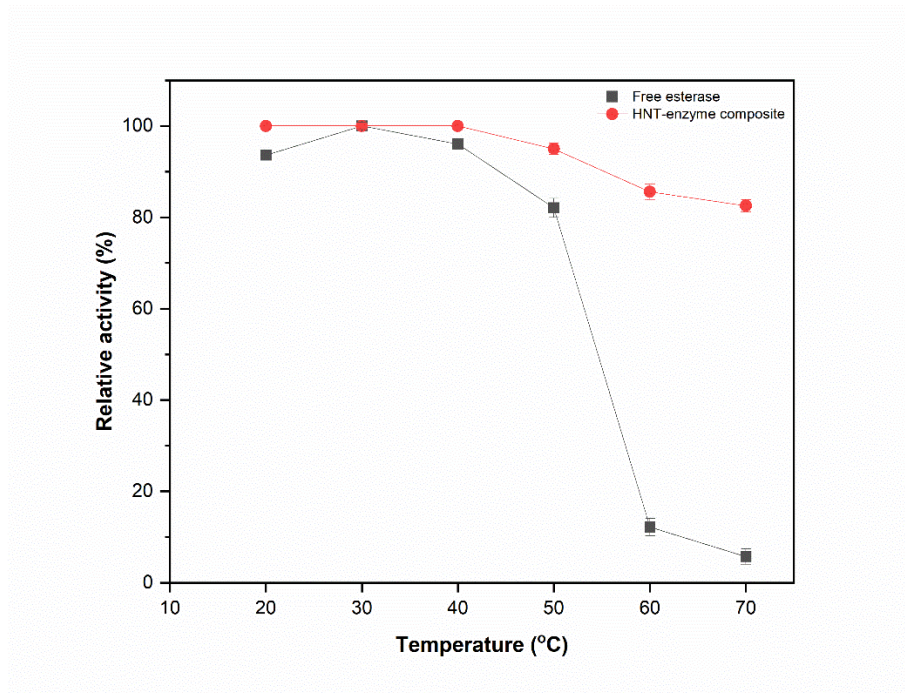


(a)

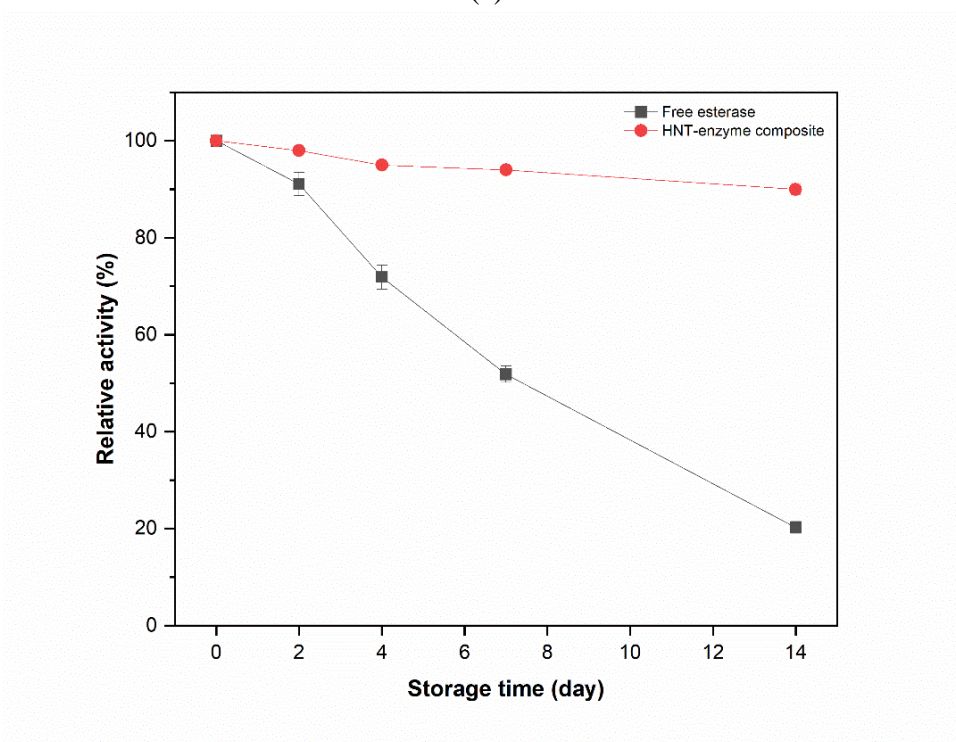


(b)

Figure B.1. (a) Enzyme activities at different temperatures and (b) DBP degradation ability of the enzymes under optimum temperature conditions for 15 min.



(a)



(b)

Figure B.2. Thermal (a) and storage stability (b) of free esterase and HNT-enzyme composite.

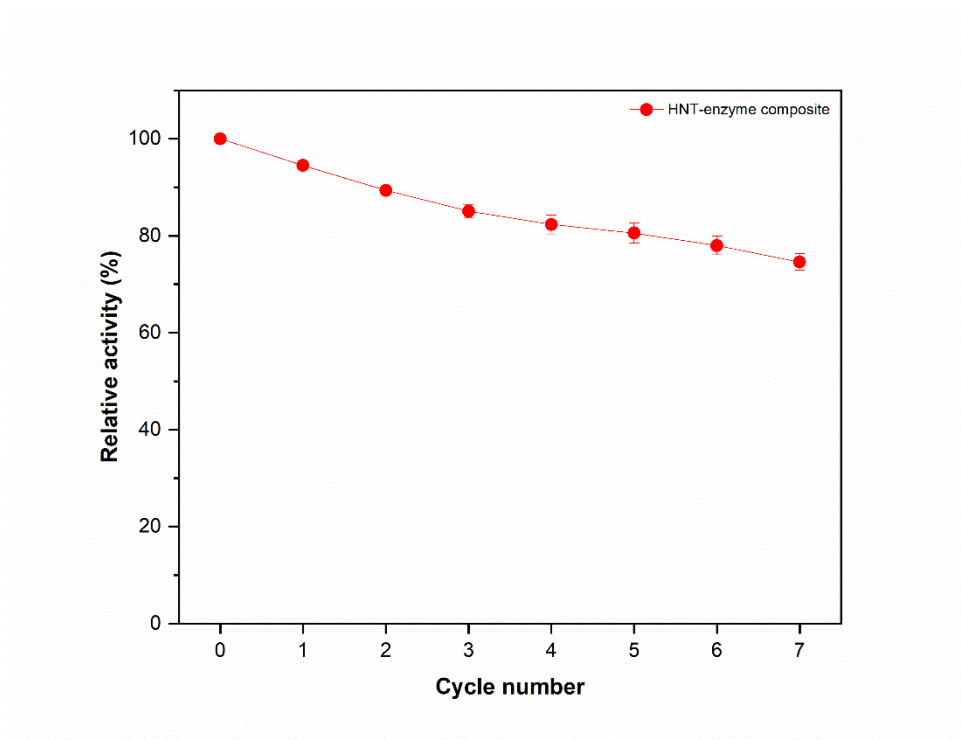


Figure B.3. Reusability of HNT-enzyme composite for 7 cycles.

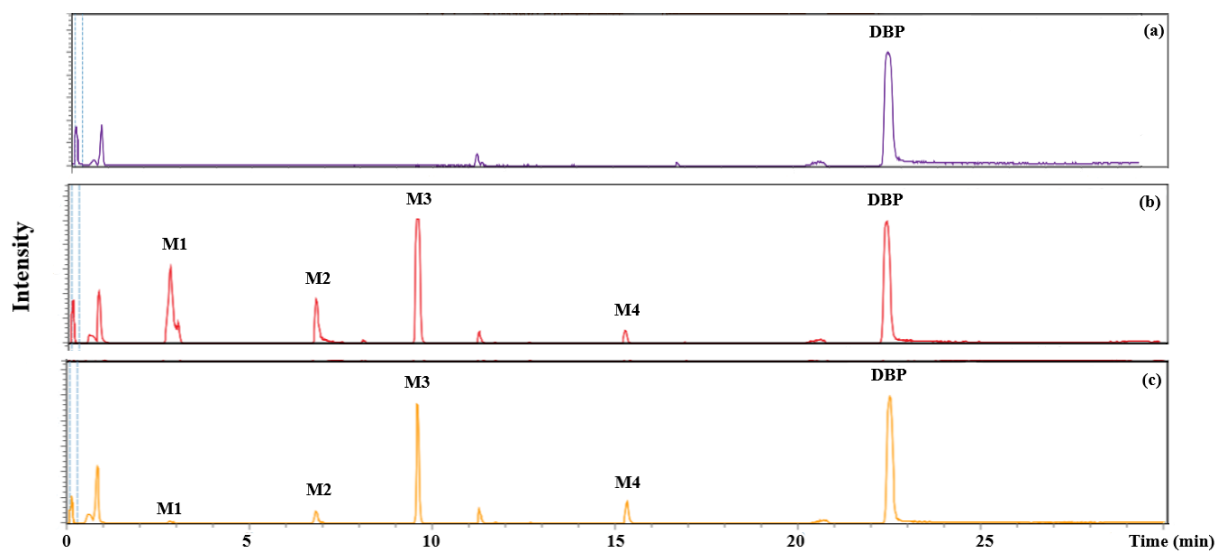
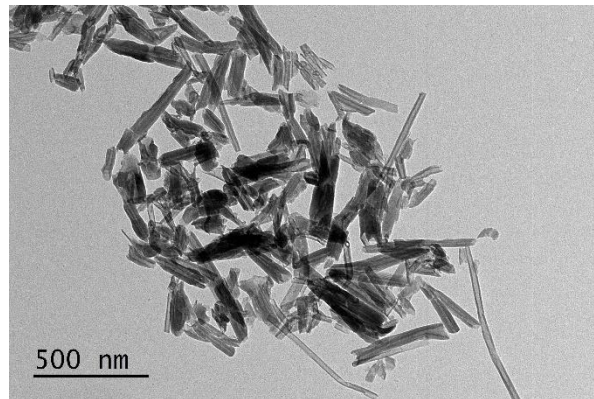


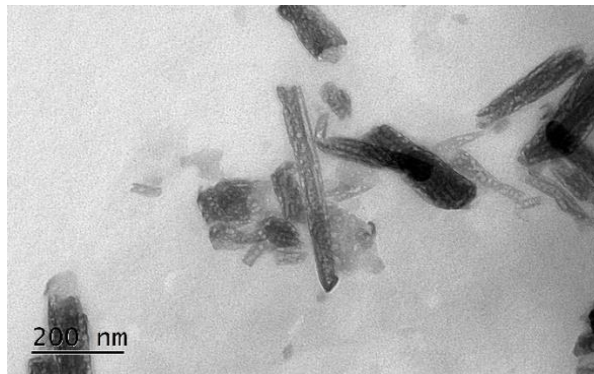
Figure B.4. HPLC-MS chromatogram of the sample before degradation experiment (a) and after degradation experiment by; free esterase (b) and HNT-enzyme composite (c).

APPENDIX C

SUPPLEMENTARY INFORMATION FOR CHAPTER 3

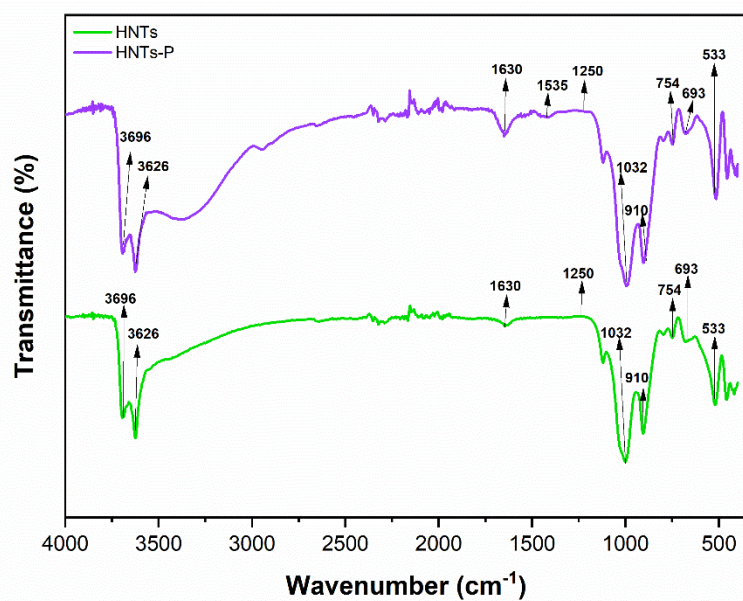


(a)

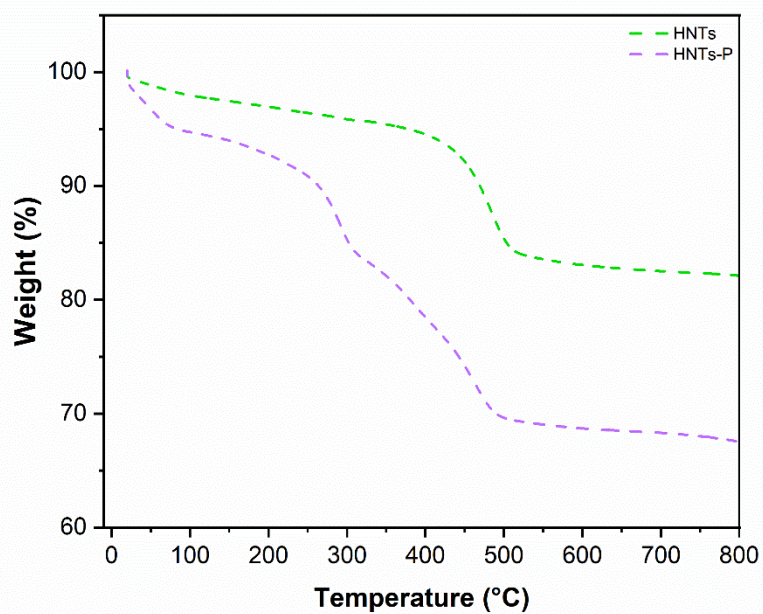


(b)

Figure C.1. TEM images of (a) pure HNTs and (b) HNTs-P composite.



(a)



(b)

Figure C.2. (a) FT-IR spectra and (b) TGA profile of HNTs (green) and HNTs-P composite (purple).

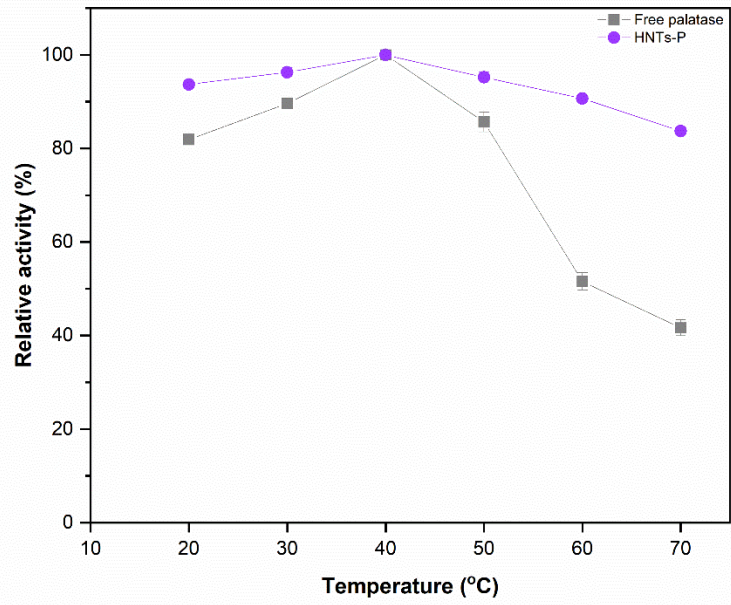


Figure C.3. Thermal stability test results: Free palatase and HNTs-P composite.

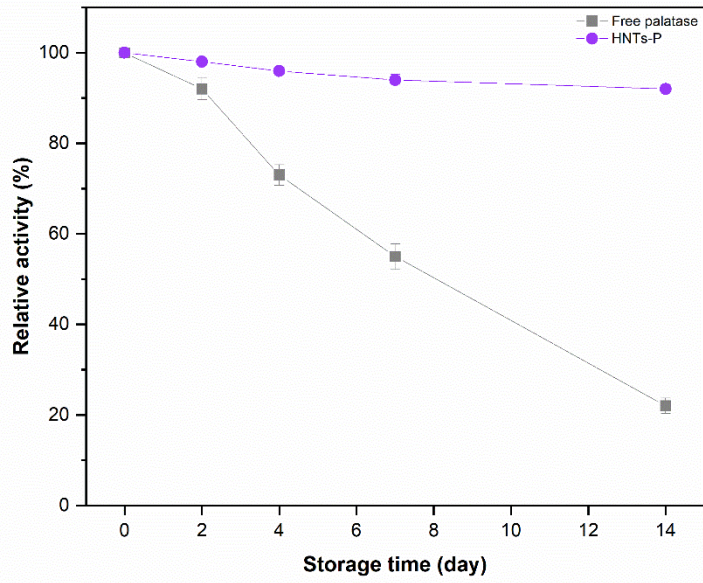


Figure C.4. Storage stability test results: Free palatase and HNTs-P composite.

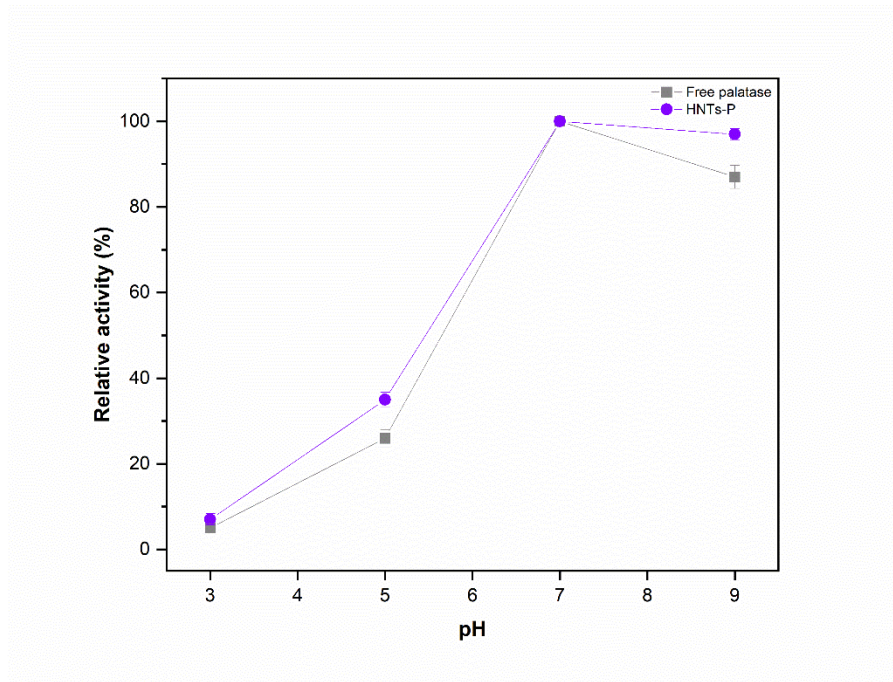
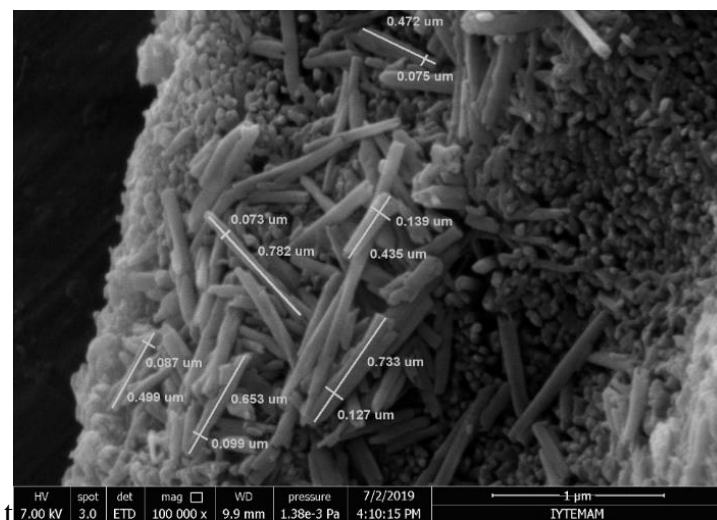


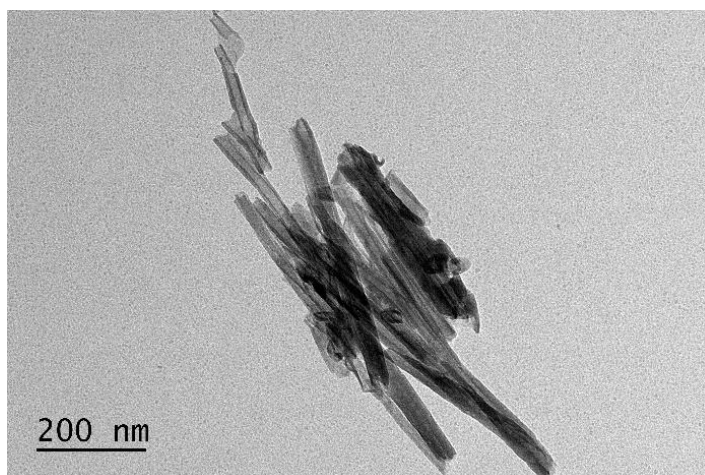
Figure C.5. pH test stability results: Free palatase and HNTs-P composite.

APPENDIX D

SUPPLEMENTARY INFORMATION FOR CHAPTER 4



(a)



(b)

Figure D.1. SEM (a) and TEM (b) images of pure HNT.

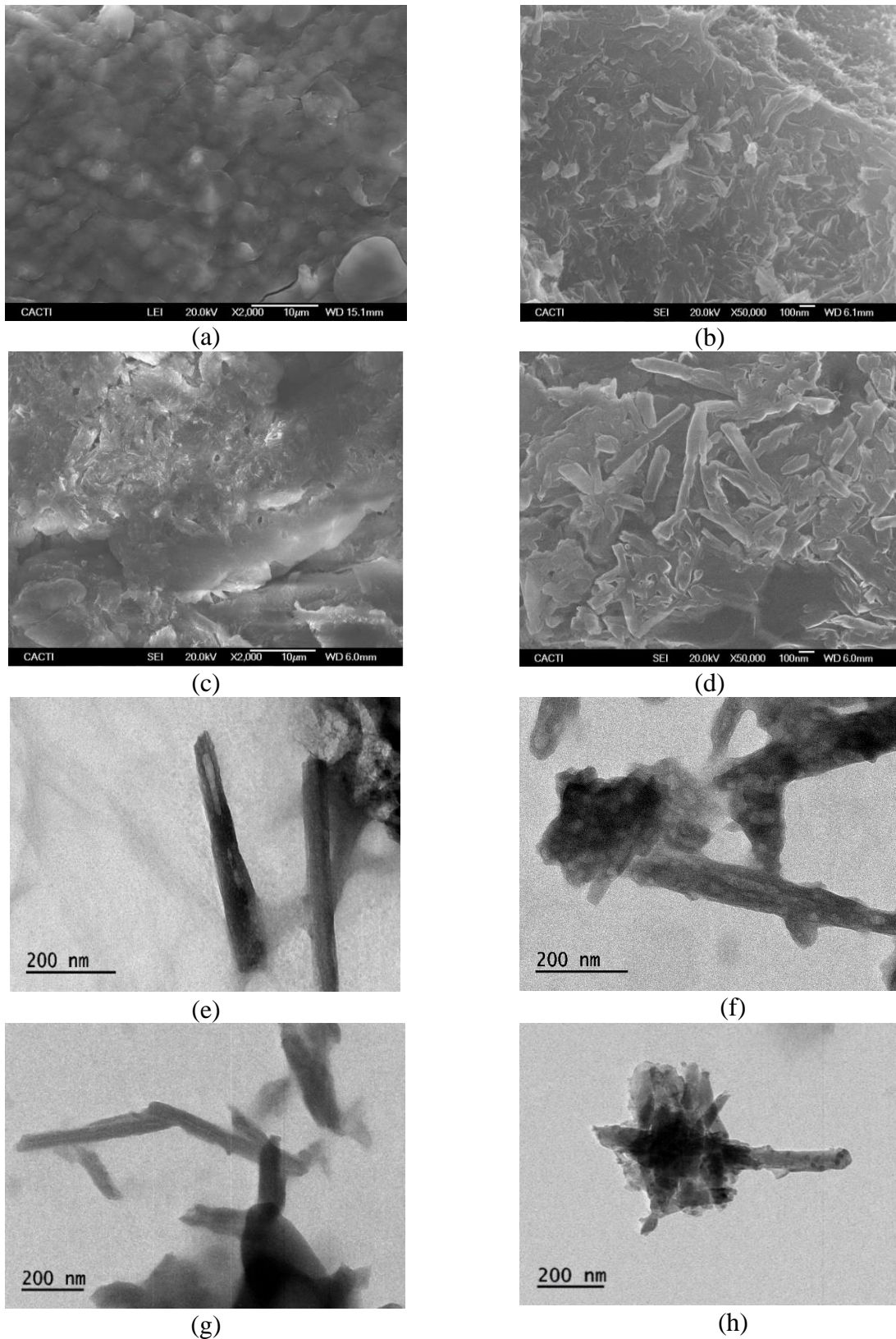


Figure D.2. SEM images of: CTS-HNT (a-b) and ALG-HNT beads (c-d). TEM images of: (e) CTS-HNT and (f) CTS-HNT-EST, (g) ALG-HNT and (h) ALG-HNT-EST.

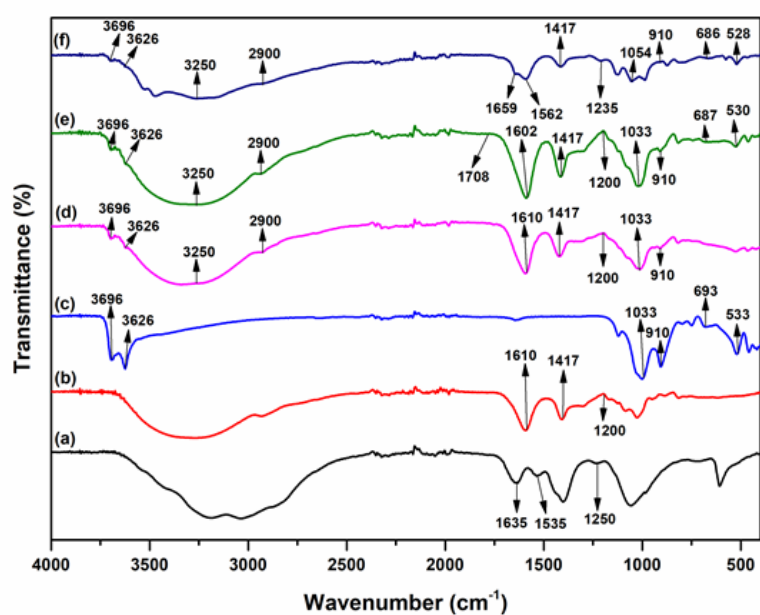
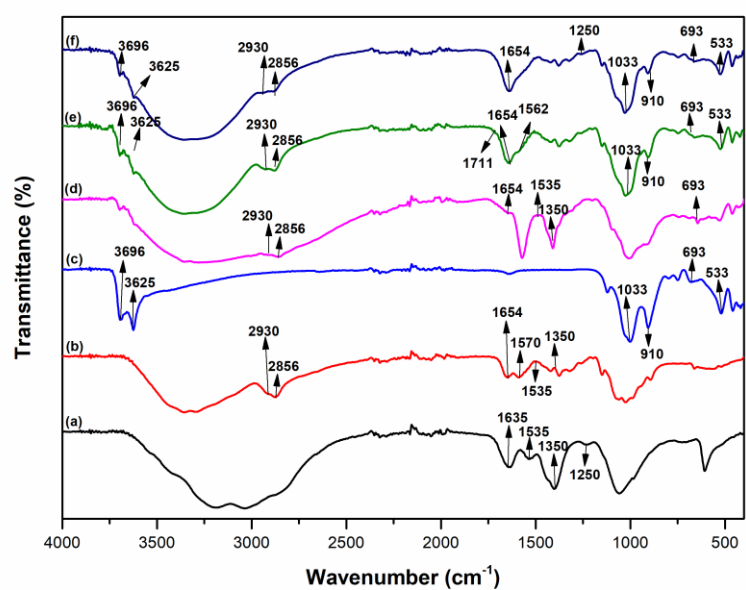


Figure D.3. In the top FT-IR spectrum of (a) the esterase (EST), (b) CTS, (c) HNT, (d) CTS-HNT, (e) CTS-HNT-GTA, and (f) CTS-HNT-GTA-EST; In the bottom FT-IR spectrum of (a) EST, (b) ALG, (c) HNT, (d) ALG-HNT, (e) ALG-HNT-GTA, and (f) ALG-HNT-GTA-EST.

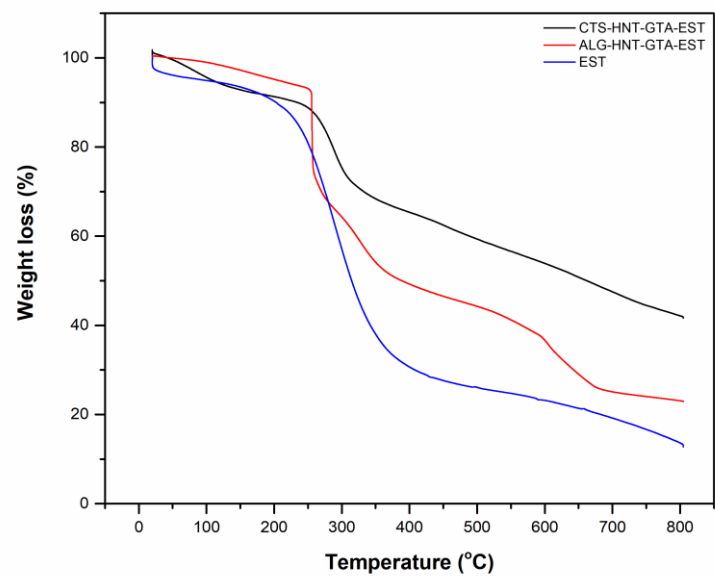
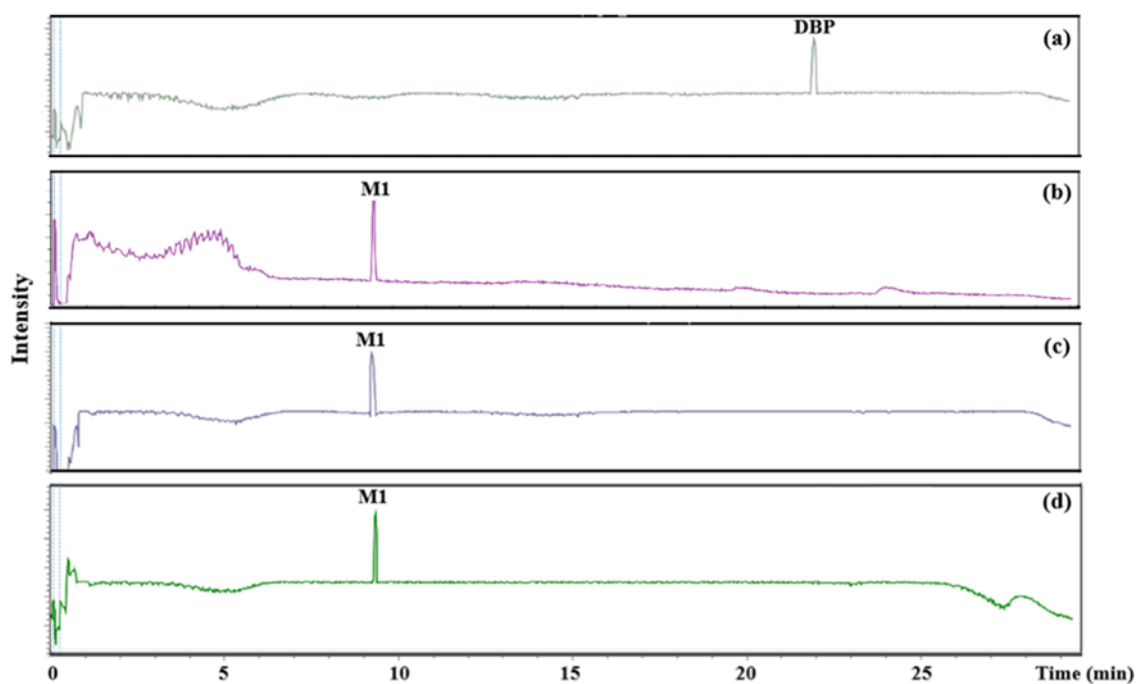
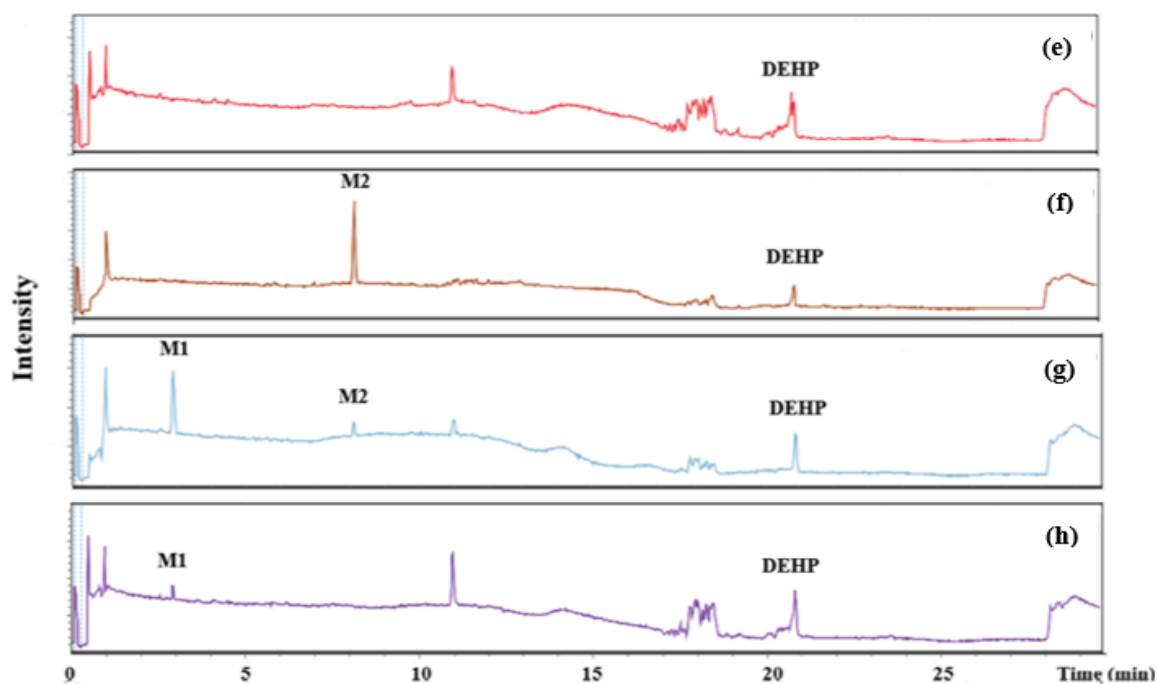


Figure D.4. Thermal analysis curve of esterase, CTS-HNT with esterase, and ALG-HNT with esterase.



A



B

Figure D5. HPLC-MS chromatogram of (A) DBP sample in DMSO before DBP degradation experiment (a), and after degradation in the presence of the free esterase (b), the esterase immobilized on the CTS-HNT (c) and ALG-HNT (d) beads; (B) DEHP before degradation experiment (e), after degradation experiment in the presence of free esterase (f), the esterase immobilized on CTS-HNT (g) and ALG-HNT (h) beads.

VITA

Education:

M.Sc. 2016

Environmental Engineering, Gebze Technical University, Kocaeli, Türkiye

Thesis: Treatment of Textile wastewater by membrane process and industrial wastewater recovery

Advisor: Prof. Dr. Coşkun AYDINER

B.S. 2013

Environmental Engineering, Istanbul University, Istanbul, Türkiye

Thesis: An Investigation of Pollution Transport Related Wastewater Dilution Performance of Kucukcekmece Marine Outfall

Advisor: Prof. Dr. Semih NEMLIOGLU

Academic Experience:

Research assistant 2017-

Environmental Engineering, Izmir Institute of Technology, Izmir, Türkiye

Researcher 2021 (10 months)

Chemical Engineering, Vigo University, Vigo, SPAIN

Project assistant 2015-2016 (18 months)

TUBITAK 113Y352 “Water Recovery and Concentrate Management with Integrated Advanced Oxidation/Membrane Filtration System in Industries Consuming a High Quantity of Water”

Project and Awards:

TUBITAK 2209-A Research Project Support Programme for Undergraduate Students, 2023

“Enzymatic bioremediation of soils containing phthalic acid ester (PAE) in the presence of esterase enzyme from *Bacillus subtilis*” (role: Supervisor).

TUBITAK 2209-A Research Project Support Programme for Undergraduate Students, 2022

“Investigation of Immobilization Efficiency of Thermoalkaliphilic Recombinant Esterase Enzyme to Halloysite Nanotube (HNT)” (role: Supervisor).

TUBITAK 2214 -A International Doctoral Research Fellowship Program, 2021

“Degradation Studies of Phthalic Acid Esters (PAEs) in Wastewater Using an Immobilized Thermophilic Enzyme” (role: Executive).

Honor Certificates

Istanbul University, Istanbul, Türkiye

2009-2013

Publications:

- Balci, E., Rosales, E., Pazos, M., Sofuoglu, A., Sanroman, M.A. 2023. Immobilization of esterase from *Bacillus subtilis* on halloysite nanotubes and applications on dibutyl phthalate degradation. *Environmental Technology and Innovation*. 30, 103113.
- Balci, E., Balci, S., Sofuoglu, A.S. 2022. Multi-purpose reverse logistics network design for medical waste management in a megacity: Istanbul, Turkey. *Environment Systems and Decisions*. 42, 372-387.
- Balci, E., Rosales, E., Pazos, M., Sofuoglu A., Sanroman, M.A. 2022. Continuous treatment of diethyl hexyl phthalates by fixed-bed reactor: Comparison of two esterase bionanocomposites. *Bioresource Technology*. 363, 127990.
- Balci, E., Genisoglu, M., Sofuoglu, S.C., Sofuoglu, A. 2020. Indoor air partitioning of Synthetic Musk Compounds: Gas, particulate matter, house dust, and window film. *Science of the Total Environment*. 729, 138798.
- Genisoglu, M., Goren, A.Y., Balci, E., Recepoglu, Y.K., Okten, H.E. 2019. Methylene Blue Removal of Fixed-Bed Column Reactor with Pumice and nZVI-Pumice: Experimental and Modelling Study, *Suleyman Demirel University Journal of Natural and Applied Science*. 23(3), 298-305.
- Aydiner, C., Mert, B.K., Dogan, E.C., Yatmaz, H.C., Dagli, S., Aksu, S., Goren, A.Y., and Balci, E. 2019. Novel hybrid treatments of textile wastewater by membrane

oxidation reactor: Performance investigations, optimizations, and efficiency comparisons, *Science of Total Environment*, 683, 411-426.

- Mert, B.K., Dogan, E.C., Balci, E., Tilki, Y.M., Goren, A.Y. and Aydiner, C., 2018. Water recovery with combined membrane system in textile industry, treatment, and management of concentrates by hybrid advanced oxidation/membrane filtration, Pamukkale University Journal of Engineering Sciences, 24(3), 468-475
- Aydiner, C., Mert, B.K., Dogan, E.C., Balci, E., Tilki, Y.M., Aksu, S. and Goren, A.Y., 2016. Investigation of Influence of Membrane Type on Water Recovery by Pressurized Membrane Processes from Textile Washing Wastewaters, *Uludag University Journal of The Faculty of Engineering*, 21(2), 319-330.

Book Chapter:

- Balci, E. and Sofuoglu, A. 2023. Fragrance emissions into the air and their impact on air quality and human health. *The Handbook of Environmental Chemistry*. 1-46. Springer, Berlin, Heidelberg.